

2014

## **Advances in targeted radiosensitiser and nanotherapeutic agents for cancer therapy**

Sianne Oktaria  
*University of Wollongong*

Follow this and additional works at: <https://ro.uow.edu.au/theses>

### **University of Wollongong**

#### **Copyright Warning**

You may print or download ONE copy of this document for the purpose of your own research or study. The University does not authorise you to copy, communicate or otherwise make available electronically to any other person any copyright material contained on this site.

You are reminded of the following: This work is copyright. Apart from any use permitted under the Copyright Act 1968, no part of this work may be reproduced by any process, nor may any other exclusive right be exercised, without the permission of the author. Copyright owners are entitled to take legal action against persons who infringe their copyright. A reproduction of material that is protected by copyright may be a copyright infringement. A court may impose penalties and award damages in relation to offences and infringements relating to copyright material.

Higher penalties may apply, and higher damages may be awarded, for offences and infringements involving the conversion of material into digital or electronic form.

Unless otherwise indicated, the views expressed in this thesis are those of the author and do not necessarily represent the views of the University of Wollongong.

---

### **Recommended Citation**

Oktaria, Sianne, Advances in targeted radiosensitiser and nanotherapeutic agents for cancer therapy, Doctor of Philosophy thesis, School of Physics, University of Wollongong, 2014. <https://ro.uow.edu.au/theses/4268>

**UNIVERSITY OF  
WOLLONGONG**



**ADVANCES IN TARGETED  
RADIOSENSITISER AND  
NANOTHERAPEUTIC AGENTS FOR  
CANCER THERAPY**

A Thesis Submitted in Partial Fulfilment of  
the Requirements for the Award of the Degree of

**Doctor of Philosophy**

from

**UNIVERSITY OF WOLLONGONG**

by

**Sianne Oktaria**

School of Physics  
Faculty of Engineering and Information Sciences

**March 2014**

---

© Copyright 2014

by

Sianne Oktaria

ALL RIGHTS RESERVED

## CERTIFICATION

I, Sianne Oktaria, declare that this thesis, submitted in partial fulfilment of the requirements for the award of **Doctor of Philosophy**, in the School of Physics, Faculty of Engineering and Information Sciences, University of Wollongong, is wholly my own work unless otherwise referenced or acknowledged. The document has not been submitted for qualifications at any other academic institution.

(Signature Required)

Sianne Oktaria  
24 March 2014



## ***Dedication***

*I dedicate this thesis for my mother who passed away on the 24th of September 2009 after less than a year strong fight against ovarian cancer. I love her beyond words. Always.*

# Table of Contents

List of Tables . . . . .	viii
List of Figures/Illustrations . . . . .	xvii
ABSTRACT . . . . .	xviii
Acknowledgements . . . . .	xxi
<b>1 Introduction &amp; Motivation</b>	<b>1</b>
1.1 Background . . . . .	1
1.2 Thesis Overview . . . . .	6
1.2.1 Objectives . . . . .	6
1.2.2 Aims . . . . .	6
<b>2 Literature Review</b>	<b>9</b>
2.1 Principles of Radiation Therapy and Radiation Biology . . . . .	9
2.1.1 Introduction to Radiotherapy . . . . .	9
2.1.2 Introduction to Radiobiology . . . . .	10
2.1.3 Physical Basis of Radiotherapy . . . . .	11
2.1.3.1 Ionising radiation . . . . .	11
2.1.3.2 Interaction of ionising radiation . . . . .	11
2.1.3.3 Radiation quality . . . . .	16
2.1.4 Biochemical and Biological Basis of Radiotherapy . . . . .	17
2.1.4.1 Radiation damage within the cell . . . . .	17
2.1.4.2 Relative biological effectiveness (RBE) . . . . .	20
2.1.4.3 Track structure model . . . . .	22
2.1.4.4 Dose-effect relationship . . . . .	24
2.1.5 Cellular Basis of Radiobiology: Mechanisms of Cell Killing	27
2.1.5.1 Cellular DNA target . . . . .	27
2.1.5.2 Radiation-induced damage to DNA . . . . .	31
2.1.5.3 DNA damage repair in irradiated cells . . . . .	34
2.1.5.4 Cell growth arrest . . . . .	36
2.1.5.5 Cell death . . . . .	40
2.2 Introduction to Nanotechnology and Nano-medicine . . . . .	40
2.3 Principles of Chemo-radiotherapy . . . . .	41
2.3.1 Introduction to Chemo-radiotherapy . . . . .	41
2.3.2 General Mechanism of Chemo-radiation Interaction . . . . .	42
2.3.3 Chemotherapeutic Agents . . . . .	42
2.3.3.1 Antimetabolites . . . . .	43
2.3.4 Radiosensitiser Drugs . . . . .	47

2.3.4.1	Halogenated pyrimidine . . . . .	47
2.4	Enhancement of radiation effect by high-Z elements . . . . .	49
2.4.1	Auger Effects . . . . .	50
2.4.1.1	Introduction . . . . .	50
2.4.1.2	Biological effect of radiation-induced Auger Effect . . . . .	51
<b>3</b>	<b>Materials and Methods</b>	<b>53</b>
3.1	Materials . . . . .	53
3.1.1	Cell Lines . . . . .	53
3.1.1.1	Cryopreservation . . . . .	54
3.1.2	Cell Culture Reagents . . . . .	54
3.1.3	Drugs and Other Chemicals . . . . .	54
3.1.4	Nanostructured particles . . . . .	55
3.1.4.1	Ceramic Nanoparticles . . . . .	55
3.1.4.2	X-ray Diffraction (XRD) . . . . .	55
3.1.4.3	Transmission Electron Microscopy (TEM) . . . . .	56
3.1.4.4	Sonicator . . . . .	56
3.1.5	X-rays Irradiated Machine . . . . .	56
3.1.5.1	Linear accelerator (LINAC) machine . . . . .	56
3.1.5.2	Kilovoltage (kV) orthovoltage machine . . . . .	57
3.1.6	Flow Cytometer . . . . .	59
3.1.6.1	Overview of flow cytometric instrumentation . . . . .	61
3.1.6.2	Fluorescence measurements . . . . .	65
3.1.7	Confocal Microscope . . . . .	65
3.2	Cell Culture Methods . . . . .	66
3.2.1	Subculture Cells . . . . .	66
3.2.2	Cell Counting . . . . .	67
3.2.3	Cryopreservation – Freezing and Thawing . . . . .	67
3.2.3.1	Freezing . . . . .	67
3.2.3.2	Thawing . . . . .	68
3.3	Cell Growth Assay . . . . .	69
3.3.1	9L cell line . . . . .	69
3.3.2	MCF-7 cell line . . . . .	69
3.3.3	U-87MG cell line . . . . .	70
3.3.4	MDCK cell line . . . . .	70
3.4	Cloning Efficiency of Plating . . . . .	70
3.5	Drugs Treatment and Cytotoxicity . . . . .	71
3.6	Nanoparticles Treatment and Cytotoxicity . . . . .	71
3.7	Cellular Irradiation Methods . . . . .	72
3.7.1	Chemotherapy Drugs Combination . . . . .	72
3.7.1.1	Megavoltage irradiations . . . . .	73
3.7.1.2	Kilovoltage irradiations . . . . .	74
3.7.2	Nanoparticles Combination . . . . .	74
3.7.2.1	Megavoltage irradiations . . . . .	75
3.7.2.2	Kilovoltage irradiations . . . . .	75

3.8	Clonogenic Survival Assay . . . . .	76
3.8.1	Fixing and Staining . . . . .	78
3.9	Flow Cytometric Detection . . . . .	78
3.9.1	Propidium Iodide (PI) Staining . . . . .	78
3.9.2	Cell Cycle Analysis . . . . .	79
3.9.3	Detection of Forward and Side Scatter (for Nanoparticles)	80
3.9.4	Immunofluorescence Staining of BrUdR) . . . . .	80
3.9.4.1	Detection of BrUdR & total DNA content si- multaneously . . . . .	81
3.10	Confocal Microscopy Analysis . . . . .	82
3.10.1	Detection of Intracellular Reactive Oxygen Species (ROS)	82
3.10.2	Immunofluorescence Staining of BrUdR . . . . .	83
3.11	Data Analysis and Statistics . . . . .	84
3.11.1	Cells Growth Analysis . . . . .	84
3.11.2	Plating Efficiency . . . . .	85
3.11.3	Cell Survival Analysis . . . . .	85
3.11.4	Flow Cytometric Data . . . . .	86
3.11.5	S-phase Fraction . . . . .	87
3.11.6	Statistical Analysis . . . . .	87
3.12	Sensitisation Defined . . . . .	89
3.12.1	Sensitisation Enhancement Ratio (SER) . . . . .	89
3.12.2	Protection Enhancement Ratio (PER) . . . . .	90
<b>4</b>	<b>Results &amp; Discussions</b>	<b>91</b>
4.1	Cell Line Characteristics and Protocols . . . . .	91
4.1.1	9L Cell Line . . . . .	92
4.1.1.1	Cell Age Effect on 9L Cells . . . . .	92
4.1.2	MCF-7 Cell Line . . . . .	92
4.1.3	U-87 MG Cell Line . . . . .	96
4.1.4	MDCK Cell Line . . . . .	97
4.2	Cloning Efficiency of Plating . . . . .	99
4.2.1	Conclusions . . . . .	101
4.3	Cytotoxicity Test . . . . .	102
4.3.1	Drugs Cytotoxicity Test on 9L Cells . . . . .	102
4.3.2	Ceramic Nanoparticles Cytotoxicity on 9L Cells . . . . .	104
4.3.2.1	Cerium Oxide ( $\text{CeO}_2$ ) . . . . .	106
4.3.2.2	Tantalum Pentoxide ( $\text{Ta}_2\text{O}_5$ ) . . . . .	106
4.3.2.3	Bismuth Oxide ( $\text{Bi}_2\text{O}_3$ ) . . . . .	107
4.3.3	Fluorodex Cytotoxicity Test on 9L Cells . . . . .	108
4.3.4	Conclusions . . . . .	109
4.4	Experimental Dose Rate of LINAC . . . . .	112
4.4.1	Background . . . . .	112
4.4.2	Results . . . . .	115
4.4.2.1	Determination of the dose-rate effect of the MV X-ray beams on clonogenic cell survival . . . . .	116

4.4.2.2	To explore the general applicability of the high-dose rate MV X-ray induce enhancement of clonogenic killing to cancer cells . . . . .	116
4.4.2.3	Cell cycle analysis . . . . .	119
4.4.3	Discussions . . . . .	121
4.4.4	Conclusions . . . . .	125
4.5	Utilisation of Nanoparticles . . . . .	127
4.5.1	Introduction . . . . .	127
4.5.2	Results – Cerium Oxide ( $\text{CeO}_2$ ) . . . . .	128
4.5.2.1	Phase and structural characterisation of $\text{CeO}_2$ .	128
4.5.2.2	Internalisation determination of $\text{CeO}_2$ . . . . .	129
4.5.2.3	Efficacy of $\text{CeO}_2$ nanoparticles – influence of different X-ray beams . . . . .	130
4.5.3	Results – Tantalum Pentoxide ( $\text{Ta}_2\text{O}_5$ ) . . . . .	135
4.5.3.1	Phase and structural characterisation of $\text{Ta}_2\text{O}_5$ .	135
4.5.3.2	Internalisation determination of $\text{Ta}_2\text{O}_5$ . . . . .	135
4.5.3.3	Efficacy of $\text{Ta}_2\text{O}_5$ nanoparticles – influence of different X-ray beams . . . . .	137
4.5.4	Results – Bismuth Oxide ( $\text{Bi}_2\text{O}_3$ ) . . . . .	143
4.5.4.1	Phase and structural characterisation of $\text{Bi}_2\text{O}_3$ .	143
4.5.4.2	Internalisation of $\text{Bi}_2\text{O}_3$ . . . . .	144
4.5.5	Discussion . . . . .	146
4.5.5.1	Cerium Oxide ( $\text{CeO}_2$ ) . . . . .	146
4.5.5.2	Tantalum pentoxide ( $\text{Ta}_2\text{O}_5$ ) and bismuth oxide ( $\text{Bi}_2\text{O}_3$ ) . . . . .	148
4.5.6	Conclusions . . . . .	150
4.6	Chemo-Auger Approach Part 1 . . . . .	152
4.6.1	Background . . . . .	152
4.6.2	Brief History of BrUdR Usage . . . . .	154
4.6.3	Results . . . . .	157
4.6.3.1	Radiosensitisation of BrUdR on 9L cells with X-rays energy of 125 kVp . . . . .	157
4.6.3.2	Radiosensitisation of methotrexate on 9L cells with X-rays energy of 125 kVp . . . . .	157
4.6.3.3	Influence of methotrexate on radiosensitising effect of BrUdR . . . . .	160
4.6.3.4	Cell cycle analysis and quantification of BrUdR incorporation into DNA simultaneously . . . . .	163
4.6.4	Discussion . . . . .	165
4.6.5	Conclusions . . . . .	172
4.7	Chemo-Auger Approach Part 2 . . . . .	173
4.7.1	Background . . . . .	173
4.7.2	Results . . . . .	174
4.7.2.1	Radiosensitisation of BrUdR + MTX on 9L cells with 50 kVp X-rays beam . . . . .	174

4.7.2.2	Radiosensitisation of BrUdR + MTX on 9L cells with 250 kVp X-rays beam . . . . .	176
4.7.2.3	Radiosensitisation of BrUdR + MTX on 9L cells with 6 MV X-rays beam . . . . .	176
4.7.2.4	Radiosensitisation of BrUdR + MTX on 9L cells with 10 MV X-rays beam . . . . .	176
4.7.2.5	Correlation between the physical X-rays beam energies and enhancement of radio sensitisation effect of BrUdR combined with MTX . . . . .	180
4.7.3	Discussions . . . . .	183
4.7.4	Conclusions . . . . .	188
4.8	Groundwork for Confocal Microscopy . . . . .	190
4.8.1	Reactive Oxygen Species Production in 9L Cells After a 24 Hour Incubation Period with Ta <sub>2</sub> O <sub>5</sub> Nanoparticles . .	190
4.8.2	BrUdR as a Radiosensitiser Drug that is Specifically Incorporated into DNA in 9L Cells . . . . .	192
4.8.3	Conclusions . . . . .	194
<b>5</b>	<b>Conclusions and Future Directions</b>	<b>195</b>
<b>A</b>	<b>Cell Line Information</b>	<b>199</b>
A.1	9L Cell Line . . . . .	200
A.2	MCF-7 Cell Line . . . . .	201
A.3	U-87 MG Cell Line . . . . .	202
A.4	MDCK Cell Line . . . . .	203
<b>B</b>	<b>Subculture Adherent Cells – Protocol</b>	<b>205</b>
B.1	Subculture Adherent Cells – Protocol . . . . .	206
<b>C</b>	<b>Cells Counting – Protocol</b>	<b>208</b>
C.1	Cells Counting – Protocol . . . . .	209
<b>D</b>	<b>Cryopreservation – Protocol</b>	<b>211</b>
D.1	Freezing Protocol . . . . .	212
D.2	Thawing Protocol . . . . .	215
<b>E</b>	<b>Cells Growth Assay – Protocol</b>	<b>217</b>
E.1	9L Cell Line . . . . .	218
E.2	MCF-7 Cell Line . . . . .	220
E.3	U-87 MG Cell Line . . . . .	222
E.4	MDCK Cell Line . . . . .	224
<b>F</b>	<b>Drugs Treatment and Cytotoxicity – Protocol</b>	<b>226</b>
F.1	Drugs Treatment and Cytotoxicity – Protocol . . . . .	227
<b>G</b>	<b>Nanoparticles Treatment and Cytotoxicity – Protocol</b>	<b>235</b>
G.1	Nanoparticles Treatment and Cytotoxicity – Protocol . . . . .	236

<b>H</b>	<b>Complete Procedure of X-rays Irradiation Experiments</b>	<b>240</b>
H.1	Experimental dose rate on LINAC . . . . .	241
H.2	Chemotherapy Drugs Combination . . . . .	245
H.3	Nanoparticles Combination . . . . .	247
<b>I</b>	<b>Flow Cytometric Detection</b>	<b>250</b>
I.1	Cell Cycle Analysis . . . . .	251
I.2	Immunocytochemical Protocol . . . . .	254
<b>J</b>	<b>List of Abbreviations</b>	<b>258</b>
<b>K</b>	<b>List of Publications and Conference Abstracts</b>	<b>264</b>
	<b>References</b>	<b>299</b>

# List of Tables

3.1	Summary of orthovoltage beams used in this study at the POWH.	57
4.1	Cell viability of control (untreated cells) of 9L cells and of treated cells with drugs for two doubling times . . . . .	103
4.2	Summary of cell survival parameters . . . . .	119
4.3	Summary of cell cycle distribution of unirradiated confluent cell populations . . . . .	121
4.4	Values of the linear-quadratic model parameters $\alpha$ and $\beta$ from 9L cells treated with ionising radiation only and combined CeO <sub>2</sub> NP plus radiation survival curves at energies 150 kVp, 6 MV, and 10 MV. XIR = radiation only; CeO <sub>2</sub> NP = cerium oxide nanoparticles (50 $\mu$ g/ml). . . . .	133
4.5	Values of the linear-quadratic model parameters $\alpha$ and $\beta$ from 9L cells treated with ionising radiation only and combined Ta <sub>2</sub> O <sub>5</sub> NP plus radiation survival curves at energies 150 kVp, 6 MV, and 10 MV. XIR = radiation only; Ta <sub>2</sub> O <sub>5</sub> NP = tantalum pentoxide nanoparticles (50 $\mu$ g/ml). N/A = Not applicable. . . . .	143
4.6	Values of the linear-quadratic model parameters $\alpha$ and $\beta$ , the $\alpha/\beta$ ratio, and SER <sub>10</sub> from 9L cells treated with ionising radiation only and MTX/BrUdR-sensitised radiation dose survival curves at energies of 125 kVp. XIR = radiation only; MTX = methotrexate (0.01 $\mu$ M) and BrUdR = bromodeoxyuridine (10 $\mu$ M); N/A = not applicable; SER <sub>10</sub> - sensitisation enhancement ratio at 10% surviving fraction. . . . .	163
4.7	Values of the linear-quadratic model parameters $\alpha$ and $\beta$ , the $\alpha/\beta$ ratio, and SER <sub>10</sub> from 9L cells treated with ionising radiation only and MTX/BrUdR-sensitised radiation dose survival curves of different energies. XIR = radiation only; DRUGS = MTX (0.01 $\mu$ M) and BrUdR (10 $\mu$ M) combination; N/A = not applicable; SER <sub>10</sub> = sensitisation enhancement ratio at 10% surviving fraction. . . . .	180
F.1	summarised of drugs concentration for cytotoxicity test on 9L cells . . . . .	229
F.2	Template for the cytotoxicity test of drugs and clonogenic assays on 01/04/11 . . . . .	234



G.1	An example of template for the cytotoxicity test and clonogenic assay of nanoparticles on 9L cells . . . . .	238
H.1	A representative of summarised of X-rays irradiation of 9L cells for clonogenic assay. The number of cell densities used are different depend on the energy of X-rays and the cell line . . . . .	244
H.2	A representative of summarised of kVp X-rays irradiation of 9L cells for clonogenic assay. The number of cell densities used are different depend on the energy of X-rays used . . . . .	246
H.3	A representative of summarised of kVp X-rays irradiation of 9L cells for clonogenic assay. The number of cell densities used are different depend on the energy of X-rays and single/combination of drugs used . . . . .	246

# List of Figures

1.1	Schematic diagram of increased lethal DNA damage by the combination of drugs and radiation in general (upper) modified from [Seiwert et al., 2007] and in this study (lower) as the increased DNA damage by the presence of drugs (i.e BrUdR and MTX) combined to radiation. Blue dots, red dots, and green square represents platinating agents (cisplatin), methotrexate/5-FU, and the high-Z agents (BrUdR/IUdR), respectively. . . . .	3
2.1	Time scale of events initiated by ionising radiation deposition in biological systems BIM biologically important molecule [Mitchell et al., 2000]. . . . .	12
2.2	Schematic diagram of the photoelectric effect and other processes that can occur as a result of the photoelectric effect (characteristic X-ray and Auger electron production). . . . .	14
2.3	Schematic diagram of the Compton effect. . . . .	15
2.4	Schematic diagram of pair production ( $h\nu$ is greater than 1.02 MeV). . . . .	15
2.5	Distribution of excitations and ionisations along particle tracks in water [Feinendegen, 1990]. . . . .	18
2.6	Direct and indirect mechanism of DNA damage by X-rays irradiation (on upper part) [Powsner and Powsner, 2006]. . . . .	21
2.7	Illustration of RBE against LET [Hall and Giaccia, 2012]. . . . .	22
2.8	Typical example of strand breakage (solid symbol) as well as base damage (open symbol)[Goodhead, 2006]. . . . .	23
2.9	Schematic representation of DNA segment with randomly selected simulated track from low-energy electron (upper) and short $\alpha$ -particle track (lower). Large and small dots are represent ionisations and excitations, respectively [Goodhead, 1994].	24
2.10	The classic linear-quadratic model as a result of the summation components of the equation (2.7): linear ( $\log S = -\alpha D$ ) and quadratic term ( $\log S = -\beta D^2$ ) [Suntharalingam et al., 2005]. . .	26
2.11	The interpretation of survival curves based on intracellular repair model [Tubiana et al., 1990]. . . . .	27
2.12	DNA within the nucleus of the cell in the chromosomes [of General Medical Science, 2006]. . . . .	28
2.13	Nucleotides as the building block of DNA. . . . .	29

2.14	Complementary base pairing predominate in DNA [Nelson and Cox, 2005]. . . . .	29
2.15	Molecular structure of DNA. a) Three-dimensional structure of DNA prepared by Watson and Crick. b) Stylised diagram of the DNA double helix [Russell, 2006]. . . . .	30
2.16	Organisation of DNA package [Wouters and Begg, 2009]. . . . .	31
2.17	Low and high LET traversing a section of the DNA helix [Powsner and Powsner, 2006]. . . . .	33
2.18	Repair mechanism of DNA double-strand break [Norbury and Hickson, 2001]. . . . .	35
2.19	Schematic model of cell cycle phase as well as the contributions of homologous recombination (HR) and non-homologous end joining (NHEJ) of ionising radiation IR-induced DSB [Rothkamm et al., 2003]. . . . .	37
2.20	Stages of a standard eukaryotic cell cycle. . . . .	38
2.21	Radiosensitivity depends on the cell cycle [Suntharalingam et al., 2005]. . . . .	39
2.22	Cell survival curves at various stages of the cell cycle. . . . .	39
2.23	Chemical structure of the antifolate MTX [Hatse et al., 1999] . . . .	44
2.24	Chemical structure of the 5-fluorouracil [Hatse et al., 1999] . . . .	45
2.25	Schematic diagram of mechanisms of methotrexate (MTX) and 5-fluorouracil (5-FU) on thymidilate cycle. DHFR= dihydrofolate reductase; TS= thymidilate synthase; FH <sub>4</sub> = tetrahydrofolate; FH <sub>2</sub> = dihydrofolate; CH <sub>2</sub> FH <sub>4</sub> = 5,10-methylene tetrahydrofolate; dUMP= deoxyuridine monophosphate; dTMP= deoxythymidine monophosphate. . . . .	46
2.26	Chemical structure of thymidine and their analogs (BrUdR and IUdR), with Van der Waals radii of atoms at 5-position represent in the circles (modified from McGinn and Kinsella [1993]). . . . .	48
2.27	Chemical structure of bromodeoxyuridine (BrUdR). . . . .	48
2.28	Schematic diagram of the target for radiosensitiser drugs. dUMP= deoxyuridine monophosphate; dTMP= deoxythymidine monophosphate; TS= thymidilate synthase; dATP= deoxyadenosine triphosphate; dTTP= deoxythymidine triphosphate; dGTP= deoxyguanosine triphosphate; dCTP= deoxycytidine triphosphate. . . . .	49
3.1	Ratio of the mass energy absorption coefficient of bromine to water relative to photon energy (MeV). . . . .	58
3.2	The output spectrum emitted from the orthovoltage X-ray unit at 50 kVp (filter 1) at the POWH. . . . .	59
3.3	The output spectrum emitted from the orthovoltage X-ray unit at 125 kVp (filter 4) at the POWH. . . . .	60
3.4	The output spectrum emitted from the orthovoltage X-ray unit at 150 kVp (filter 5) at the POWH. . . . .	60

3.5	The output spectrum emitted from the orthovoltage X-ray unit at 250 kVp (filter 7) at the POWH. . . . .	61
3.6	Becton Dickinson fluorescence-activated cell sorting (FACS) flow cytometer (BD LSR II; BD Biosciences, USA) at IHMRI, Wollongong, Australia. . . . .	62
3.7	Flow chamber of a flow cytometer (longitudinal cross-sectional view) [Dean and Hoffman, 2007]. In this work, FACS LSR II from BD [BD, 2007] . . . . .	63
3.8	Forward scatter (FSC) and side scatter (SSC) [BD, 2000, 2007] .	63
3.9	Schematic of flow cytometer systems . . . . .	65
3.10	Leica confocal laser scanning microscope (Leica TCS SP5 Advanced System – UV-VIS-IR and X1-Port Access with SMD FCS and CO <sub>2</sub> incubation chamber, Germany at IHMRI. . . . .	66
3.11	Set up of sonication procedure using the Branson Sonifier® S-250D digital with double-stepMicro-tip (Consonic Pty Ltd., NSW, Australia). . . . .	72
3.12	Schematic diagram of experimental setup for cellular irradiation (MV with or without drugs). . . . .	73
3.13	Photograph of experimental setup for cellular irradiation (with or without drugs). . . . .	74
3.14	Photograph of experimental setup for cellular irradiation (MV with or without nanoparticles). . . . .	75
3.15	Example of photograph of cells plated immediately after the irradiation (approximately of 120 plates for each set of single experiment). The assays of all irradiations treatment conditions (with or without drugs/NPs treated) were performed at least three times independently, unless otherwise specified. . . . .	77
3.16	Photograph of fix and staining the cells. . . . .	78
3.17	Example of photograph of the stained plates. . . . .	79
3.18	Direct (A) vs. indirect (B) immunofluorescence staining. . . . .	81
3.19	Cells grown onto <sup>TM</sup> Lab-Tek <sup>TM</sup> II Chamber Slide <sup>TM</sup> System 4 wells (growth area = 1.8cm <sup>2</sup> ) (Thermo-Scientific). . . . .	83
3.20	Schematic diagram of cell culture technique (i.e clonogenic assay) to produce a cell survival curve. . . . .	86
3.21	A representative typical data analysed on BD LSR II flow cytometer and an illustration of gating using FlowJo software (from 9L cells stained with PI). (a) Dot plot (or cytogram) which showing forward scatter (FSC) versus side-scatter (SSC). (b) Histogram plot which showing positive population of cells (ungated). (c) Dot plot, which was gated shown as 74% cells (singlets). (d) Histogram which showing gated on singlet cells only. . . . .	88
3.22	A schematic diagram of cell cycle, showing flow cytometric components of each phase (www.phoenixflow.com). . . . .	89

4.1	Analysis of exponential growth of 9L cells (passage 47). The assay was performed three times, and a representative result is shown. Experimental points are shown, along with exponential fit describe in methods section (Eq 3.2). Bars are $\pm$ one standard deviation. . . . .	93
4.2	Analysis of exponential growth of 9L cells passage 54 (new) vs. passage 89 (old). Experimental points are shown, along with exponential fit describe in methods section (Eq 3.2). Bars are $\pm$ one standard deviation (error bars are too small). . . . .	94
4.3	Analysis of exponential growth of MCF-7 cells in DMEM vs. RPMI-1640. Experimental points are shown, along with exponential fit describe in methods section (Eq 3.2). Bars are $\pm$ one standard deviation. . . . .	95
4.4	Analysis of exponential growth of U-87MG cells. Experimental points are shown, along with exponential fit describe in methods section (Eq 3.2). Bars are $\pm$ one standard deviation. . . . .	96
4.5	Analysis of exponential growth of MDCK cells. Experimental points are shown, along with exponential fit describe in methods section (Eq 3.2). Bars are $\pm$ one standard deviation. . . . .	98
4.6	Photograph of colonies of unirradiated MCF-7 cells. Plating efficiency of cells densities of 200, 500, 1000 and 1500cells/plate are shown. . . . .	99
4.7	Plating efficiency of 9L, MCF-7, U-87 MG, and MDCK cells. Bars are $\pm$ one standard deviation. . . . .	100
4.8	Drugs cytotoxicity test at the concentration of $0.1 - 10\mu\text{M}$ on 9L cells. F = 5-fluorouracil; B = bromodeoxyuridine; M = methotrexate. Bars are $\pm$ one standard deviation. . . . .	105
4.9	The surviving fraction of 9L cells exposed to cerium oxide ( $\text{CeO}_2$ ) and tantalum pentoxide ( $\text{Ta}_2\text{O}_5$ ) nanoparticles following a 24 hour exposure at a concentration of $50\mu\text{g/ml}$ . The toxicity was measured using the clonogenic survival assay. Bars are $\pm$ one standard deviation. . . . .	106
4.10	Comparison of cytotoxicity tests of $\text{Bi}_2\text{O}_3$ (air vs. argon techniques) as the number of clonogenic survival of unirradiated 9L and MDCK cells at the concentration of $50\mu\text{g/ml}$ . Bars are $\pm$ one standard deviation. . . . .	108
4.11	Comparison of cytotoxicity test of 5-FU (to allow for comparison) and fluorodex on 9L cells at the concentration of $0.01 - 0.1\mu\text{M}$ of fluorodex and the combination with $10\mu\text{M}$ BrUdR. Bars are $\pm$ one standard deviation. . . . .	109
4.12	Comparison of cytotoxicity test of fluorodex on MDCK cells at the concentration of $0.005 - 0.05\mu\text{M}$ . Bars are $\pm$ one standard deviation. . . . .	110

4.13	Radiation survival curves of 9L cells irradiated at dose rate of 0.5 Gy/min vs. dose rate 5 Gy/min. The data were fitted to the linear quadratic model. Each data point represents the means $\pm$ standard deviation of three independent experiments. . . . .	117
4.14	Survival curves of MCF-7 cells irradiated at dose rate of 0.5 Gy/min vs. dose rate 5 Gy/min. The data were fitted to the linear quadratic model. Each data point represents the means $\pm$ standard deviation of three independent experiments. 8 Gy data point is not included as they are too sensitive – number of colonies obtained were less than 50. . . . .	118
4.15	Survival curves of 9L and MCF-7 irradiated at a dose-rate of 5 Gy/min. The data were fitted to the LQ model. Each data point represents the means $\pm$ standard deviation of three independent experiments. 8 Gy data point is not included in MCF-7 as the cells are too sensitive – number of colonies obtained were less than 50 . . . . .	120
4.16	Schematic representation of high-Z secondary radiation mechanism (also known as indirect radiation therapy, IRT) [Nawroth et al., 2008] . . . . .	128
4.17	(A) XRD spectrum and (B) high resolution TEM of the CeO <sub>2</sub> NP sample synthesised by spray pyrolysis with size between 6-8 nm. Data was acquired using an automated GBC @eMMA X-ray Diffractometer. X-ray diffraction peaks were assigned Miller indices in correlation with the ICSD Briggs et al. [2013]. . . . .	129
4.18	Flow cytometric analysis of forward scatter (FSC) and side scatter (SSC) of 9L cells incubated for 24 hours with 50 $\mu$ g/ml cerium oxide (CeO <sub>2</sub> ) (right) and its control of untreated cells (left). . . . .	130
4.19	Ratio of the mass energy absorption coefficient of CeO <sub>2</sub> to water relative to photon energy (MeV) [Briggs, 2011]. . . . .	131
4.20	Radiation dose-survival curves of confluent cultures of 9L cells after irradiation with 150 kVp photon beam at a dose rate of approximately 75 MU/min, with or without 50 $\mu$ g/ml cerium oxide (CeO <sub>2</sub> ) treatment for 24 hours using T12.5 cm <sup>2</sup> flask with a 6 mm depth of medium. Each data point represents the means $\pm$ standard deviation of three independent experiments. Experimental results modified from Briggs et al. [2013]. . . . .	132
4.21	Radiation dose-survival curves of confluent cultures of 9L cells after irradiation with a 6 MV photon beam at a dose rate of 5 Gy/min, with or without 50 $\mu$ g/ml cerium oxide (CeO <sub>2</sub> ) treatment for 24 hours using T12.5 cm <sup>2</sup> flask filled with HBSS. Each data point represents the means $\pm$ standard deviation of three independent experiments. Experimental results modified from Briggs [2011]. . . . .	134

4.22	Radiation dose-survival curves of confluent cultures of 9L cells after irradiation with a 10 MV photon beam at a dose rate of 5 Gy/min, with or without 50 $\mu\text{g}/\text{ml}$ cerium oxide ( $\text{CeO}_2$ ) treatment for 24 hours using T12.5 $\text{cm}^2$ flask filled with HBSS. Each data point represents the means $\pm$ standard deviation of three independent experiments. Experimental results modified from Briggs et al. [2013]. . . . .	136
4.23	(A) XRD spectrum and (B) high resolution TEM of the $\text{Ta}_2\text{O}_5$ NP sample. Data was acquired using an automated GBC®eMMA X-ray Diffractometer. X-ray diffraction peaks were assigned Miller indices in correlation with the ICSD [Brown et al., 2013].	137
4.24	Flow cytometric analysis of forward scatter (FSC) and side scatter (SSC) of 9L cells incubated for 24 hours with 50 $\mu\text{g}/\text{ml}$ tantalum pentoxide ( $\text{Ta}_2\text{O}_5$ ) (right) and its control of untreated cells (left). . . . .	138
4.25	Ratio of the mass energy absorption coefficient of $\text{Ta}_2\text{O}_5$ to water relative to photon energy [Brown, 2011]. . . . .	138
4.26	Radiation dose-survival curves of confluent cultures of 9L cells after irradiation with 150 kVp photon beam at a dose rate of approximately 75 MU/min, with or without 50 $\mu\text{g}/\text{ml}$ tantalum pentoxide ( $\text{Ta}_2\text{O}_5$ ) treatment for 24 hours using T12.5 $\text{cm}^2$ flask with a 6 mm depth of medium. Each data point represents the means $\pm$ standard deviation of three independent experiments. Experimental results modified from [Brown et al., 2013]. . . . .	140
4.27	Radiation dose-survival curves of confluent cultures of 9L cells after irradiation with a 6 MV photon beam at a dose rate of 5 Gy/min, with or without 50 $\mu\text{g}/\text{ml}$ tantalum pentoxide ( $\text{Ta}_2\text{O}_5$ ) for 24 hours using T12.5 $\text{cm}^2$ flask filled with HBSS. Each data point represents the means $\pm$ standard deviation of three independent experiments. Experimental results modified from [Brown et al., 2013]. . . . .	141
4.28	Radiation dose-survival curves of confluent cultures of 9L cells after irradiation with a 10 MV photon beam at a dose rate of 5 Gy/min, with or without 50 $\mu\text{g}/\text{ml}$ tantalum pentoxide ( $\text{Ta}_2\text{O}_5$ ) for 24 hours using T12.5 $\text{cm}^2$ flask filled with HBSS. Each data point represents the means $\pm$ standard deviation of three independent experiments. Experimental results modified from [Brown et al., 2013]. . . . .	142
4.29	XRD spectrum of $\text{Bi}_2\text{O}_3$ NP via precipitate in argon and air annealed; high resolution TEM (insert). Data was acquired using an automated GBC®eMMA X-ray Diffractometer. X-ray diffraction peaks were assigned Miller indices in correlation with the ICSD [Stewart et al., 2014]. . . . .	144
4.30	TEM image of $\text{Bi}_2\text{O}_3$ [Stewart, 2012]. . . . .	145

4.31	Flow cytometric analysis of forward scatter (FSC) and side scatter (SSC) of 9L cells incubated for 24 hours with 50 $\mu\text{g/ml}$ bismuth oxide ( $\text{Bi}_2\text{O}_3$ ) (right) and its control of untreated cells (left).	145
4.32	Radiation dose-survival curves of confluent cultures of 9L cells after irradiation at energies of 125kVp, with and without exposure to 10 $\mu\text{M}$ BrUdR for 72 hours. Normalised of data for BrUdR-treated cells was done with unirradiated, BrUdR-treated cells sample. Each data point represents the means $\pm$ standard deviation ( $\pm\text{SD}$ ) of at least three independent experiments.	158
4.33	Radiation dose-survival curves of confluent cultures of 9L cells after irradiation, at energies of 125 kVp, with or without 0.01 $\mu\text{M}$ MTX treatment for 72 hours. Normalised of data for MTX-treated cells was done with unirradiated, MTX-treated cells sample. Each data point represents the means ( $\pm\text{SD}$ ) of at least three independent experiments.	159
4.34	Radiation dose-survival curves of confluent cultures of 9L cells after irradiation at energies of 125 kVp, with or without drugs combination (0.01 $\mu\text{M}$ MTX and 10 $\mu\text{M}$ BrUdR) treatment for 72 hours. Normalised of data for drugs-treated cells was done with unirradiated, drugs-treated cells sample. Each data point represents the means ( $\pm\text{SD}$ ) of at least three independent experiments.	161
4.35	Radiation dose-survival curves of confluent cultures of 9L cells after irradiation at energies of 125 kVp, with or without drugs (0.01 $\mu\text{M}$ MTX and/or 10 $\mu\text{M}$ BrUdR) treatment for 72 hours. Each data point represents the means ( $\pm\text{SD}$ ) of at least three independent experiments.	162
4.36	Representative of single parametric DNA diagrams of 9L cells stained with PI – gated shown represents each cell phase. DNA histogram were analysed with the FlowJo for Mac software.	164
4.37	Single parametric DNA diagrams of 9L cells stained with PI. Measurements were performed on a FACS LSR II flow cytometer after 72 h without drugs/irradiation (control) (a), 0.01 $\mu\text{M}$ MTX (b), 10 $\mu\text{M}$ BrUdR (c), 0.01 $\mu\text{M}$ MTX +10 $\mu\text{M}$ BrUdR (d), and 0.01 $\mu\text{M}$ MTX +10 $\mu\text{M}$ BrUdR combined with 5Gy X-rays radiation of 125 kVp (e). DNA histograms were analysed with the FlowJo for Mac software. The assay was performed at least three times, a representative example is shown.	166



4.38	Dot plots of bivariate DNA/BrUdR distributions of 9L cells. Measurements were performed on a FACS LSR II flow cytometer after 72 h without drugs/irradiation (control) ( <b>a</b> ), 10 $\mu$ M BrUdR ( <b>b</b> ), 0.01 $\mu$ M MTX +10 $\mu$ M BrUdR ( <b>c</b> ). Total DNA content (red fluorescence – 575/26-A) versus amount of incorporated BrUdR (green fluorescence – 515/20-A) shown on the x-axis and y-axis, respectively. DNA histograms were analysed with the FlowJo for Mac software. The assay was performed at least three times, a representative example is shown. . . . .	167
4.39	Radiation dose-survival curves of confluent cultures of 9L cells after irradiation at energies of 50 kVp, with or without drugs combination (0.01 $\mu$ M MTX and 10 $\mu$ M BrUdR) treatment for 72 hours. Each data point represents the means $\pm$ standard deviation of at least two independent experiments. . . . .	175
4.40	Radiation dose-survival curves of confluent cultures of 9L cells after irradiation at energies of 250 kVp, with or without drugs combination (0.01 $\mu$ M MTX and 10 $\mu$ M BrUdR) treatment for 72 hours. Each data point represents the means $\pm$ standard deviation of at least two independent experiments. . . . .	177
4.41	Radiation dose-survival curves of confluent cultures of 9L cells after irradiation at energies of 6 MV, with or without drugs combination (0.01 $\mu$ M MTX and 10 $\mu$ M BrUdR) treatment for 72 hours. Each data point represents the means $\pm$ standard deviation of at least two independent experiments. . . . .	178
4.42	Radiation dose-survival curves of confluent cultures of 9L cells after irradiation at energies of 10 MV, with or without drugs combination (0.01 $\mu$ M MTX and 10 $\mu$ M BrUdR) treatment for 72 hours. Each data point represents the means $\pm$ standard deviation of at least two independent experiments. . . . .	179
4.43	The effect of BrUdR plus MTX on 9L cells after irradiation with different energies of radiation analysed with LQ model (Eq.2.6). Each data point represents the means standard deviation of at least two independent experiments are shown. Control represents as the average of the irradiated controls from all different energies without drugs treated. . . . .	181
4.44	Sensitisation enhancement ratio at 10% surviving fraction ( $SER_{10}$ ) in function of radiation energies. . . . .	182
4.45	The effect of drugs on 9L cells after irradiation with energies of 50, 125, and 250 kVp at dose of 5 Gy. MTX = methotrexate (0.01 $\mu$ M); Br = bromodeoxyuridine (10 $\mu$ M). . . . .	183

4.46	Microphotograph of intracellular ROS induced by Ta <sub>2</sub> O <sub>5</sub> nanoparticles in 9L cells detected with DCFD dye and counterstained with PI. (A) Untreated cells (control). (B) Cells were treated with 50 $\mu$ g/ml of Ta <sub>2</sub> O <sub>5</sub> nanoparticles for 24 hours. All the chamber slides were analysed for fluorescence with a 488 nm excitation laser on a Leica confocal laser scanning microscope and the images were captured using the same parameters to allow comparison. Overlay image corresponding to the fluorescence of intracellular PI and DCFD fluorescence image. . . . .	191
4.47	Exposure of 9L cells to Ta <sub>2</sub> O <sub>5</sub> nanoparticles (50 $\mu$ g/ml) for 24 hours, results in uptake of agglomerates surround the cell nucleus (black dots) (on left) and the magnification (on right). Light microscopy images were obtained using a Leica confocal laser scanning microscope. . . . .	192
4.48	Microphotograph of intracellular 5-bromo-2'-deoxyuridine (BrUdR) in 9L cells. (A) Cells with no treatment was used as negative control. (B) Treatment of cells with 0.01 $\mu$ M of MTX was used as positive control. (C) Cells treated with 10 $\mu$ M BrUdR. Detection of BrUdR by direct fluorescent microscopy after 30 mins incubation with fluorescently labeled anti-BrUdR antibody (MoBU-1) (green signal) and cell nuclei labeled with PI (red signal). All the chamber slides were analysed for fluorescence with a 488 nm excitation laser on a Leica confocal laser scanning microscope and the images were captured using the same parameters to allow comparison. Overlay image corresponding to the fluorescence of intracellular PI and MoBU-1 fluorescence image. . . . .	193
C.1	A typical hemocytometer . . . . .	210
C.2	Counting chamber of a hemocytometer . . . . .	210
D.1	Schematic diagram of master and working stocks of cells (e.g. U-87 MG cells) . . . . .	214
H.1	Schematic diagram of cell culture technique (i.e clonogenic assay).243	

ADVANCES IN TARGETED RADIOSENSITISER AND  
NANOTHERAPEUTIC AGENTS FOR CANCER THERAPY

Sianne Oktaria

A Thesis for **Doctor of Philosophy**

School of Physics

University of Wollongong

## ABSTRACT

Although the treatment of cancer continues to improve, the treatment of high-grade gliomas remains a major challenge; current treatments are palliative rather than curative. This is despite a variety of multimodal treatments options including surgery, chemotherapy and radiotherapy. The median survival for patients with glioblastoma multiforme is less than one year after diagnosis and generally no patients survive five years post treatment.

The hypothesis underlying the work presented in this thesis is that local tumour control can be improved by exploiting elements with a high atomic number ( $Z$ ) so as to increase the energy deposited in the tumour cells. The main aim is to use *in vitro* experiments to better understand, and consequently optimise, the role of the high- $Z$  element for combination with chemo-radiotherapy and dose enhancement radiotherapy. This work goes part of the way to prove that combination chemo-radiotherapy can lead to outcomes that are more than simply additive and that high-atomic number nanostructured particles can be customised for radiotherapy to increase radiation-induced effects for the very radioresistant 9L cancer cells.

In preliminary studies carried out to develop and test all cell related protocols an interesting and unexpected result was observed in *in vitro* experiments that investigated the response of two asynchronous cancer cell lines, 9L (rat gliosarcoma) and MCF-7 (human breast carcinoma), exposed to 10 MV X-ray radiation at dose-rates of 0.5 Gy/min and 5 Gy/min. Namely that although the 9L cells did not demonstrate any noticeable dose-rate effect, the radiosensitive cell line MCF-7 exhibited an inverse dose-rate effect. The different efficacy of the treatments was measure quantitatively by a significant increase of 20% in the absorbed radiation dose necessary in the 5 Gy/min experiment to deliver the same 10% cell-surviving fraction as in the 0.5 Gy/min experiment.

A second strand of experiments investigated the effect of ceramic nanoparticles (NPs) containing high atomic number elements on the radiation response of 9L cells *in vitro*. The NPs investigated were cerium oxide ( $\text{CeO}_2$ ), tantalum pentoxide ( $\text{Ta}_2\text{O}_5$ ), and bismuth oxide ( $\text{Bi}_2\text{O}_3$ ). I developed the cell culture protocols, investigated cytotoxicity, performed experiments using flow cytometry to determine internalisation of the NPs inside the cells and used confocal microscopy to investigate the effect of NPs upon reactive oxygen species (ROS) production.

The bulk of the research carried out for this thesis involved an investigation into the effectiveness of concurrent chemo-radiotherapy (using BrUdR and MTX drugs) in an attempt to reduce the radioresistivity of 9L cells. *In vitro* experiments were performed by analysing cell cultures irradiated with common radiation radiotherapy modalities, a conventional orthovoltage x-ray unit and a LINAC in the radiotherapy clinic at the Prince of Wales Hospital, Sydney.

Results of the clonogenic assay show that the surviving fraction of 9L cells was

significantly reduced when BrUdR and MTX drugs were combined together with photon irradiation, compared to the cases of irradiation alone or either drug and irradiation. Cells irradiated in a 125 kVp X-ray field showed the greatest sensitisation enhancement ratio (SER) value of 2.3 compared to all other energies investigated (50 kVp, 250 kVp, 6MV, or 10MV). These results support not only the feasibility of chemotherapy drug-enhanced radiotherapy through the improved biological effectiveness of the X-ray irradiation but also validate the application of chemo-radiotherapy in conventional X-ray radiotherapy modality fields.

The ability of high atomic number elements to act as radiosensitising components has been demonstrated. The results presented in this thesis may have future application in radiotherapy to increase the biological effectiveness of such treatment and consequently to improve local tumour control. Finally, although the use of nanoparticles enhances the biological effect of irradiation halogenated pyrimidine is a more effective radiosensitiser due to its ability to be incorporated into the DNA of dividing cells.

This Ph.D. thesis is the first from the newly created Targeted Nano-Therapies (TNT) Team at the University of Wollongong, which is a multidisciplinary research team that brings together Medical Physicists, Materials Engineers, Chemists, Biologists and Clinicians to improve the outcomes of cancer treatment.

**KEYWORDS:** radiosensitiser, high-Z, bromodeoxyuridine, methotrexate, nanoparticles, *in vitro*, conventional X-rays.

# Acknowledgements

I am sincerely grateful to my supervisory committee, Prof. Anatoly Rosenfeld, A/Prof. Michael Lerch, Dr. Stéphanie Corde and Dr. Moeava Tehei for their continued support and encouragement throughout my PhD journeys for the past three years. They have all provided me with extensive personal and professional guidance and have always been shared their experience in their respective areas of expertise. Their knowledge, criticism and encouragements were invaluable for the completion of this research project. Thank you for belief in me. I couldnt have done it without you!

I am truly grateful to Prof. Rosenfeld for directing me to this fascinating project and introducing me to the radiobiology field. He has always been interested in my studies since my Bachelor degree in Biological Science at the University of Wollongong in 2005 and I feel privileged to have been taught by him. I would especially like to thank A/Prof. Lerch for his excellent assistance, as well as many useful discussions and helpful advice throughout my studies. I would like to sincerely thank Dr. Moeava Tehei and Dr. Stéphanie Corde Tehei. This project was their brainchild, but they trust me to work throughout on it to what I hope they consider a success. Special thank you also to Stéphanie for her time to come and run the Linac machine on the weekend.

I also wish to thank Dr. Shivashni Deo and Dr. Myth Mok from the Westmead Millennium Institute (WMI) for their guidance in cells biology. I would also like to thank Dr. Justin Yerbury from the Illawarra Health and Medical Research Institute (IHMRI) for his help in flow cytometry and confocal microscopy work and also Dr. Jude Taylor for his help in FlowJo. Dr. Konstantin Konstantinov from the Institute for Superconducting and Electronic Materials (ISEM).

Thank you also to Targeted Nano-therapies Team (TNT) and Dixon research group of the Centre for Medical and Molecular Bioscience (CMMB) for the start of new friendship. To Adam Briggs, Ryan Brown, Callum Stewart, Marjorie McDonald, Lee Taylor, Dean Cardillo (for teaching and help me with LaTeX), and Natalia Roberts, thank you for creating such a friendly working environment and the laughter in every meeting. Special thank you to members of the Centre for Medical Radiation Physics (CMRP) group, past and present, for making an enjoyable and pleasant office to work at (Amir, Jeannie Wong, Amy Ziebell, Norlaili Ahmad, Cheryl Lian, Elise Pogson, Dean Cutajar, Michael Weaver, Ash Cullen, Anthony Espinoza, Linh Tran, Sally McKinnon, Julian Steele, and Claudiu Porumb).

In addition, I thank Karen Ford and Sunny Skipp from CMRP for their kind in handling all the administration, all the lab technical officers (Katie, Claire, Tanya, and Linda) and receptionists (Beth, Dy, and Aleta) at IHMRI for their continued support. Thank you to the Centre for Medical Radiation Physics and the University of Wollongong for financial support through a Matching Scholarship and International Postgraduate Tuition Award (IPTA), respectively.

I would like to thank my family, whose love is with me in whatever I pursue. Last and most importantly, I wish to thank my loving, kindly and supportive fiancé Mark Nelson, who provides me endless inspirations, encouragement, and unconditional love. He also taught me about scientific research in general and has shown me what a good researcher (and person) should be.



# Chapter 1

## Introduction & Motivation

### 1.1 Background

Despite significant advances in surgery, radiotherapy, and chemotherapy, cancer is the second largest cause of death in developed countries. In Australia, more than 80,000 people develop cancer every year with more than 60% of patients surviving long term following an appropriate treatment plan. Radiotherapy forms a major treatment strategy for cancer patients, being second after surgery in contributing to the cure of cancer. In some cases radiotherapy is used as an alternative to surgery, particularly for those cases where surgery is not an option due to the need to preserve critical organs such as in the treatment of deep-seated gliomas.

The ongoing challenge in radiation therapy treatment is the controlled delivery of a lethal dose to the tumour whilst minimising damage to the surrounding normal tissue. Improvements in radiation dose delivery techniques provide improvements in local tumour control, e.g. intensity modulation radiation therapy (IMRT) and stereotactic radiotherapy (SRT) are two of the most commonly used external beam radiation therapies (EBRT). IMRT is the most commonly

used technique in radiotherapy of the central nervous system (CNS) while SRT is an extremely precise radiation treatment technique for the delivery of a large single dose fractionation within the brain (e.g. gamma knife).

In the most common form of clinical radiotherapy megavoltage linear accelerators (LINACs) are used to irradiate the target by X-rays. Modern medical LINACs are also used for electron beam radiotherapy where electrons are not directed onto a target (x-ray target is retracted) but used directly to a tumour site, which only be used in special procedures such as total body electron skin irradiation [Metcalf et al., 2007]. A less common form of radiotherapy, using lower energy kilovolt (kV) X-rays from an orthovoltage machine, is primarily used for superficial cancer treatment. Another type of radiotherapy is hadron therapy, which uses particles such as neutrons, protons, and light or heavy ions to treat cancer. Theoretically hadron therapy offers the potential of both physical (protons and ions) and biological (neutrons and ions) advantages in the treatment of localised tumours [Lodge et al., 2007] as well as the treatment of radioresistant tumours and tumours located near critical body structures (e.g. spinal cord) [Petti and Lennox, 1994].

All types of radiation therapy used in cancer treatment have been extensively studied in terms of their quality of dose distributions, linear energy transfer (LET), and most importantly, in terms of their ability to confine the high-dose treatment to the tumour volume and thus minimise the radiation dose delivered to the surrounding healthy tissue. In patients with more advanced local-regional disease, tumour control is often unsatisfactory with 85% of patients with glioblastoma [Krex et al., 2007] and 30 – 40% of patients with unresectable pancreatic carcinoma and head & neck cancers suffering a local recurrence [Sohn et al., 2000]. For this reason considerable research has been

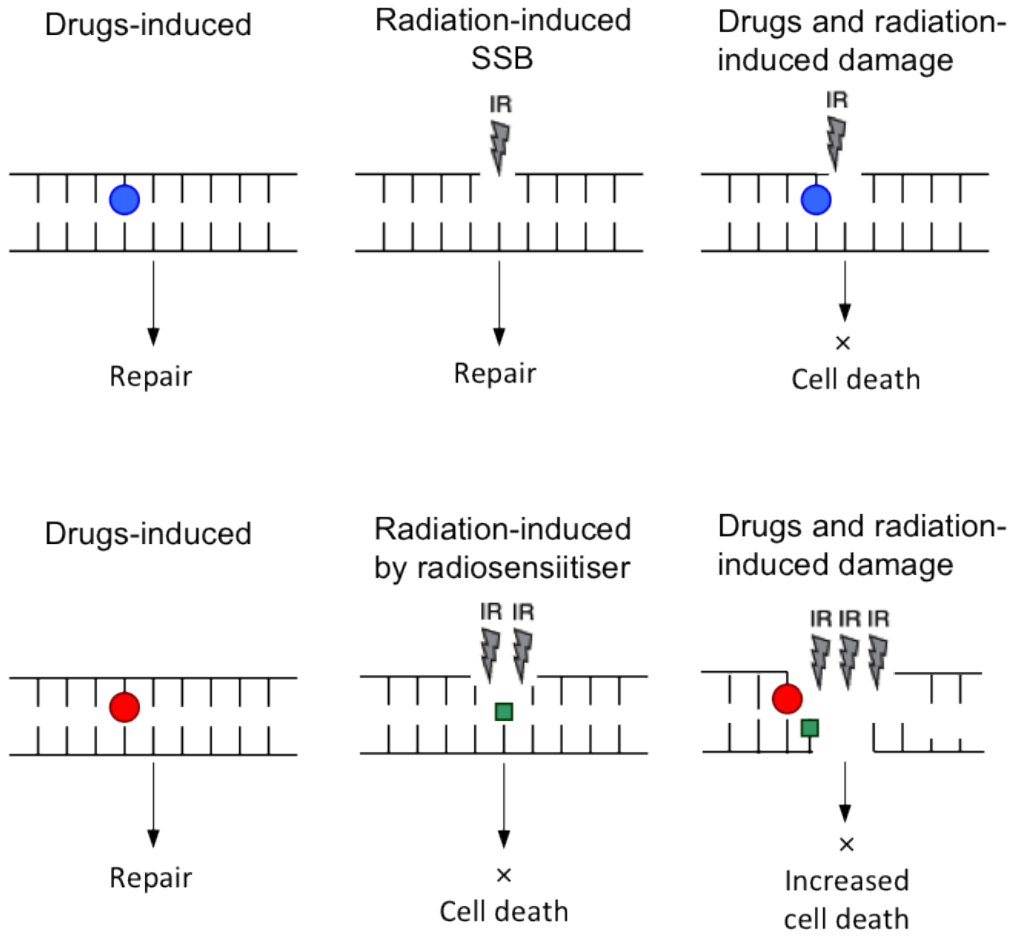


Figure 1.1: Schematic diagram of increased lethal DNA damage by the combination of drugs and radiation in general (upper) modified from [Seiwert et al., 2007] and in this study (lower) as the increased DNA damage by the presence of drugs (i.e BrUdR and MTX) combined to radiation. Blue dots, red dots, and green square represents platinating agents (cisplatin), methotrexate/5-FU, and the high-Z agents (BrUdR/IUdR), respectively.

performed into enhancing the cytotoxicity effect of radiotherapy focussing on the use drugs-and/or nanoparticles (NPs) to enhance radiotherapy. This is one of the strategies used in the work presented in this thesis, as illustrated in Figure 1.1.

The combined use of chemotherapy and radiosensitiser drugs containing platinum ( $Z = 78$ , K-edge at 78.4 keV) has recently shown promising results in clinical radiotherapy [Rousseau et al., 2010]. This method is designed to in-

crease the radiation dose delivered to the target tissue by using elements that have large photoabsorption (i.e. photoelectric effect) cross-sections. However, in Rousseau et al. [2010] mega-electron X-rays were used. The photon absorption mechanisms present at these energies are not as efficient as those present at kilo-voltage X-ray energies. This suggests that the technique can be improved by using lower X-ray energies. In the presence of highly absorbing elements in the tumours, X-ray photoabsorption in the tissue can theoretically be enhanced by tuning the X-ray energy to that of the inner-shell absorption edge of the targeted elements [Kobayashi et al., 2010].

In 2004, Corde et al. proposed the concept of radiotherapy enhancement in the presence of iodine compounds by irradiating with photons of energy just above the K-absorption edge of iodine (33.2 keV). They succeeded in demonstrating that 50 keV photons were the most effective for this element. More recently, researchers have investigated using the combination of platinum nanoparticles with hadron therapy. In both cases the required energy sources (intense monochromatic X-rays and carbon or proton ions facilities) are very expensive high-tech treatment options, making them less viable as a treatment option. The strategy proposed in this thesis is based upon utilising more traditional cancer treatment modalities such as conventional X-ray machines, which are both much more readily available in hospitals worldwide and cheaper.

Other cancer radiation treatment options relevant to this thesis to obtain the synergy of enhanced absorption and tumour specificity are brachytherapy and radionuclide-targeted therapy. Brachytherapy (BT) is a form of radiotherapy which involves the use of radioisotopes (e.g. low dose rate (LDR-BT) iodine-125 seeds or a high dose rate (HDR-BT) Ir-192 seed) implanted directly into the tumour, either temporarily (in the case of HDR-BT) or permanently (in

the case of LDR-BT). BT is often used for treating cancer in organs that incorporate or are in close proximity to critical structures (e.g. urethra, rectum). In such cases dose escalation for better tumour treatment is difficult to achieve without compromising the dose restrictions for these critical organs. The nanoparticles (NPs) used in this thesis may allow such dose escalation via direct injection of the NPs into the target prior to BT treatment. While BT sources are not used in this thesis, low energy (kilovoltage) X-rays are used and have some overlap with BT radiation fields. The associated findings therefore have some relevance to BT.

In the case of radionuclide therapy radiolabelled pharmaceuticals (e.g. I-131, P-32, Yt-90), more commonly used in nuclear medicine for diagnostic imaging, are used to locate molecular and functional targets within tumor sites. Recent studies have reported the use of radiosensitisers combined with radionuclide therapy in order to improve the tumoricidal effect of Auger electron therapy [DeNardo and Denardo, 2006; Wong, 2006]. However, it is still a major challenge to achieve the high dosage to the tumour necessary for satisfactory therapeutic benefit. For this reason the strategy proposed in this thesis of using external X-ray beams may be an effective option to significantly further boost the local dose delivered to the tumour.

In order to increase the radio-sensitivity of the tumour radiosensitizer agents, such as halogenated pyrimidine analogs, can be administered during radiotherapy [Sano et al., 1965, 1968]. These agents are incorporated into the DNA of dividing tumour cells; their uptake is aided by the addition of a very small dosage of antimetabolites, methotrexate (MTX) or 5-fluorouracil (5-FU). It should be noted that throughout this thesis, the term cell killing or cell death refers to the loss of unlimited reproductive capability.

## 1.2 Thesis Overview

### 1.2.1 Objectives

Improvements in radiation dose delivery to ensure a more efficient killing of cancer cells is needed for targeted cancer treatments which aim to provide an improvement in local tumour control and consequently reduced tumour recurrence. The objective of this thesis work is to gain a better understanding of how to significantly enhance tumour cell damage using:

1. Ceramic nanostructured particles (based on Ce, Ta and Bi) as compounds of high-Z element, combined with external X-ray radiation beams and
2. An experimental therapeutic combination of anticancer drugs (MTX or 5-FU) and halogenated thymidine analogs (BrUdR) with X-ray radiation

The experimental approach is discussed in detail below.

### 1.2.2 Aims

The research program outlined in this thesis aims to:

1. Establish tissue culture methods and techniques by growing cells, counting and splitting them and by setting up clonogenic assays. (**SECTION 4.1 & 4.2**)
2. Test the cytotoxicity of the pharmacological drugs and ceramic NPs combined with the radiosensitiser drugs for optimal enhancement of drug-enhanced radiotherapy by measuring the viability of cells and clonogenic survival. (**SECTION 4.3**)
3. Establish irradiation conditions for the optimal enhancement of the chemopair therapy induced by conventional megavoltage X-ray beams by in-

investigating the effect of dose rates of 0.5 and 5 Gy/min and by comparing a radioresistant (9L) and radio-sensitive (MCF-7) cancer cell lines (**SECTION 4.4**).

4. Determine the general applicability of the protocol by using ceramic NPs (**SECTION 4.5**) and different chemo-drugs (i.e. 5-FU or Fluorodex) (**SECTION 4.3**).
5. Establish irradiation conditions for the optimal enhancement of the chemo-Auger therapy induced by conventional kilovoltage X-ray beams (**SECTION 4.6**).
6. Demonstrate radiation-induced increases in cell killing in the presence of chemo- and radiosensitiser drugs combination assessed by clonogenic survival analysis and quantification of the intra-cellular and intra-DNA halogen uptake (**SECTION 4.6**).
7. Investigate the influence of energy dependence on enhanced radiosensitising effect by BrUdR plus MTX by investigating the effect on different energies range. (**SECTION 4.7**).
8. Establish the groundwork for confocal microscopy studies. (**SECTION 4.8**).

The remaining chapters of this study are arranged as follows.

**CHAPTER 2** reviews the research literature pertaining to radiation therapy, radiation biology, chemo-radiation, and the enhancement of radiobiological effects by high-Z elements. Additionally the chapter develops and validates the theoretical hypothesis underpinning the proposed experimental investigation combining pharmacological drugs with radiosensitiser drugs and/or nanoparticles concomitantly with external therapeutic X-ray beams.

**CHAPTER 3** describes the materials and methods used in the experimental procedures in this thesis.

**CHAPTER 4** presents and discusses all of the experimental results in the context of the aims and objectives of the thesis.

**CHAPTER 5** contains the concluding remarks of this study.

The research reported in this thesis is original. Although the combination of a high-Z material (i.e. radiosensitiser drugs), anti-cancer drugs and external beam radiation in order to enhance biological effects have been investigated by previous researchers, these studies did not investigated the influence of the X-ray energy. Our research hypothesis is driven by knowledge of the influence of Auger electrons and the importance of cluster damage produced by these low energy electrons.

This thesis work is part of a collaborative program between the Centre for Medical Radiation Physics (CMRP), the Centre for Medical and Molecular Bioscience (CMMB), and the Institute for Superconducting and Electronic Materials (ISEM) of the University of Wollongong (UOW). Research was mostly conducted at the Illawarra Health and Medical Research Institute (IHMRI) of the UOW utilising their cell and molecular biology research infrastructure and using the X-ray irradiation facility in the Department of Radiation Oncology in the Prince of Wales Hospital (POWH).



# Chapter 2

## Literature Review

### 2.1 Principles of Radiation Therapy and Radiation Biology

#### 2.1.1 Introduction to Radiotherapy

Cancer is a disease in which cell proliferation is out of control. The invasion surrounding normal tissues by tumour cells and spread to other sites in the body (by either entering the blood stream or the lymphatic system) is known as metastasis and this is what makes cancer lethal. Radiation therapy (radiotherapy) is a cancer treatment using a beam of ionising radiation which aims to kill all cancer cells within a defined target volume and therefore leading to significant tumour shrinkage or a curative clinical outcome.

The use of ionising radiation was a revolutionary step in the evolution of the diagnosis and treatment of cancer. It is called ionising radiation because the radiation is of enough energy to ionise the material it is traversing, thus forming ions as it passes through human tissue. Without radiation, many conditions would not be diagnosed and some cancers would not be treatable. Radiation

is the primary treatment for many kinds of cancer and is also used in conjunction with surgery and/or chemotherapy for other types of cancer. Over the past 100 years, radiotherapy has become an increasingly important modality for most cancer treatment. Currently, radiotherapy plays an important role in the management of benign and malignant disease throughout the body in both children and adults with over 50% of cancer patients receiving some form of radiotherapy treatment as part of their cancer management plan [Delaney et al., 2005]. Radiotherapy also offers an effective means of palliative care when a curative outcome is not possible [Mundt et al., 2000].

### **2.1.2 Introduction to Radiobiology**

Cells may eventually die or lose their ability to divide when they are exposed to ionising radiation. The explanation of this effect lies partially in physics and partially in biology [Hirst, 2007]. Some of the interesting aspects of radiobiology are concerned with attempts to link these two fields [Lawrence, 1971]. Radiobiology is a field that studies fundamental changes in irradiated cells and helps understand the responses of normal tissue and tumours to ionising radiation [Bernier et al., 2004]. In other words, radiobiology is a branch of science that combines two disciplines: radiation physics and biology, and is concerned with the action of ionising radiation on biological tissue and living organism [Hall and Giaccia, 2012; Suntharalingam et al., 2005].

### 2.1.3 Physical Basis of Radiotherapy

#### 2.1.3.1 Ionising radiation

Ionising radiation is a form of electromagnetic radiation and is physical concept in which energy is transmitted through space without necessarily the need or aid of a material medium [Lawrence, 1971]. The ionisation process involves the ejection of electrons from the atoms that make up the medium in which the radiation is traversing and this initial interaction is the major event in the action of radiation. Radiation absorbed by aqueous systems such as cells can cause excitation and ionisation, as well as free radical production. The biological consequences of exposure to ionising radiation are mediated by a series of processes, which can be classified into four stages [Adams, 1989]: physical, chemical, biochemical, and cellular responses, which are initiated after the deposition of the radiation in the medium [Mitchell et al., 2000] (Figure 2.1).

The time scale over which energy is transferred to an atom or a small molecule during irradiation is extremely short (less than  $10^{-15}$  s) and is governed by the particle velocity, the dimensions of the atom or molecule, and the amount of energy lost in the process [Adams, 1989], which then produces water radicals and other chemical lesions (less than 1 s) that diffuse through and/or react with molecules in the cell, thereby creating biomolecular lesions which can last a relatively long time [Curtis, 1986].

#### 2.1.3.2 Interaction of ionising radiation

In modern clinical radiotherapy, ionising radiation is delivered to tissues primarily with high-energy photons (gamma rays and X-rays) and charged particles (electrons, protons, heavy ions, pions etc). Gamma rays (such as those

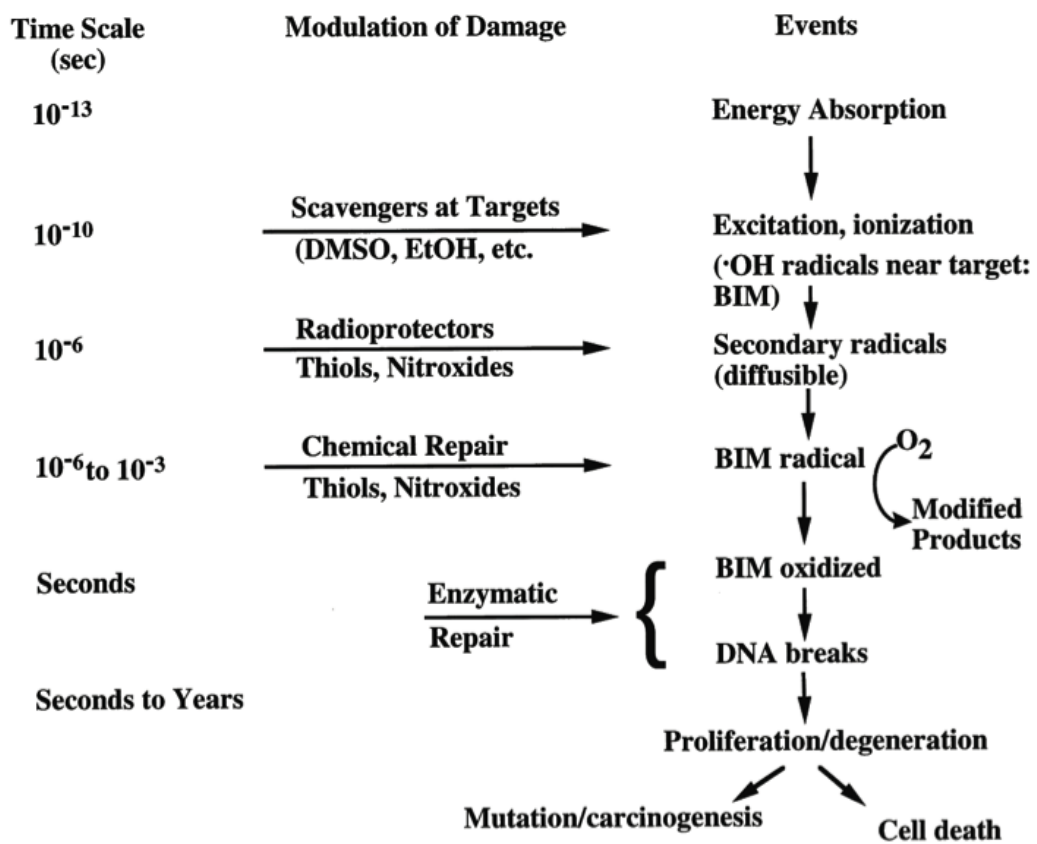


Figure 2.1: Time scale of events initiated by ionising radiation deposition in biological systems BIM biologically important molecule [Mitchell et al., 2000].

used in brachytherapy) originate from within the nucleus of an atom while X-rays (such as those used in external beam radiotherapy) originate from the outside the nucleus of an atom. Within a linear accelerator (LINAC), a narrow beam of electrons is accelerated to nearly the speed of light before striking a tungsten target [Khan, 2010]. As the electrons decelerate, bremsstrahlung radiation (X-rays) is emitted with a spectrum ranging from zero to their maximum kinetic energy. The beam quality is expressed in terms of the highest-energy photons related to the electron accelerating voltage, kVp (kilovolts peak) or MV (megavoltage) [Mundt et al., 2000]. In the energy range most widely used in external X-ray beam radiotherapy (50kVp up to 25MV), the relevant interactions of X-rays photons with tissue are the photoelectric effect, the Compton effect, and pair production [Attix, 2004; Khan, 2010].

### Photoelectric Effect

The photoelectric effect refers to light (photo-) causing the ejection of electrons (electric) from a material. In the photoelectric effect, an incident photon is completely absorbed by an inner shell electron with the subsequent ejection of an electron known as a photoelectron (Figure 2.2). The probability of photoelectric absorption,  $\tau$  depends strongly on atomic number,  $Z$  [Attix, 2004; Khan, 2010]:

$$\frac{\tau}{\rho} = \frac{Z^3}{(hv)^3} \quad (2.1)$$

where  $\rho$  is the density ( $\text{g/cm}^3$ ) and  $hv$  is the energy of the incident photon. Therefore, photoelectric absorption becomes more important as the atomic number increases and as the photon energy decreases.

### Compton Effect

In the Compton effect, the photon behaves like a particle as it collides with a

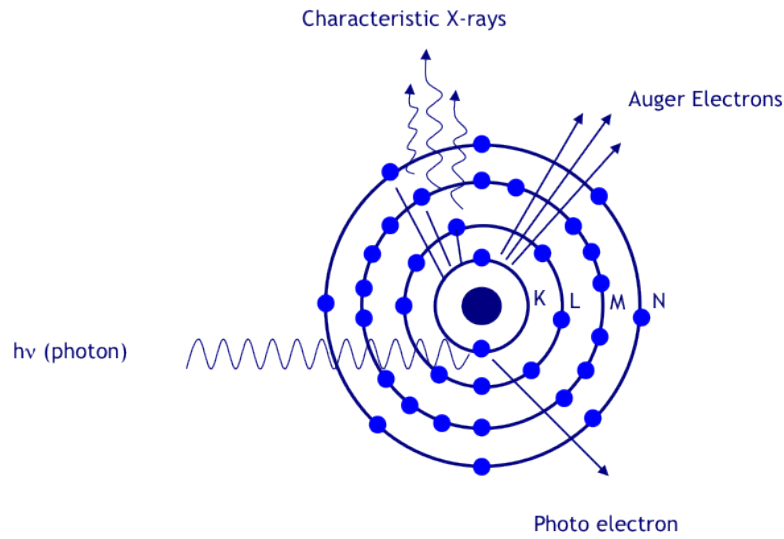


Figure 2.2: Schematic diagram of the photoelectric effect and other processes that can occur as a result of the photoelectric effect (characteristic X-ray and Auger electron production).

loosely bound outer orbital electron. The incident photon is deflected (scattered) and imparts kinetic energy to the electron (Figure 2.3). The probability of this interaction is proportional to the number of electrons per unit mass ( $\propto Z/A$ ) and is related inversely to the energy of photon [Attix, 2004; Khan, 2010; Metcalfe et al., 2007].

### Pair Production

A photon may decay to an electron and a positron provided the energy of the photon greater than 1.022 MeV. After losing all or some of its kinetic energy, the positron annihilates with an electron. In the case where the photon loses all of energy prior to annihilation, two 511 keV photons travelling in opposite directions are produced [Attix, 2004; Khan, 2010] (Figure 2.4). The probability of pair production is roughly proportional to  $Z^2$ , which varies with  $Z^2$  per atom,  $Z$  per electron and  $Z$  per gram [Khan, 2010].

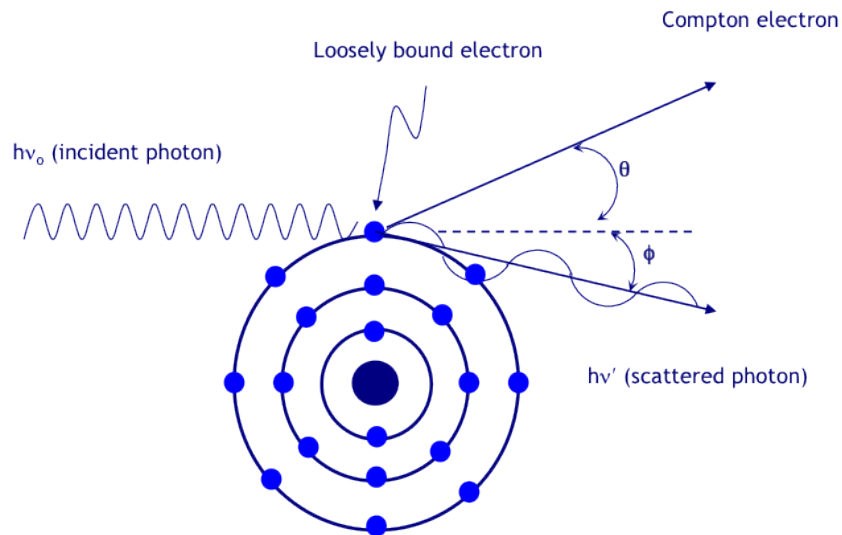


Figure 2.3: Schematic diagram of the Compton effect.

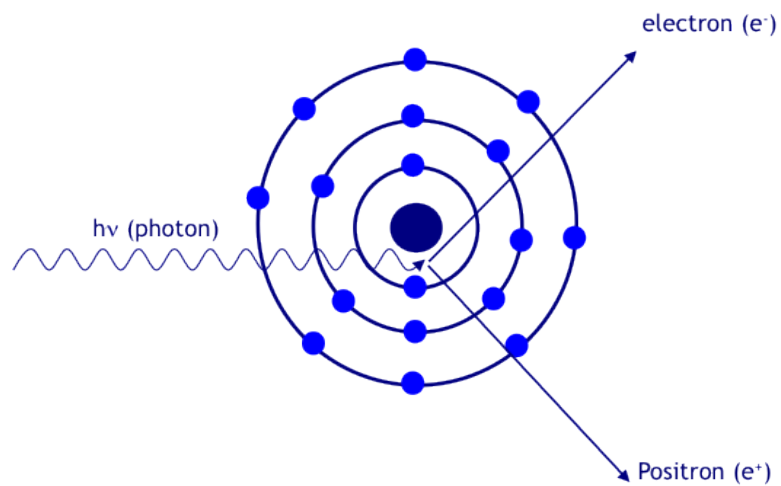


Figure 2.4: Schematic diagram of pair production ( $h\nu$  is greater than 1.02 MeV).

### 2.1.3.3 Radiation quality

In radiation biology, radiation quality refers to beam characteristics that must be specified in order to determine interactions at the microscopic level that may influence the ability of an irradiation field to produce biological effects. Principally, radiation quality refers to those radiation characteristics that describe the spatial distribution of energy transfer by charged particles when other physical factors are kept constant (e.g. absorbed dose) [on Radiation Units and Measurements, 1979].

#### Radiation absorbed dose

Absorbed dose is the accepted unit of measurement that represents the energy absorbed per unit mass. The SI unit of absorbed dose is the Gray (Gy), which is defined as the absorption of 1 Joule of energy per kilogram of mass (J/kg).

#### Linear energy transfer (LET)

Linear energy transfer (LET) is a physical quantity expressing radiation quality for radiobiological purposes. The International Commission on Radiation Units and Measurements (ICRU) defines the LET as: LET of charged particles in a medium is the quotient  $dE/dl$ , where  $dE$  is the average energy locally imparted to the medium by a charged particle of specified energy in traversing a distance of  $dl$ . The unit of LET is  $\text{keV}/\mu\text{m}$  difficult to measure but, in the case of electrons, can be approximated by dividing the energy of the electron by the range of the electron in a given material [Suntharalingam et al., 2005].

High LET radiations such as neutrons and  $\alpha$ -particles normally deposit substantial amounts of energy by individual heavily ionising tracks [Hill et al., 2002]. These could have a greater biological effectiveness than the sparsely ionising radiation fields with low LET such as that from X-rays and  $\gamma$ -rays



[Goodhead, 1999]. However, it should be noted that the photoionisation processes in matter due to Auger processes can also produce significant enhancement of the energy deposition events surrounding photoabsorption sites. Thus, one of the major aims of this project is to increase the dose delivery to the tumour target by the presence of highly absorbing elements in the tumours (i.e. high-Z elements) that have large photo-absorption cross-sections (as detailed in section 2.4).

## 2.1.4 Biochemical and Biological Basis of Radiotherapy

### 2.1.4.1 Radiation damage within the cell

As described in section 2.1.3.1, the interaction of ionising radiation with biological matter proceeds through several stages which results in a variety of biological end effects. More specifically, deoxyribonucleic acid (DNA) damage caused by X-ray radiation is mediated through direct ionisation and indirect mechanisms. In direct actions, the radiation interacts directly with DNA as a critical target in the cell (i.e. electrons ionise DNA molecules). The atoms of DNA itself may be ionised or excited through interactions (e.g. photoelectric effect) that lead to a chain of physical and chemical events, eventually resulting in biological damage. In indirect actions, the radiation interacts with other molecules and atoms, mainly water (80% of a cell is composed of water), within the cell to produce free radicals (e.g. hydroxyl radicals). Both  $\text{H}_2\text{O}^+$  (water ion) and the  $\text{OH}^\bullet$  (hydroxyl radical) are extremely reactive free radicals, which can diffuse and attack DNA [Gofman, 1990; Nias, 1990; Casarett, 1968].

#### Direct action – primary and secondary electron

Between collisions, electrons primarily travel through a medium in straight lines, although one will occasionally suffer a major deflection and travel in

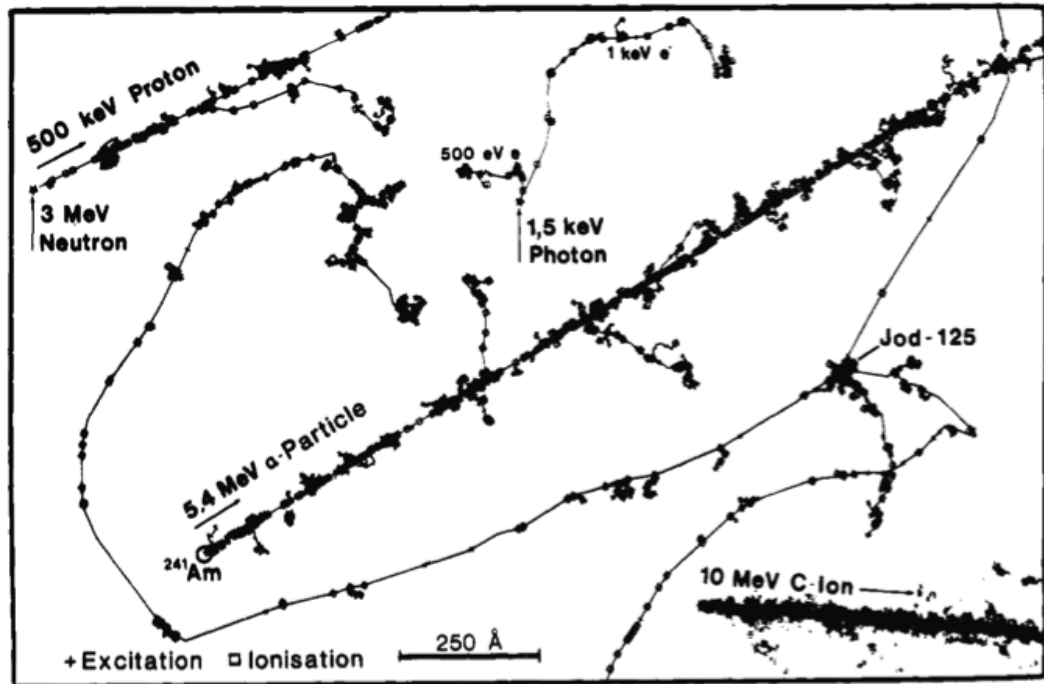


Figure 2.5: Distribution of excitations and ionisations along particle tracks in water [Feinendegen, 1990].

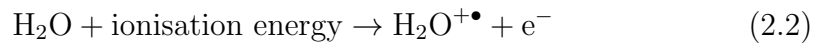
another straight line. The distance travelled depends on the initial electron energy as well as the composition and density of the medium. A primary electron sets secondary electrons, which have their own tracks, into motion at irregular intervals. These electrons are called delta rays, and several hundreds of such ionisations are produced per  $\mu\text{m}$  of track [Feinendegen, 1990]. Their tracks, being typically only a few nanometres long [Gofman, 1990], are generally much shorter than the track of the primary electron. A set of particle tracks in matter with a density close to that of tissue (i.e. water), including those from electrons (photon absorption and  $^{125}\text{I}$  Auger effect), a recoil proton, a  $\alpha$ -particle, and a heavy ion is shown in (Figure 2.5).

#### Indirect action - free radicals formation

The indirect action of X-ray radiation in producing biological damage involves

several steps described below:

Pairs of abnormal ions, formed as the consequences of X-ray irradiation, are called free radical ions. An excited water molecule transfers its energy and forms a positive ion and a free electron as a result of the ejection of an electron [Gofman, 1990; Nias, 1990]:



$\text{H}_2\text{O}^{+\bullet}$  is a free radical ion (with the dot representing an unpaired electron), which is very unstable and extremely reactive. This is the primary event of water molecule ionisation and is followed by a series of reactions leading to the formation of various free radicals. The electron,  $\text{e}^-$ , is picked up by another water molecule and will become hydrated ( $\text{e}_{aq}^\bullet$ ):



The free radical ion  $\text{H}_2\text{O}^{+\bullet}$  reacts with a water molecule to produce the highly reactive hydroxy radical  $\text{OH}^\bullet$ :



The indirect effect of radiation is especially important in aqueous systems, where a water molecule may be ionised and then transfer this energy to another molecule [Gofman, 1990; Casarett, 1968]. Molecules produced by the irradiation of water molecules such as hydrogen peroxide ( $\text{H}_2\text{O}_2$ ), can have a variety of effects on other molecules in biological systems [Tubiana et al.,

1990]:



Secondary electrons, which cause the direct effects, are responsible for the majority of the ionisations and excitations produced in DNA. The indirect mechanism is mediated free radical formation within the cell, mostly from water ( $\text{H}_2\text{O}$ ) molecules (Figure 2.6). Through the chain reaction above water is also sequentially converted to free radicals, such as  $\text{H}^\bullet$  and  $\text{HO}^\bullet$ , and peroxides, such as  $\text{ROO}^\bullet$  (radical peroxide) and  $\text{ROOH} + \text{R}'^\bullet$  (hydroperoxide). These are highly reactive molecules which are known as reactive oxygen species (ROS) [Tubiana et al., 1990]. The indirect mechanism is thought to account for about two-thirds of all mammalian DNA damage caused by X-rays [Hall and Giaccia, 2012].

#### 2.1.4.2 Relative biological effectiveness (RBE)

As mentioned above, different types of radiations have different degrees of relative biological effectiveness (RBE). RBE compares the dose of given test radiation to the dose of standard radiation to produce the same biological effect. The RBE is defined by the following ratio [on Radiation Units and Measurements, 1979; Lawrence, 1971; Suntharalingam et al., 2005]:

$$\text{RBE} = \frac{\text{Dose from standard radiation to produce a given biological effect}}{\text{Dose from test radiation to produce a given biological effect}}$$

For historical reasons, the standard radiation is 250 kVp X-rays, but the use of  $^{60}\text{Co}$   $\gamma$  rays is now recommended. RBE depends on radiation quality (LET).

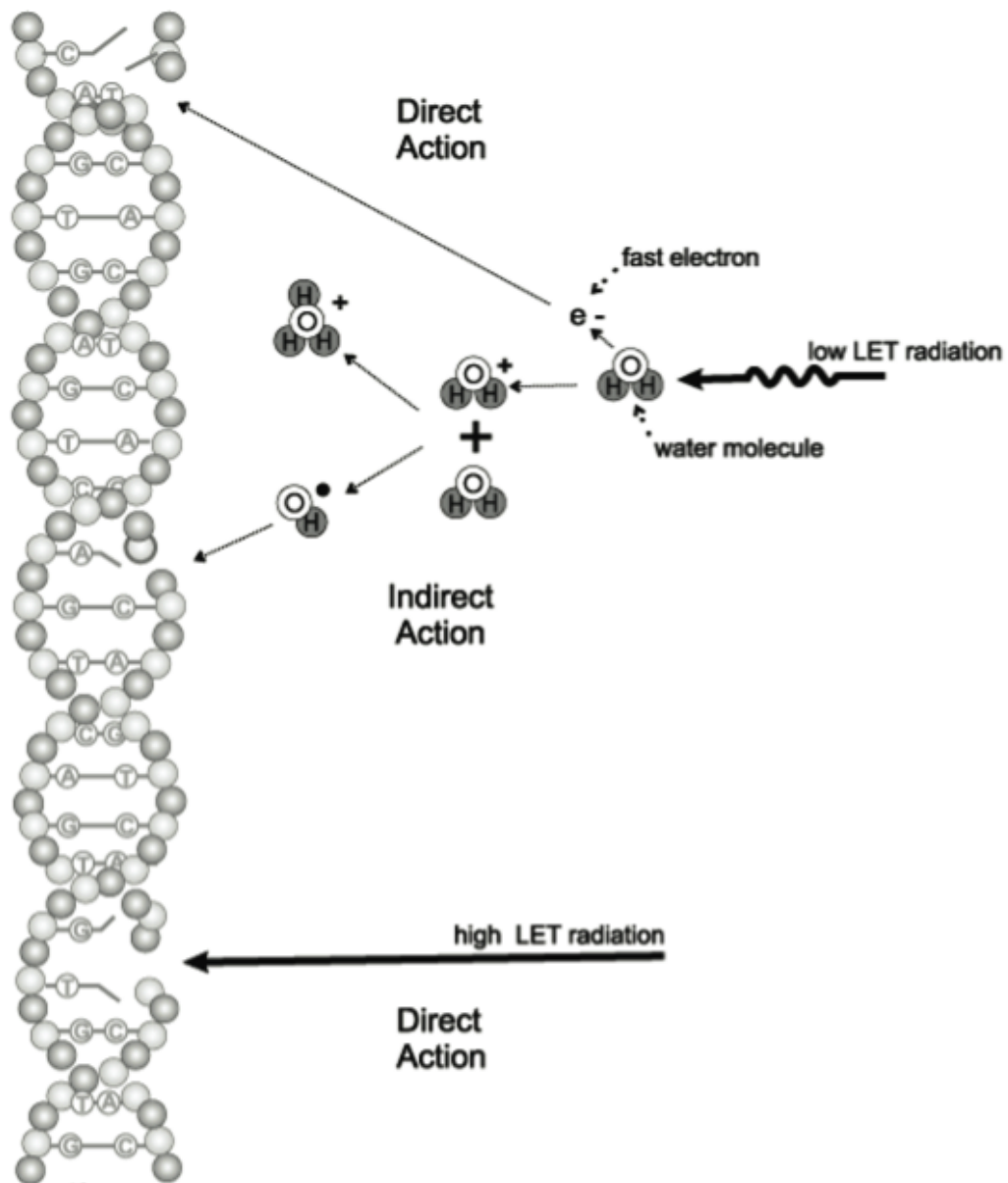


Figure 2.6: Direct and indirect mechanism of DNA damage by X-rays irradiation (on upper part) [Powsner and Powsner, 2006].

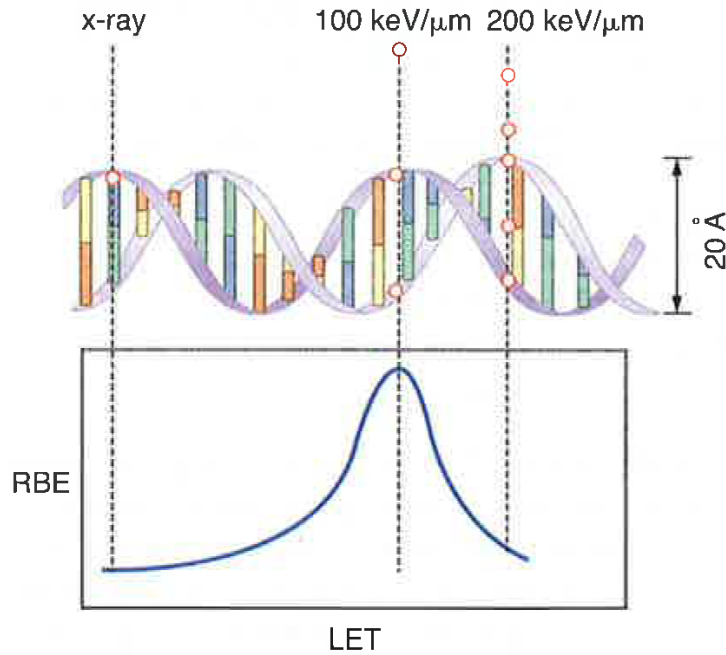


Figure 2.7: Illustration of RBE against LET [Hall and Giaccia, 2012].

As the LET of radiation increases, the ability of radiation to produce biological damage also increases. The RBE depends on the radiation dose, the number of dose fractions, the dose rate, and the biological system. In general, the RBE increases with the LET to reach a maximum RBE of 3 – 8, depending on the level of cell kill [Suntharalingam et al., 2005] at a LET of 100 keV/μm [Hall and Giaccia, 2012] and then decreases with a further increase in the LET due to energy overkill (Figure 2.7).

#### 2.1.4.3 Track structure model

Ionising radiation differs from other DNA damage agents due to its ability to produce clusters of adjacent damages over distances of a few nanometers and is characterised by the radiation track structure reflecting this critical property could be suitable for DNA lesions yields calculation [Michalik, 1992]. Studies of track structure provide a powerful tool for investigating the microscopic

### Clustered DNA damage

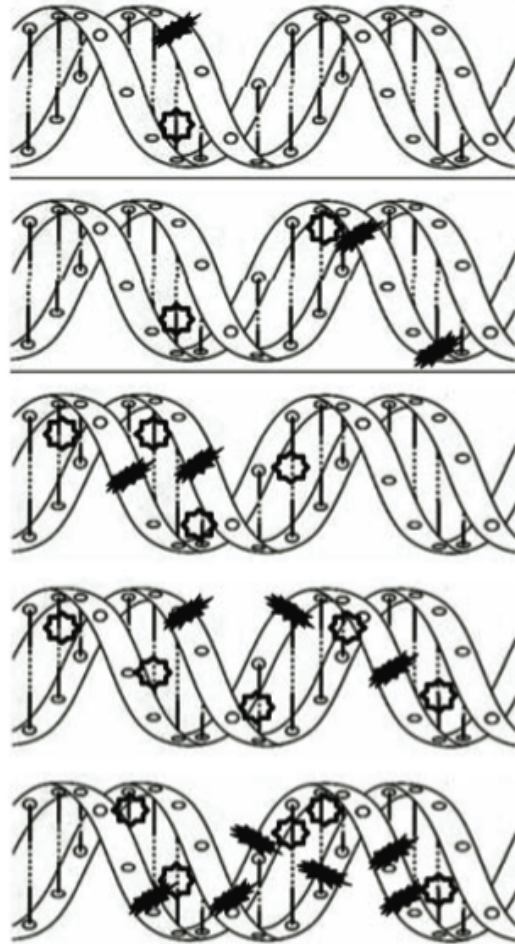


Figure 2.8: Typical example of strand breakage (solid symbol) as well as base damage (open symbol)[Goodhead, 2006].

features of ionising radiation and the nature of molecular damage to DNA [Nikjoo et al., 1998]. Based on the physical and chemical analysis of microscopic features of radiation tracks, it has been demonstrated that clustered damage (Figure 2.8) is a major factor in the biological effectiveness of radiation [Nikjoo et al., 1998; Goodhead et al., 1980; Goodhead, 1994].

The efficiency with which ionising radiations produce clustered damage depends on the local ionisation clusters within the tracks, both directly in the DNA (direct mechanism) and also via hydroxyl radicals from water within

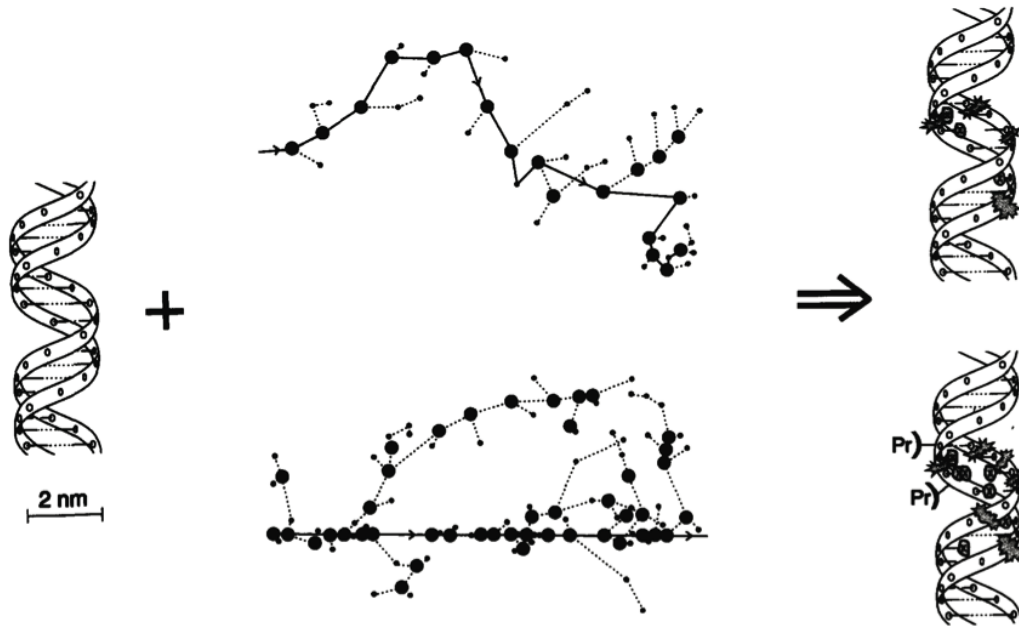


Figure 2.9: Schematic representation of DNA segment with randomly selected simulated track from low-energy electron (upper) and short  $\alpha$ -particle track (lower). Large and small dots are represent ionisations and excitations, respectively [Goodhead, 1994].

a few nanometers of the DNA (indirect mechanism) [Goodhead, 2006]. The complex clustered damage in DNA that can be produced from low energy X-rays is shown in a track structure simulation (Figure 2.9).

#### 2.1.4.4 Dose-effect relationship

##### Cell survival curves

Principally, the survival fraction of a cell population is measured rather than the fraction that is killed [on Radiation Units and Measurements, 1979]. The cell survival curves, which are exponentially based, are shown as the response of a population of single cells as a function of dose,  $D$  [Metcalf et al., 2007]. In this case, the surviving fraction of cells is the fraction of irradiated cells that maintain their reproductive integrity (clonogenic cells). Graphically, cell survival as a function of radiation dose is represented by plotting the surviving



fraction on a logarithmic scale (on y-axis) against dose on a linear scale (on x-axis).

#### Linear-quadratic (LQ) model

The clonogenic impairment of mammalian cells, which is commonly known as a cell reproductive death, can be described adequately by a linear-quadratic function of radiation dose,  $D$ , [Barendsen, 1991]:

$$F(D) = \alpha D + \beta D^2 \quad (2.6)$$

This yields the survival curve, assuming that there are two components to cell kill by radiation [Chadwick and Leenhouts, 1973; Tubiana et al., 1990], represented by:

$$\frac{S(D)}{S(0)} = \exp(-\alpha D - \beta D^2) \quad (2.7)$$

where  $S(D)$  is the cell survival fraction at dose  $D$ ,  $S(0)$  is the cell survival fraction at a dose equal to 0,  $\alpha$  is a constant which measures the initial slope of the cell survival curve, representing single-hit killing kinetics which dominates the radiation responses at low doses, and  $\beta$  represents the quadratic component of cell killing (i.e. two hit, single target – quadratic model). The non-zero value of  $\beta$  causes the curve to bend at higher doses (Figure 2.10). The broad initial shoulder at low doses indicates that X-rays are relatively inefficient at killing cells [Borek and Hall, 1973].

This is the simplest and most widely used form for the cell-survival relationship [Deschavanne et al., 1990; Steel, 1989]. From the view point of radiobiology, it can be converted to a linear relationship which can be used to obtain the  $\alpha$  and  $\beta$  parameters:

$$-\frac{\ln(SF)}{D} = \alpha + \beta D \quad (2.8)$$

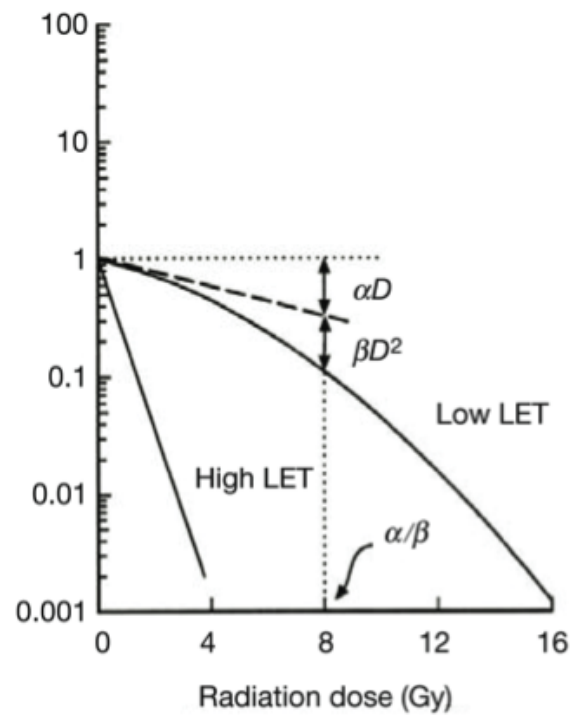


Figure 2.10: The classic linear-quadratic model as a result of the summation components of the equation (2.7): linear ( $\log S = -\alpha D$ ) and quadratic term ( $\log S = -\beta D^2$ ) [Suntharalingam et al., 2005].

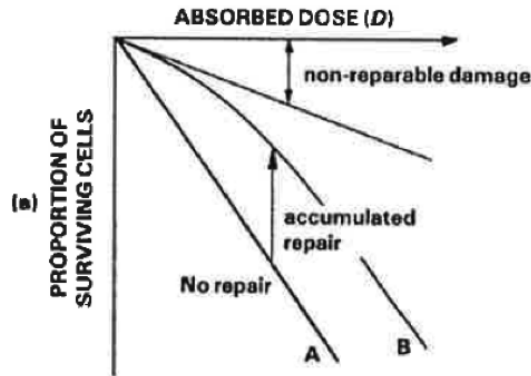


Figure 2.11: The interpretation of survival curves based on intracellular repair model [Tubiana et al., 1990].

where SF is the cell survival fraction at dose,  $D$ , the parameter  $\alpha(\text{Gy}^{-1})$  represents the initial slope of the cell survival curve related to the radio-sensitivity, and  $\beta(\text{Gy}^{-2})$  represents the accumulation of damage repair. This is according to a model based on intracellular repair shown in figure 2.11, where curve A and curve B represent the surviving fraction due to cellular damage without repair and modified by repair, respectively [Tubiana et al., 1990].

## 2.1.5 Cellular Basis of Radiobiology: Mechanisms of Cell Killing

### 2.1.5.1 Cellular DNA target

Deoxyribonucleic acid (DNA) molecules, as the genetic material, are the most important targets for biological damage induced by ionising radiation. DNA organised into chromosome is located within the nucleus of the eukaryotic cell (Figure 2.12).

DNA is a polymer, a large molecule consisting of many similar smaller molecules monomers that are linked together. The monomers that make up DNA are called nucleotides. Nucleotides as the building blocks of DNA have three dis-

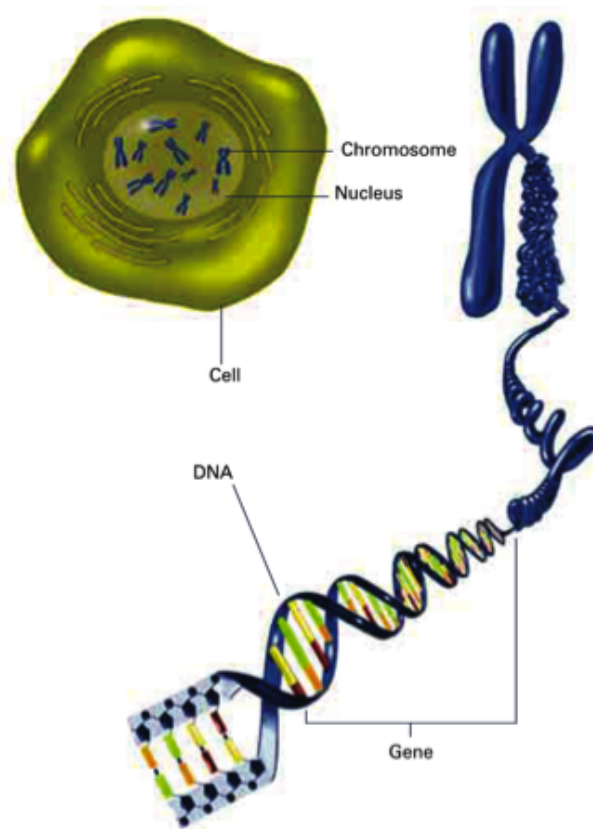


Figure 2.12: DNA within the nucleus of the cell in the chromosomes [of General Medical Science, 2006].

tinct components: a pentose (five-carbon) sugar (deoxyribose), a nitrogenous (nitrogen-containing) base, and a phosphate group (Figure 2.13).

Two classes of nitrogenous bases are purine and pyrimidine. DNA contain two major purine bases: adenine (A) and guanine (G), and two major pyrimidines bases: cytosine (C) and thymine (T). The hydrogen-bonding patterns in the base pairs are A bonds specifically to T (double hydrogen bond) and G bonds to C (triple hydrogen bond). These two types of base pairs predominate in double-stranded DNA, which was defined by Watson and Crick in 1953 (Figure 2.14) [Nelson and Cox, 2005].

In other words, DNA exists as a double-stranded helix. Each strand consists of

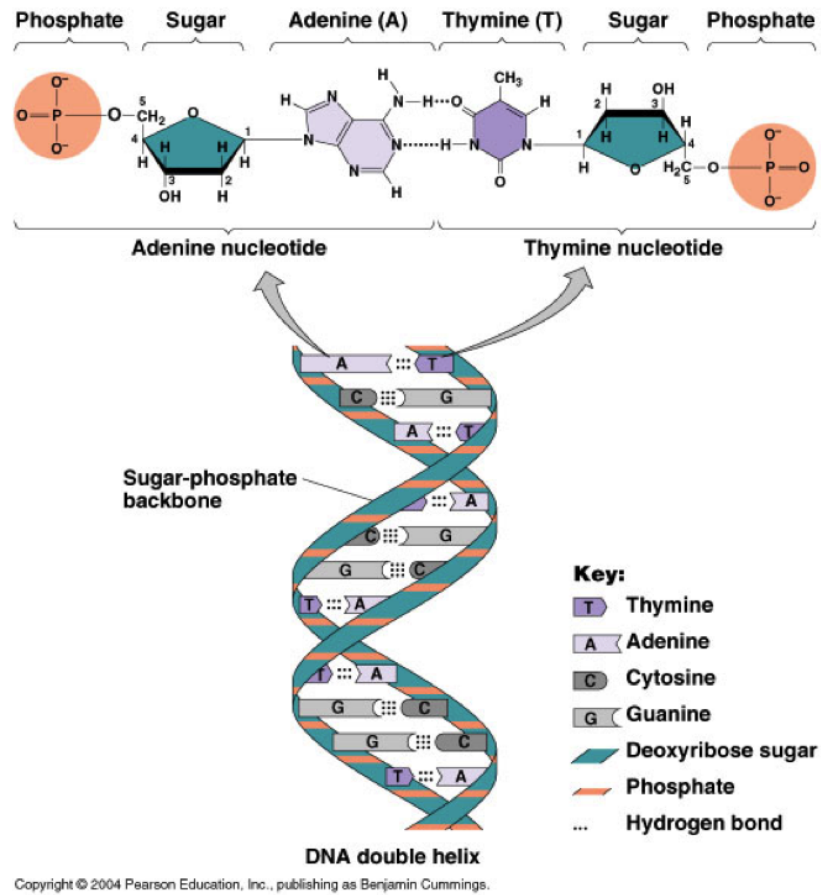


Figure 2.13: Nucleotides as the building block of DNA.

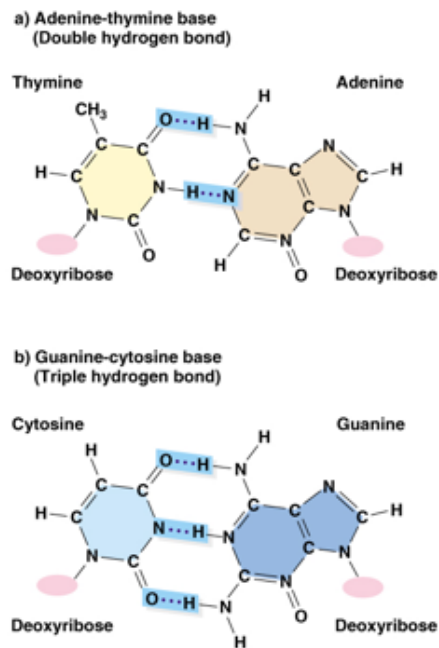


Figure 2.14: Complementary base pairing predominate in DNA[Nelson and Cox, 2005].

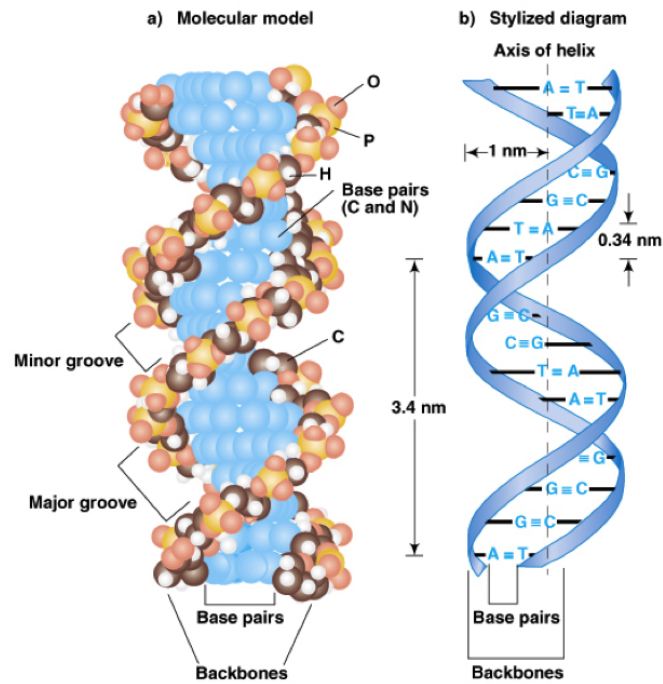


Figure 2.15: Molecular structure of DNA. a) Three-dimensional structure of DNA prepared by Watson and Crick. b) Stylised diagram of the DNA double helix [Russell, 2006].

base-sugar-phosphates. The strands are linked by hydrogen bonds between the bases, and the entire structure is coiled into a helical configuration [Casarett, 1968]. The distance from one base pair to the next is 0.34 nm and one full turn of the DNA helix is 3.4 nm, so there are 10 base pair (bp) in a complete turn. The diameter of a double-stranded DNA helix is 2 nm shown in Figure 2.15.

To make DNA more compact, double-stranded DNA molecules are wound around globular protein complexes (two each of histones H2A, H2B, H3 and H4) to make DNA more compact, which made up the nucleosome, the basic structural units of chromatin (complex of DNA and proteins in cell nucleus) [Felsenfeld and Groudine, 2003] (Figure 2.16). Hence, the least compact form is the 10 nm chromatin fibre that has a characteristic bead-on-a-string with about 10 nm diameter of the beads [Russell, 2006], which are then piled up to

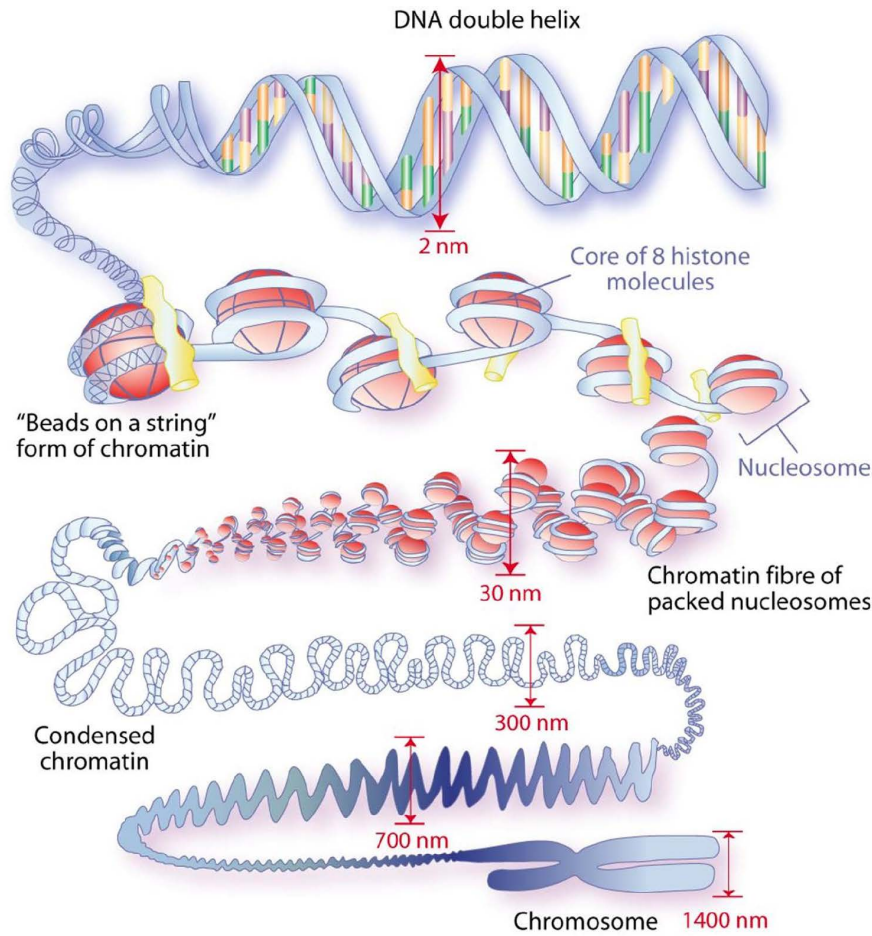


Figure 2.16: Organisation of DNA package [Wouters and Begg, 2009].

form chromatin fibres of nucleosomes, folded and rolled up in irregular spirals to form the chromosome which are visible under the microscope [Wouters and Begg, 2009; Tubiana et al., 1990].

#### 2.1.5.2 Radiation-induced damage to DNA

There are three main types of damage induced in DNA: direct strand breakage (single-strand breaks, SSBs and double strand breaks, DSBs), base damage, and cross-linkage [Bryant, 1989; Radford, 1986]. The proportion of these damage types leads to differences in radiosensitivity and RBE [Barendsen, 1994]. Even at doses as low as  $\sim 1$  Gy, ionising radiation is capable of inducing all of three types of DNA damage type in both isolated and clustered lesions (1–10

bp apart) [Georgakilas, 2008]. For instance, 1 Gy of irradiation will cause approximately  $10^5$  ionisations, more than 1000 DNA bases damages, around 1000 SSBs and around 20–40 DSBs [Wouters and Begg, 2009].

Based on theoretical calculations, it is predicted that in addition to isolated lesions, low-LET radiation can create clusters with as many as 10 lesions [Goodhead, 1994; Sutherland et al., 2000]. Low-LET radiation produces SSB, which are relatively easily repaired whereas radiation of relatively high-LET or a high dose of low-LET may produce SSB in close proximity to each other in both strands (DSB) (Figure 2.17). It is generally accepted that DSBs are the most important lesions in terms of cell death, as well as latent effect such as chromosomal aberrations and tumourigenesis, following exposure to ionising radiation [Collis et al., 2004, 2002]. Another lesions produced by ionising radiation is destructions of the deoxyribose sugars. These are rare and not well understood [Tubiana et al., 1990].

### Clustered DNA damage

Ward [1981] introduced the idea of clustered DNA damage as local multiply damaged sites (LMDS), which are several closely spaced lesions within a short DNA segment produced by ionising radiation. LMDS are caused by the non-uniform energy deposition events followed the passage of secondary electrons through matter and the presence of radicals that attack DNA [Ward, 1981, 1994]. Clustered lesions are estimated to be 50–80% of the total complex DNA damage (DSB and non-DSB clustered DNA lesions) produced by ionising radiation [Georgakilas, 2008]. Clustered DNA damage in cells is produced by low doses of ionising radiation [Sutherland et al., 2000].



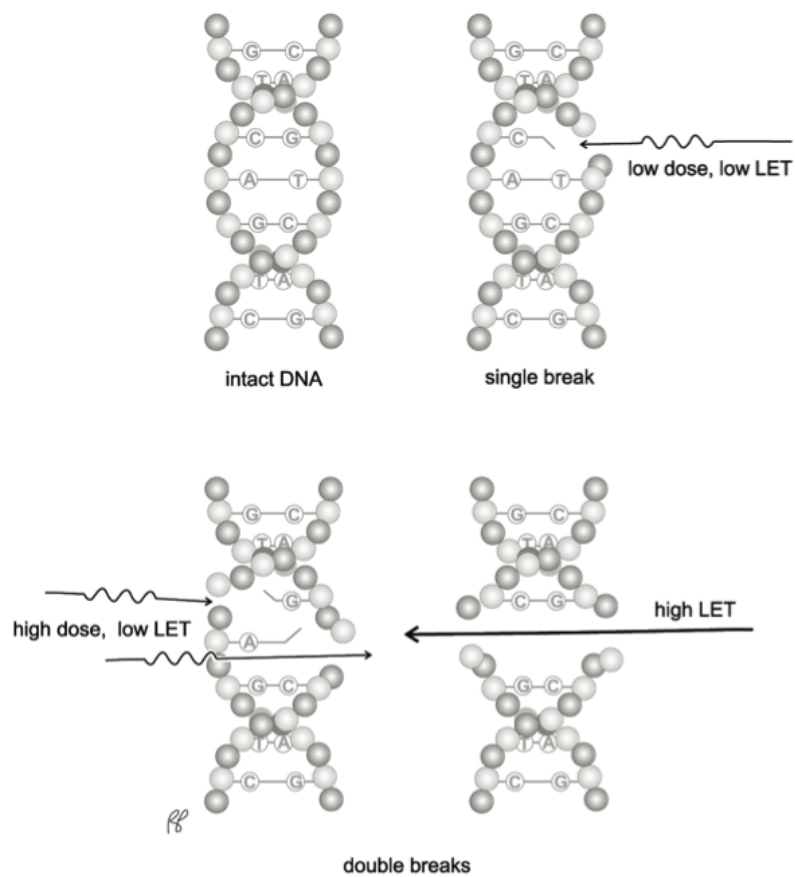


Figure 2.17: Low and high LET traversing a section of the DNA helix [Powsner and Powsner, 2006].

### 2.1.5.3 DNA damage repair in irradiated cells

Numerous studies have shown that most radiation-induced DNA damage can be repaired. However, the rates of repair of different types of lesions vary [Bryant, 1989]. As DSB are both the most important lesion and the main focus of this project, only the repair of DSB DNA is explained.

#### DNA DSB repair

DNA DSB can result in permanent cell cycle arrest, apoptosis, or mitotic cell death if left unrepaired [Olive, 1998]. The two major repair mechanisms of DNA double-strand breaks are non-homologous end joining (NHEJ) and homologous recombination (HR) ([Khanna and Jackson, 2001; Helleday et al., 2007]. These involve different multi-protein processes [Friedberg, 2003] (Figure 2.18).

Non-homologous end joining (NHEJ) is due to the ligation of DNA double strand breaks that do not require sequence homology. The process of NHEJ is divided into four steps [Hall and Giaccia, 2012]. These are end recognition, end processing, fill-in synthesis, and ligation. DNA-dependent protein kinase (DNA-PKc), DNA end-binding protein KU (Ku70 and Ku80), DNA ligase IV, and XRCC4 in human are all the critical components of the NHEJ repair pathway [Norbury and Hickson, 2001].

End-recognition occurs when DNA-PK, which is composed of a heterodimer DNA-binding component, named Ku70/Ku80, forms a ring that binds specifically to either blunt or staggered DNA ends at the double-strand break. This DNA-KU complex then activates and recruits the large catalytic subunit kinase (DNA-PKc), a serine/threonine protein kinase.

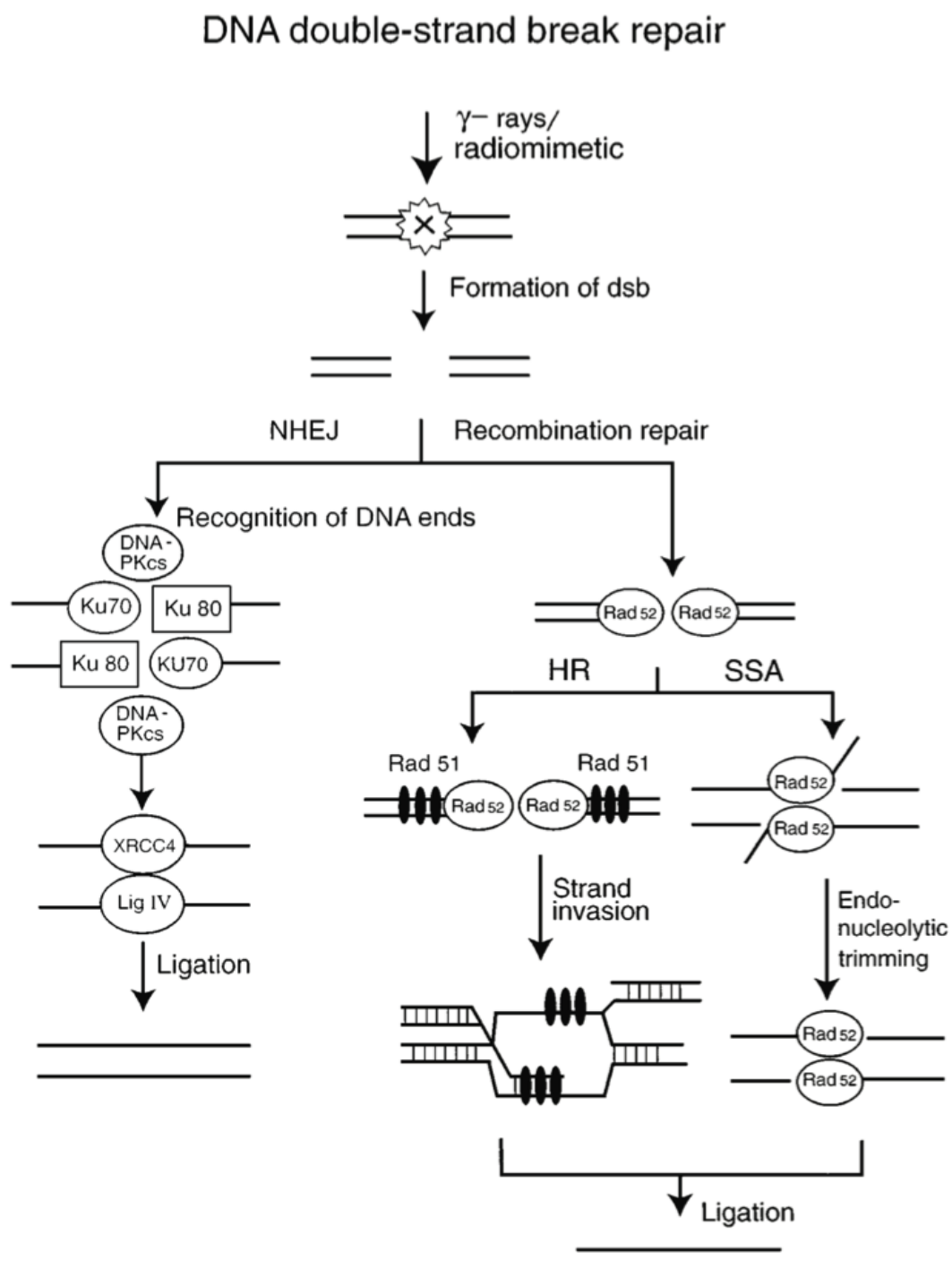


Figure 2.18: Repair mechanism of DNA double-strand break [Norbury and Hickson, 2001].

After binding to the two ends of the DNA the Ku/DNA-PKc complex undergoes autophosphorylation and may recruit additional proteins to the damaged site as potential phosphorylation substrate such as the NBS1, MRE111, and RAD50 proteins and the Artemis. The XRCC4 bind to DNA ligase IV (Lig IV) and then finally ligates the breaks to create intact DNA strands. It is unclear what signal is used for the fill-in reaction, but the XRCC4 gene products bound to DNA Lig IV have been found to be associated and may serve as the polymerase for the fill-in reaction when the broken ends become available for ligation [Helleday et al., 2007; Kao et al., 2005].

In contrast, HR is much more accurate and complex than NHEJ [Kao et al., 2005] but appears to be less important than NHEJ for repairing IR-induced breaks in higher eukaryotes [Rothkamm et al., 2003]. HR utilises extensive homology to restore the sequence at break site and processing involve the mediator protein Rad52 that plays a role in the search for a homologous DNA sequence [Kao et al., 2005]. Briefly, Rad51 as primary recombinase in eukaryotic cells initiates HR through catalysing homologous pairing and DNA strand exchange. Rad52 also acts during the single-strand annealing (SSA) [Norbury and Hickson, 2001].

Moreover, Rothkamm et al. [2003] first showed that both NHEJ and HR contribute to repair and radioresistance. As NHEJ is important in all cell cycle phases, HR is particularly important in late S/G<sub>2</sub> phases of the cell cycle [Willers et al., 2004] (Figure 2.19).

#### 2.1.5.4 Cell growth arrest

##### Cell cycle

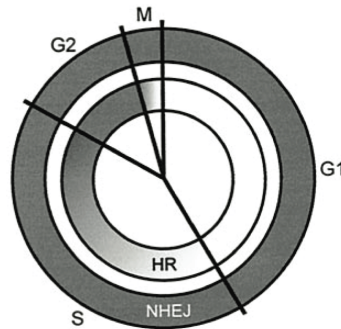


Figure 2.19: Schematic model of cell cycle phase as well as the contributions of homologous recombination (HR) and non-homologous end joining (NHEJ) of ionising radiation IR-induced DSB [Rothkamm et al., 2003].

In a population of dividing cells, whether inside the body (*in vivo*) or in a culture dish (*in vitro*), each cell passes through a series of defined stages, which constitutes the cell cycle [Karp, 2005] and is depicted in Figure 2.20. In contrast, the cell cycle for stem cells is up to 10 days [Suntharalingam et al., 2005]. The four phases of the cell cycle are the pre-DNA synthetic phase ( $G_1$ ), the DNA synthetic phase (S), the post-DNA synthetic phase ( $G_2$ ), and mitosis (M). Another phase,  $G_0$ , which is not part of the cell cycle, is a state where cells are not actively proliferating and have exited the cell cycle [Prasad, 1995].

As temporarily resting cells, the cells in  $G_0$  phase may enter the cell cycle or remain permanently outside (differentiated cells). By knowing the doubling time of cells in the culture, the timescale of the cell cycle (i.e the duration of each phase) can be estimated from the percentage of cells in this phase determined by flow cytometry (i.e univariate analysis of cellular DNA – section 3.9.2). For instance, for mammalian cells growing in culture: the S-phase (6–8 h), the M-phase (less than an hour),  $G_2$  (2–4 h), and  $G_1$  (1–8 h), making the total cell cycle of the order of 10–20 h [Suntharalingam et al., 2005].

### Cells radiosensitivity

Radiation sensitivity, expressed as loss of reproductive ability, depends on the

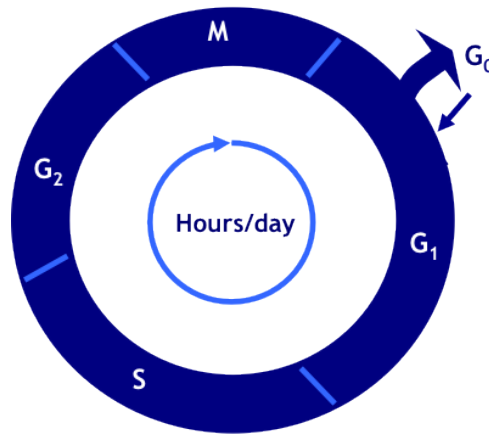


Figure 2.20: Stages of a standard eukaryotic cell cycle.

cell cycle phase in which the cells are exposed [Kiefer, 1990] (Figure 2.21). Generally, cells are most radiosensitive in the M and G<sub>2</sub> phase, and most radioresistant in the late S-phase (Figure 2.22), depending on the cell line studied.

#### DNA damage checkpoints

A checkpoint was defined originally as a specific point in the cell cycle when the DNA integrity was examined (checked) before allowing progression through the cell cycle. There are four distinct checkpoints in response to irradiation. Firstly, a checkpoint at the transition between G<sub>1</sub> and S phases, which plays an important role in deciding whether the cells initiate division or not. Secondly, the S-phase checkpoint causing the reduction of DNA synthesis which results in increasing the overall length of time to replicate DNA. Thirdly, the G<sub>2</sub> early checkpoint, which is activated by relatively low doses of radiation (e.g  $\sim 1$  Gy) and blocks the cell cycle progression at the end of G<sub>2</sub>. The final checkpoint, the G<sub>2</sub> late checkpoint, is commonly observed after irradiation. It causes a long G<sub>2</sub> delay before entry into mitosis [Wouters and Begg, 2009]. Therefore, the DNA damage checkpoints are biochemical pathways that delay or arrest cell-cycle progression in response to DNA damage [Sancar et al., 2004].

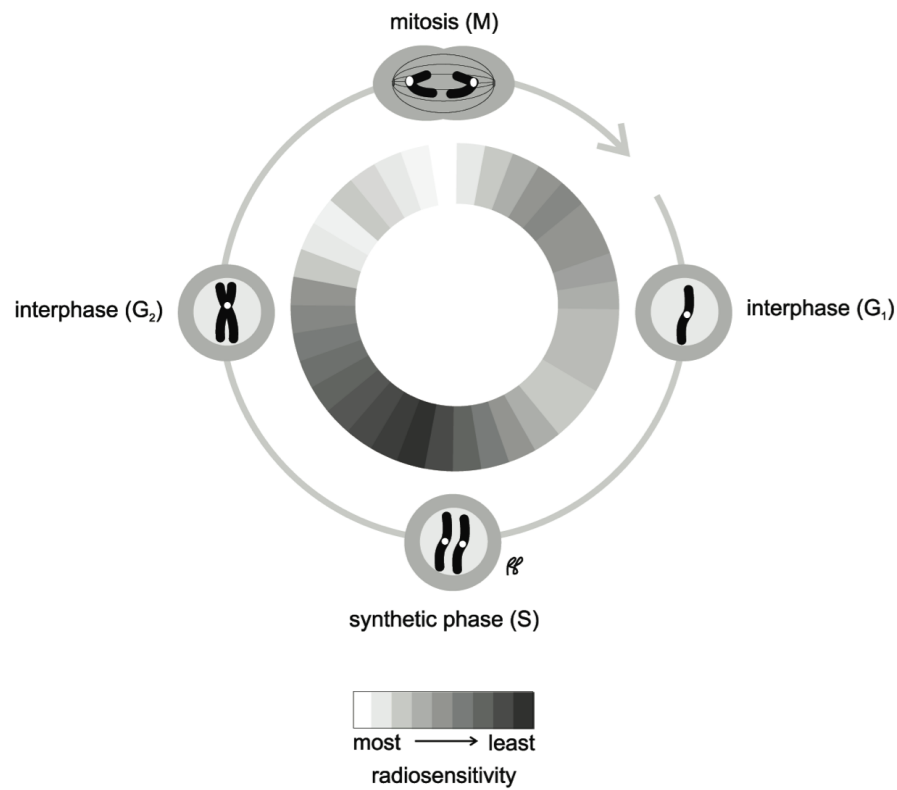


Figure 2.21: Radiosensitivity depends on the cell cycle [Suntharalingam et al., 2005].

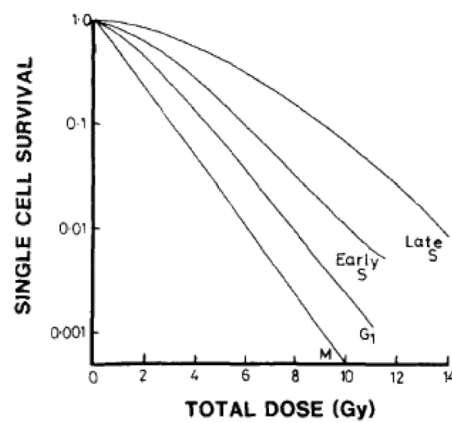


Figure 2.22: Cell survival curves at various stages of the cell cycle.

Following the ionising radiation, cells arrest at the checkpoints. Consequently, the failure to achieve completion of the cell cycle events may lead to cell death.

#### **2.1.5.5 Cell death**

Apoptosis or programmed cell death is a series of morphological and biochemical changes that take place in cells, which have been instructed to die. In radiobiology, a cell is commonly defined as dead when it fails to produce a colony of more than fifty descendant cells, this is more accurately called a loss of proliferative capacity [Lawrence, 1971]. Investigation of radiation-induced cell death in terms of a loss of proliferating capacity is used in this study.

## **2.2 Introduction to Nanotechnology and Nano-medicine**

The application of nanotechnology to medicine, also known as nanomedicine, concerned with the use of nanomaterials with unique physicochemical properties, such as small size, large surface area (SA) and a high reactivity different from bulk materials [Moreno-Vega et al., 2012]. It provides an innovative approach that can enhance the effectiveness of radiotherapy [Allard et al., 2010].

Over recent years, ceramic nanoparticles have been widely used in biomedical applications because of their biocompatibility with tissues and cells. Among many nanomaterials studied for cancer diagnosis and therapy, the engineered nanostructure particles (NSPs) used in this study were cerium oxide, which has a potential as a radioprotectant, and tantalum pentoxide and bismuth oxide, which both have potential as radiosensitisers.



## 2.3 Principles of Chemo-radiotherapy

### 2.3.1 Introduction to Chemo-radiotherapy

Chemo-radiotherapy is a combination of chemotherapy and radiotherapy, widely being researched for use in the treatment of cancer. Radiotherapy uses high-energy X-rays to instigate tumour cell apoptosis via secondary electrons. The drugs utilised in chemotherapy have specific mechanisms to inhibit tumour cells from dividing, this ensuring that they stop growing or eventually die. Thus, the combination of radiotherapy with chemotherapy represents an exciting opportunity to give rise to a method to enhance the cancer cell killing effect.

When both chemotherapy and radiotherapy are administered concomitantly, lower doses of one or both are often needed, thus reducing toxicity on healthy cells [Hahn and Maity, 2009]. Moreover, the chemoradiation may help overcome the radioresistance of tumour cells and sensitise them to the cytotoxic effects of ionising radiation. This is expected to enhance tumour control and minimise the radiation toxicity of healthy tissues by allowing dose reduction [Bischoff et al., 2009]. This is one of the main aims of this thesis, where it is proposed to use the synergy of pharmacological drugs and radiations that will either:

*allow for the reduction of the required dose of both radiation and targeted chemotherapy drugs without compromising the desired treatment outcome,*  
*and/or*  
*increase the lethal damage to the tumour target with equivalent or less toxicity to the surrounding normal tissue.*

### 2.3.2 General Mechanism of Chemo-radiation Interaction

DNA damage can be induced by chemotherapy and radiotherapy acting synergistically as ionising radiation induced DNA damage (e.g. SSB and DSB). The addition of chemotherapy drugs (e.g. cisplatin that target DNA) can also work in combination to make the damage induced by the radiation dose significantly more difficult to repair.

There are several other specific mechanisms of chemotherapy and radiotherapy such as platinum analogs, taxane-based, mitomycin-C-based, tirapazamine-based, and temozolomide-based chemoradiotherapy. In this project, only anti-metabolite-based chemo-radiotherapy is used. Consequently, only those are described in more detail.

The hypothesis of the work described in this thesis is based around one of the general mechanisms of chemotherapy in that it can inhibit post-radiation damage repair. Since DNA synthesis and repair share common pathways, the rationale for using thymidine antimetabolites (i.e MTX as DNA synthesis inhibitors) is that they act as the agents that affect nucleoside and nucleotide metabolism with radiation as a means of inducing more cytotoxic damage to tumour cells when combined with halogenated pyrimidine analog (i.e BrUdR).

### 2.3.3 Chemotherapeutic Agents

Most anticancer drugs act by disrupting the function of DNA and are classed as cytotoxic. Some act directly on the DNA whilst others (e.g. antimetabolites) act indirectly by inhibiting the enzymes involved in DNA synthesis or

its nucleotide building blocks [Hall and Giaccia, 2012; Patrick, 2005].

### 2.3.3.1 Antimetabolites

Antimetabolites can be defined as analogues of the metabolites required for cell function and replication. They damage cells by interacting with enzymes and interfering with their structure by any of its mode of actions to incorporate with nucleic acids. This inhibits their normal function and induces apoptosis (cell death process). They also compete for binding sites of the enzymes. In other words, antimetabolites are drugs that interfere with normal cellular function, particularly the DNA synthesis that is required for replication [Siu and Moore, 2005], with the added possibility of selectivity toward cancer cells due to their faster division [Avendaño and Menéndez, 2008]. Some of the many clinically useful metabolites are purine or pyrimidine analogs (i.e. 5-fluorouracil). These metabolites inhibit the synthesis of DNA (and sometimes RNA) by either inhibiting the formation of the normal nucleotides or interacting with DNA to prevent further new DNA strand extension, leading to an inhibition of the cell division [Siu and Moore, 2005; Avendaño and Menéndez, 2008].

Among the many compounds known to inhibit the reactions of the DNA biosynthesis pathway, only methotrexate (MTX) and 5-fluorouracil (5-FU) are used in this project as these two drugs have been widely used as anticancer drugs worldwide for more than 50 years. Thus, it was proposed to use both MTX and 5-FU as competitive inhibitors of enzymes, dihydrofolate reductase (DHFR) and thymidilate synthase (TS), respectively. This is described in more detail below.

**Methotrexate (MTX)** is not a nucleoside analogue, it is an analogue of

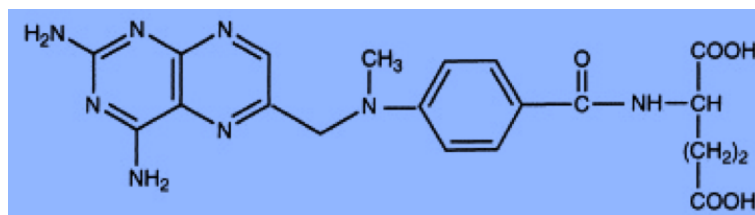


Figure 2.23: Chemical structure of the antifolate MTX [Hatse et al., 1999]

the vitamin folic acid (Figure 2.23). MTX is one of the anti folates that are not nucleoside analogues and prevent the formation of reduced folates, which is required for DNA synthesis. Reduced folate is required for transfer of methyl groups in purines biosynthesis and in the conversion of deoxyuridine monophosphate (dUMP) to deoxythymidine monophosphate (dTMP), which is a reaction catalysed by thymidilate synthase (TS). In the latter reaction, reduced folate becomes oxidised and its generation is dependent on the enzyme dihydrofolate reductase (DHFR).

DHFR is a critical enzyme that catalyses the reduction of dihydrofolate ( $\text{FH}_2$ ) to tetrahydrofolate ( $\text{FH}_4$ ), which is essential for DNA synthesis. MTX (with similar structure to  $\text{FH}_2$ ) is a competitive inhibitor of DHFR, a key enzyme in the thymidilate cycle, which is resulting the  $\text{FH}_4$ , is then not produced. A result of this inhibition may be blocking of the DNA synthesis due there being no available dTMP and/or purines, which can lead to cell death (by inhibiting the *de novo* synthetic pathways) [Siu and Moore, 2005; Kamen and Drachtman, 2000; Tehei et al., 2006; Huennekens, 1994; Hatse et al., 1999].

**5-Fluorouracil (5-FU)** is halogenated pyrimidine analog, a drug that resembles the pyrimidine bases uracil (RNA) and thymine (DNA) [Siu and Moore, 2005] (Figure 2.24) by inhibiting the TS. As mentioned above, TS catalyses the conversion of dUMP to dTMP, in a reductive methylation that involves the transfer of a carbon atom from 5,10-methylene tetrahydrofolate ( $\text{CH}_2\text{FH}_4$ )



Figure 2.24: Chemical structure of the 5-fluorouracil [Hatse et al., 1999]

to the 5-position of the pyrimidine ring [Avendaño and Menéndez, 2008].

5-FU is converted in the body to the fluorinated analogue of 2-deoxyuridylic acid monophosphate (FdUMP), which then combines with the enzyme and the  $\text{CH}_2\text{FH}_4$  to form a suicide substrate *in situ* and the reaction mechanism proceeding normally. The  $\text{FH}_4$  has formed a covalent bond to the uracil skeleton via the methylene unit, which is usually transferred to uracil. At this stage, things start to go wrong when a proton is usually lost from the 5-position of uracil, but 5-FU has a fluorine (F) atom at that position instead of hydrogen (H) atom. The fluorouracil remains covalently and irreversibly bound to the active site as uracil. As a result, thymidine synthesis is now terminated, which in turn stops the DNA synthesis [Patrick, 2005] and 5-FU could be incorporated in DNA. 5-fluorouracil is the main inhibitor of TS [Pinedo and Peters, 1988; Shewach and Lawrence, 2007].

Thus, MTX has an indirect effect on thymidilate synthase by lowering the amount of  $\text{CH}_2\text{FH}_4$ , whereas 5-FU acts to inhibit TS directly. These mechanisms are illustrated in (Figure 2.25).

Moreover, an investigation to the parenteral 5-FU and folinic acid formulations also presented in parallel to this study (termed Fluorodex) [Locke et al., 2009; Stutchbury et al., 2010].

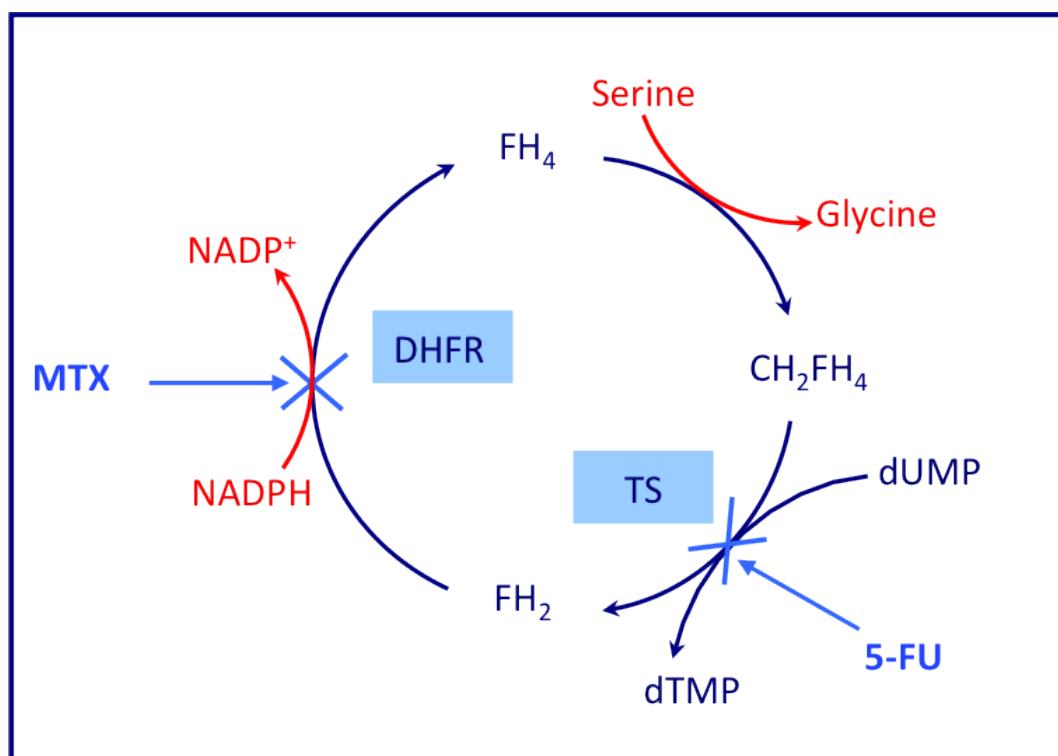


Figure 2.25: Schematic diagram of mechanisms of methotrexate (MTX) and 5-fluorouracil (5-FU) on thymidilate cycle. DHFR= dihydrofolate reductase; TS= thymidilate synthase;  $\text{FH}_4$ = tetrahydrofolate;  $\text{FH}_2$ = dihydrofolate;  $\text{CH}_2\text{FH}_4$ = 5,10-methylene tetrahydrofolate; dUMP= deoxyuridine monophosphate; dTMP= deoxythymidine monophosphate.

## 2.3.4 Radiosensitiser Drugs

### 2.3.4.1 Halogenated pyrimidine

Numerous studies have shown that pyrimidine analogues, especially halogenated deoxyuridine, that are incorporated into deoxyribonucleic acid (DNA) of dividing cells act as radiosensitisers. Of these agents, iododeoxyuridine (IUdR) and bromodeoxyuridine (BrUdR), which is incorporated into DNA as a thymidine substitute, show good radiosensitising activity at non-toxic doses [Djordjevic and Szybalski, 1960]. The halogen atom (i.e Br or I) replaces the hydrogen at the 5-position on the pyrimidine ring of deoxyuridine. The Van der Waals radii of bromine (Br) and iodine (I) are 1.95 Å and 2.15 Å, respectively, which closely resembles the methyl group of the thymidine (2.0 Å). Therefore, they are known as pyrimidine thymidine analogues [Djordjevic and Szybalski, 1960; McGinn and Kinsella, 1993; Tubiana et al., 1990] (Figure 2.26). There is a large literature on these compounds. Only the literature for BrUdR is relevant for this thesis.

The 5-bromo-2'-deoxyuridine or bromodeoxyuridine (BrUdR) (Figure 2.27) is one of the most well-known radiosensitisers for use in radiotherapy treatment of cancer. It has been studied in the lab and clinical setting for more than 50 years. BrUdR has been shown to enhance cytotoxicity when administered concurrently with radiation [Shewach and Lawrence, 2007] by either increasing DNA DSBs or inhibiting their repair [Iliakis and Kurtzman, 1989].

Figure 2.28 illustrates the main mechanism of cytotoxicity through which radiosensitiser drugs (i.e BrUdR and IUdR) act as nucleoside analogues via incorporation into the DNA. Its effect is to alter the deoxynucleotide pools (i.e dATP, dTTP, dGTP, dCTP) and may contribute to radiosensitisation [Shewach

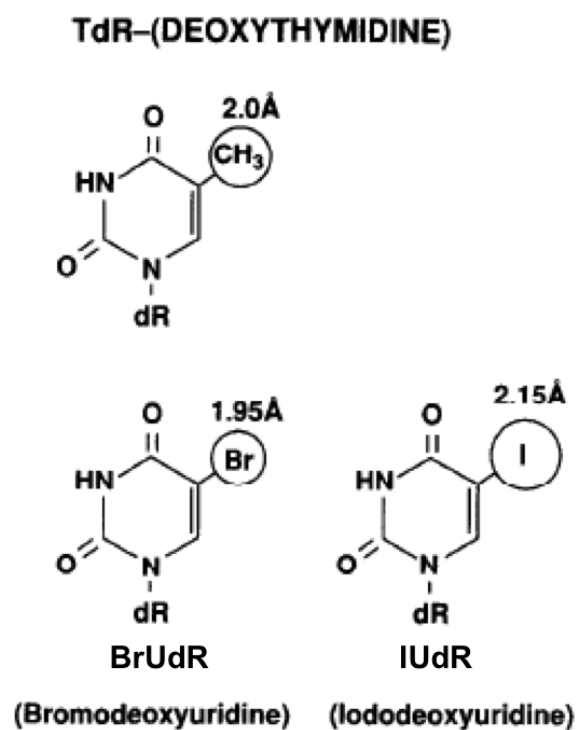


Figure 2.26: Chemical structure of thymidine and their analogs (BrUdR and IUdR), with Van der Waals radii of atoms at 5-position represent in the circles (modified from McGinn and Kinsella [1993]).

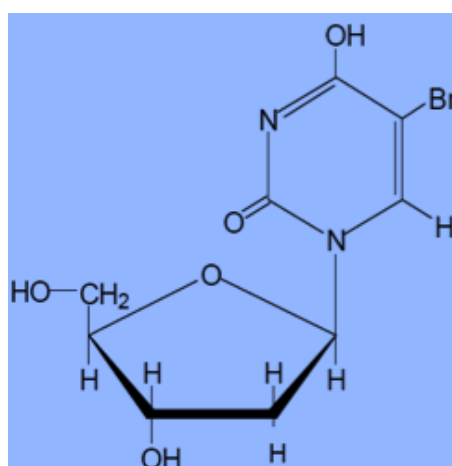


Figure 2.27: Chemical structure of bromodeoxyuridine (BrUdR).



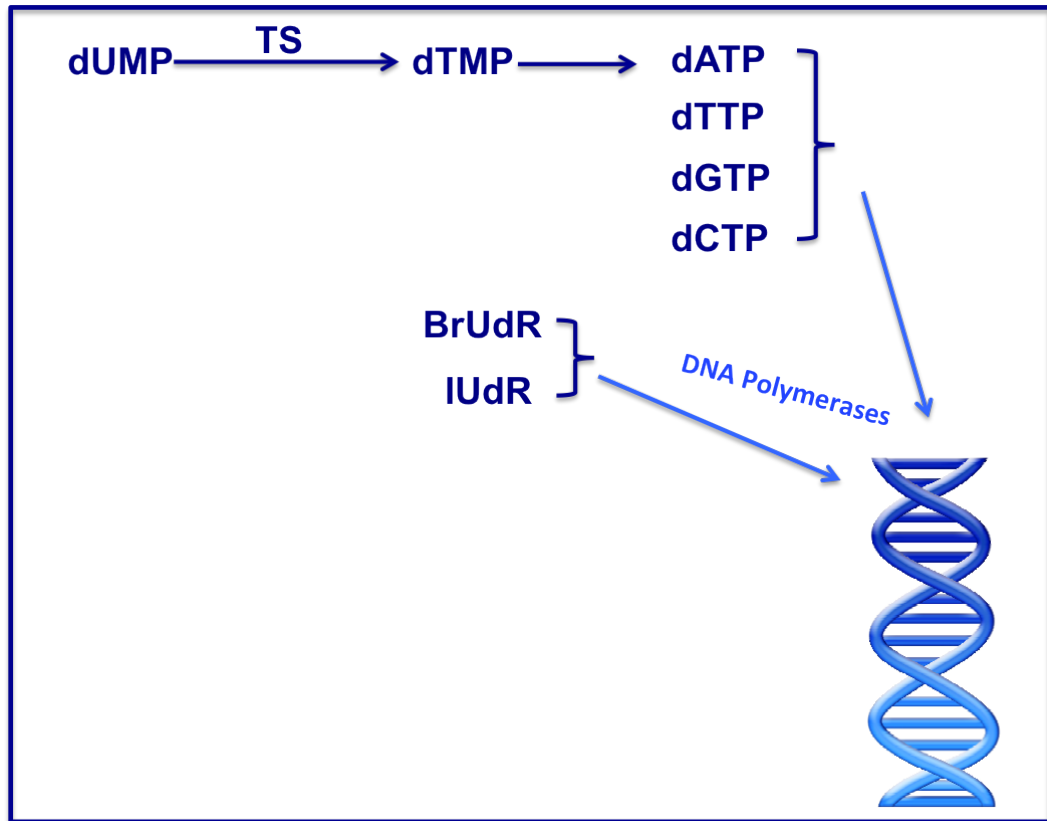


Figure 2.28: Schematic diagram of the target for radiosensitiser drugs. dUMP= deoxyuridine monophosphate; dTMP= deoxythymidine monophosphate; TS= thymidilate synthase; dATP= deoxyadenosine triphosphate; dTTP= deoxythymidine triphosphate; dGTP= deoxyguanosine triphosphate; dCTP= deoxycytidine triphosphate.

and Lawrence, 2007] (Figure 2.28).

## 2.4 Enhancement of radiation effect by high-Z elements

As mentioned above, using photons in the kilo-electron voltage (keV) range enhances the radiation dose enhancement mainly as a result of the additional photoelectric interactions arising from the increased interaction cross section, which are highly Z dependant, of the high-Z material.

Furusawa et al. [1991] studied Auger enhancement by a bromine atom, which was incorporated in phage DNA as bromodeoxyuridine and showed that enhancement of radiobiological effects by bromine atom is caused by the K-shell ionisation followed by Auger effects. Shinohara et al. [1985] were the first to report data on the enhanced killing of mammalian cells pre-labeled with 5-bromodeoxyuridine for mammalian cells. Similar work was carried out done by sensitising the mammalian cells with 5-bromodeoxyuridine [Larson et al., 1989] and with 5-iododeoxyuridine [Laster et al., 1990, 1993]. It was also demonstrated that a platinum-containing molecule acts as a radiosensitiser when photons with energy close to that of the absorption edge of the inner shell of platinum are used [Le Sech et al., 2000, 2001]. In the work of this thesis, the enhanced radiosensitivity effects of BrUdR to external X-ray irradiation were investigated, using the 9L rat gliosarcoma cells.

### **2.4.1 Auger Effects**

#### **2.4.1.1 Introduction**

In 1925, a 26-year old French physicist, Pierre Victor Auger described a new phenomenon that later became known as the Auger effect. He was investigating the pattern of electron tracks produced by irradiation of a cloud chamber with low-energy X-rays and noted the production of multiple electron tracks ([Kassis et al., 2004; Hofer, 2000]). He concluded that this event was caused by electron transitions that are initiated when low energy X-ray photons impinge on target atoms and eject inner shell electrons [Hofer, 2000]. The resulting vacancy leads to the emission of characteristic X-rays (a radiative process) and low-energy Auger electrons (a non-radiative process – Auger process), in the emission of Auger, Coster-Kronig, and super Coster-Kronig electrons [Hofer, 2000; Howell, 2008]. It was later shown that the Auger effect occurs in many

radionuclides that decay by electron capture (EC) or internal conversion (IC) ([Kassis et al., 2004; Hofer, 2000]).

In the case of the photons utilised in this study, when their energy is higher than the inner-shell binding energy of the target atom, an electron can absorb the photons via a photoelectric effect and thus a vacancy is produced. The probability of photoelectric interaction depends upon both the photon energy and the targeted element (as mentioned earlier). The ionisation of a specific inner-shell state is effectively induced by choosing an appropriate energy of the incident X-rays, synchrotron radiation is the only light source that gives access to intense monoenergetic photon sources. However, it should be noted that Auger effects are induced very frequently in X-ray irradiated samples even though X-rays are not monochromatised [Kobayashi et al., 2010].

#### **2.4.1.2 Biological effect of radiation-induced Auger Effect**

The biological significance of Auger electrons for therapeutic purposes was neglected for many years because of their low energy, and consequent short range, compared to the energy released from a decaying radionuclide [Hofer, 2000; Kassis, 2003]. Auger electrons travel a distance of 2 – 500 nm, which results in a high-LET radiation that in the range of 2 – 25 keV/ $\mu\text{m}$  ([Kassis et al., 2004; Sastry, 1992; Charlton et al., 1987]. Investigations and applications of the photoabsorption spectra at the X-rays energy level have failed due to the polychromatic nature of X-rays from X-ray tubes [Kobayashi et al., 2010]. This was the state of play until the founding meeting in 1975 that was organised by Ludwig Feinendegen in Jülich, Germany that focused on the biological aspects of the Auger process [Howell, 2008].

In this thesis, the radiobiological effects of Auger electrons released as the consequence of photoelectric effect (induced by external X-ray beams) is mainly investigated in the presence of chemotherapeutic drugs (MTX) and radiosensitiser drugs containing a high-Z material (i.e. BrUdR) loaded and incorporated into DNA to produce more lethal damage.

Experimental investigations into BrUdR were initiated in the 1960s but fell out of favour in the late 1980s. The emphasis was on determining the optimum concentration of the drugs used or designing a new radionuclide. However, there were no studies that investigated optimising X-ray beam energies using conventional X-rays machines or LINACs (i.e polychromatic). Beam energies of 50 – 250kVp, 6 MV, and 10 MV are explored as part of the work described in this thesis.

# Chapter 3

## Materials and Methods

### 3.1 Materials

Nalgene® cryogenic vials and Mr.Frosty freezing container were purchased from Thermo Fisher Scientific, VIC, Australia. Unless otherwise noted, all tissue culture plasticware were from Becton-Dickinson (BD Falcon™).

#### 3.1.1 Cell Lines

The rat gliosarcoma (9L), human glioblastoma (U-87 MG), and Madin Darby Canine Kidney (MDCK) cell lines were obtained from the European Collection of Cell Cultures (ECACC) distributed by Westmead Children Hospital and Sigma-Aldrich, Australia. The human breast carcinoma (MCF-7) cell line was obtained from the American Type Culture Collection (ATCC), kindly provided by A/Prof. Marie Ranson from IHMRI (Illawarra Health and Medical Research Institute), Wollongong, Australia. Detailed information about the cell lines used in this study are provided in Appendix A.

### 3.1.1.1 Cryopreservation

Dimethylsulfoxide (DMSO) is the most commonly used cryoprotective agent, which prevents ice crystal forming and the fragmenting of membranes [Macleod and Langdon, 2004]. The freezing medium Gibco<sup>TM</sup> (90% medium; 10% DMSO) were used for 9L cell line, whilst freezing mixtures of (95% medium; 5% DMSO) were freshly made for U-87MG, MCF-7 and MDCK cell lines. The cell stocks of all the cell lines is stored in liquid nitrogen at  $-196^{\circ}\text{C}$ .

### 3.1.2 Cell Culture Reagents

Dulbeccos modified eagles medium (DMEM), foetal bovine serum (FBS), penicillin/streptomycin (Pen Strep), trypsin-ethylenediaminetetraacetic acid (Trypsin-EDTA), phosphate buffer solution (PBS), and Hanks balanced salt solution (HBSS) were purchased from Gibco<sup>TM</sup> (Invitrogen Life Technologies, NSW, Australia).

### 3.1.3 Drugs and Other Chemicals

Methotrexate (MTX), 5-bromo-2'-deoxyuridine (BrUdR), 5-fluorouracil (5-FU), propidium iodide (PI), 2',7'-Dichlorofluorescein diacetate (DCFDA) and all other reagents were purchased from Sigma-Aldrich (Sigma-Aldrich Chemicals, MO, USA) unless specified otherwise. Fluorodex is kindly provided by A/Prof. Ranson from IHMRI.

### 3.1.4 Nanostructured particles

The nanomaterials  $\text{CeO}_2$  and  $\text{Ta}_2\text{O}_5$  were synthesised by Dr Konstantinov, a TNT member of Institute for Superconducting and Electronic Materials (ISEM). All the nanoparticles were dried and sterilised at  $121^\circ\text{C}$  before addition to the cells.

#### 3.1.4.1 Ceramic Nanoparticles

All the nanoparticles samples were synthesised at the ISEM. Cerium oxide was synthesised using a spray-pyrolysis technique derived from previous work [Briggs et al., 2013]. Tantalum pentoxide was synthesised using  $\text{Ta}(\text{OEt})_5$  via an ethoxide decomposition reaction with water, which is derived from Kominami et al. [2001]. Bismuth oxide was synthesised from bismuth (III) nitrate pentahydrate –  $\text{Bi}(\text{NO}_3)_3$  using two techniques: a precipitate method (in argon and air annealed) [Stewart et al., 2014] and a citrate gel method derived from [Patil et al., 2005] and Anilkumar et al. [2005], respectively.

#### 3.1.4.2 X-ray Diffraction (XRD)

After the nanoparticles were synthesised, they were analysed using X-ray diffraction (XRD). The XRD analysis was performed using an automated GBC® eMMA X-ray Diffractometer (GBC, Vic, Australia). Phase identification was extracted by comparing the recorded diffraction pattern with the Inorganic Crystal Structure Database (ICSD). The average nanoparticle crystallite size ( $\overline{Tc}$ ) is extracted from the X-ray diffraction data using Scherrers equation:

$$\overline{T_c} = \frac{K\lambda}{\beta \cos(\theta_B)} \quad (3.1)$$

where  $K$  is the shape factor constant ( $K = 0.89$ ),  $\lambda$  is the X-ray beam wavelength,  $\beta$  is the FWHM (full-width half-maximum) in radians and  $\theta_B$  is the Bragg angle.

#### 3.1.4.3 Transmission Electron Microscopy (TEM)

The particle size and morphology of the nanoparticles were determined by high resolution Transmission Electron Microscopy (TEM). TEM was performed using a JEOL 2011 high-resolution (HR) instrument.

#### 3.1.4.4 Sonicator

The Branson Sonifier® S-250D digital with double-step Micro-tip (Consonic Pty Ltd., NSW, Australia) was used for sonication of nanoparticles.

### 3.1.5 X-rays Irradiated Machine

#### 3.1.5.1 Linear accelerator (LINAC) machine

The Axesse Elekta LINAC with beam modulator (Elekta AB, Kungstensgatan, Stockholm, Sweden) in the radiation oncology department at the Prince of Wales Hospital (Randwick, NSW, Australia) was used for cellular irradiations in the megavoltage (MV) energies range. X-ray energies of 6 and 10 MV were used to irradiate the cells. The dose rate was 0.5 and 5 Gy/min for 10 MV and 5 Gy/min for 6 MV. All doses (1, 2, 3, 5 and 8 Gy) were delivered in single



fractions at room temperature. The dose rate is altered by changing the beam dose rate in the LINAC without removing the flattening filter.

### 3.1.5.2 Kilovoltage (kV) orthovoltage machine

The Nucletron Oldelft Therapax DXT 300 Series 3 Orthovoltage unit (Nucletron B.V., Veenendaal, The Netherlands) in the radiation oncology department at the Prince of Wales Hospital (POWH) (Randwick, NSW, Australia) was used for cellular irradiations in the kilovoltage (kV) energies range. X-ray energies at 50, 125, 150 and 250 kVp were used to irradiate the cells for the same range of dose as MV above. Details of orthovoltage beams characteristic (e.g. mA and half-value layer HVL) used at the POWH is summarised in Table 3.1.

Table 3.1: Summary of orthovoltage beams used in this study at the POWH.

Filter no.	Energy (kv)	mA	HVL 30 cm FSD (cm) mm Al	HVL 50 FSD (cm) mm Cu	FSD (cm) mm Al
1	50	26	1.48		1.57
2	75	30	2.47		2.62
3	100	22	3.77		3.9
4	125	20	6.52		6.7
5	150	20		0.67	
6	200	15		1.47	
7	250	11		2.38	
8	300	10		3.66	

The mechanism for activation of high-Z materials requires an ionisation of one of its atom (i.e for BrUdR, it requires an ionisation of the bromine atom). This is the simplest and most important concept that underlies the understanding of what kind of radiation is required to give enough activation of the drug in order to maximise the dose enhancement effect. For instance, the synchrotron experimentation by [Corde et al., 2004] confirmed that the iodine

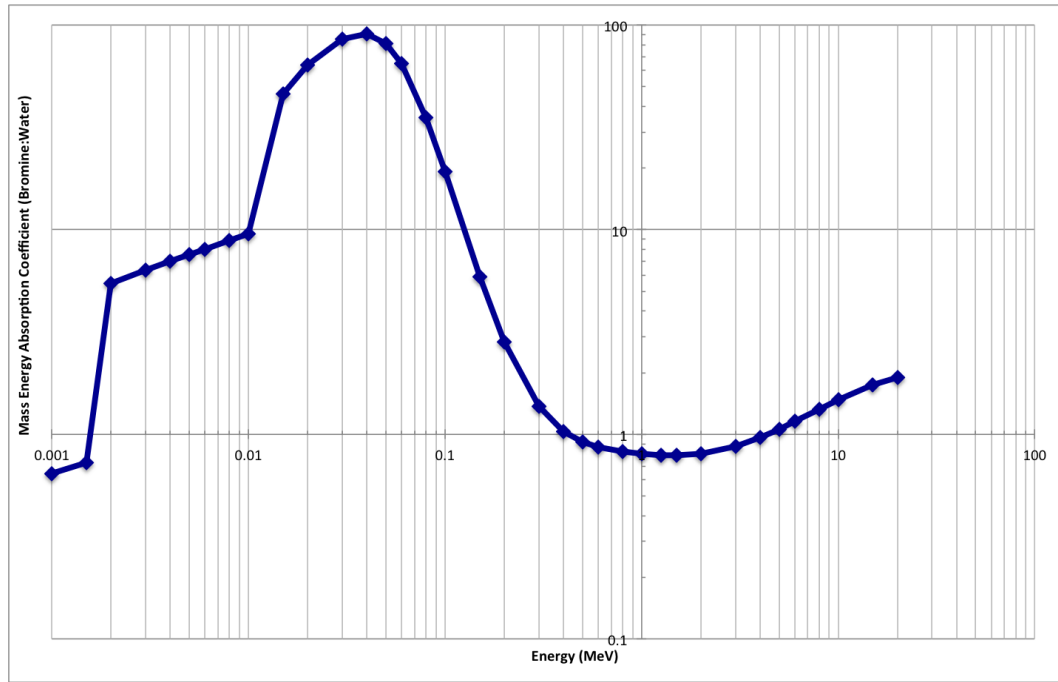


Figure 3.1: Ratio of the mass energy absorption coefficient of bromine to water relative to photon energy (MeV).

atom is ionised most efficiently just above its K-edge, with the peak of absorption compared to water occurs in the spectrum around  $\sim 50$  keV.

In this study, as in the case of BrUdR, the peak of absorption contrast relative to water in the spectrum around  $\sim 40$  keV is illustrated in Figure 3.1). Briefly, the full mass-energy absorption coefficients  $((\mu_{\text{en}}/\rho)_E)$  of bromine and water were obtained from the National Institute of Standards and Technology (NIST) and the ratio were then graphed as a function of energy (Figure 3.1).

Since the radiation photoactivation source used in this study is not monochromatic (i.e polychromatic), the optimum energy has to be carefully chosen. It is by using the available beam filters and their associated HVL (Table 3.1), the attenuation coefficient can be calculated. These were then interpolated to those listed by John and Cunningham [1983] to obtain the effective energies for our radiation spectrum. As the rule of thumb, the mean effective energy

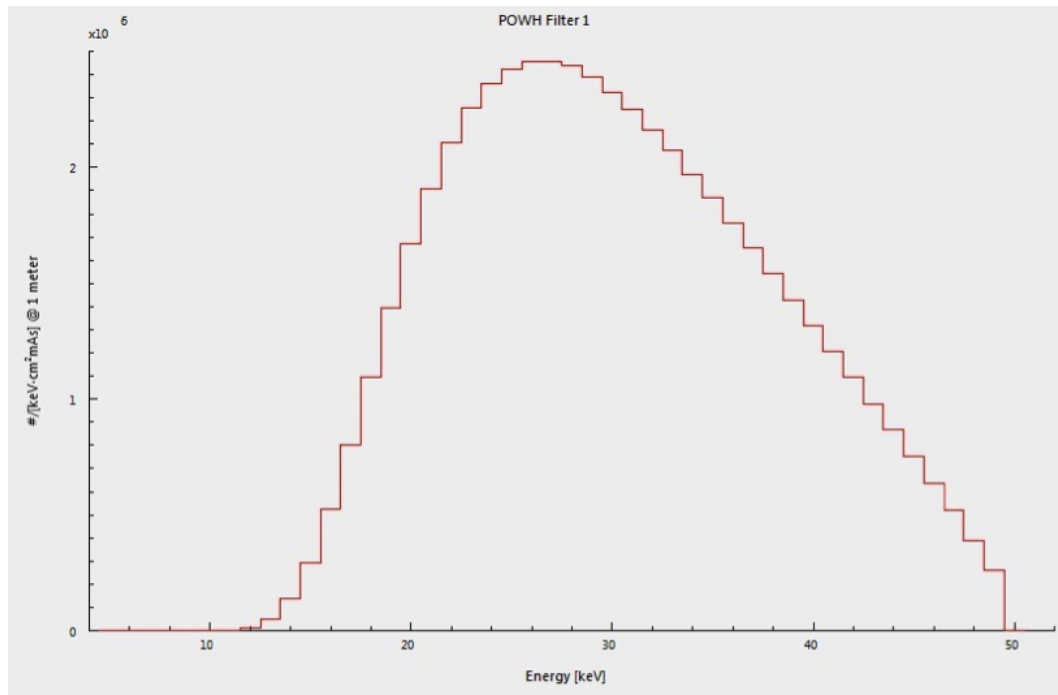


Figure 3.2: The output spectrum emitted from the orthovoltage X-ray unit at 50 kVp (filter 1) at the POWH.

delivered is about one-third of the maximum beam energy.

For instance, filter 4 (125 kVp) and filter 5 (150 kVp) was chosen as the optimal energy for both irradiation with BrUdR and the nanoparticles (cerium and tantalum details in section 4.5), respectively. To confirm this, the output spectra emitted from the orthovoltage machine was also generated by simulation. The SpekCalc X-ray spectrum generator [Poludniowski et al., 2009] was used to simulate the output spectra emitted from the X-ray unit of every filter used (Figures 3.2 – 3.5).

### 3.1.6 Flow Cytometer

Flow cytometry is an invaluable technique that has been applied extensively to many areas of radiation research at both the experimental and clinical level. It is used as an investigational technique in molecular radiobiology to iden-

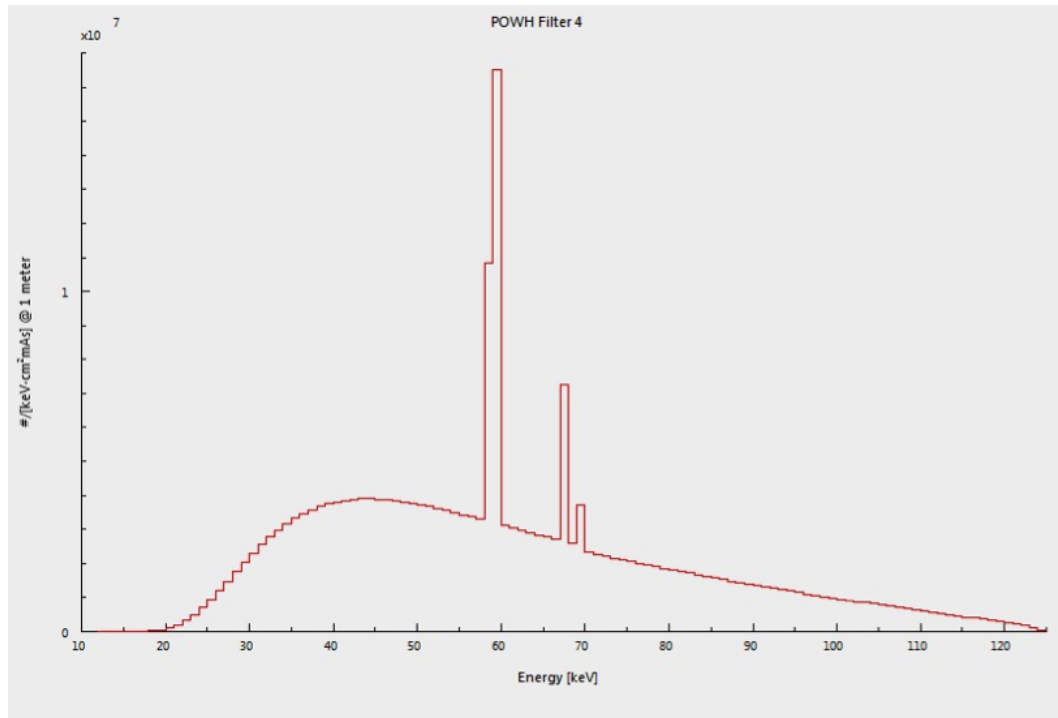


Figure 3.3: The output spectrum emitted from the orthovoltage X-ray unit at 125 kVp (filter 4) at the POWH.

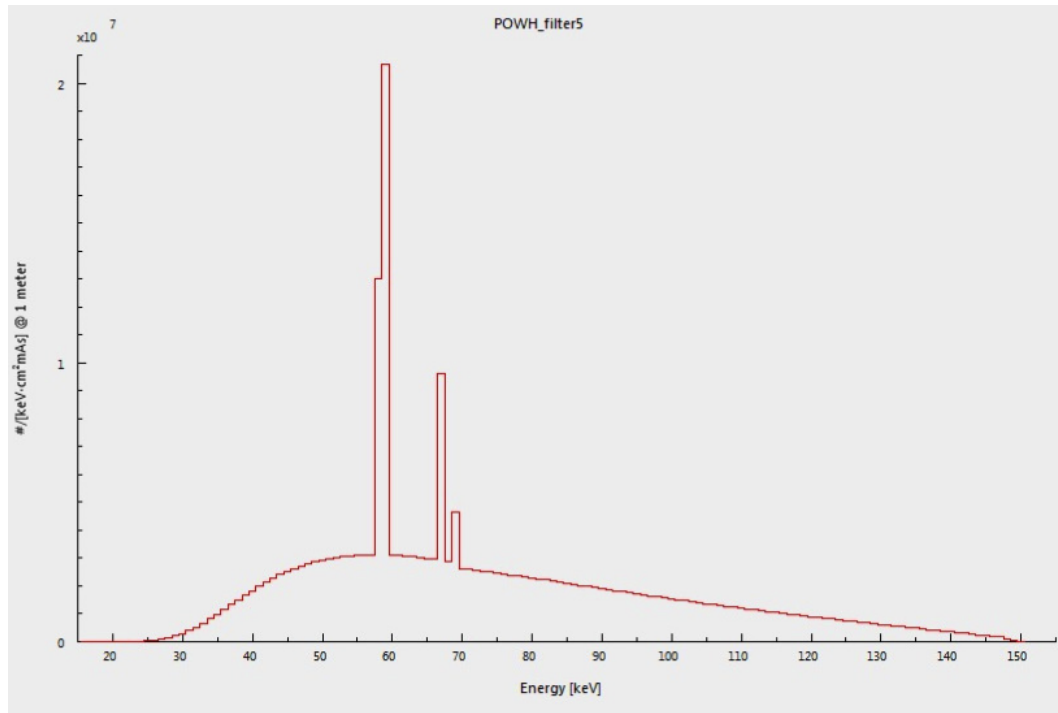


Figure 3.4: The output spectrum emitted from the orthovoltage X-ray unit at 150 kVp (filter 5) at the POWH.

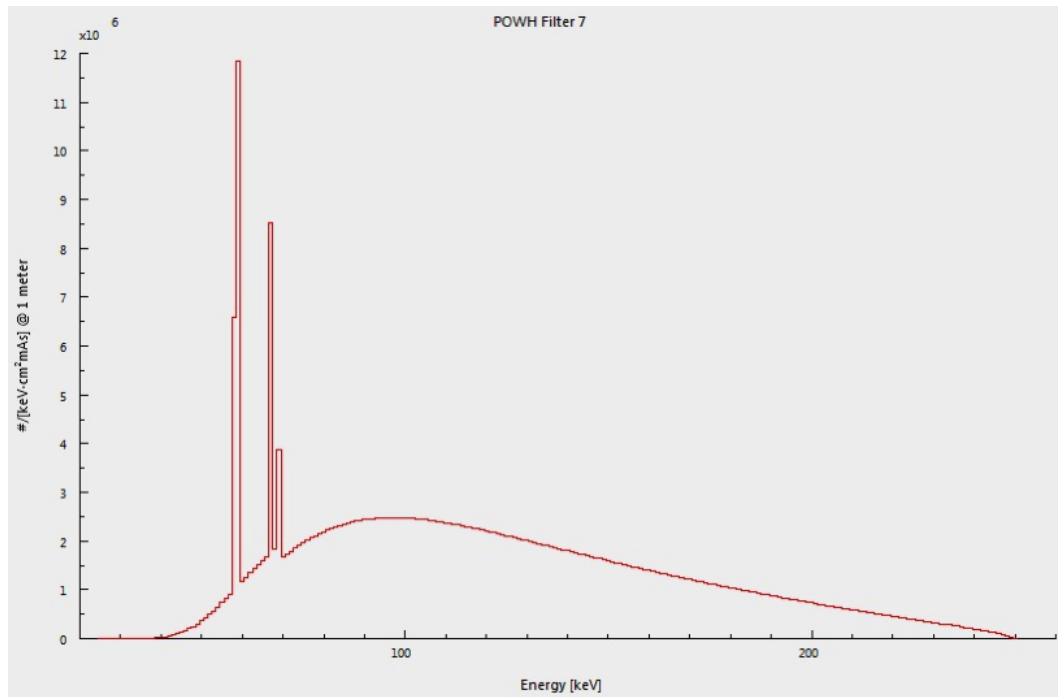


Figure 3.5: The output spectrum emitted from the orthovoltage X-ray unit at 250 kVp (filter 7) at the POWH.

tify and characterise the temporal response of cells to radiation damage such as those involved with cell cycle kinetics and DNA damage sensing and repair [Wilson and Marples, 2007]. It is a laser-based technology that is used to measure the physical and biochemical characteristics of biological particles [Radcliff and Jaroszeski, 1997]. Becton Dickinson fluorescence-activated cell sorting (FACS) flow cytometer (BD LSR II; BD Biosciences, USA) at IHMRI, Wollongong, Australia (Figure 3.6) was used for all flow cytometry analysis.

### 3.1.6.1 Overview of flow cytometric instrumentation

Flow cytometers scan single particles or cells in suspension [Dean and Hoffman, 2007] as they flow one at a time through a flow chamber (Figure 3.7) past an excitation light source [Radcliff and Jaroszeski, 1997]. Certain properties such as size and internal complexity of the particles are measured [BD, 2000, 2007]. To do this, a flow cytometer needs a combined system of: fluidics, optics and

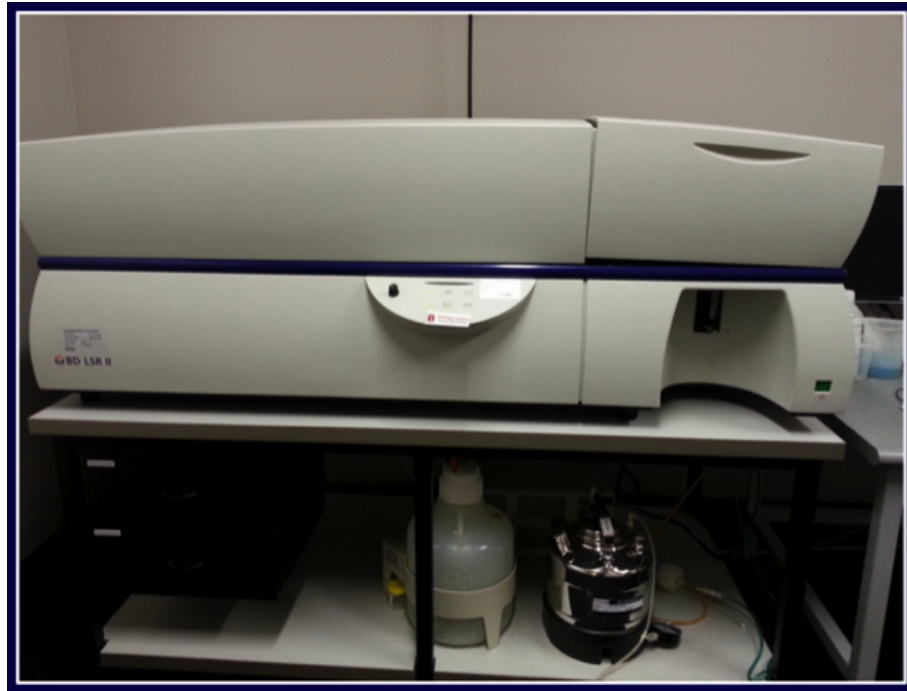


Figure 3.6: Becton Dickinson fluorescence-activated cell sorting (FACS) flow cytometer (BD LSR II; BD Biosciences, USA) at IHMRI, Wollongong, Australia.

electronic systems [BD, 2000, 2007].

**Fluidics system** A fluidics system in a flow cytometer moves cells in the fluid through a flow chamber (i.e. flow cell), past a light source (i.e. laser beam) and then into a waste tank [BD, 2000]. Figure 3.7 illustrates that a sheath stream is introduced to the flow chamber. Due to its higher flow rate ( $\sim 10\text{ml/min}$ ) than the sample ( $\sim 100\mu\text{l/min}$ ), it serves to compress the sample particles in a stable stream and confine them through the center of the flow chamber. This technique is known as hydrodynamic focusing [Dean and Hoffman, 2007].

**Optics system** When a cell or particle passes through a focused laser beam, laser light is scattered and emitted in all directions ( $360^\circ$ ). Light that scatters

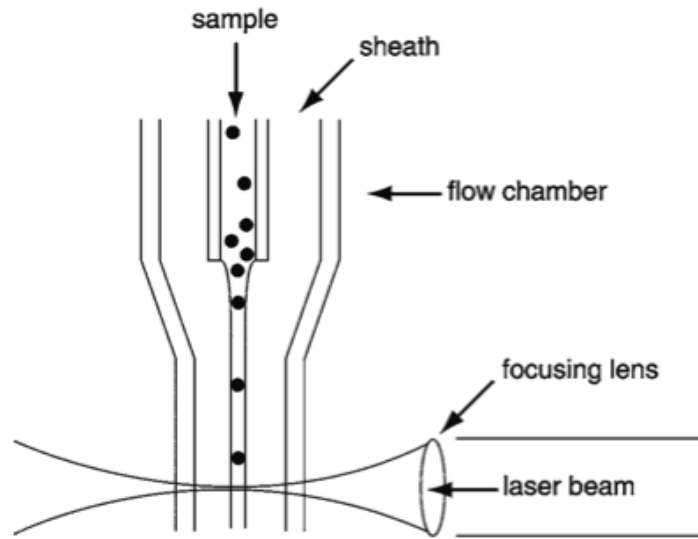


Figure 3.7: Flow chamber of a flow cytometer (longitudinal cross-sectional view) [Dean and Hoffman, 2007]. In this work, FACS LSR II from BD [BD, 2007]

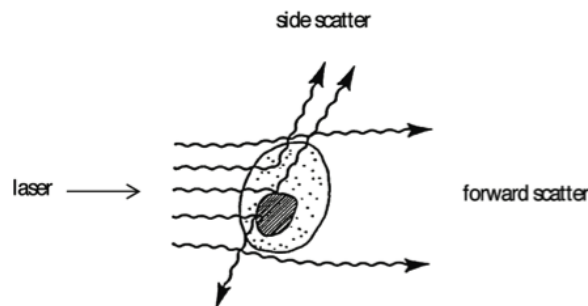


Figure 3.8: Forward scatter (FSC) and side scatter (SSC) [BD, 2000, 2007]

roughly in the forward direction is called forward scatter (FSC) and light that is scattered roughly perpendicular ( $90^\circ$ ) is called side scatter (SSC). Forward scattered light is a result of diffraction and indicates relative differences in the size of the cells or particles whereas side-scattered light, as a result of reflected and refracted light, indicates relative differences in the internal complexity or granularity of the cells (Figure 3.8) [Radcliff and Jaroszeski, 1997; BD, 2000, 2007].

The optics systems consist of excitation and collection optics. Excitation op-

tics include lasers as light source, filters and mirrors that route the laser light to the fluidic stream and modify the spectral distribution of light scatter and fluorescence directed to detectors.

Collection optics consist of detectors that collect and convert light signals into electrical signals that can be processed by the electronic system [BD, 2000]. Two types of signal detectors are used: the photodiode and the photomultiplier tube (PMT). The photodiode is used when the FSC signal is strong and photomultipliers that are very sensitive to light, are used when the light signal generated by SSC and fluorescence [Dean and Hoffman, 2007; BD, 2000].

**Electronic system** After light scatter and fluorescence is converted to electrical signals by the optical system, the resulting information is converted into digital data before being interpreted and stored by the computer. A schematic of the flow cytometry components is shown in (Figure 3.9).

Flow cytometry is particularly important for biological investigations because it allows both qualitative and quantitative examinations of whole cells and cellular constituents that have been labelled with dyes or monoclonal antibodies. It has become a powerful tool for use in clinical research due to its capability to process thousands of individual particles in a matter of seconds. In addition, it also has the powerful ability to sort particles based on light scattering and fluorescent emission characteristics [Radcliff and Jaroszeski, 1997; BD, 2000]. A more comprehensive review of the flow cytometer can be found in [Saphiro, 1988; Ormerod, 1999].



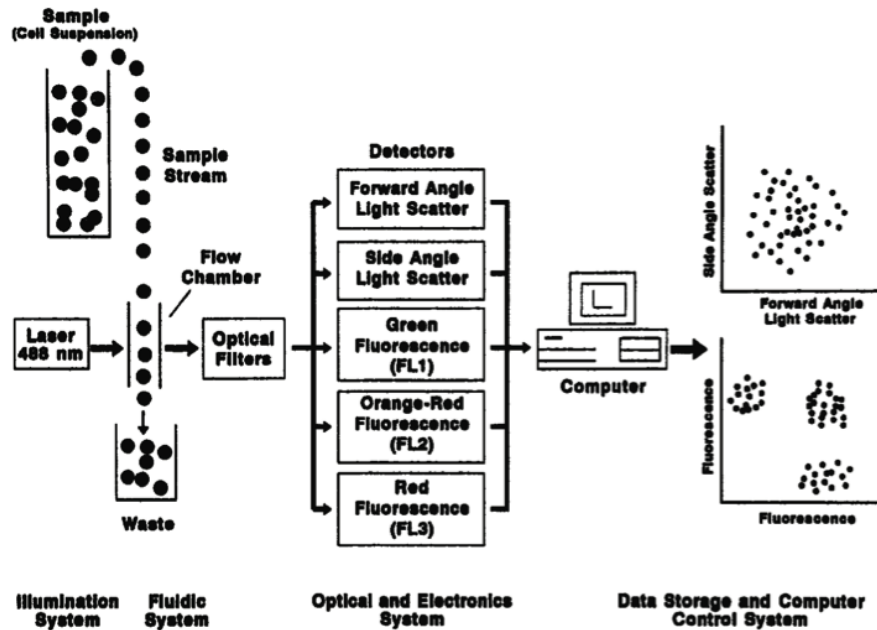


Figure 3.9: Schematic of flow cytometer systems

### 3.1.6.2 Fluorescence measurements

The stained nuclei were analysed for both DNA-PI and anti-BrUdR mouse monoclonal antibody (Clone MoBU-1) conjugated with Alexa Fluor 488 fluorescence on the FACS with excitation at 488 nm. The linear red fluorescence intensity was measured with a long-pass filter at 620 nm for PI detection. The log green fluorescence intensity was measured with a band-pass filter at 515 – 570 nm for the detection of Alexa Fluor 488 anti-BrUdR. A minimum of 10,000 single cell events was analysed for each sample in each experiment.

### 3.1.7 Confocal Microscope

Light and fluorescence microscopy images were obtained using a Leica confocal laser scanning microscope (Leica TCS SP5 Advanced System – UV-VIS-IR and X1-Port Access with SMD FCS and CO<sub>2</sub> incubation chamber, Germany) and the accompanying image manager software Leica Application Suite Advanced Fluorescence (LAS AF, v.2.6.1–7314, Germany) at IHMRI,

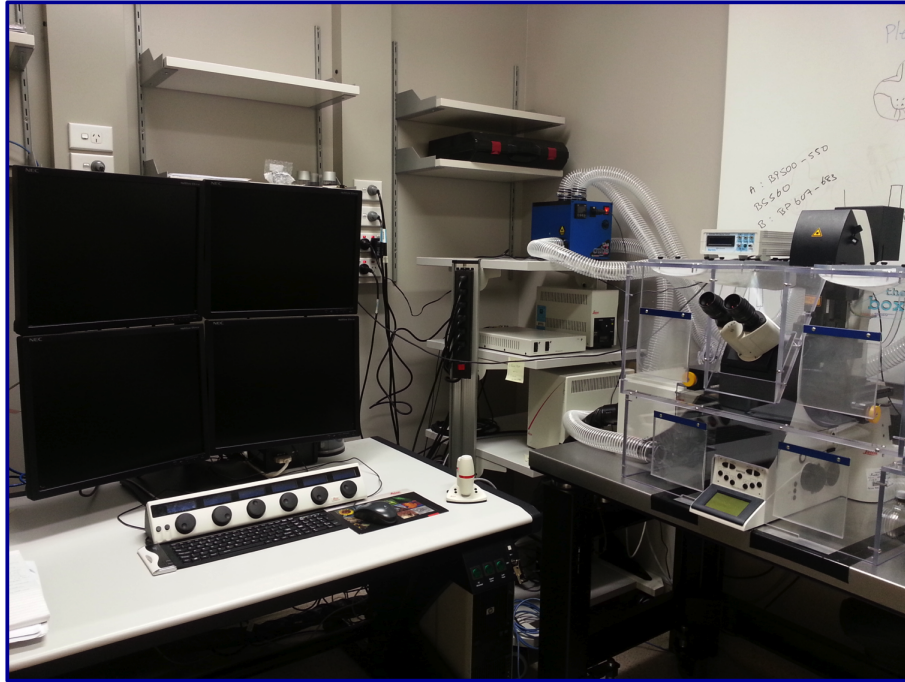


Figure 3.10: Leica confocal laser scanning microscope (Leica TCS SP5 Advanced System – UV-VIS-IR and X1-Port Access with SMD FCS and CO<sub>2</sub> incubation chamber, Germany at IHMRI.

Wollongong, Australia (Figure 3.10).

## 3.2 Cell Culture Methods

### 3.2.1 Subculture Cells

Cells were routinely maintained in the exponential growth phase in 75cm<sup>2</sup> cell culture flasks with a vented screw cap (Greiner Bio-one) in complete DMEM containing L-Glutamine and supplemented with 10% (v/v) FBS and 1% (v/v) Pen Strep) for 9L and MCF-7; and complete DMEM with sodium pyruvate supplemented with 10% (v/v) FBS and 1% (v/v) Pen Strep for U87-MG. All cells were maintained in a 37°C humidified 5% (v/v) CO<sub>2</sub> cell culture incubator (Heracell 150i). The cell concentration was maintained at  $2-4 \times 10^4$  cells/cm<sup>2</sup> and was routinely passaged upon reaching confluence for up to 30 passages. Following removal of the media, the monolayer was washed with PBS (Ca<sup>2+</sup>

and  $\text{Mg}^{2+}$  free), and the cell detached by incubating with 0.05% trypsin–EDTA at 37°C for 2-3 mins. Cell lines were routinely tested for mycoplasma contamination. All the cell culture experiments were carried out using cells in the exponential growth phase at IHMRI, Wollongong, Australia. Details of the procedure is provided in Appendix B.

### 3.2.2 Cell Counting

The most common way to determine the concentration of cells in a suspension is by using the Neubauer haemocytometer. Typically, the procedure is carried out after mixing an equal volume of the cell suspension with a solution of the dye Trypan blue. Trypan blue is excluded by live cells (which appear clear) but enters dead cells and stains them blue. So, with only the clear cells counted, the result indicates live cells per ml. All the counting procedures mentioned in this thesis were carried out using this technique. The details of procedure are provided in Appendix C.

### 3.2.3 Cryopreservation – Freezing and Thawing

#### 3.2.3.1 Freezing

Briefly, cells (in the exponential growth phase from 4 – 6 of T75cm<sup>2</sup> flasks) were washed and trypsinised as described above. A small aliquot of the cell suspension is taken and counted. Cells were then pelleted by centrifugation (e.g. 1500 rpm for 5 mins) and resuspended with the freezing medium to give a final concentration of  $2 - 4 \times 10^6$  cells/ml to each Nalgene® cryogenic vial. All cryogenic vials were then labelled (i.e cell name, passage number, date) and placed in a Nalgene® Mr.Frosty freezing container containing 250 mL

isopropanol to freeze the cells at a cooling rate between 1– 3°C/min and kept at –80°C in a freezer overnight. Then, all vials were transferred to a gas phase liquid nitrogen permanent storage vessel. The details of procedure are provided in Appendix D.1.

Shortly after freezing (after 24 hour in liquid nitrogen vessel), one vial of master stock was revived (to check the viability). The cells were then being expanded to freeze more vials (i.e. as working stock). The working stock will then be revived and is used until there are only 2 – 3 vials remaining. Then, when the working stock is depleted, another vial of master stock is revived to create another batch of working cell stocks. Details, including a schematic diagram and table, are provided in the Appendix D.1.

### **3.2.3.2 Thawing**

The cryogenic vial from the liquid nitrogen is placed in a 50 mL tube containing pre-warmed 70% ethanol. The tube was then rapidly warmed into a 37°C water bath. Once thawed, the cells were transferred into a new sterile flask and pre-warmed complete culture medium (i.e DMEM) was added. The medium was added dropwise while gently swirling the flask in a circular motion to slowly equilibrate the cells to the medium. At first, only few mLs were added very slow (e.g. 1 drop per second and then speeded up). The cells were pipette up and down gently and a small aliquot was taken and counted to check the viability of the cells. The cells were then maintained in a 37°C humidified 5% (v/v) CO<sub>2</sub> cell culture incubator (Heracell 150i). Once the cells have attached and had a chance to expel the DMSO, the media was removed and fresh media added. After the cells reach ~ 90% confluent, they were washed and detached as described above. The cell suspensions were then centrifuged (if required –

as this will effectively remove the DMSO from the cells) and the cell pellet were resuspend in the media. Then, the cells are maintain and subculture as necessary. The details of the procedure are provided in Appendix D.2.

### 3.3 Cell Growth Assay

#### 3.3.1 9L cell line

Cells were plated in a 60-mm petri dish (growth area = 21.3 cm<sup>2</sup>) in complete DMEM. Briefly, monolayers were washed and detached as above. Cell suspensions were diluted in a DMEM medium and were counted using a haemocytometer. The final concentration of  $5 \times 10^4$  cells in 5 ml was then plated into each 60-mm petri dish. Cell numbers were counted daily (triplicate for each day) for up to 10 days. Three independent experiments were performed. The second and third experiments were done with higher cell seeding on day 0 (i.e.  $2 \times 10^5$  cells) in 100-mm petri dish. The details of the procedure are provided in Appendix E.1.

#### 3.3.2 MCF-7 cell line

Cells were plated in a 100-mm petri dish (growth area = 58.95 cm<sup>2</sup>) either in complete DMEM or RPMI-1640 supplemented with 5% (v/v) FBS and 1% (v/v) Pen Strep. Briefly, monolayers were washed and detached as above. Cell suspensions were diluted in a DMEM medium and were counted using a hemocytometer. The final concentration of  $2 \times 10^5$  cells in 10 ml was plated into each 100-mm petri dish. Cell numbers were counted daily (triplicate for each day) for 7 days. The details of this procedure are provided in Appendix E.2.

### 3.3.3 U-87MG cell line

Cells were plated in a 60-mm petri dish (growth area = 21.3 cm<sup>2</sup>) in complete DMEM. Briefly, monolayers were washed and detached as above. Cell suspensions were diluted in a DMEM medium and were counted using a hemocytometer. The final concentration of  $1.5 \times 10^5$  cells in 5 ml was plated into each 60-mm petri dish. Cell numbers were counted daily (triplicate for each day) for 10 days. The details of this procedure are provided in Appendix E.3.

### 3.3.4 MDCK cell line

Cells were plated in a 100-mm petri dish (growth area = 58.95 cm<sup>2</sup>) in complete DMEM. Briefly, monolayers were washed and detached as above. Cell suspensions were diluted in a DMEM medium and were counted using a hemocytometer. The final concentration of  $2 \times 10^5$  cells in 10 ml was plated into each 100-mm petri dish. Cell numbers were counted daily (triplicate for each day) for 7 days. Extra plates and flasks were also used. The details of this procedure are provided in Appendix E.4.

## 3.4 Cloning Efficiency of Plating

A clonogenic survival assay (see Section 3.8) with different densities of cells plated was performed to test the cloning efficiency. Fourteen densities of 200 cells/plate, 500 cells/plate, 1000 cells/plate, 1500 cells/plate, 2000 cells/plate, 2500 cells/plate, 3000 cells/plate, 4000 cells/plate, 5000 cells/plate, 6000 cells/plate, 7000 cells/plate, 8000 cells/plate, 9000 cells/plate, and 10,000 cells/plate were performed using 100-mm petri dishes for each cell line in 10 ml of their corresponding complete media and were incubated for 15 doubling times.

### 3.5 Drugs Treatment and Cytotoxicity

Stock solutions of methotrexate (MTX), 5-fluorouracil (5-FU) and 5-bromo-2'-deoxyuridine (BrUdR) were prepared in Hanks Balanced Salt Solution (HBSS) and stored at  $-20^{\circ}\text{C}$ . Fluorodex was prepared using the method derived from previous work (Locke et al 2009). Exponentially growing culture of 9L cells were seeded in vented T12.5 cm<sup>2</sup> tissue culture flasks in complete DMEM at a density of  $8-10 \times 10^4$  cells per flask. Cells were allowed to attach and divide for 48 hours. Then, the medium was replaced and cells were incubated with 0.01–0.1  $\mu\text{M}$  MTX/5-FU and/or 1–10  $\mu\text{M}$  BrUdR. After a two doubling times incubation period with the drugs, the cytotoxic effect of the drugs was determined by clonogenic assay (refer to section 3.8). The number of cells plated was chosen based on the count of toxicity on cells (with reference of the corresponding controls for each cell line). Details of the procedure are provided in Appendix F.

### 3.6 Nanoparticles Treatment and Cytotoxicity

The nanoparticles were freshly prepared and dispersed in PBS ( $\text{Ca}^{2+}$  and  $\text{Mg}^{2+}$ ) to solubilise them. Sonication and vortex mixing was used to minimise the size of nano particle aggregates and increase the homogeneity of dispersion prior to exposure. The set up for sonication experiment is shown in (Figure 3.11). A concentration of 50  $\mu\text{g}/\text{ml}$  was applied to the cells for subsequent analysis. Details of the procedure are provided in Appendix G.



Figure 3.11: Set up of sonication procedure using the Branson Sonifier® S-250D digital with double-stepMicro-tip (Consonic Pty Ltd., NSW, Australia).

## 3.7 Cellular Irradiation Methods

### 3.7.1 Chemotherapy Drugs Combination

All experiments were carried out with confluent cultures grown as monolayer in  $12.5\text{cm}^2$  cell culture flasks with a vented screw cap (BD Falcon™). For the control (untreated cells or radiation-treated cells only), it contain 5 mL of DMEM medium and 30 mL of Hanks balanced salt solution (HBSS). For the drug-treated cells (following a two doubling times incubation period with drugs), just prior to irradiation, drugs-containing medium was added to make up the total of 35 ml (same conditions as controls above with concentration of drugs being adjusted). Unirradiated control samples were kept at room temperature in the control room while the other samples were irradiated in the treatment room. The complete procedures for irradiated cells in the absence of drugs (i.e the experimental on dose rate) and the irradiated cells combined with drugs (with its correspond control) are provide in Appendix H.1 and Appendix H.2, respectively.



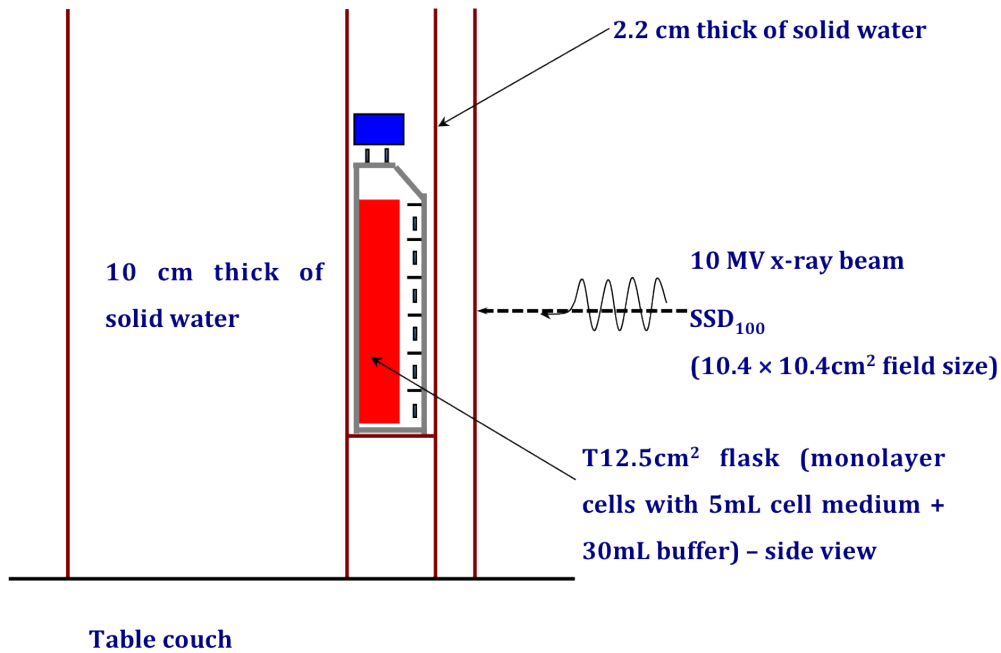


Figure 3.12: Schematic diagram of experimental setup for cellular irradiation (MV with or without drugs).

### 3.7.1.1 Megavoltage irradiations

The cell flasks were placed vertically facing the beam and were positioned at a depth of 2.2 cm and 1.7 in solid water (water-equivalent material) to match the Dmax depth of the 10 MV and 6 MV photon field, respectively. An additional thickness of 10 cm of solid water was placed behind the flask to assure adequate scattering conditions. To maintain electronic equilibrium conditions within the flasks during the irradiation, the flask was also surrounded by solid water slabs. The irradiation field size used for all experiments was  $10.4 \times 10.4$  cm<sup>2</sup> and the source-to-surface distance (SSD) was 100 cm. Figure 3.12 shows a schematic diagram of the setup for cellular irradiation – MV X-rays for combination with and without chemotherapy drugs (the dose rate experimental on LINAC).



Figure 3.13: Photograph of experimental setup for cellular irradiation (with or without drugs).

#### 3.7.1.2 Kilovoltage irradiations

The irradiation field size used for all experiments was  $6 \times 8 \text{ cm}^2$  at the source-to-surface distance (SSD) of 50 cm, with the tissue culture flasks positioned as described previously (irradiated in a vertical orientation facing the beam directly) with solid water placed both behind and around the sides of the flasks, primarily to maintain adequate backscattering effects and to stabilise electronic equilibrium. Figure 3.13 shows the real setup for cellular irradiation combined with chemotherapy drugs.

#### 3.7.2 Nanoparticles Combination

The confluent cell cultures were irradiated in non-vented T12.5  $\text{cm}^2$  tissue culture flasks (BD Falcon<sup>TM</sup>) following a 1-day incubation period with nanopar-

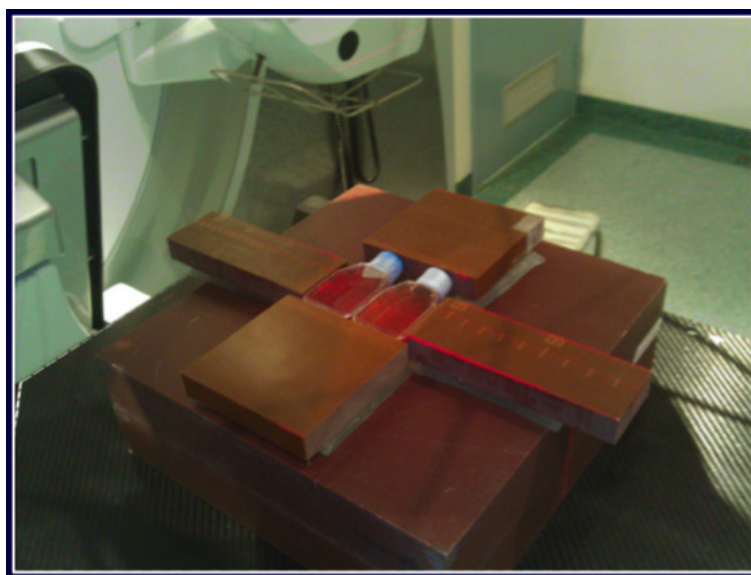


Figure 3.14: Photograph of experimental setup for cellular irradiation (MV with or without nanoparticles).

ticles at a concentration of  $50 \mu\text{g}/\text{ml}$ . The complete procedure is provided in Appendix H.3.

### 3.7.2.1 Megavoltage irradiations

Prior to irradiation, all the flasks were filled completely with HBSS to ensure no air bubbles were present inside the flask. Tissue culture flasks were irradiated in a horizontal orientation with solid water placed both underneath and around the sides of the flasks, primarily to maintain adequate backscattering effects and to stabilise electronic equilibrium (Figure 3.14).

### 3.7.2.2 Kilovoltage irradiations

Kilovoltage irradiation was performed using a 6 mm depth of medium in an attempt to maximise the accuracy of the dose delivered to the cell monolayer. Only beam energies of 150 kVp were explored. Tissue culture flasks were irradiated in a horizontal orientation with solid water placed both underneath and

around the sides of the flasks, primarily to maintain adequate backscattering effects and to stabilise electronic equilibrium.

### 3.8 Clonogenic Survival Assay

In 1956, Puck and Marcus were the first to describe a cell culture technique for mammalian cells, which were plated in cultured dishes with a suitable medium. They determined the first X-ray radiation dose survival curve for irradiated HeLa cells in culture [Puck and Marcus, 1956]. Subsequently, many studies have performed clonogenic assays or colony formation assay as the method of choice to determine cell reproductive death after treatment with ionising radiation or to determine the effectiveness of other cytotoxic agents [Munshi et al., 2005; Franken et al., 2006; Rafehi et al., 2011]. It is an *in vitro* cell survival assay based on the ability of a single cell to grow into a colony consisting of at least 50 cells. It is commonly regarded as the gold standard cellular sensitivity assay [Plumb, 2004].

In this project, both the control and irradiated/treated cells were plated immediately after the irradiation experiments. The medium was removed and the confluent cells were washed gently with DPBS ( $\text{Ca}^{2+}/\text{Mg}^{2+}$  free), then detached using Trypsin-EDTA. The disassociated cells were counted with a hemocytometer and seeded at low densities to achieve approximately 100 colonies after fifteen doubling times into 100-mm tissue culture dishes (BD Falcon™) containing 10 mL of complete cell growth medium (i.e. DMEM containing L-Glutamine and supplemented with 10% (v/v) FBS and 1% (v/v) PenStrep). Depending on the prescribed dose, each experiment involved a minimum of three cells densities with triplicate dishes for each density (Figure 3.15). The



Figure 3.15: Example of photograph of cells plated immediately after the irradiation (approximately of 120 plates for each set of single experiment). The assays of all irradiations treatment conditions (with or without drugs/NPs treated) were performed at least three times independently, unless otherwise specified.

numbers of cells plated per petri dish were determined by preliminary experiments designed in order to determine the radio-sensitivity of the cell lines. The cells in petri dishes were then incubated to allow colonies to form in a 37°C humidified 5% (v/v) CO<sub>2</sub> cell culture incubator (Heracell 150i). The details of this procedure are provided in figure H.1 (Appendix H). We believe our protocol to be free of major flaws and that clonogenic assay is the most robust technique for biological endpoint measurement after irradiation.

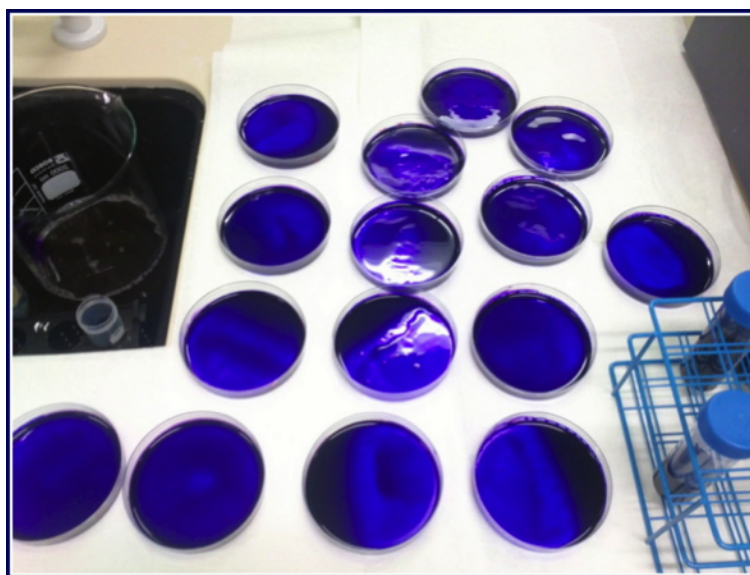


Figure 3.16: Photograph of fix and staining the cells.

### 3.8.1 Fixing and Staining

After fifteen doubling times, the colonies were fixed and stained with a mixture solution of 25% (v/v) crystal violet and 75% (v/v) ethanol for five minutes, washed, and air-dried (Figure 3.16). Only the numbers of colonies containing more than 50 cells were counted, as observed by microscope (Figure 3.17).

## 3.9 Flow Cytometric Detection

### 3.9.1 Propidium Iodide (PI) Staining

Propidium Iodide (PI) is the most commonly used dye for DNA cell cycle analysis by flow cytometry. This technique was also used as *in vitro* chemosensitivity test to detect DNA damage induced by anticancer drugs [Iwadate and Fujimoto, 1997]. Briefly, cells were harvested by trypsinisation as above and centrifuged at 1500 rpm for 5 min at 4°C and then washed once with cold phosphate buffer solution (PBS) which is  $\text{Ca}^{2+}/\text{Mg}^{2+}$  free. Then, resuspend with PBS at cell density of  $1 \times 10^6$  cells/mL and transferred to labelled FAC-



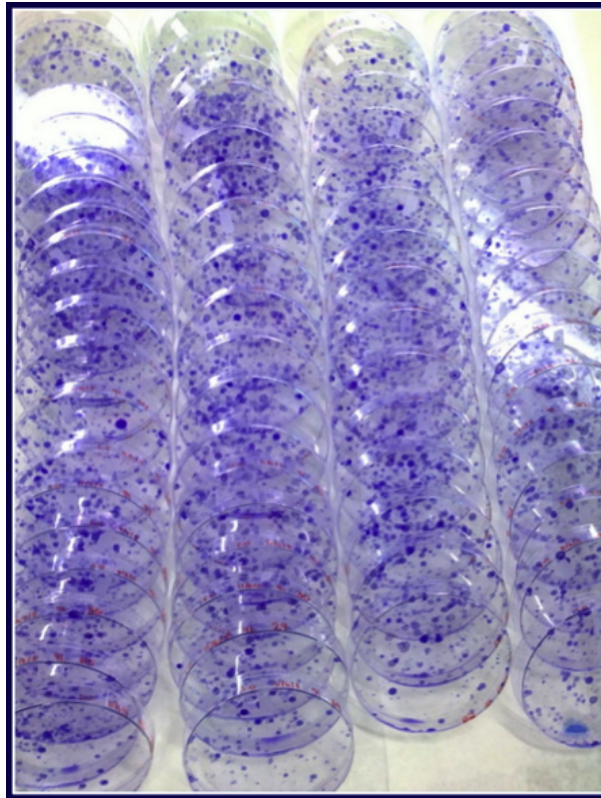


Figure 3.17: Example of photograph of the stained plates.

Stubes. PI of 1 mg/mL was added to give a final concentration of 10  $\mu\text{g/mL}$  just before the analysis is run on a flow cytometer.

### 3.9.2 Cell Cycle Analysis

Measurements of the cell cycle distribution were performed by flow cytometric analysis using propidium iodide (PI) staining. The method used was derived from previous work [Vine et al., 2007]. Cells ( $2 \times 10^6$ ) were centrifuged at 1500 rpm for 5 min at 4°C and washed twice with cold phosphate buffer solution (PBS) pH 7.4 ( $\text{Ca}^{2+}/\text{Mg}^{2+}$  free) then finally fixed by drop wise addition of 1 mL ice-cold ethanol (70%) and stored at  $-20^\circ\text{C}$  for up to 7 days before DNA analysis. The ethanol was then removed via a centrifuge process, washed twice with cold PBS. The cells were then stained with a solution containing 40

$\mu\text{g/mL}$  PI, 100  $\mu\text{g/mL}$  RNase A, and PBS (pH 7.4) at 37°C for 1 hour. The stained nuclei were analysed for DNA-PI fluorescence using a FACS flow cytometer. A minimum of 10,000 single cell events was analysed for each sample in each experiment and at least three independent experiments was performed. Details of this procedure are provided in Appendix I.1.

### 3.9.3 Detection of Forward and Side Scatter (for Nanoparticles)

After exposure to nanoparticles for 24 h, cells were harvested by trypsinisation, centrifuged at 1500 rpm for 5 min at 4°C and washed twice with cold phosphate buffer solution (PBS) with  $\text{Ca}^{2+}/\text{Mg}^{2+}$  free. Flow cytometric measurements were performed and a minimum of 10,000 cells were analysed for each sample. Cell doublets and aggregates were gated out using a two-parameter histogram of FL2-Area versus FL2-Height. The decrease in size of forward scatter (FSC) and the increase of side scatter (SSC) associated with the granularity were evaluated.

### 3.9.4 Immunofluorescence Staining of BrUdR)

Immunofluorescence staining is the staining of cells with antibodies and other specific ligands directly or indirectly with fluorescent molecule [Radbruch, 1992] to detect the presence of antigen (antibody-generating substance) on or in a cell by the fluorescence emitted by the bounded antibody. Direct staining is by using antibody-fluorescent conjugated directly whereas indirect staining is using unconjugated antibodies (primary antibody) and then detected using secondary antibody that fluorescent-conjugated (Figure 3.18). In this project,



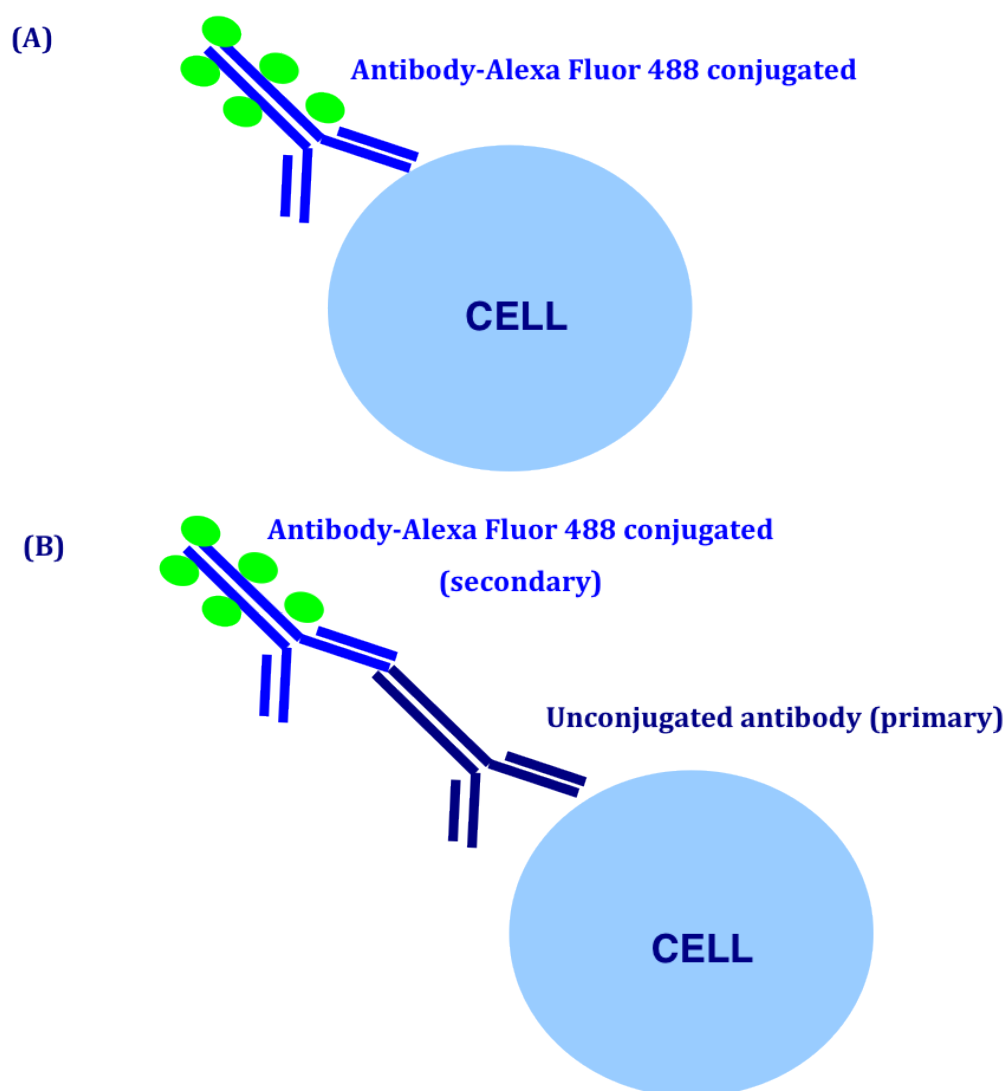


Figure 3.18: Direct (A) vs. indirect (B) immunofluorescence staining.

direct staining with antibodies conjugated to fluorescent is used (i.e. anti-BrUdR antibodies conjugated to Alexa Fluor 488). Therefore, the detection of anti-BrUdR antibody binding level by flow cytometry showed to be correlated with the number of Br uptake into cells.

#### 3.9.4.1 Detection of BrUdR & total DNA content simultaneously

Cells that had incorporated BrUdR during drug the incubation procedure were detected by fluorescently labelled anti-BrUdR antibodies. In this study, the

anti-BrdU mouse monoclonal antibody (Clone MoBU-1) that is highly specific for BrdU incorporated into DNA was used. The clone MoBU-1 conjugated with Alexa Fluor 488 was purchased from Molecular Probe (Invitrogen Life Technologies, NSW, Australia). The assay was carried out using an acid denaturation method as per the manufacturers references with minor modifications.

Briefly, cells were incubated with 10  $\mu$ M BrUdR as described previously, harvested and fixed at least overnight after the addition of 1mL of ice-cold 70% ethanol as above. The cells were washed twice with cold PBS and then treated with 4M HCl (Sigma) for 20 min at room temperature. After this, the cells were washed with a phosphate/acid buffer at pH 7.4 and were washed a second time with antibody diluting buffer (PBS with Triton X-100 and bovine serum albumin (Sigma)). After washing, the cells were then incubated with the clone MoBU-1 antibody for 30 min, followed by antibody diluting buffer washing. The pelleted cells were then counterstained with PI staining solution (10  $\mu$ g/ml PI, 100 $\mu$ /ml RNase A, and PBS pH 7.4) for 30 min at room temperature. The stained nuclei were then analysed using flow cytometer. Details of this procedure are provided in Appendix I.2.

## 3.10 Confocal Microscopy Analysis

### 3.10.1 Detection of Intracellular Reactive Oxygen Species (ROS)

The formation of ROS in 9L cells following treatment by nanoparticles was assessed using confocal laser scanning microscopy. Briefly,  $1 \times 10^5$  cells were seeded onto Nunc <sup>TM</sup>Lab-Tek<sup>TM</sup>II Chamber Slide<sup>TM</sup>System 4 wells (growth

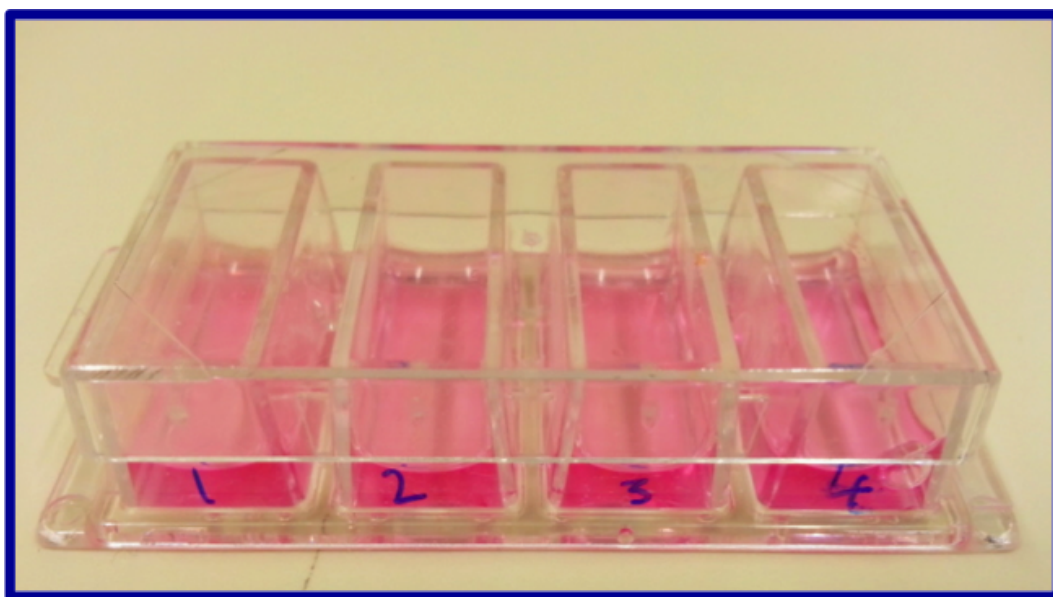


Figure 3.19: Cells grown onto <sup>TM</sup>Lab-Tek<sup>TM</sup>II Chamber Slide<sup>TM</sup>System 4 wells (growth area = 1.8cm<sup>2</sup>) (Thermo-Scientific).

area = 1.8cm<sup>2</sup>) (Thermo-Scientific) (3.19) in fresh culture medium (complete medium) containing nanoparticles. Only tantalum pentoxide (Ta<sub>2</sub>O<sub>5</sub>) nanoparticles have been tested, with a concentration of 50 µg/ml. After 24 hours of incubation, 10 µg/ml of propidium iodide (PI) and 10µM of 2',7'-Dichlorofluorescein diacetate (DCFDA) dye were added. Stained cells were then visualised immediately by confocal microscopy. Confocal laser scanning microscopy were acquired using a Leica TCS SP system with a water immersion objective lens. As DCFDA is very light sensitive, the procedures were performed in the dark.

### 3.10.2 Immunofluorescence Staining of BrUdR

The immunofluorescence staining procedure was carried out in a similar method as described for flow cytometry (section 3.9). Briefly,  $7.5 \times 10^4$  cells were seeded onto Nunc<sup>TM</sup>Lab-Tek<sup>TM</sup>II Chamber Slide<sup>TM</sup>System 4 wells (growth area = 1.8cm<sup>2</sup>) (Thermo-Scientific) (Figure 3.19). After an incubation period with drugs (MTX or BrUdR) or without drugs (negative control) corresponding

to 15 doubling times, cells were fixed with 70% ethanol at 4°C for 30 mins, washed twice with cold PBS and treated with 4M HCl for 20 mins at room temperature. Cells were then washed with phosphate/acid buffer (pH 7.4) and washed three times with an antibody diluting buffer containing Triton X-100 and bovine serum albumin. The cells were then incubated with MoBU-1 antibody for 30 mins, followed by antibody diluting buffer washing. The cells were then counterstained with PI staining solution (10  $\mu$ g/ml PI, 100 $\mu$ /ml RNase A, and PBS pH 7.4) for 30 mins at room temperature. Stained cells were then visualised by confocal microscopy. Confocal laser scanning microscopy were acquired using a Leica TCS SP system with an oil immersion objective lens.

## 3.11 Data Analysis and Statistics

### 3.11.1 Cells Growth Analysis

The exponential growth curves for all the cells were plotted as the number of cells against time, which is based on the equation:

$$N = N_0 \exp(\lambda t), \quad (3.2)$$

where  $N$  = the concentration of cells at time,  $t$ ,  $N_0$  = the initial concentration of the cells, and  $\lambda$  is the growth constant. The doubling time,  $t_2$ , is the time required for the cells to double in population is obtained from the equation:

$$t_2 = \ln \frac{2}{\lambda}. \quad (3.3)$$

### 3.11.2 Plating Efficiency

The plating efficiency (PE) was calculated as the number of surviving colonies divided by the number of cells seeded:

$$PE = \frac{\text{Number of colonies counted}}{\text{Number of cells seeded}} \quad (3.4)$$

### 3.11.3 Cell Survival Analysis

The number of colonies that arise after irradiation, which is expressed in terms of PE, is called the surviving fraction (SF):

$$SF(D) = \frac{PE(D)}{PE(0)} \quad (3.5)$$

where  $SF(D)$  is the cell survival fraction at dose  $D$  (Gy),  $PE(D)$  is the plating efficiency at the dose (irradiated cells), and  $PE(0)$  is the plating efficiency at zero dose (unirradiated cells or control). The values of  $PE(D)$  and  $PE(0)$  are the average over the replicate samples for each dose. The radiation dose-survival curves were generated by plotting the SF as a function of the dose on a semi-logarithmic scale. The radiation dose survival curves were fitted by a linear quadratic function (LQ model) (Eq. 2.6) used to describe *in vitro* radio-sensitivity [Fertil and Malaise, 1981, 1985].  $\alpha$  and  $\beta$  parameters were determined in order to quantify the radio-sensitivity [Curtis, 1986]. A schematic diagram of the overall procedure is illustrated in Figure 3.20, where the clonogenic assay (Section 3.8) was initiated. Details of the procedures are provided in Appendix H.

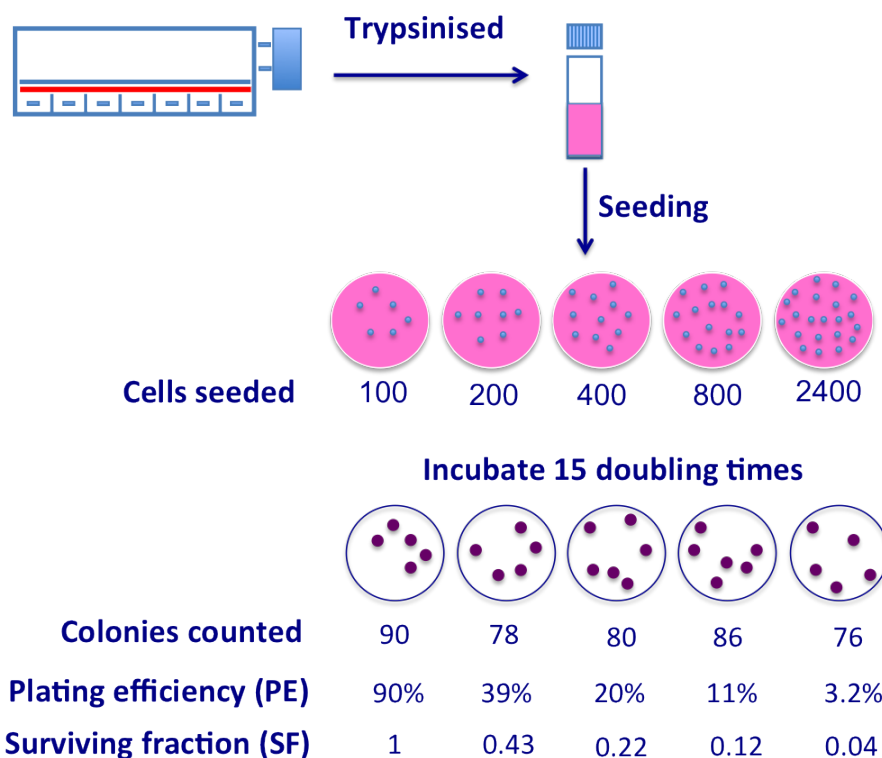


Figure 3.20: Schematic diagram of cell culture technique (i.e clonogenic assay) to produce a cell survival curve.

### 3.11.4 Flow Cytometric Data

Cell doublets and aggregates were usually gated out using a two-parameter histogram of FL2-Area versus FL2-Height. In this study, the FSC-A vs SSC-A gate was sufficient. Figure 3.21a is a two-dimensional dot plot of FSC vs. SSC, show the bulk of the cells as the dense population of dots and each dot represents one acquired event. The intensity of fluorescence (i.e. red fluorescence in this case as PI used) is displayed in a histogram plot (Figure 3.21b). In figure 3.21c, a gate has been drawn around the dense cell population of interest on the plot to exclude cell doublets and debris from analysis, which give a better histogram plot shown in Figure 3.21d.

The resulting DNA distribution was then analysed on the basis of histograms using FlowJo software Mac version (V9.6.2, Tree Star Inc., USA) for the pro-

portion of cells in  $G_0/G_1$ , S and  $G_2/M$  phases of the cell cycle. Figure 3.22 show a typical cell cycle of each phase by flow cytometry, with  $G_0/G_1$  phase and  $G_2/M$  phase represents as diploid (2N) and tetraploid (4N) DNA content, respectively (where N as a single complement of chromosomes, the haploid content). Therefore, by fluorescence labelling of the nuclei cells with PI, the population of each phase cells can be determined by analysing its fluorescence properties. The  $G_0/G_1$  phase (2N) with one copy of DNA will have 1X fluorescence intensity whereas the  $G_2/M$  phase (4N) with two copies of DNA will have 2X intensity. For the S-phase, the fluorescence values are between 1X and 2X as they are synthesising DNA. All data were stored by the computer system in a flow cytometer standard (FCS) format.

### 3.11.5 S-phase Fraction

The S-phase fraction (SPF) was calculated as the number of S-phase fraction divided by the number of total fraction seeded:

$$SPF = \frac{\text{S-phase fraction}}{\text{total fraction}} \quad (3.6)$$

### 3.11.6 Statistical Analysis

The cell growth curves are fitted using equation (3.2), weights in the fit by the standard deviation at each point. The plating efficiencies (PEs) for each irradiation were calculated and were normalised to 100% survival controls at zero dose (unirradiated cells). PEs for each irradiation combined with drugs, the data were normalised to 100% survival controls of unirradiated drugs-treated cells.

The cell survivals are then given as the mean values from the pooled data of

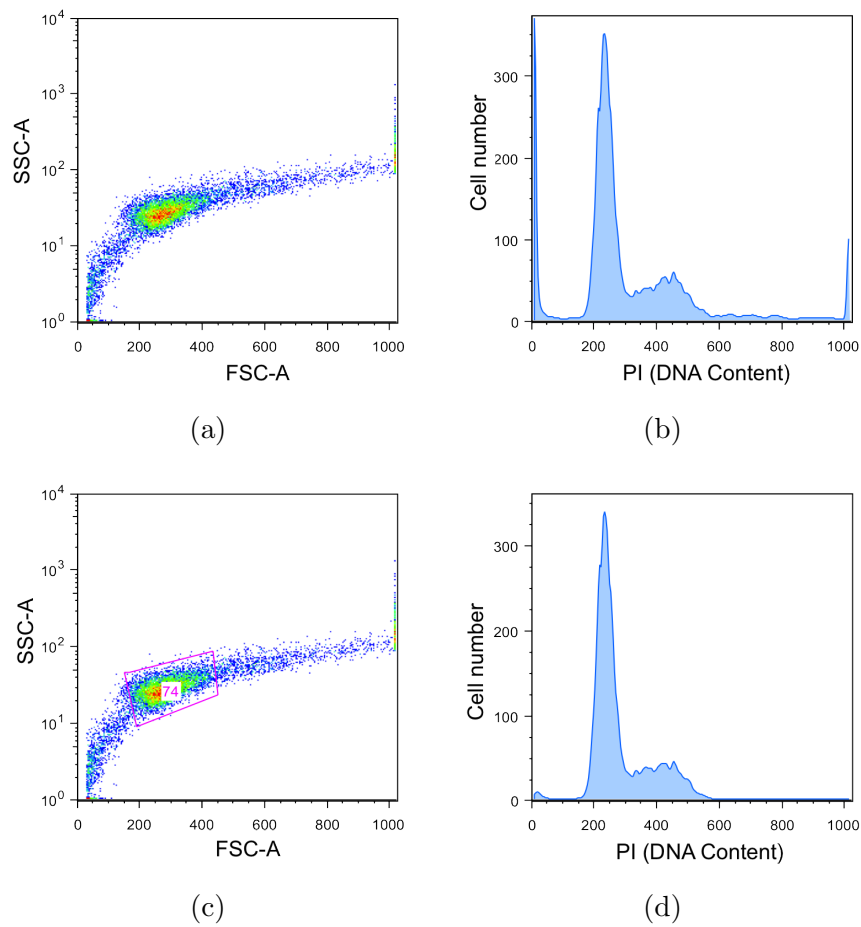


Figure 3.21: A representative typical data analysed on BD LSR II flow cytometer and an illustration of gating using FlowJo software (from 9L cells stained with PI). (a) Dot plot (or cytogram) which showing forward scatter (FSC) versus side-scatter (SSC). (b) Histogram plot which showing positive population of cells (ungated). (c) Dot plot, which was gated shown as 74% cells (singlets). (d) Histogram which showing gated on singlet cells only.



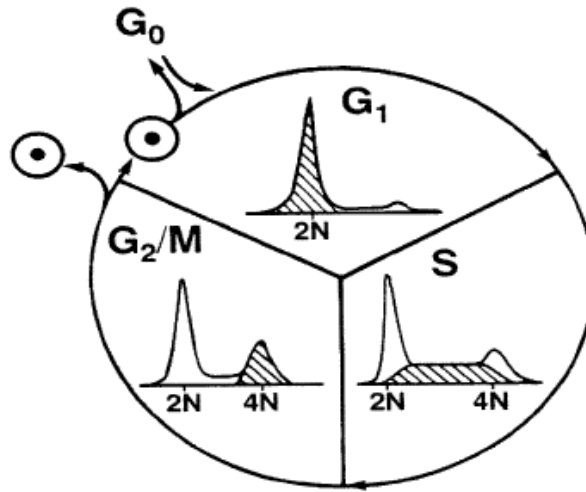


Figure 3.22: A schematic diagram of cell cycle, showing flow cytometric components of each phase ([www.phoenixflow.com](http://www.phoenixflow.com)).

at least six-replicate samples (each triplicate from a minimum of three independent experiments, unless specified otherwise) for each data point, with the experimental uncertainty given as one standard deviation (mean  $\pm$  SD). The LQ model was fitted to cell survival data using IGOR Pro software (V.6.21, WaveMetrics, Inc. Oregon, USA). The fit of the data is weighted by the reported error at each dose in the determination of the radiobiological constants of the LQ model (non-linear least squares algorithm). FACS plots and histograms are representative of at least two independent experiments.

## 3.12 Sensitisation Defined

### 3.12.1 Sensitisation Enhancement Ratio (SER)

There are two major sensitisation enhancement ratios (SER) defined in the literature: horizontal and vertical. For the horizontal ratio, the values are given as the ratio of the dose required to kill a given surviving percentage in the control group to the dose required in the treated group (e.g.  $SER_{10}$ ). For vertical ratios, the SER is defined as the ratio of the surviving fraction in the

control to the surviving fraction in the treated group in particular dose (e.g.  $SER_{2Gy}$ ). Researchers often choose 2 Gy because of its practical value when used as prescribed dose (per fraction) in fractionation RT. In this study,  $SER_{10}$  is used as a way to measure the dose-enhancement by different energies (e.g. kVp vs. MV).

### 3.12.2 Protection Enhancement Ratio (PER)

For cerium oxide nanoparticles in this study, we defined a protection enhancement ratio,  $PER_{10}$ , as the ratio of the dose required to protect 10% surviving fraction in the control group to the dose required in the treated group.

# Chapter 4

## Results & Discussions

### 4.1 Cell Line Characteristics and Protocols

This thesis is part of the foundation research and development associated with the recently formed Targeted Nano-Therapy (TNT) team at the University of Wollongong. The TNT team is made up of collaborating members from the Centre for Medical Radiation Physics (CMRP), the Centre for Medical Bioscience (CMB), and the Institute for Superconducting and Electronic Materials (ISEM) of the University of Wollongong. The initial research, carried out at the Illawarra Health and Medical Research Institute (IHMRI), centred on the establishment of a variety of cell lines and cell handling protocols.

This chapter examines the exponential growth of all the cell lines used in this thesis: 9L, MCF-7, U87-MG, and MDCK. The cell growth analysis of MCF-7, U87-MG, and MDCK has also been performed as groundwork analysis only.

### 4.1.1 9L Cell Line

The 9L is an adherent, fibroblast-like, radioresistant rat gliosarcoma cell line derived from a N-nitrosomethylurea-induced tumor. The mean population doubling time of 9L cells over a series of three experiments was approximately 32 – 34 hours (Figure 4.1). This doubling time is comparable to reported doubling times of 1.3 days [Ghulam Muhammad et al., 2009]. The 9L cells are also similar to some human high-grade glioma cells that are relatively resistant to X-rays irradiation [Malaise et al., 1987]. As is generally true for most glioma cell lines, the 9L cell line is aggressive and less radio-sensitive than other rat tumour cell lines [Henderson et al., 1981; Bencokova et al., 2008]. It is the best and most widely used of all rat brain tumour models for research [Barth, 1998] as well as a preclinical model used in brain radiotherapy [Vinchon-Petit et al., 2010] and has been utilised in such experiments for more than 30 years [Kimler, 1994].

#### 4.1.1.1 Cell Age Effect on 9L Cells

An additional preliminary cell growth assay of 9L cells was performed to check whether there is an effect on cell age (Figure 4.2). 9L cells on passage 54 (new) were compared to cells on passage 89 (old). The doubling time for the old passage is shorter (26 hours) than the newer passage (32 – 34 hour). From this result, it was recommend to use cells for up to 30 passages.

### 4.1.2 MCF-7 Cell Line

MCF-7 is an adherent, epithelial-like, radiosensitive breast adenocarcinoma cell line established from a 69-year-old female. There is no significant different in growth of MCF-7 between using the DMEM (27 hours) or RPMI-1640

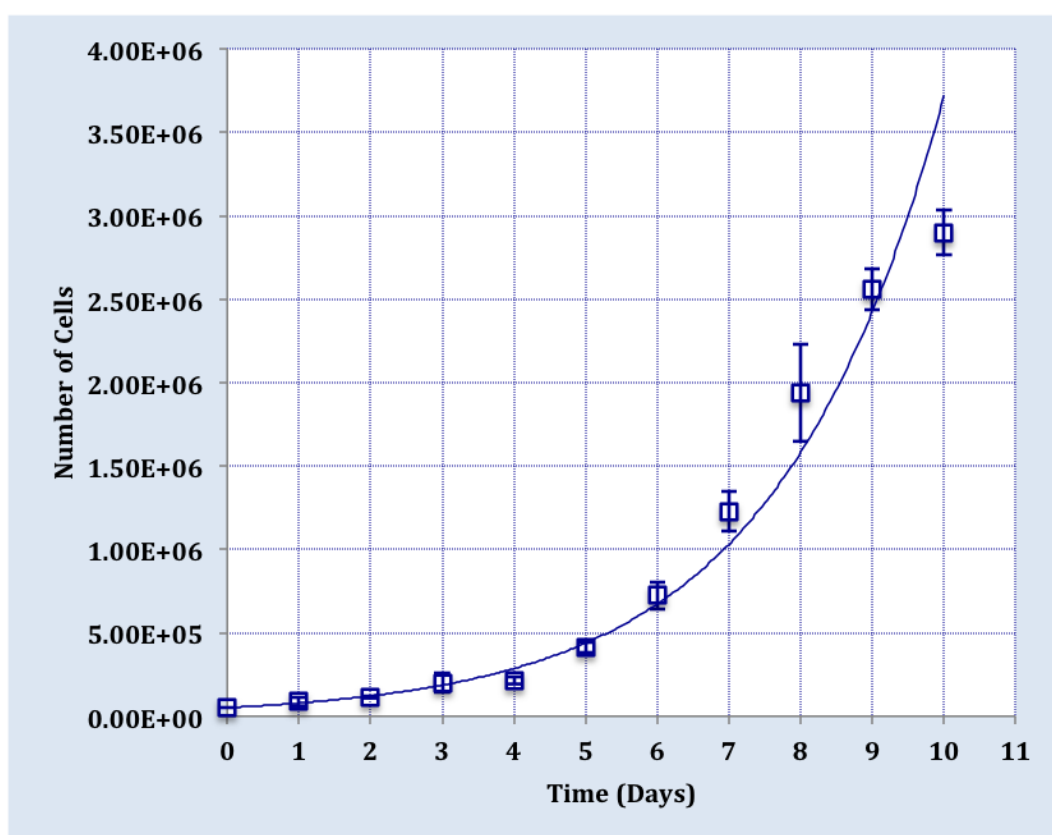


Figure 4.1: Analysis of exponential growth of 9L cells (passage 47). The assay was performed three times, and a representative result is shown. Experimental points are shown, along with exponential fit describe in methods section (Eq 3.2). Bars are  $\pm$  one standard deviation.

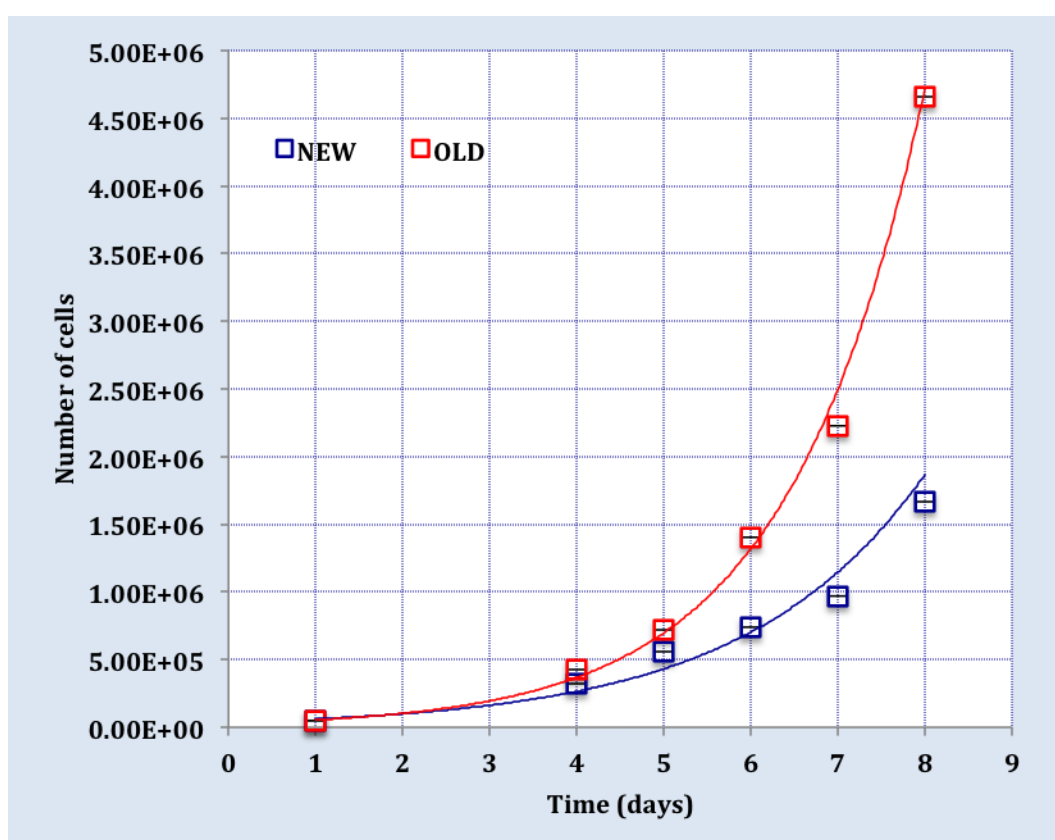


Figure 4.2: Analysis of exponential growth of 9L cells passage 54 (new) vs. passage 89 (old). Experimental points are shown, along with exponential fit describe in methods section (Eq 3.2). Bars are  $\pm$  one standard deviation (error bars are too small).

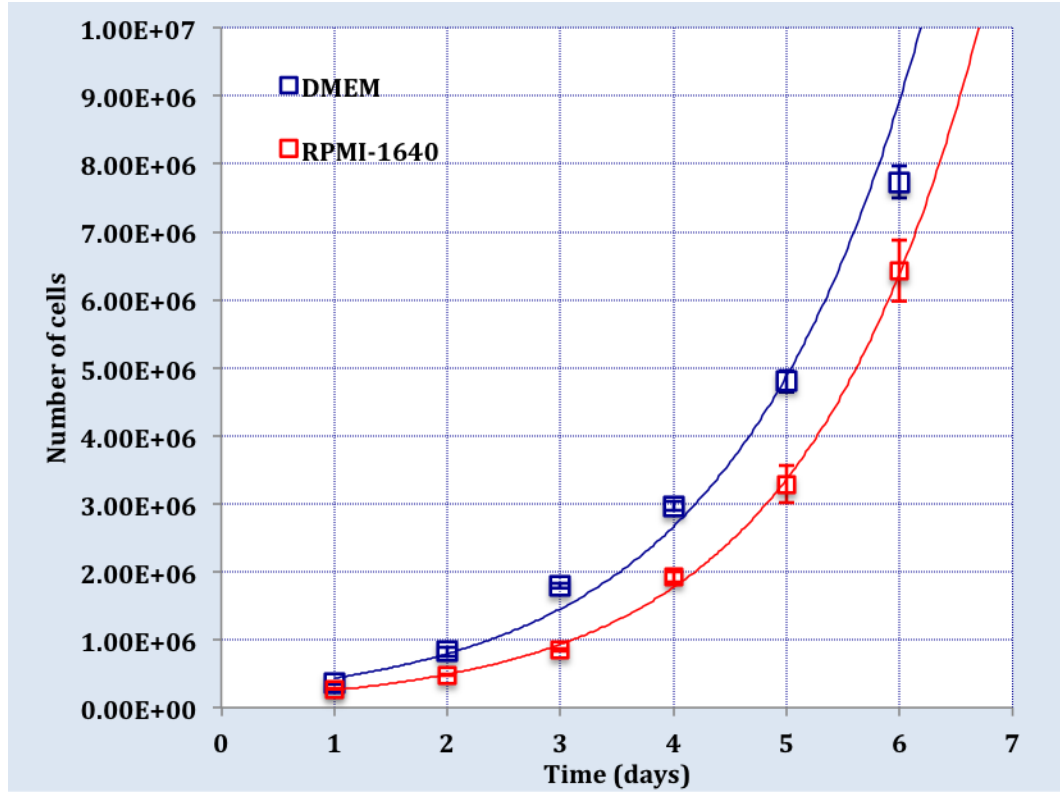


Figure 4.3: Analysis of exponential growth of MCF-7 cells in DMEM vs. RPMI-1640. Experimental points are shown, along with exponential fit describe in methods section (Eq 3.2). Bars are  $\pm$  one standard deviation.

(26 hours) media (Figure 4.3). Thus, in order to keep the same experimental conditions for all the cell line used in this study, DMEM medium is chosen for MCF-7. The mean population doubling time of MCF-7 cells over a series of two experiments was approximately 25 – 27 hours (Figure 4.3). This doubling time is comparable to reported doubling times of 24 hour (ATCC - American Type Culture Collection). The MCF-7 cell line represents a well-adopted pre-clinical model of breast tumour tissue. It has provided the basis of many breast cancer biology studies [Tutt and Yarnold, 2006]. These cells are relatively more radio-sensitive [Matthews et al., 1989] than 9L cells.

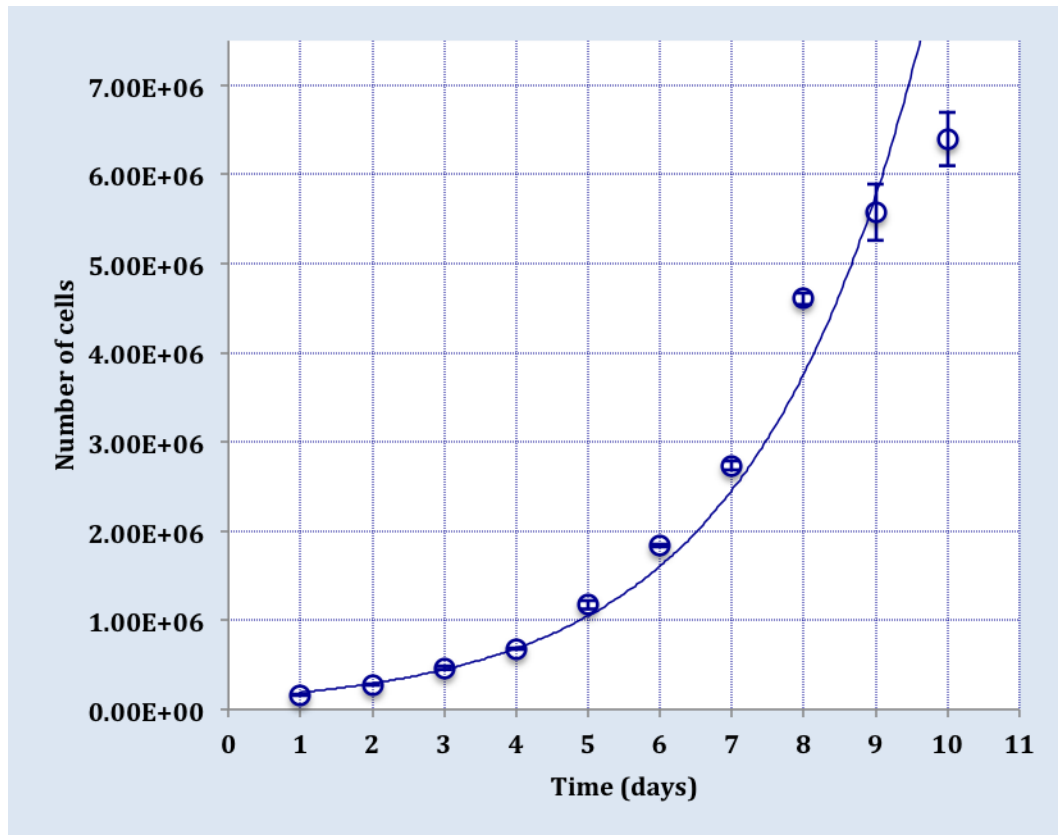


Figure 4.4: Analysis of exponential growth of U-87MG cells. Experimental points are shown, along with exponential fit describe in methods section (Eq 3.2). Bars are  $\pm$  one standard deviation.

### 4.1.3 U-87 MG Cell Line

The analysis of exponential growth for U-87 MG cells was performed as ground-work analysis. The mean population doubling time of U-87 MG cells was approximately 36 – 38 hours (Figure 4.4). This doubling time is comparable to the reported doubling times of 34 hours (ATCC). Glioblastoma cells were reported as very highly aggressive cells and highly vascularised tumours [Jensen, 1998]. Therefore, the U87-MG glioblastoma cells were chosen as a highly radioresistant cell line [Leith et al., 1994; Williams et al., 2008] to be comparable with the radioresistant 9L cells for future work.



#### 4.1.4 MDCK Cell Line

As it is generally difficult to maintain primary culture, we chose a continuous non-malignant cell line that is easy to maintain (i.e. the MDCK – Madin Darby Canine Kidney) cells. The MDCK cell line is the most well studied epithelial cell [Simons and Virta, 2006]. It is derived from a normal dog kidney [Madin and Darby, 1958; Gaush et al., 1966]. MDCK cells were chosen to mimic the model for glioma (i.e. 9L), which is used for the preliminary nanoparticles work presented in this study. MDCK was chosen as a model for permeation experiments on blood brain barrier (BBB) [Veronesi, 1996; Garberg et al., 2005; Hombach and Bernkop-Schnurch, 2009]. The mean population doubling time of MDCK cells was approximately 19 hours (Figure 4.5). This doubling time is comparable to reported doubling times of 21 hours (ATCC).

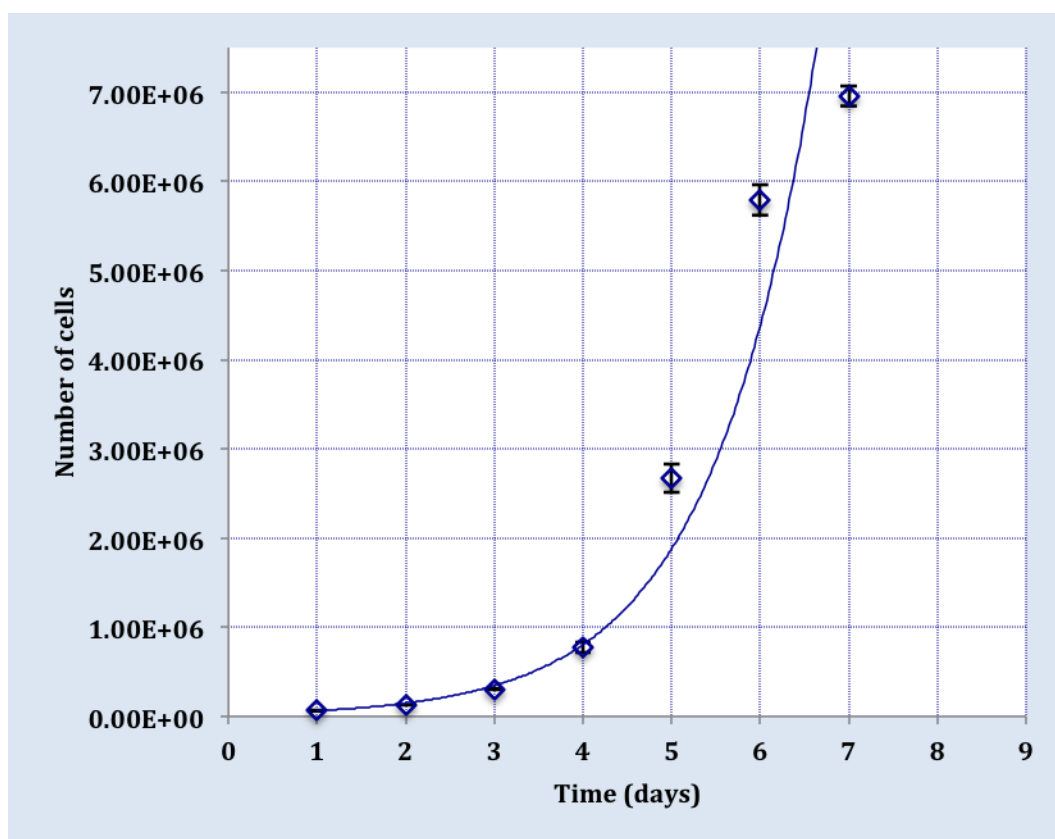


Figure 4.5: Analysis of exponential growth of MDCK cells. Experimental points are shown, along with exponential fit describe in methods section (Eq 3.2). Bars are  $\pm$  one standard deviation.

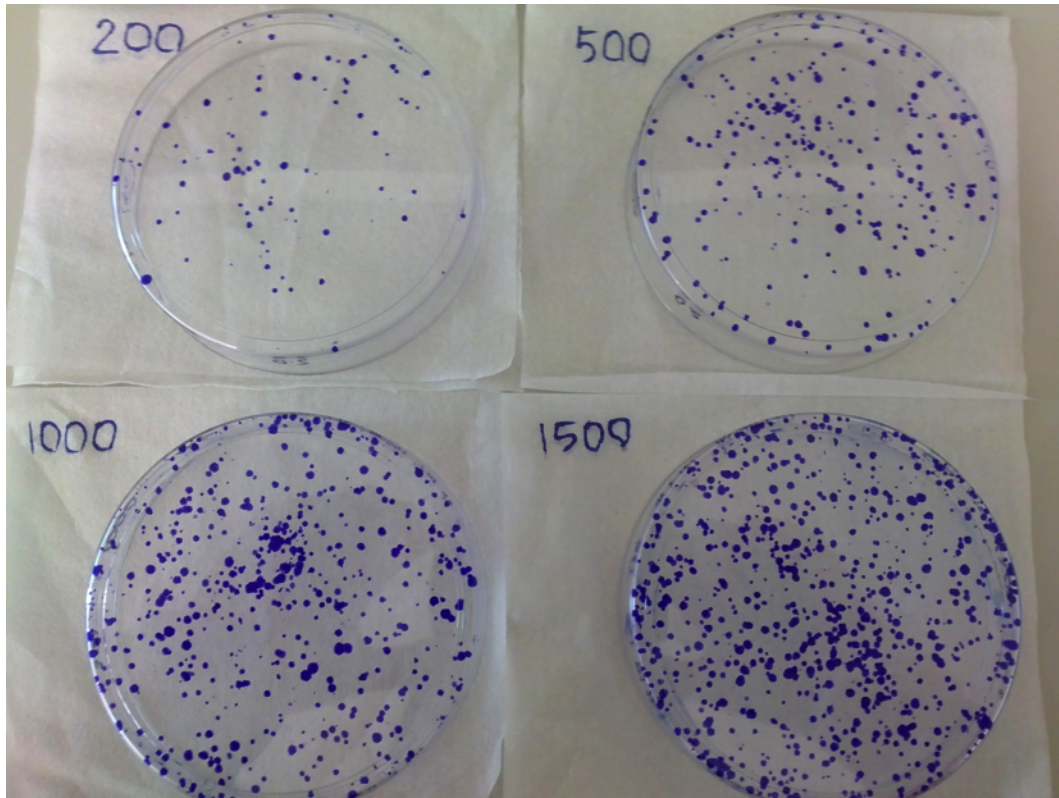


Figure 4.6: Photograph of colonies of unirradiated MCF-7 cells. Plating efficiency of cells densities of 200, 500, 1000 and 1500 cells/plate are shown.

## 4.2 Cloning Efficiency of Plating

Different cell lines have different plating efficiency [Franken et al., 2006]. Under our experimental conditions, the range of plating efficiencies (Figure 4.6) at low density for 9L and MCF-7 was approximately 8–10% and 50–70%, respectively. The plating efficiency for U87-MG and MDCK has also been performed as groundwork analysis. The range of plating efficiencies at low density for U87-MG and MDCK was approximately 6–8% and 15–20%, respectively (Figure 4.7).

A clonogenic assay was also performed to investigate whether there is an effect on cells while travelling to the POWH for irradiation experiment. Two samples of unirradiated cells, both 9L and MCF-7 (not travelling), were tested as well as with or without filter cap for the 9L cells. There were no differences

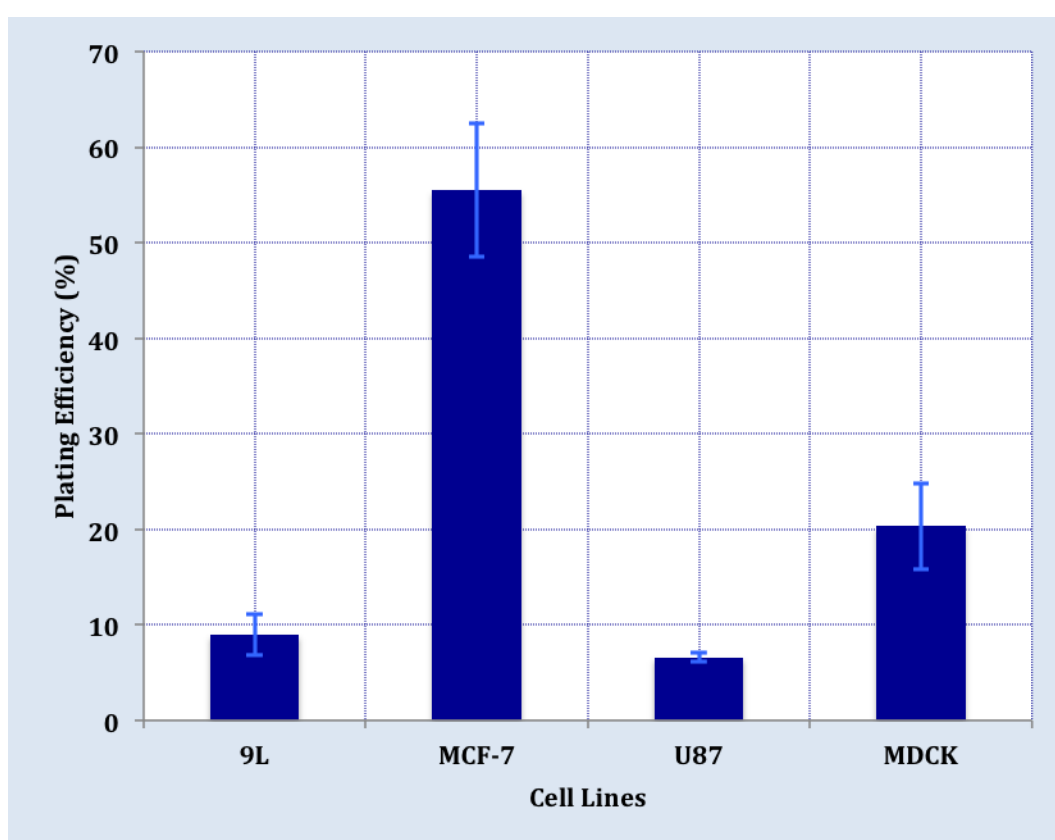


Figure 4.7: Plating efficiency of 9L, MCF-7, U-87 MG, and MDCK cells. Bars are  $\pm$  one standard deviation.

observed in any of the treatments (data not shown). This suggests that the traveling period for the irradiation experiment (approximately 3 hours) has no additional effect on the cells.

For the irradiation experiment, there are always two controls used in each treatment conditions. One sample of each control was plated immediately whereas another was plated at the end (i.e. after all the remaining samples are plated) in order to anticipate the effect of timing on the last sample being plated.

#### 4.2.1 Conclusions

The cell proliferation rate was determined by calculating the doubling time of each cell line. For our experimental conditions, it showed that 9L, MCF-7, U-87 MG, and MDCK cells grow exponentially with doubling times of 32 – 34 hours, 24 – 27 hours, 36 – 38 hours, and 19 – 21 hours, respectively. These doubling times are consistent with literature values, which are 1.3 days for 9L [Ghulam Muhammad et al., 2009], 24 hours for MCF-7 (ATCC), 34 hour for U-87 MG (ATCC), and 21 hours for MDCK (ATCC). Thus, the observed exponential growth of cells proved validity of the tissue culture technique used in this project.

## 4.3 Cytotoxicity Test

This section is concerned with the toxicity assessment of both the drugs and the nanoparticles on cells. The first part of this section describes the cytotoxicity of drugs and the reasons how the optimum concentration used in this study was chosen. The second part describes the cytotoxicity of the ceramic nanoparticles (cerium oxide –  $\text{CeO}_2$ , tantalum pentoxide –  $\text{Ta}_2\text{O}_5$ , and bismuth oxide –  $\text{Bi}_2\text{O}_3$ ) on 9L cells and only bismuth on the non-malignant cells. Finally, the last part describes the cytotoxicity test of a new pro-drug of 5-fluorouracil (fluorodex).

### 4.3.1 Drugs Cytotoxicity Test on 9L Cells

The present study involved two kinds of cytotoxicity tests. The toxicity of the drugs (MTX, 5-FU, and/or combination with BrUdR) was first investigated over a period of two doubling times by counting the viable cells using a haemocytometer. This first investigation (i.e. cell viability assay) was required in order to determine the cell density required for the second cytotoxicity test, i.e. cell clonogenic assay. The number of cells plated in the second investigation was based on the percentage toxicity rate in the initial investigation (a detailed procedure is given in Appendix F1 of the thesis).

In the second investigation the toxicity of the drugs was assessed over fifteen doubling times using clonogenic assay. Only the cytotoxicity on 9L cells is presented in this study. There was no significant decrease in the number of viable cells following exposure to drugs at a concentration of  $0.01 \mu\text{M}$  for either MTX or 5-FU alone or when either of these was combined with BrUdR (at a concentration of either 1 or  $10 \mu\text{M}$ ). Under these conditions both of these

doses of BrUdR can be considered non-toxic. Only when the dose of MTX was (i.e.  $0.1 \mu\text{M}$ ), both alone and combined with  $1 \mu\text{M}$  BrUdR, was significant toxicity indicated by a decrease in the number of viable cells to less than 20%. These results are summarised in Table 4.1.

Table 4.1: Cell viability of control (untreated cells) of 9L cells and of treated cells with drugs for two doubling times

Treatment	Cell viability (%)
Control	100
MTX $0.01 \mu\text{M}$	65.9
MTX $0.1 \mu\text{M}$	17.4
BrUdR $1 \mu\text{M}$	63.5
BrUdR $10 \mu\text{M}$	65.9
5-FU $0.01 \mu\text{M}$	54.8
5-FU $0.1 \mu\text{M}$	55.5
MTX $0.01 \mu\text{M}$ ; BrUdR $1 \mu\text{M}$	63.5
MTX $0.01 \mu\text{M}$ ; BrUdR $10 \mu\text{M}$	67.5
MTX $0.1 \mu\text{M}$ ; BrUdR $1 \mu\text{M}$	19.0
MTX $0.1 \mu\text{M}$ ; BrUdR $10 \mu\text{M}$	50.8
5-FU $0.01 \mu\text{M}$ ; BrUdR $1 \mu\text{M}$	54.7
5-FU $0.01 \mu\text{M}$ ; BrUdR $10 \mu\text{M}$	79.4
5-FU $0.1 \mu\text{M}$ ; BrUdR $1 \mu\text{M}$	54.7
5-FU $0.1 \mu\text{M}$ ; BrUdR $10 \mu\text{M}$	59.5

An interesting observation in the cell viability test results is that when either MTX or 5-FU is combined with a higher dose of  $10 \mu\text{M}$  BrUdR, there is an increase in the number of viable cells compared to when they are combined with a lower dose ( $1 \mu\text{M}$  BrUdR). These results not only suggest that BrUdR is non-toxic but also support the general mechanism of BrUdR. When the DNA synthesis of cells is blocked by MTX or 5-FU, the cells can mistakenly uptake and incorporate the BrUdR into the newly formed DNA chains.

Cells cultured for two doubling times when exposed to a low dose of MTX ( $0.01 \mu\text{M}$ ) alone or combined with either low or high doses of BrUdR show about a 40% decrease in the clonogenic survival fraction. In the case of a higher

dose of MTX alone ( $0.1 \mu\text{M}$ ) or combined with either a low or high dose of BrUdR, the clonogenic surviving fraction of cells was significantly decreased. Cells cultured for two doubling times when exposed to a low or high ( $0.01 \mu\text{M}$  and  $0.1 \mu\text{M}$ ) dose of 5-FU alone or combined with  $1 \mu\text{M}$  BrUdR did not show any significant decrease in survival. Only when the 5-FU was combined with  $10 \mu\text{M}$  BrUdR, did the surviving fraction decrease by 40%. These results are presented in figure 4.8.

The high dose of MTX (i.e.  $0.1 \mu\text{M}$ ) can therefore be considered to be toxic since the results in Table 4.1 and Figure 4.8 are consistent. This is clearly indicated by the significant decrease in the number of viable cells and cell survival fraction. Interestingly, this is not the case for 5-FU. The cells grown in  $0.1 \mu\text{M}$  5-FU showed an increased in clonogenic survival cell compared to the control (Figure 4.8). These results in Figure 4.8 are also in a good agreement with Wakisaka [1979]. The latter author found the optimum range of MTX and BrUdR concentration for a synergistic effect was  $0.01$  to  $0.02 \mu\text{M}$  and  $0.3$  to  $30 \mu\text{M}$ , respectively tested on L5 mouse fibroblast cells [Wakisaka, 1979].

#### 4.3.2 Ceramic Nanoparticles Cytotoxicity on 9L Cells

The nanoparticles are tested for biocompatibility, as they are expected to interact with biological systems. The current understanding of the mechanisms which determine the level of such interaction is limited. As described previously, a concentration of  $50 \mu\text{g}/\text{ml}$  of each ceramic nanoparticles ( $\text{CeO}_2$ ,  $\text{Ta}_2\text{O}_5$ , and  $\text{Bi}_2\text{O}_3$ ) was tested on 9L cells for a 1-day incubation. Biocompatibility testing on MDCK cells was carried out, but for  $\text{Bi}_2\text{O}_3$  only.



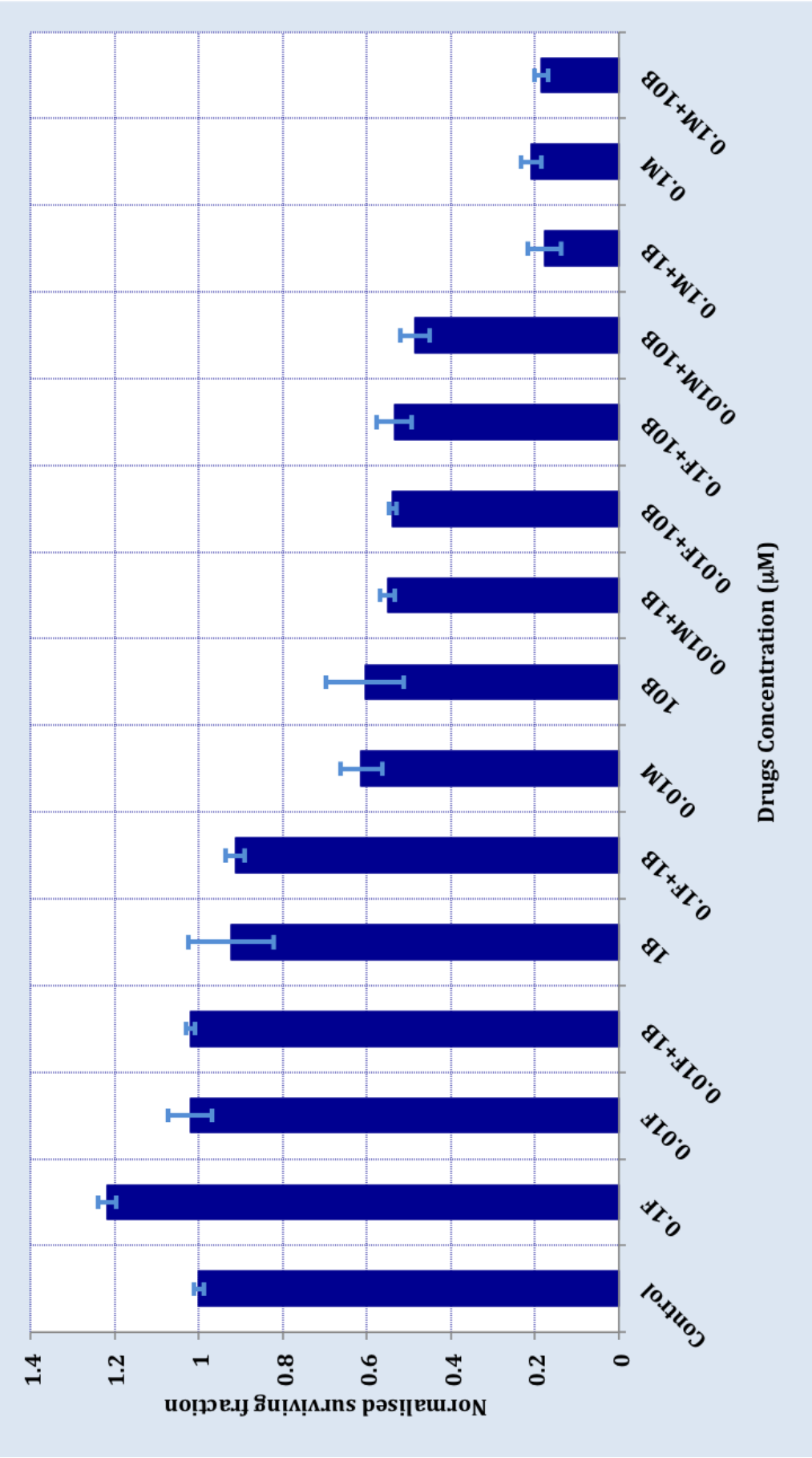


Figure 4.8: Drugs cytotoxicity test at the concentration of  $0.1 - 10\mu\text{M}$  on 9L cells. F = 5-fluorouracil; B = bromodeoxyuridine; M = methotrexate. Bars are  $\pm$  one standard deviation.

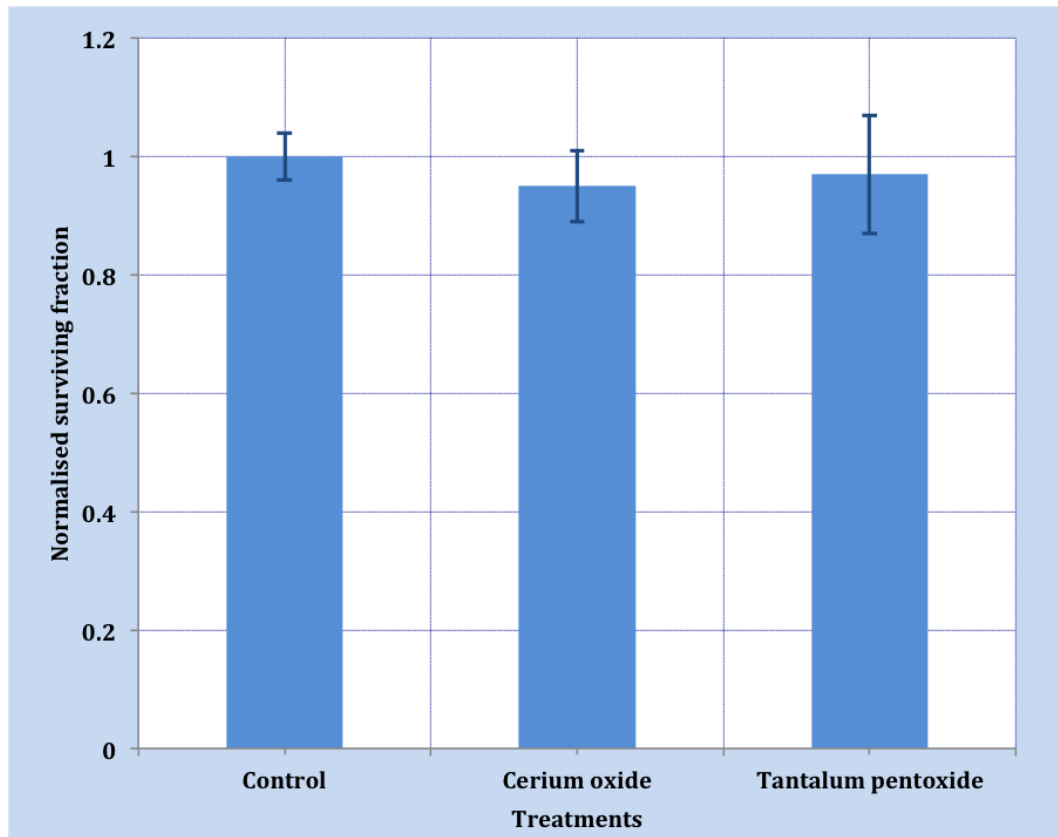


Figure 4.9: The surviving fraction of 9L cells exposed to cerium oxide ( $\text{CeO}_2$ ) and tantalum pentoxide ( $\text{Ta}_2\text{O}_5$ ) nanoparticles following a 24 hour exposure at a concentration of  $50 \mu\text{g/ml}$ . The toxicity was measured using the clonogenic survival assay. Bars are  $\pm$  one standard deviation.

#### 4.3.2.1 Cerium Oxide ( $\text{CeO}_2$ )

The toxicity of  $\text{CeO}_2$  nanoparticles to 9L cells is shown in Figure 4.9. There is no significant toxic effect on the survival fraction of 9L cells (Figure 4.9) at a nanoparticle concentration of  $50 \mu\text{g/ml}$ , this is consistent with the literature [Colon et al., 2009; Tarnuzzer et al., 2005; Xia et al., 2008].

#### 4.3.2.2 Tantalum Pentoxide ( $\text{Ta}_2\text{O}_5$ )

Tantalum is a known biocompatible material that has been used in orthopaedic surgery [Zardiackas et al., 2001]. Given the high atomic number of tantalum, the TNT group decided to develop a ceramic nano structured material based

on the hypothesis that one could exploit both its biocompatibility and the high-Z ( $Z = 73$ ) nature of this element to produce an effective radiosensitiser.

Tantalum pentoxide ( $\text{Ta}_2\text{O}_5$ ) is one of the many unexplored ceramic nanomaterials that contain potentially desirable characteristics as high-Z material to be used as radiosensitiser. The toxicity of the synthesised  $\text{Ta}_2\text{O}_5$  nanoparticles to 9L cells is shown in Figure 4.9. There is no significant toxic effect on the clonogenic survival fraction of 9L cells (Figure 4.9). This is unsurprising as tantalum is a known biocompatible material that has been used in orthopaedic surgery [Zardiackas et al., 2001] and consequently is non-toxic to healthy cells.

#### 4.3.2.3 Bismuth Oxide ( $\text{Bi}_2\text{O}_3$ )

The toxicity of the synthesised  $\text{Bi}_2\text{O}_3$  nanoparticles to 9L cells and MDCK cells are shown in (Figure 4.10). A toxic effect was observed for  $\text{Bi}_2\text{O}_3$  nanoparticles synthesised by precipitation in air on the clonogenic survival fraction of both 9L and MDCK cells at a concentration of  $50 \mu\text{g}/\text{ml}$  (Figure 4.10). However, there was no significant toxic effect on the clonogenic survival fraction of both 9L and MDCK cells at a concentration of  $50 \mu\text{g}/\text{ml}$  when exposed to  $\text{Bi}_2\text{O}_3$  synthesised by precipitation in argon. This result suggests that the presence of the argon environment in the manufacturing process appears to passivate the surface of the nanoparticles. Therefore, only the  $\text{Bi}_2\text{O}_3$  synthesised by precipitation in an argon environment was used in further experiments.

This biocompatibility result shown by the  $\text{Bi}_2\text{O}_3$  synthesised by precipitation in argon supports the use of many other bismuth compounds (e.g. bismuth subsalicylate and bismuth oxychloride) that are widely used in medicines and other biological application [Von Recklinghausen et al., 2008; Tripathi et al.,

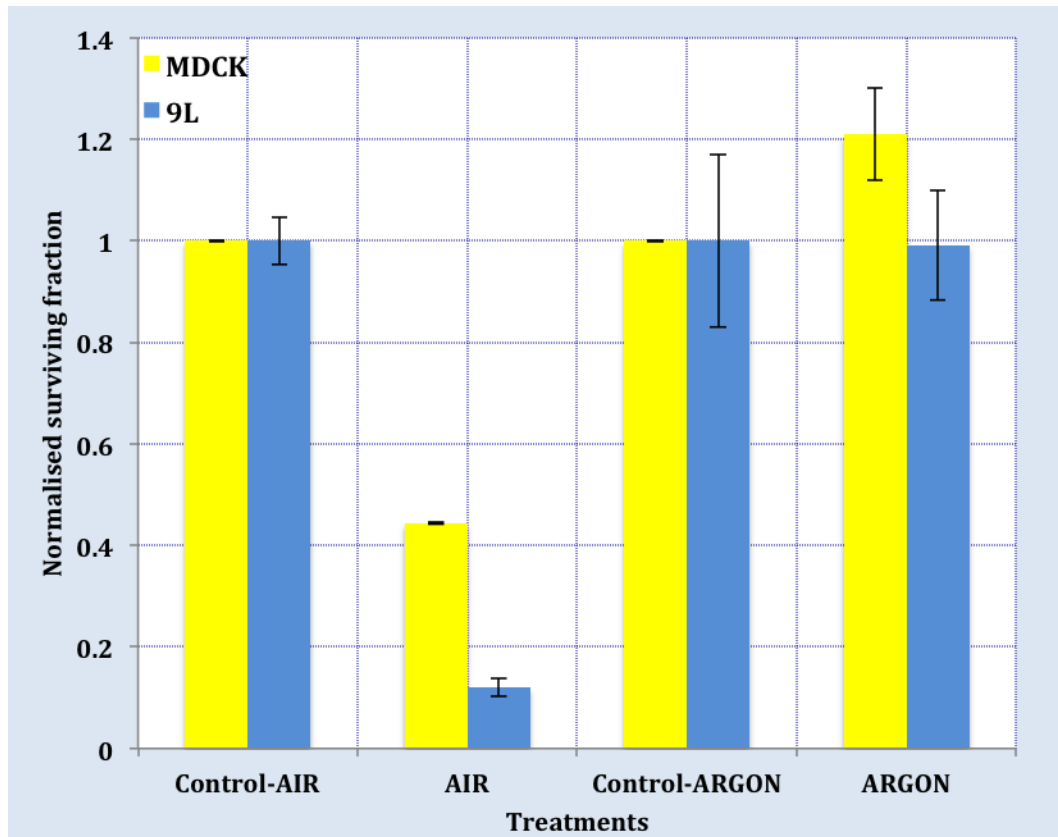


Figure 4.10: Comparison of cytotoxicity tests of  $\text{Bi}_2\text{O}_3$  (air vs. argon techniques) as the number of clonogenic survival of unirradiated 9L and MDCK cells at the concentration of  $50 \mu\text{g}/\text{ml}$ . Bars are  $\pm$  one standard deviation.

2011; Lambert and Midolo, 1997; Fugiwara et al., 2005].

### 4.3.3 Fluorodex Cytotoxicity Test on 9L Cells

5-FU is an anticancer drug that has widely used for more than 50 years. However, the major drawbacks of its use in a clinical setting is in the administration of these drugs, which includes phlebitis, thromboembolic events and catheter blockages. Fluorodex is the clinical term used for pH neutral parenteral 5-FU and folinic acid formulations that are improved injectable forms of 5-FU that may reduce the occurrence of these limitations [Locke et al., 2009; Stutchbury et al., 2010]. The toxicity effect of Fluorodex on 9L cells is shown in Figure 4.11, which show that it is more toxic compared to 5-FU alone as well as with

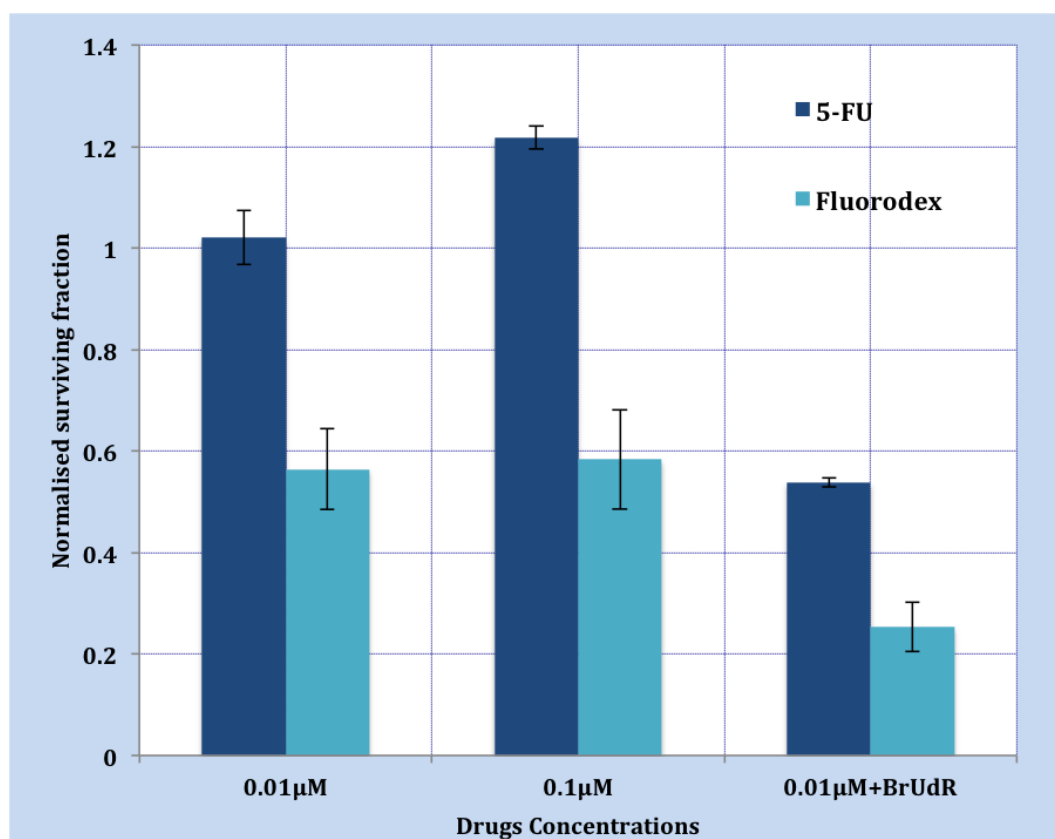


Figure 4.11: Comparison of cytotoxicity test of 5-FU (to allow for comparison) and fluorodex on 9L cells at the concentration of 0.01 – 0.1  $\mu\text{M}$  of fluorodex and the combination with 10  $\mu\text{M}$  BrUdR. Bars are  $\pm$  one standard deviation.

the combination with 10  $\mu\text{M}$  BrUdR (Figure 4.11).

Interestingly, the MDCK cells grown in fluorodex at all concentrations showed an increased clonogenic survival of MDCK cells compared to the control cells (untreated) (Figure 4.12).

#### 4.3.4 Conclusions

By taking into account the toxicity effect of the anti-cancer drugs alone, optimum drug doses of 0.01  $\mu\text{M}$  was chosen for MTX and 5-FU. The optimum concentration of 10  $\mu\text{M}$  is chosen for BrUdR since there was either no or only a slight toxicity observed in this case with or without the combination of the

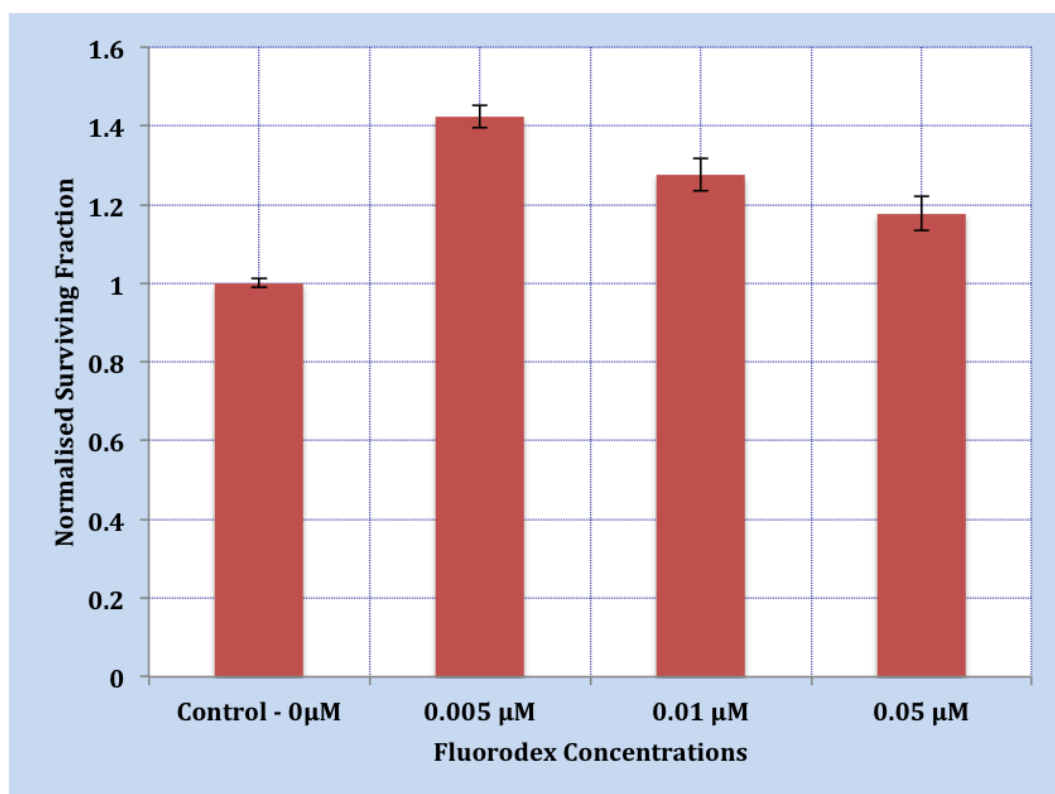


Figure 4.12: Comparison of cytotoxicity test of fluorodex on MDCK cells at the concentration of 0.005 – 0.05  $\mu\text{M}$ . Bars are  $\pm$  one standard deviation.

anticancer drugs. In other words, the optimum drugs doses within a medium range of toxicity were chosen as when they are combined with radiation, the experiments did not lead to an over killing of the cells (i.e. cell survival viability was still countable). It appears that the effect of exposure to either BrUdR or MTX alone on unirradiated cells has an inhibitory effect on the cell proliferation to a similar extent.

For the biocompatible nanostructured particle work, all of the new engineered nanomaterials:  $\text{CeO}_2$ ,  $\text{Ta}_2\text{O}_5$ , and  $\text{Bi}_2\text{O}_3$  (except when synthesised by precipitation in air) showed an excellent biocompatibility at the concentration tested. Furthermore, they are potentially suitable as high-Z agents to study the interaction of such materials with biological systems.

The results of the toxicity experiments indicate that there is significant potential for future research effort directed towards investigating the use of 5-FU in combination with BrUdR as well as Fluorodex in combination with radiations. Especially with Fluorodex, since it exhibits toxicity effect on cancerous cells (9L) but not on non-malignant cells (MDCK).

## 4.4 Experimental Dose Rate of LINAC

The aim of this section is to establish conditions for the optimal enhancement of megavoltage (MV) X-ray radiation upon the survival curves. We do this by investigating the effect of the dose rate delivered by the LINAC. This investigation is carried out prior to the main projects, which investigate the use of pharmaceutical agents and the parallel studies using nanoparticles.

Research investigating the biological effect of differing dose-rates for 10 MV X-ray irradiation delivered from a LINAC is highly significant in predicting outcomes of new generation of intensity modulation radiation therapy (IMRT), which is commercially available using technology that enable the delivery X-rays with high dose-rates. To our best knowledge, this is the first time that the biological effectiveness of 10 MV X-ray radiation doses on 9L and MCF-7 cell lines has been investigated. The significance in the findings of this study are discussed with regard to observations on the radio-sensitivity of the 9L and MCF-7 cells, concepts of radiobiology, and potential implications for new methods of dose delivery of IMRT.

### 4.4.1 Background

Radiation therapy (RT) is an important modality for many cancer treatments, with over 50% of cancer patients receiving some form of RT as part of their cancer management plan. The ongoing challenge in RT treatment is the controlled delivery of a lethal dose to the tumour whilst minimising damage to the surrounding normal tissue. Modern radiotherapy techniques such as intensity modulation radiation therapy (IMRT), intensity modulated arc therapy (IMAT) or volumetric-modulated arc therapy (VMAT), and stereotactic ra-



diatherapy (SRT)[Tubiana and Eschwege, 2000; Benedict et al., 2001; Siochi, 1999] have improved local tumour control through better precision of the delivered radiation dose. These technologies consequently often deliver more complex treatment fields than conventional techniques.

Clinically, IMRT has become an important modality and it has been widely used in radiotherapy for over 15 years. The capabilities of IMRT have been extensively described in the literature in terms of physical advantages, such as target coverage conformity, better dose uniformity, and sparing the adjacent normal tissue, which make IMRT technique superior compared to conventional or three-dimensional conformal external radiotherapy (3D-CRT) [Group, 2001; Cheung, 2006]. However, in IMRT an increased number of monitor units (MUs) is required and thus IMRT (beam-on time) generally involves a longer dose delivery time than conventional RT. The radiobiological advantages of IMRT have been extensively debated in the literature [Wang et al., 2003; Mu et al., 2003; Moiseenko et al., 2007; Fowler et al., 2004; Srensen et al., 2011; Lohse et al., 2011]. The suspicion that IMRT could possibly decrease tumour control due to the increase of the overall treatment time does not have any clinical evidence and this would be offset by the advantages linked to the better conformation of physical doses to the target volumes and therefore better sparing of critical organs.

Improvement in clinical outcomes can be achieved by reducing patient intra fraction movements. Recent technical developments have therefore focused on increasing the clinical dose rates to minimise the effect of such movements. Increasing the dose rate also has the added benefit of reducing the overall patient treatment time, thus allowing an increase in patient throughput. One recent development is the removal of flattening filters in the linear accelerator

heads (flattening filter free (FFF) linac configuration), which has proven to be particularly beneficial for IMRT and SRT [Fu et al., 2004; Stathakis et al., 2009; Kragl et al., 2009]. The absence of the flattening filter, leading to a significant decrease in the number of MUs for a given photon treatment delivery, has been reported in the literature for both Varian (energies 6 MV and 18 MV) [Stathakis et al., 2009] and Elekta (energies 6 MV and 10 MV) [Kragl et al., 2009] clinical LINACs. It is thus important to, and would be hazardous not to, investigate the biological effectiveness of physical radiation doses delivered with differing dose rates.

Recently published radiobiological data has emphasised the radiobiological effect of a high instantaneous dose rate and indicated that there is no effect of the instantaneous dose rate of FFF LINACs on clonogenic cell survival [Srensen et al., 2011]. Other data however, showed that the radiobiological effect of the FFF beam is dependent on dose per pulse and suggested that it might become a crucial factor that influences the cancer cell survival [Lohse et al., 2011]. Ling et al. [1995] reviewed the dose rate effect in external beam radiotherapy and concluded that it is the overall beam-on time that determines tumour cell survival, not the average dose-rate of the LINAC nor the instantaneous dose-rates within LINAC pulses. In this work, we are primarily focused on the overall time of irradiation and its influence on the survival of two cell lines with significantly different radiosensitivities.

Dose-rate sparing is usually known to involve a decreased biological response to radiation exposure at a low dose rate compared to a high dose rate, as theoretically predicted by Lajtha and Oliver [1961]. To the contrary, Mitchell and Bedford [1977] and Mitchell et al. [1979] first identified the decrease in survival of HeLa cells irradiated at a low dose rate of 37 cGy/h compared with a high

dose rate of 1.54 Gy/h; this was referred to as the inverse dose-rate effect. Similar studies by Furre et al. [1999] also observed an inverse dose-rate effect on NHIK 3025 cells. These data suggest that for some cell lines, a monotonic increase in dose-rate does not produce a similar increase in cell killing. Moreover, in some specific cell lines increasing the dose rate actually decreases the cell killing effectiveness.

#### 4.4.2 Results

RT is rapidly evolving toward the adoption of equipment delivering higher dose rates. The safe adoption of these latest technologies in clinical practice necessitates a thoughtful evaluation of all the relevant parameters. However, the radiobiological advantages of the use of higher dose rates has been the subject of much recent debate in the literature. In this work, the results of in vitro experiments in which the biological effect of differing dose-rates for 10 MV X-ray irradiation delivery from a LINAC has been assessed by colony forming assay. The dose is delivered using clinical dose rates of 0.5 Gy/min compared to a 10-fold higher dose rate of 5 Gy/min. 9L and MCF-7 cell lines were used because they represent a good pre-clinical model of brain and breast tumour tissues respectively. Their intrinsic radio-sensitivity is different, the 9L being considered to be more radiation resistant than the MCF-7.

Clonogenic assay was used to determine cell reproductive death after treatment with ionising radiation as first described by Puck and Marcus [1956]. In the present study, this assay was performed to measure the capability of each cell line to proliferate and produce colonies after the irradiation, which can be modelled by a linear-quadratic function of radiation dose.

#### 4.4.2.1 Determination of the dose-rate effect of the MV X-ray beams on clonogenic cell survival

The results for the 10 MV X-rays irradiation experiment at a dose-rate of 0.5 Gy/min compared to 5 Gy/min on 9L and MCF-7 cells are shown in Figure 4.13 and Figure 4.14, respectively. The reduction of dose-rate appears to have no effect on the clonogenic survival of 9L cells (Figure 4.13). However, with MCF-7 cells, the lower dose-rate irradiation results in a decreased clonogenic survival (Figure 4.14). Analysis of the data using the LQ model is shown in Table 4.2 and reveals that the  $\alpha$  value for MCF-7 cells irradiated at 0.5 Gy/min ( $0.83 \pm 0.01 \text{ Gy}^{-1}$ ) is larger than the corresponding value when irradiated at 5 Gy/min ( $0.47 \pm 0.03 \text{ Gy}^{-1}$ ). Hence, a change in the efficacy of treatments was found, as measured quantitatively by a significant reduction of 20% in the necessary absorbed radiation dose in order to achieve the same 10% cell-surviving fraction.

Since there is no dose-rate effect observed on clonogenic survival of 9L cells (Figure 4.13), the high dose-rate of 5 Gy/min is chosen for all the megavoltage irradiation experiments used in combination with the drugs/nanoparticles in this study (i.e. including the 6 MV).

#### 4.4.2.2 To explore the general applicability of the high-dose rate MV X-ray induce enhancement of clonogenic killing to cancer cells

The cell survival curves of the 9L and MCF-7 cells after irradiation with 10 MV X-rays at a dose-rate of 5 Gy/min are plotted on the same graph to allow comparison of the relative radio-sensitivities of the two cell lines (Figure 4.15). From the graph it can be seen that 9L cells are about 2.2 times more resistant

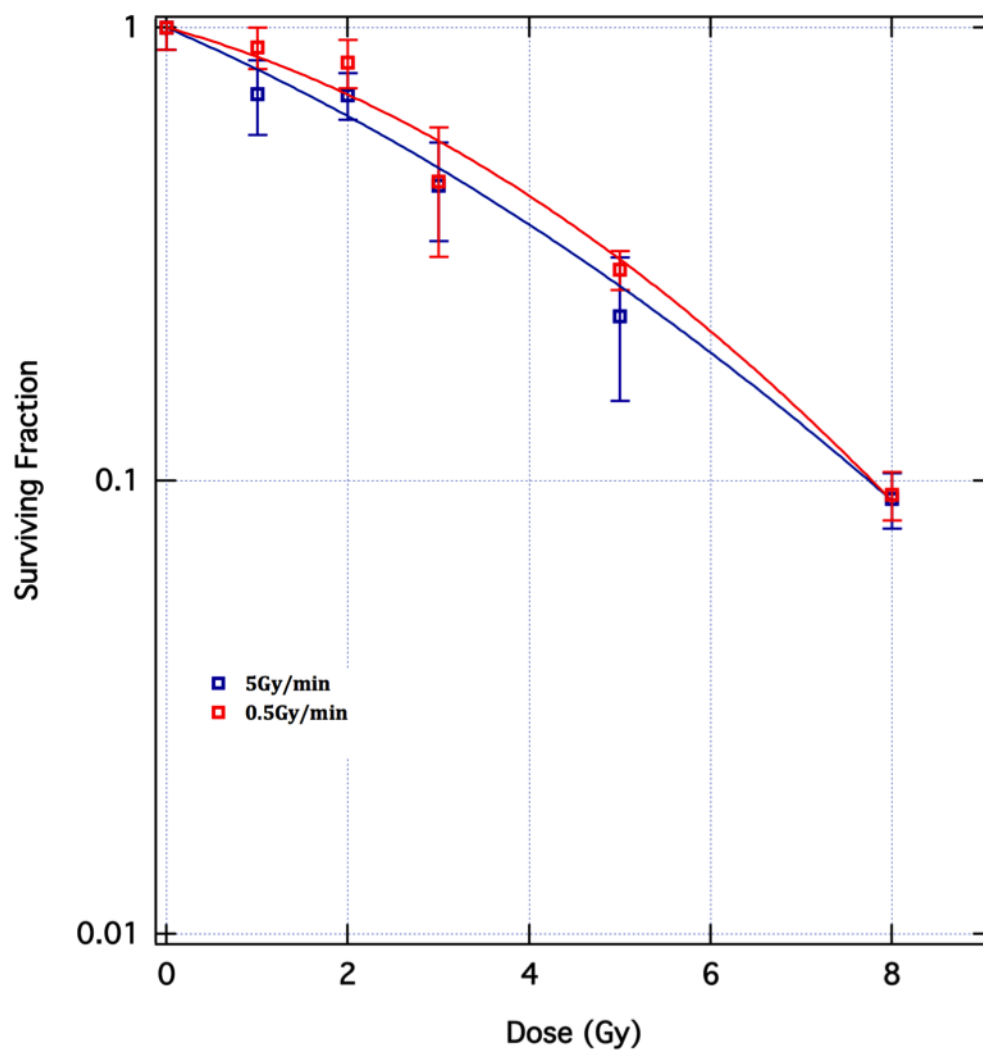


Figure 4.13: Radiation survival curves of 9L cells irradiated at dose rate of 0.5 Gy/min vs. dose rate 5 Gy/min. The data were fitted to the linear quadratic model. Each data point represents the means  $\pm$  standard deviation of three independent experiments.

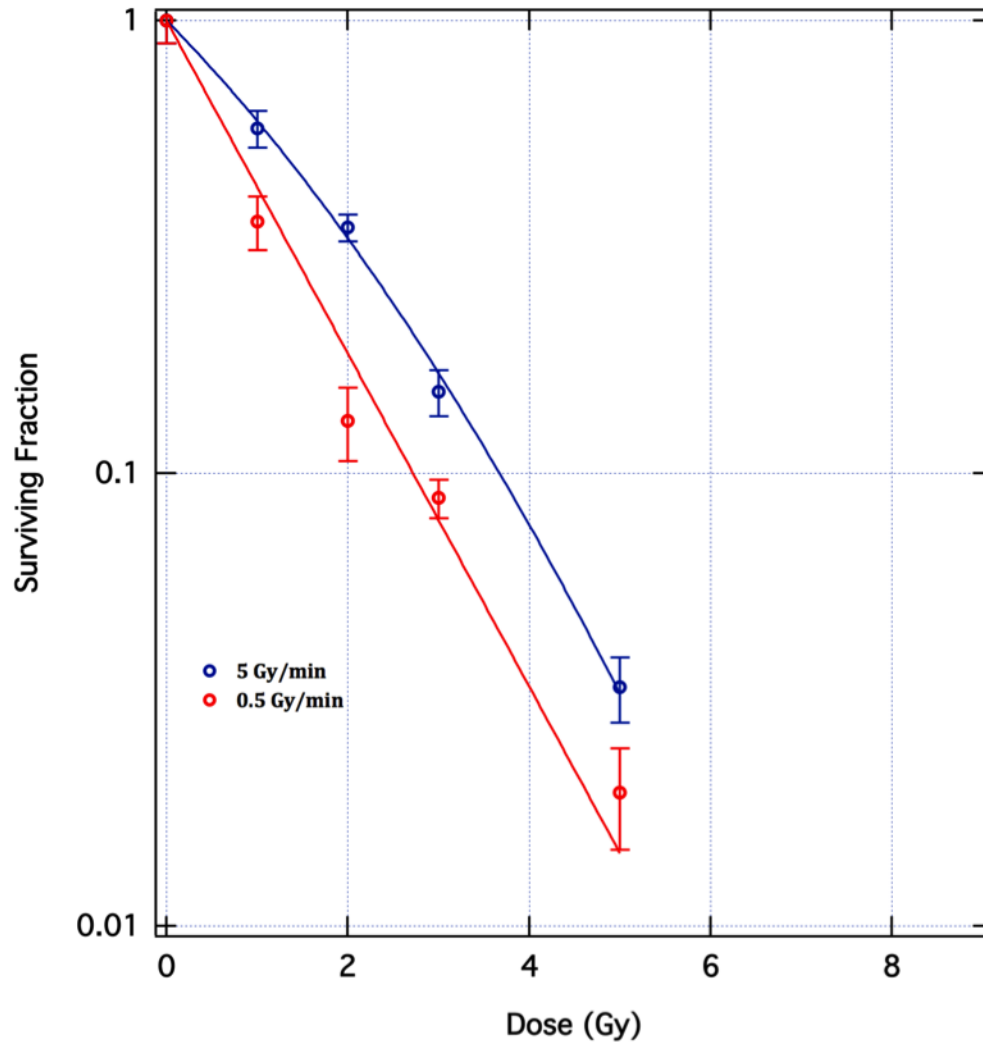


Figure 4.14: Survival curves of MCF-7 cells irradiated at dose rate of 0.5 Gy/min vs. dose rate 5 Gy/min. The data were fitted to the linear quadratic model. Each data point represents the means  $\pm$  standard deviation of three independent experiments. 8 Gy data point is not included as they are too sensitive – number of colonies obtained were less than 50.

than MCF-7 cells. The 10% survival doses ( $D_{10}$ ) in 9L and MCF-7 are 8 Gy and 3.7 Gy, respectively. The data point of 8 Gy is not included in MCF-7 as the cells are too sensitive (number of colonies counted were less than 50). It is not possible to increase the number of cell density for the clonogenic assay in order to get more than 50 colonies due to the limited size of the flask used (T12.5 cm<sup>2</sup>).

Table 4.2 presents the radiobiological parameters and indicates that the 9L cell line, with  $\alpha = 0.20 \pm 0.06 \text{ Gy}^{-1}$  and  $\beta = 0.013 \pm 0.008 \text{ Gy}^{-2}$ , is more radio-resistant than MCF-7, with  $\alpha = 0.47 \pm 0.03 \text{ Gy}^{-1}$  and  $\beta = 0.04 \pm 0.007 \text{ Gy}^{-2}$ . These findings are consistent with values published in the literature, which are  $\alpha = 0.24 \text{ Gy}^{-1}$ ;  $\beta = 0.029 \text{ Gy}^{-2}$  for glioblastomas and  $\alpha = 0.45 \text{ Gy}^{-1}$  and  $\beta = 0.039 \text{ Gy}^{-2}$  for adenocarcinoma [Malaise et al., 1987].

Table 4.2: Summary of cell survival parameters

Cell line	Dose rate (Gy/min)	$\alpha \text{ (Gy}^{-1}\text{)}$	$\beta \text{ (Gy}^{-2}\text{)}$
9L	0.5	$0.13 \pm 0.04$	$0.021 \pm 0.007$
	5	$0.20 \pm 0.06$	$0.013 \pm 0.008$
MCF-7	0.5	$0.84 \pm 0.02$	0.00
	5	$0.47 \pm 0.03$	$0.040 \pm 0.007$

#### 4.4.2.3 Cell cycle analysis

In an effort to evaluate whether the observed inverse dose-rate effect is linked to the proportion of cells in radio-resistant and sensitive phases of the cell cycle, a FACS analysis was performed. Under asynchronous confluent conditions, the percentages of cells in  $G_0/G_1$ , S, and  $G_2/M$  in both cell lines are summarised in Table 4.3. In the case of the 9L cell line, 64.2% of the population is in the  $G_0/G_1$  phase, while MCF-7 has only 58.7%. The percentage of cells in the S-phase in 9L and MCF-7 is 12.6% and 13.2%, respectively. The percent-

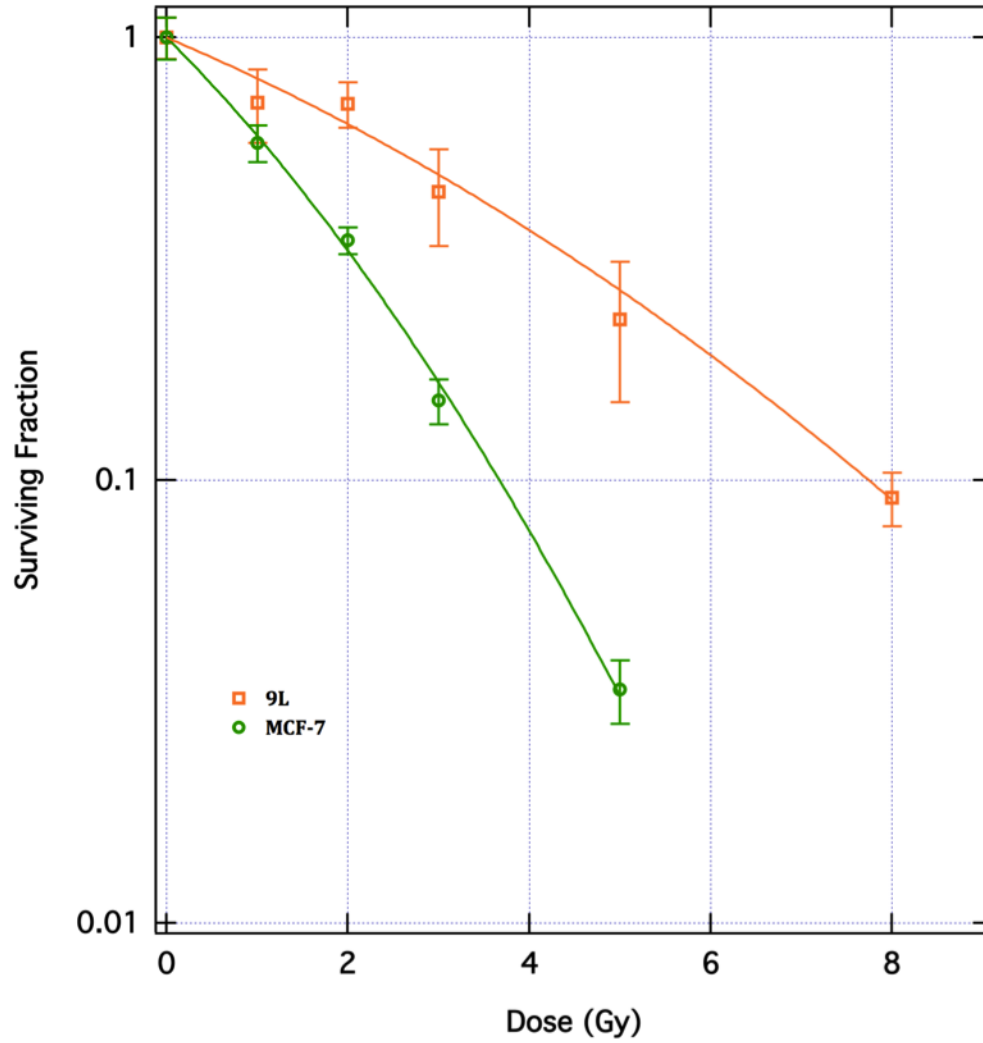


Figure 4.15: Survival curves of 9L and MCF-7 irradiated at a dose-rate of 5 Gy/min. The data were fitted to the LQ model. Each data point represents the means  $\pm$  standard deviation of three independent experiments. 8 Gy data point is not included in MCF-7 as the cells are too sensitive – number of colonies obtained were less than 50



age of 9L cells in G<sub>2</sub>/M is 23.2%, in contrast to 28.1% of MCF-7 cells in G<sub>2</sub>/M.

Table 4.3: Summary of cell cycle distribution of unirradiated confluent cell populations

Cell line	G0/G1 (%)	S (%)	G2/M (%)
9L	64.2	12.6	23.2
MCF-7	58.7	13.2	28.1

### 4.4.3 Discussions

As is generally true for most glioma cell lines, the 9L cell line is aggressive and less radio-sensitive than other rat tumour cell lines [Henderson et al., 1981; Bencokova et al., 2008]. It is the best and most widely used of all rat brain tumor models for research [Barth, 1998] as well as for preclinical model used in brain radiotherapy [Vinchon-Petit et al., 2010], it has been utilised in such experiments for more than 30 years [Kimler, 1994]. The MCF-7 cell line represents a well adopted pre-clinical model of breast tumour tissue. It has provided the basis of many breast cancer biology studies [Tutt and Yarnold, 2006] and are relatively more radio-sensitive than the other breast cancer cell line [Matthews et al., 1989].

No differences in the survival curves of the 9L cell line were observed at dose rates of 0.5 Gy/min and 5 Gy/min (Figure 4.13). Interestingly, an inverse dose rate effect was observed for the MCF-7 cells (Figure 4.14), where the lower dose rate of 0.5 Gy/min induced an increased cell killing compared to that for the 5 Gy/min dose rate. The inverse dose rate effect is complemented with a linearisation of the cell survival curve when the lower dose rate experiment at 0.5 Gy/min is performed. The results observed above suggest that the optimum dose rate radiotherapy can be significantly different depending on the tumour cells type.

Several studies have shown that by decreasing the radiation dose rate, recovery processes are allowed to take place during irradiation (i.e. within the first few hours). This usually leads to a reduced biological effect Steel [1989]; Hall [1972]. This traditional key characteristic of the dose-rate effect appears to be inversed in this study.

The mechanisms underlying the cause of the inverse nature of the dose-rate effect are not well understood. Possible explanations for this finding could be that the effect is dependent on the intrinsic radio-sensitivity that varies along the cell cycle [Ling et al., 1995] at the time of irradiation, the cell type [Fertil and Malaise, 1981], the doubling time [Mitchell et al., 1979], cell age [Biade et al., 1997] and, more clinically, the histology type [Ramsay et al., 1992].

Numerous studies have shown that the X-ray induced deficiency in DNA synthesis depends on the cell cycle phase of cells at the time of irradiation [Denekamp, 1986; Griffiths and Tolmach, 1975; Rowley and Leeper, 1985]. In this study, while the mechanism of the change in the efficacy of treatments by 20% is unclear, these positive data support further exploration to investigate the dose-rate effect on the biological effectiveness of megavoltage X-ray radiation doses.

Radiation sensitivity, expressed as loss of reproductive ability, depends on the cell cycle phase in which the cells are exposed. The variation in the cell cycle response to ionising radiation is believed to be due to the intrinsic radio-sensitivity of some human tumour cells [Biade et al., 1997]. A lower dose rate would then be expected to be more effective if a phase of the cell cycle (i.e. G<sub>2</sub>/M-phase) was correlated with the radio-sensitivity [Knox et al., 1993; Marples, 2004; Wilson, 2004].

Numerous studies have found that plateau-phase cultures are generally more radio-sensitive than exponentially growing cells. On the contrary, some studies have observed the development of radio-resistance in plateau phase with V79 cells [Durand and Sutherland, 1973] and 9L cells [Mendonca et al., 1989; Kimler and Henderson, 1982]. This condition is minimised in this study since all experiments were carried out with confluent cultures, where the cell number remained constant throughout the irradiation.

Flow cytometry experiments were used to evaluate whether the observed inverse dose-rate effect is linked to the differences in the intrinsic radiosensitivity between these two cell lines. FACS analysis was performed to analyse the cell cycle distribution and DNA content, this indicated that the proportion of cells in the same phase were similar for the two different cell lines studies. Cells are most radiosensitive in phases  $G_2/M$ , have intermediate radiosensitivity in  $G_0/G_1$  and are most radio-resistant in the S-phase [Tubiana et al., 1990]. It is reasonable then to consider that *in vitro* radiosensitivity of a cell line may be influenced by the proportion of cells in the different phases of the cell cycle. However, our flow cytometry results indicate that the cells phase distribution may not play an important role in the observed differences in the radiation sensitivities of the two cell lines.

This study has potential implications for external radiation delivery techniques, where the dose-rate is greatly increased. It is hypothesised that *in vitro* cellular radio-sensitivity is correlated with *in vivo* tissue response [Deacon et al., 1984]. For instance, the  $\alpha$  parameter predicts best for intrinsic radio-sensitivity of tumour cells irradiated at a dose of 2 Gy (SF2) [Fertil and Malaise, 1981; Malaise et al., 1987].

The clinical implementation of different dose-response parameters on biologically optimised IMRT in breast cancer has been studied by Ferreira et al. [2008], their results suggest that it can only be maximised by predicting the individual patient radio-sensitivity. Our studies support that individualised radiation therapy may significantly increase the benefits for patients with extreme radio-sensitivity or radio-resistance.

Since no single molecular factor has been identified which is common to all the cancer cell lines that can explain their radiation sensitivity to radiation dose-rate, an improved understanding of the intrinsic radio-sensitivity and damage repair mechanisms should lead to personalised enhanced cancer RT treatments. The results presented in this study may contribute to clinically significant radiobiological effects as the lower dose-rate induced an increased cell killing in MCF-7 cells. It suggests that some patients with breast cancer would not benefit from the latest technological advances and would require dose delivery with a lower dose rate (rather than a higher) for a better treatment outcome.

The various external beam conformal RT techniques such as 3D-CRT, IMRT, and VMAT have been reviewed for partial breast irradiation (PBI) treatment [Njeh et al., 2012] and for malignant glioma of the brain [Wagner et al., 2009]. Furthermore, there are many interesting papers in the literature showing that VMAT, which enables the delivery of higher effective clinical dose-rates, can be the most efficient treatment option in terms of plan quality and treatment time (better conformal dose distributions with fewer MUs).

Although VMAT offers the potential to provide improved target coverage and should be favored because of the shorter treatment time compared to conven-

tional RT techniques, *in vitro* experimental evidence specific to VMAT and its optimisation with the biological response of the tumour is lacking. Therefore, there is a need for a definitive radiobiological and clinical aspect for VMAT patient selection. Our data demonstrated that for certain types of cancer cell lines, a higher effective dose rate can lead to a decreased radiobiological response and therefore a less favourable treatment outcome. Hence, even for radiosensitive patients, the simple treatment technique (i.e 3D-CRT) is sufficient to maximise the outcome.

It is worth restating that only two dose rates were used in these experiments. Namely, a low dose rate of 0.5 Gy/min and a dose rate of 5 Gy/min, the latter is used clinically for external-beam radiotherapy. The radiobiological effect of the chosen dose rates may differ with alternative higher- or lower- dose rate irradiation. The most important feature of the data presented here is the significant difference in response to low dose rate (0.5 Gy/min) irradiation for the two cell lines. This finding is supportive of the hypothesis that dose rate effects contribute to clinically significant radiobiological effects.

To investigate whether the results presented here are applicable to other types of cells with similar radiobiological characteristics (radioresistant or radiosensitive), a variety of dose rates needs to be studied. Furthermore, to confirm if the proposed relationship between the intrinsic radiosensitivity parameters and dose rate effects is valid a variety of tumour types should be studied.

#### 4.4.4 Conclusions

The data presented in this study have focused on cell survival following the delivery of 10 MV X-rays radiation doses at a dose-rate of 0.5 Gy/min com-

pared to a 10-fold higher dose-rate of 5 Gy/min. To date, there has been no published literature on any change in the biological effectiveness of 10 MV X-ray radiation doses in 9L and MCF-7 cell lines with dose-rate. The *in vitro* experiments presented in this study show that the lower dose rate induced a larger effect in cell killing in the MCF-7 cell line.

This observation emphasises the importance of taking into account not only the physical dose but also the radiobiological responses when planning a particular cancer treatment and may help clinicians to individualise patient treatment decisions so as to maximise the efficacy of treatment and hence the clinical outcome of the RT treatment. The results of this study may provide important information to predict whether all cancer patients or perhaps only those with particular tumour types, since we have demonstrated a variation in radiosensitivity, will benefit from the new advances in the technologies of RT that enable the delivery of X-rays with high dose-rates.

## 4.5 Utilisation of Nanoparticles

In the following section, there is no attempt to deal with this topic in any more than a superficial manner. The main objective of this parallel project was to investigate the possibility of using new modern engineered materials (i.e. ceramic nanoparticles) for the same function as high-Z elements, either as radiosensitiser or radioprotectant agents. The investigation of the ceramic nanoparticle involved the synthesis of the particles, phase and structure characterisation using X-ray diffraction (XRD) and transmission electron microscopy (TEM), internalisation and testing cytotoxicity (section 4.3) on both cancer cells (9L) and non-malignant cells (MDCK) as well as exploring the effect on different energies of the X-rays beam. There are three ceramic nanoparticles currently under investigation by the TNT team: cerium oxide ( $\text{CeO}_2$ ), tantalum pentoxide ( $\text{Ta}_2\text{O}_5$ ), and bismuth oxide ( $\text{Bi}_2\text{O}_3$ ).

### 4.5.1 Introduction

Nanomaterials, commonly called as nanoparticles, are very attractive for both basic science and technologies (i.e. nanotechnology). With the rapid growth of nanotechnology, engineered nanomaterials are providing new opportunities that can improve therapeutic ratio in medical field such as by targeting cancer cells and limiting cytotoxicity to healthy normal tissue. An example of this is in indirect radiation therapy (IRT) (Figure 4.16), which inactivates cancer cells by secondary radiation products evolving from incorporated target material inside the body upon specific absorption of an external radiation therapy beam (one of the possible methods, known as photon activation therapy – PAT is defined later in detail in section 4.6).

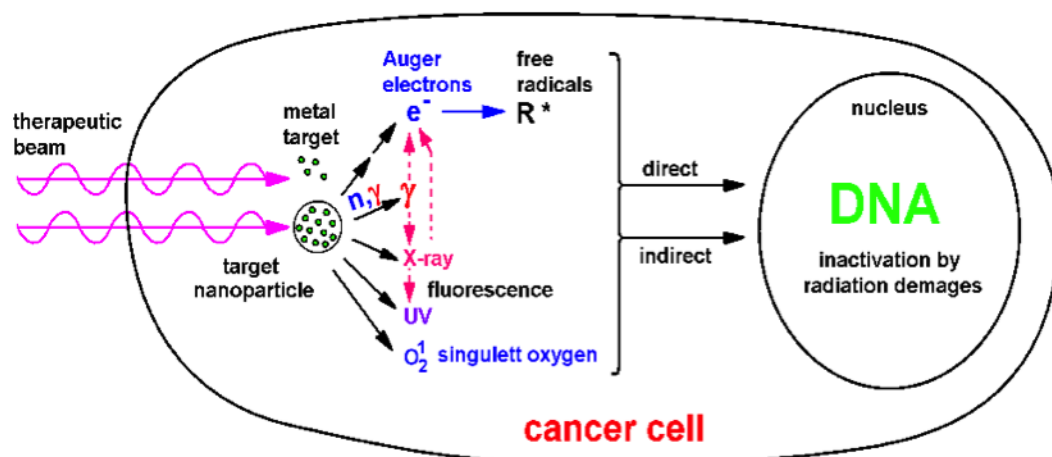


Figure 4.16: Schematic representation of high-Z secondary radiation mechanism (also known as indirect radiation therapy, IRT) [Nawroth et al., 2008]

## 4.5.2 Results – Cerium Oxide ( $CeO_2$ )

### 4.5.2.1 Phase and structural characterisation of $CeO_2$

The biochemical effects of nanoparticles are dependent on their structural and physical characteristics. Characteristics of particular interest include phase composition, structure and crystallite size.

Figure 4.17A shows first order diffraction peaks that have been labeled by correlating recorded data against the ICSD (PDF card no. 01-089-8436). The cerium oxide nanoparticles phase is confirmed to exist as  $CeO_2$ . This phase is known to provide protection against radiation [Madero-Visbal et al., 2012; Colon et al., 2009; Rzigalinski et al., 2003; Tarnuzzer et al., 2005]. The  $CeO_2$  NP sample has a simple cubic crystalline structure with a single lattice parameter,  $a = 5.4112 \text{ \AA}$ . The average crystallite size can be extracted from the XRD peaks using Scherrers equation [Patterson, 1939] (Eq. 3.1).

The average crystallite size was calculated to lay in the range of 6 – 8 nm, which is consistent with the crystallite sizes observed in the TEM image (Fig-



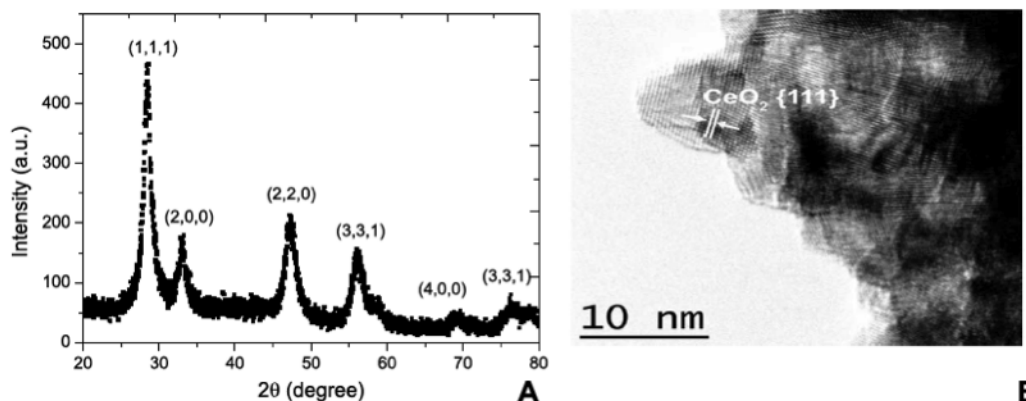


Figure 4.17: (A) XRD spectrum and (B) high resolution TEM of the CeO<sub>2</sub> NP sample synthesised by spray pyrolysis with size between 6-8 nm. Data was acquired using an automated GBC @eMMA X-ray Diffractometer. X-ray diffraction peaks were assigned Miller indices in correlation with the ICSD Briggs et al. [2013].

ure 4.17B). This shows clear lattice fringes with a fringe spacing ( $d$ ) of 3.15 Å, which corresponds to the distance between the 111 lattice planes of CeO<sub>2</sub>.

#### 4.5.2.2 Internalisation determination of CeO<sub>2</sub>

The internalisation or cellular uptake of the CeO<sub>2</sub> nanoparticles was analysed using flow cytometry (Figure 4.18). The flow cytometry analysis of side scatter (SSC), a parameter that indicates the internal complexity or granularity of the cells, showed that nanoparticle internalisation correlates with an increase in cell side scatter [Celardo et al., 2011]. The CeO<sub>2</sub> NPs affected the cell side scatter, evidenced by the increase of sparseness on the dot plots (Figure 4.18) and the increase of SSC mean value of 393 to 734.

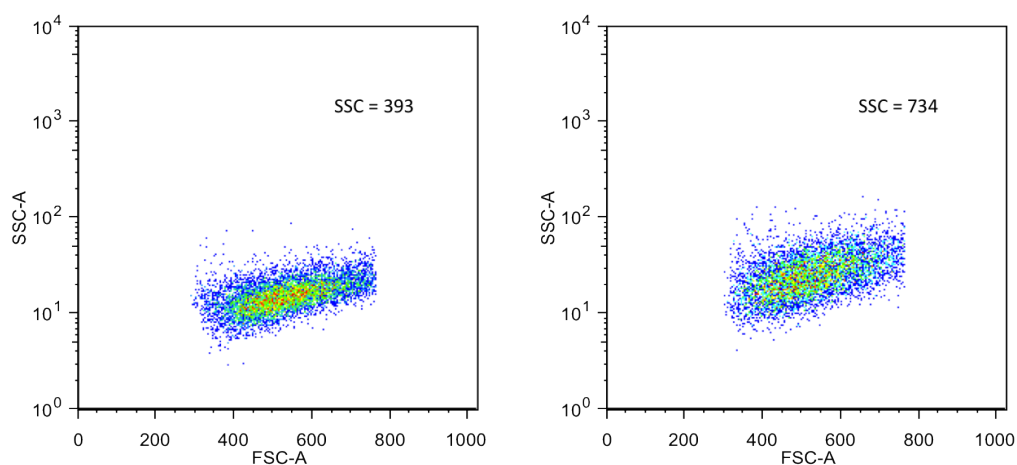


Figure 4.18: Flow cytometric analysis of forward scatter (FSC) and side scatter (SSC) of 9L cells incubated for 24 hours with 50  $\mu\text{g}/\text{ml}$  cerium oxide ( $\text{CeO}_2$ ) (right) and its control of untreated cells (left).

#### 4.5.2.3 Efficacy of $\text{CeO}_2$ nanoparticles – influence of different X-ray beams

As mentioned earlier in section 3.1.5.2, based on the atomic number of  $\text{CeO}_2$   $Z = 54$ , 150 kVp X-rays energy is believed to maximise the probability of interaction between X-ray and the high- $Z$  atoms of  $\text{CeO}_2$ . The peak of absorption of  $\text{CeO}_2$  contrast relative to water in the spectrum around 50 keV is illustrated in Figure 4.19 and it matches with the 150 kVp spectrum output defined in section 3.1.5.2 (Figure 3.4) with the effective energy of 65 keV.

Consequently, 9L cells were exposed to a range of doses up to 8 Gy using the 150 kVp, 6 MV, and 10 MV X-ray beam to probe the effectiveness of  $\text{CeO}_2$  NPs. Clonogenic assays were then performed to obtain radiation survival curves. The results show that the 9L cell line has a response that varies with treatment beam energy (Figures 4.20 – 4.22).

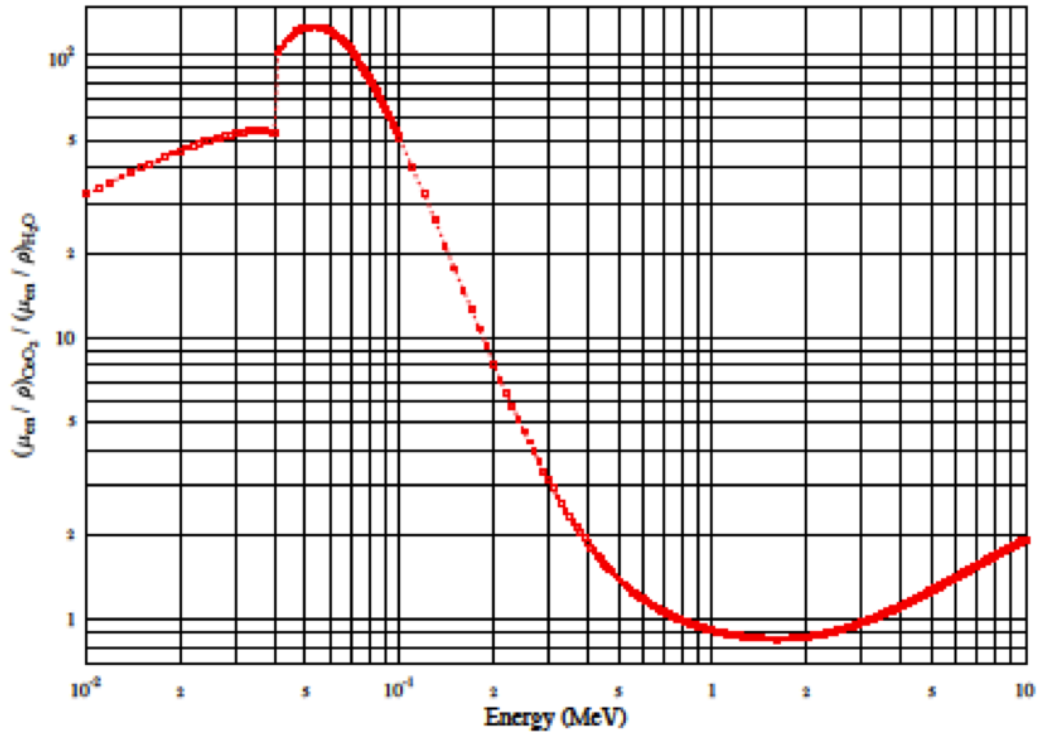


Figure 4.19: Ratio of the mass energy absorption coefficient of  $\text{CeO}_2$  to water relative to photon energy (MeV) [Briggs, 2011].

**150 kVp irradiation** The survival curves of 9L cells following irradiation with 150 kVp alone and radiation combined with  $\text{CeO}_2$  NPs ( $50 \mu\text{g}/\text{ml}$  for 24 hours) are presented in Figure 4.20. This shows that  $\text{CeO}_2$  NPs had a radiation enhancement effect on cells, instead of providing protection against radiation. A comparison of the 10% surviving fraction of cells in the presence and absence of  $\text{CeO}_2$  NPs induced a sensitisation enhancement ratio ( $\text{SER}_{10}$ ) of 1.02. This is also reflected in the  $\alpha$  value ( $\pm\text{SD}$ ) for 9L cells irradiated with  $\text{CeO}_2$  NPs ( $0.302 \pm 0.042 \text{ Gy}^{-1}$ ) being higher than that of irradiated cells without  $\text{CeO}_2$  NPs (controls) ( $0.212 \pm 0.025 \text{ Gy}^{-1}$ ) at 150 kVp (Table 4.4).

**6 MV photon beam Irradiation** The survival curves of 9L cells following irradiation with 6 MV alone and radiation combined with  $\text{CeO}_2$  NPs ( $50 \mu\text{g}/\text{ml}$  for 24 hours) are presented in Figure 4.21. This shows that  $\text{CeO}_2$  exhibits ra-

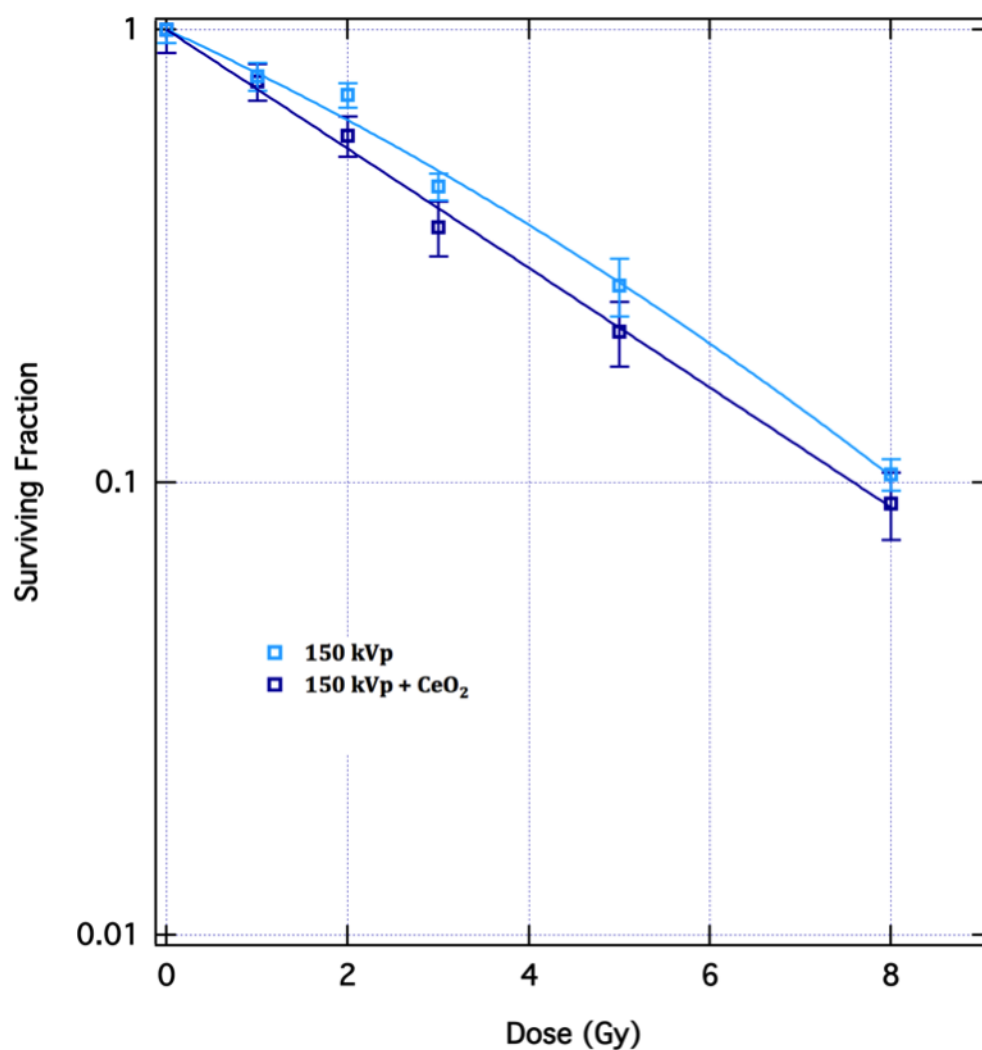


Figure 4.20: Radiation dose-survival curves of confluent cultures of 9L cells after irradiation with 150 kVp photon beam at a dose rate of approximately 75 MU/min, with or without 50  $\mu\text{g/ml}$  cerium oxide ( $\text{CeO}_2$ ) treatment for 24 hours using T12.5  $\text{cm}^2$  flask with a 6 mm depth of medium. Each data point represents the means  $\pm$  standard deviation of three independent experiments. Experimental results modified from Briggs et al. [2013].

diation protection. Instead of ( $\text{SER}_{10}$ ), a comparison of the 10% surviving fraction of cells in the presence and absence of  $\text{CeO}_2$  NPs induced a protection enhancement ratio ( $\text{PER}_{10}$ ) of 1.07. This is also reflected in the lower  $\alpha$  value ( $\pm\text{SD}$ ) for 9L cells irradiated with  $\text{CeO}_2$  NPs ( $0.193 \pm 0.015 \text{ Gy}^{-1}$ ) compared to irradiated cells without  $\text{CeO}_2$  NPs (controls) ( $0.220 \pm 0.021 \text{ Gy}^{-1}$ ) at 6 MV Table 4.4. This confirms the radioprotective ability of  $\text{CeO}_2$  NPs.

Table 4.4: Values of the linear-quadratic model parameters  $\alpha$  and  $\beta$  from 9L cells treated with ionising radiation only and combined  $\text{CeO}_2$  NP plus radiation survival curves at energies 150 kVp, 6 MV, and 10 MV. XIR = radiation only;  $\text{CeO}_2$  NP = cerium oxide nanoparticles ( $50 \mu\text{g/ml}$ ).

Energies	Treatment	$\alpha (\text{Gy})^{-1}$	$\beta (\text{Gy})^{-2}$
150 kVp	XIR	$0.212 \pm 0.025$	$0.009 \pm 0.004$
	$\text{CeO}_2$ NP	$0.302 \pm 0.042$	$0.000 \pm 0.007$
6MV	XIR	$0.220 \pm 0.021$	$0.021 \pm 0.003$
	$\text{CeO}_2$ NP	$0.193 \pm 0.015$	$0.016 \pm 0.003$
10MV	XIR	$0.200 \pm 0.060$	$0.0013 \pm 0.008$
	$\text{CeO}_2$ NP	$0.060 \pm 0.040$	$0.019 \pm 0.005$

**10 MV photon beam irradiation** The survival curves of 9L cells following irradiation with 10 MV alone and radiation combined with  $\text{CeO}_2$  NPs ( $50 \mu\text{g/ml}$  for 24 hours) are presented in Figure 4.22. This shows that when irradiated with 10 MV,  $\text{CeO}_2$  provides a protective effect to 9L cells. This is evidenced by the higher surviving fraction of 9L cells at all doses in the presence of  $\text{CeO}_2$  NPs compared to the irradiated controls only (Figure 4.22). A  $\text{PER}_{10}$  value of 1.23 is achieved during the 10 MV treatment, again confirming the radioprotective ability of  $\text{CeO}_2$  NPs. This is also reflected in the lower  $\alpha$  value ( $\pm\text{SD}$ ) for 9L cells irradiated with  $\text{CeO}_2$  NPs ( $0.060 \pm 0.040 \text{ Gy}^{-1}$ ) compared to irradiated cells without  $\text{CeO}_2$  NPs (controls) ( $0.200 \pm 0.060 \text{ Gy}^{-1}$ ) at 10 MV (Table 4.4). Table 4.4 summarises the LQ parameters of 9L cells obtained following analyses of the radiation dose-survival curves for irradiation

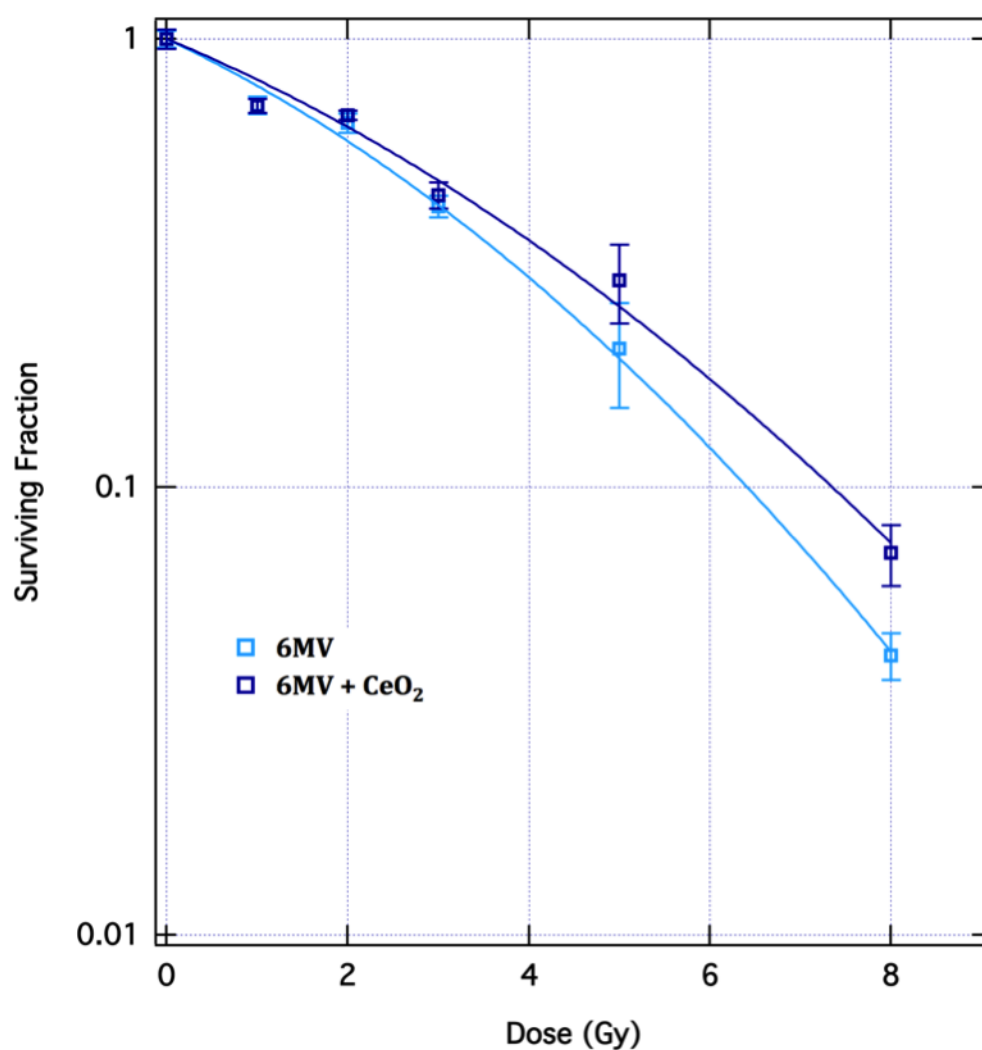


Figure 4.21: Radiation dose-survival curves of confluent cultures of 9L cells after irradiation with a 6 MV photon beam at a dose rate of 5 Gy/min, with or without 50  $\mu\text{g/ml}$  cerium oxide ( $\text{CeO}_2$ ) treatment for 24 hours using T12.5  $\text{cm}^2$  flask filled with HBSS. Each data point represents the means  $\pm$  standard deviation of three independent experiments. Experimental results modified from Briggs [2011].

alone and following combined irradiation and CeO<sub>2</sub> NPs at energies of 150 kVp, 6 MV, and 10 MV.

### 4.5.3 Results – Tantalum Pentoxide (Ta<sub>2</sub>O<sub>5</sub>)

#### 4.5.3.1 Phase and structural characterisation of Ta<sub>2</sub>O<sub>5</sub>

The XRD pattern for tantalum pentoxide nanoparticles, with the crystal planes of reflection corresponding to each peak, is shown in (Figure 4.23A). The peak analysis of the resulting diffraction pattern established the presence of a single beta Ta<sub>2</sub>O<sub>5</sub> phase, orthorhombic in nature with parameters a= 6.20 Å, b=3.66 Å, and c=3.89 Å (PDF card no. 01-089-2843).

The average crystallite size was calculated to be 56 nm, consistent with the crystallite sizes observed in the TEM image (Figure 4.23B). This revealed that the average crystallite size observed is relatively large compared to the cerium oxide nanoparticles (6 – 8 nm as in section 4.5.2).

#### 4.5.3.2 Internalisation determination of Ta<sub>2</sub>O<sub>5</sub>

The internalisation or the cellular uptake of Ta<sub>2</sub>O<sub>5</sub> NPs were analysed using flow cytometry (Figure 4.24). Unlike CeO<sub>2</sub>, this showed that the Ta<sub>2</sub>O<sub>5</sub> NPs did not affect cell side scatter, as evidenced by only a slight increase in the mean SSC value from 451 to 499. This is consistent with the TEM image (Figure 4.23B) that the majority of the Ta<sub>2</sub>O<sub>5</sub> NPs aggregates are too big to be internalised within the cells. The slight increase in SSC observed was probably due to the effect of the size distributions. The aggregates of the smaller Ta<sub>2</sub>O<sub>5</sub> NPs in latter confocal laser scanning microscopy experiments confirmed that the nanoparticles had been internalised by the 9L cells (Figure 4.47, section 4.8).

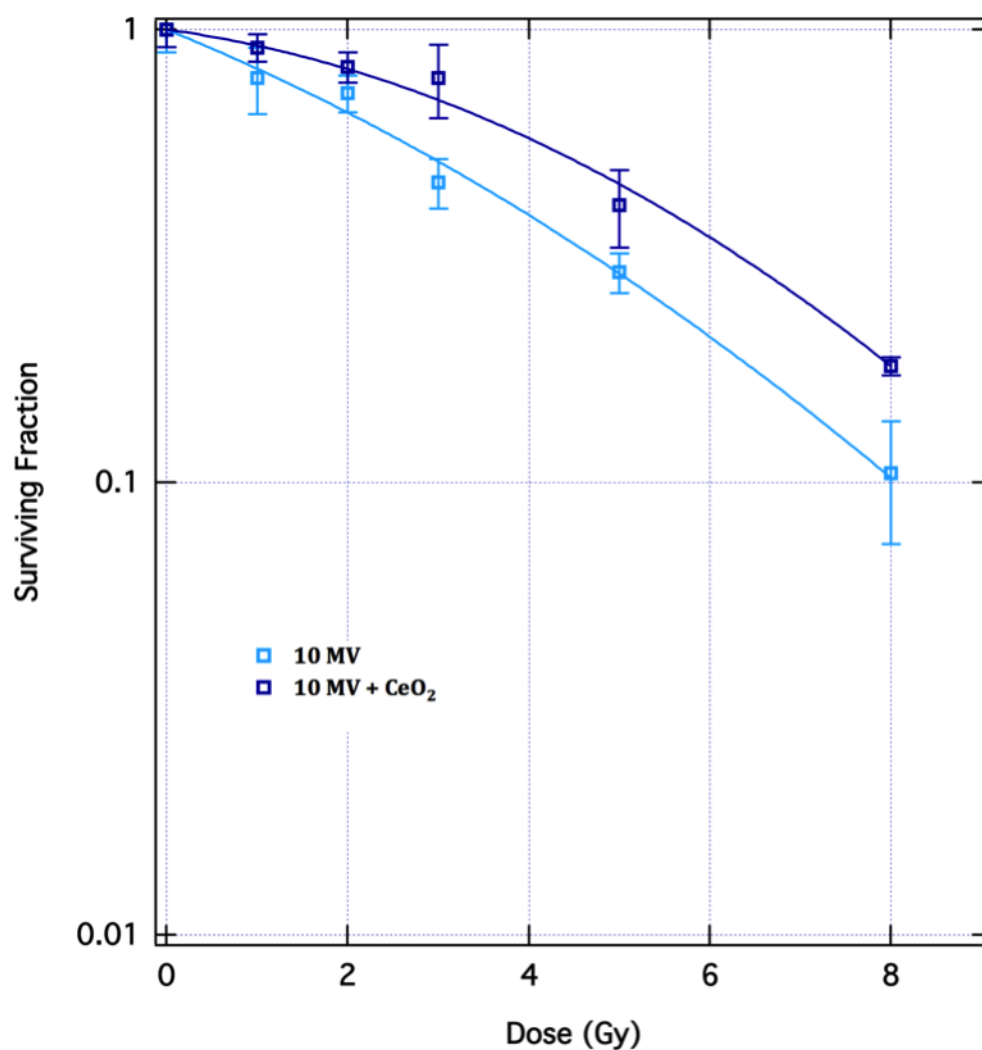


Figure 4.22: Radiation dose-survival curves of confluent cultures of 9L cells after irradiation with a 10 MV photon beam at a dose rate of 5 Gy/min, with or without 50  $\mu\text{g}/\text{ml}$  cerium oxide ( $\text{CeO}_2$ ) treatment for 24 hours using T12.5  $\text{cm}^2$  flask filled with HBSS. Each data point represents the means  $\pm$  standard deviation of three independent experiments. Experimental results modified from Briggs et al. [2013].



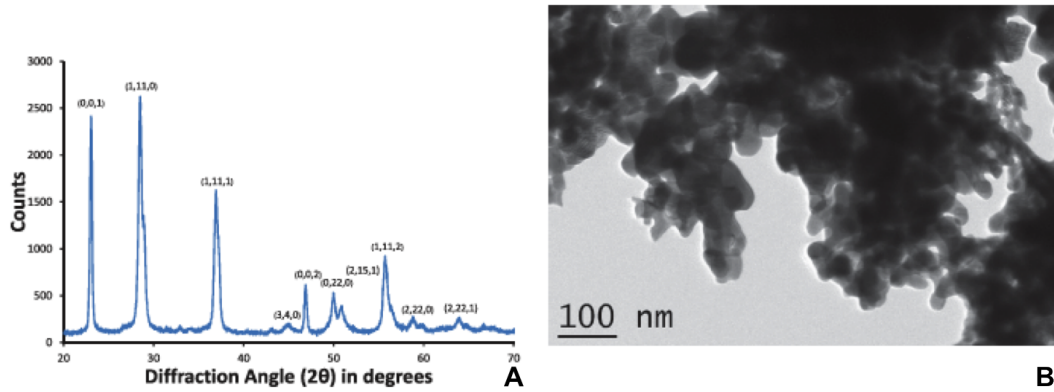


Figure 4.23: (A) XRD spectrum and (B) high resolution TEM of the Ta<sub>2</sub>O<sub>5</sub> NP sample. Data was acquired using an automated GBC®eMMA X-ray Diffractometer. X-ray diffraction peaks were assigned Miller indices in correlation with the ICSD [Brown et al., 2013].

#### 4.5.3.3 Efficacy of Ta<sub>2</sub>O<sub>5</sub> nanoparticles – influence of different X-ray beams

As mentioned earlier in section 3.1.5.2, based on the atomic number,  $Z = 73$  for tantalum (Ta), the 150kVp X-rays energy is believed to maximise the probability of interaction between X-rays and the high- $Z$  atoms of Ta<sub>2</sub>O<sub>5</sub>. The peak of absorption of Ta<sub>2</sub>O<sub>5</sub> contrast relative to water in the spectrum around 60 keV is illustrated in Figure 4.25 and it matches with the 150 kVp spectrum output defined in section 3.1.5.2 (Figure 3.4) with the effective energy of 65 keV.

**150 kVp irradiation** The survival curves of 9L cells following irradiation with 150 kVp alone and radiation combined with Ta<sub>2</sub>O<sub>5</sub> NPs (50 µg/ml for 24 hours) are presented in Figure 4.26. This shows that Ta<sub>2</sub>O<sub>5</sub> NPs had a radiation enhancement effect on cells. A comparison of the 10% surviving fraction of cells in the presence and absence of Ta<sub>2</sub>O<sub>5</sub> NPs induced a sensitisation enhancement ratio (SER<sub>10</sub>) of 1.07 (no sensitisation). This is also reflected

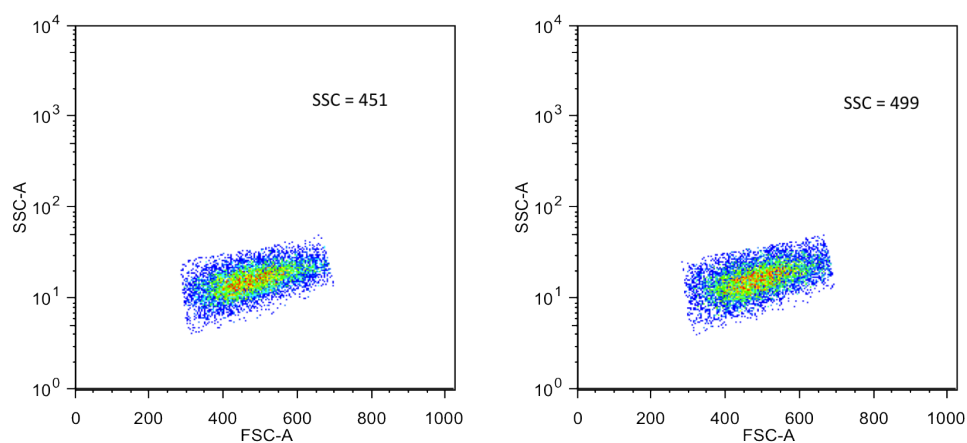


Figure 4.24: Flow cytometric analysis of forward scatter (FSC) and side scatter (SSC) of 9L cells incubated for 24 hours with 50  $\mu\text{g/ml}$  tantalum pentoxide ( $\text{Ta}_2\text{O}_5$ ) (right) and its control of untreated cells (left).

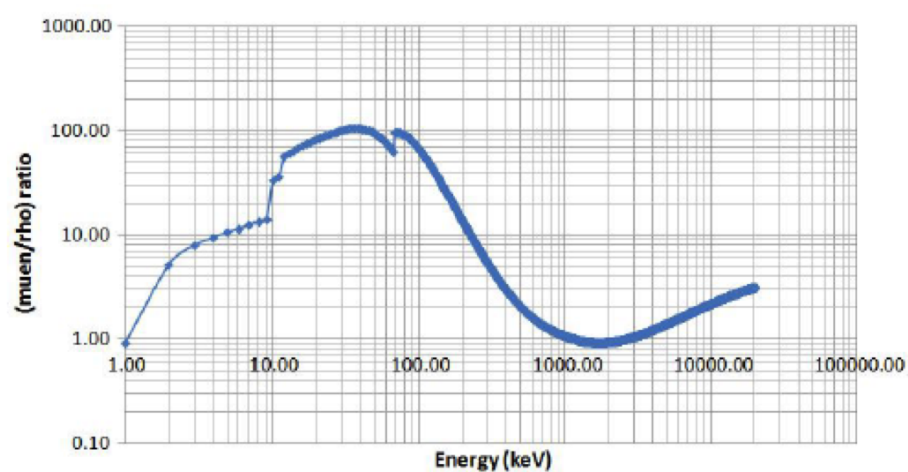


Figure 4.25: Ratio of the mass energy absorption coefficient of  $\text{Ta}_2\text{O}_5$  to water relative to photon energy [Brown, 2011].

in the  $\alpha$  value ( $\pm$ SD) for 9L cells irradiated with Ta<sub>2</sub>O<sub>5</sub> NPs ( $0.319 \pm 0.045$  Gy<sup>-1</sup>) being higher compared to irradiated cells without Ta<sub>2</sub>O<sub>5</sub> NPs (controls) ( $0.301 \pm 0.043$  Gy<sup>-1</sup>) at 150kVp (Table 4.5).

**6 MV irradiation** The survival curves of 9L cells following irradiation with 6 MV alone and radiation combined with Ta<sub>2</sub>O<sub>5</sub> NPs (50  $\mu$ g/ml for 24 hours) are presented in Figure 4.27. This shows that Ta<sub>2</sub>O<sub>5</sub> has a radiation enhancement effect on cells. A comparison of the 10% surviving fraction of cells in the presence and absence of Ta<sub>2</sub>O<sub>5</sub> NPs induced a sensitisation enhancement ratio (SER<sub>10</sub>) of 1.07. This is also reflected in the  $\alpha$  value ( $\pm$ SD) for 9L cells irradiated with Ta<sub>2</sub>O<sub>5</sub> NPs ( $0.335 \pm 0.055$  Gy<sup>-1</sup>) being higher compared to the value for irradiated cells without Ta<sub>2</sub>O<sub>5</sub> NPs (controls) ( $0.300 \pm 0.021$  Gy<sup>-1</sup>) at 6 MV (Table 4.5).

**10 MV irradiation** The survival curves of 9L cells following irradiation with 10 MV alone and radiation combined with Ta<sub>2</sub>O<sub>5</sub> NPs (50  $\mu$ g/ml for 24 hours) is shown in Figure 4.28. This shows that Ta<sub>2</sub>O<sub>5</sub> had a radiation enhancement effect on cells. A comparison of the 10% surviving fraction of cells in the presence and absence of Ta<sub>2</sub>O<sub>5</sub> NPs induced a sensitisation enhancement ratio (SER<sub>10</sub>) of 1.33, which is higher than the corresponding values at the other two lower energies. This is also reflected in the  $\alpha$  value ( $\pm$ SD) for 9L cells irradiated with Ta<sub>2</sub>O<sub>5</sub> NPs ( $0.381 \pm 0.040$  Gy<sup>-1</sup>) being higher compared to the value of irradiated cells without Ta<sub>2</sub>O<sub>5</sub> NPs (controls) ( $0.187 \pm 0.045$  Gy<sup>-1</sup>) at 10 MV (Table 4.5). This confirms a significant degree of radiation dose enhancement.

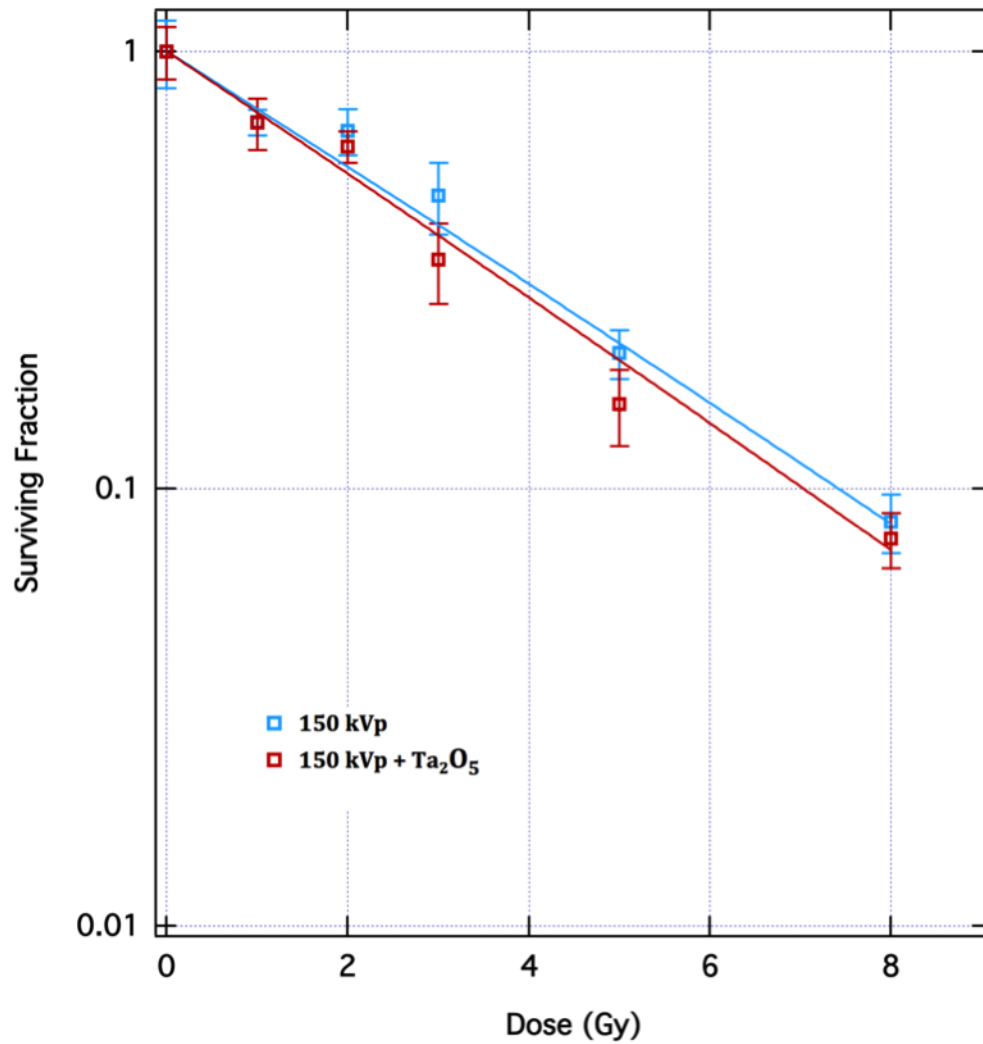


Figure 4.26: Radiation dose-survival curves of confluent cultures of 9L cells after irradiation with 150 kVp photon beam at a dose rate of approximately 75 MU/min, with or without 50 µg/ml tantalum pentoxide (Ta<sub>2</sub>O<sub>5</sub>) treatment for 24 hours using T12.5 cm<sup>2</sup> flask with a 6 mm depth of medium. Each data point represents the means  $\pm$  standard deviation of three independent experiments. Experimental results modified from [Brown et al., 2013].

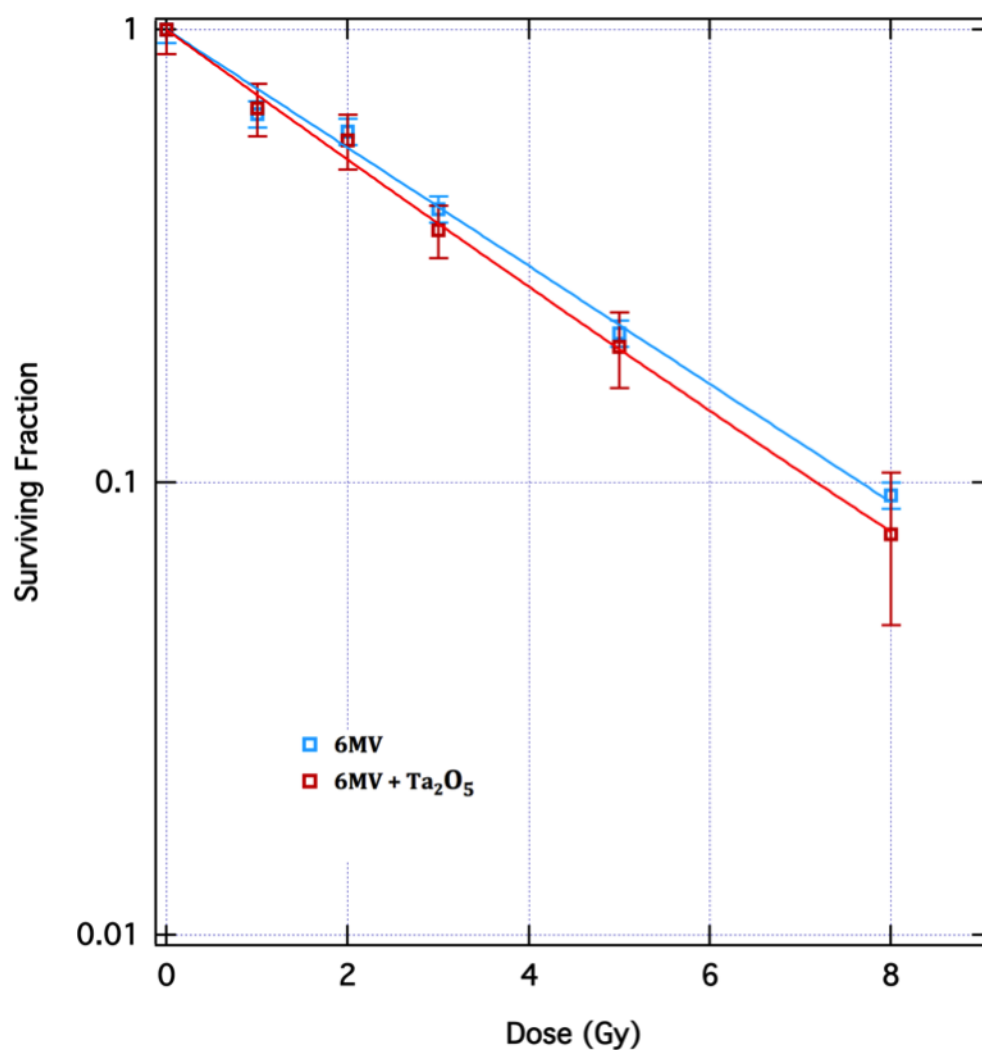


Figure 4.27: Radiation dose-survival curves of confluent cultures of 9L cells after irradiation with a 6 MV photon beam at a dose rate of 5 Gy/min, with or without 50  $\mu\text{g/ml}$  tantalum pentoxide ( $\text{Ta}_2\text{O}_5$ ) for 24 hours using T12.5  $\text{cm}^2$  flask filled with HBSS. Each data point represents the means  $\pm$  standard deviation of three independent experiments. Experimental results modified from [Brown et al., 2013].

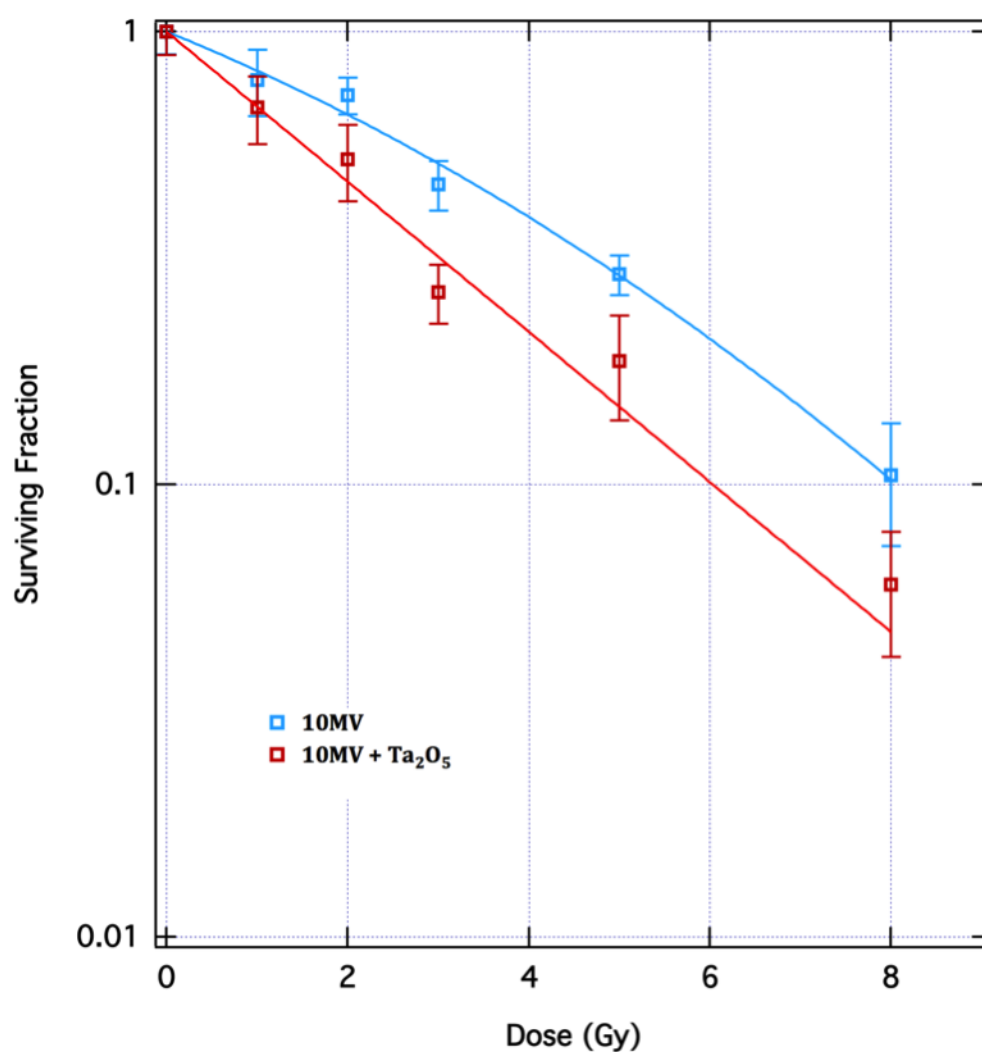


Figure 4.28: Radiation dose-survival curves of confluent cultures of 9L cells after irradiation with a 10 MV photon beam at a dose rate of 5 Gy/min, with or without 50  $\mu\text{g}/\text{ml}$  tantalum pentoxide ( $\text{Ta}_2\text{O}_5$ ) for 24 hours using T12.5  $\text{cm}^2$  flask filled with HBSS. Each data point represents the means  $\pm$  standard deviation of three independent experiments. Experimental results modified from [Brown et al., 2013].

Table 4.5: Values of the linear-quadratic model parameters  $\alpha$  and  $\beta$  from 9L cells treated with ionising radiation only and combined Ta<sub>2</sub>O<sub>5</sub> NP plus radiation survival curves at energies 150 kVp, 6 MV, and 10 MV. XIR = radiation only; Ta<sub>2</sub>O<sub>5</sub> NP = tantalum pentoxide nanoparticles (50 $\mu$ g/ml). N/A = Not applicable.

Energies	Treatment	$\alpha (\text{Gy})^{-1}$	$\beta (\text{Gy})^{-2}$
150 kVp	XIR	$0.301 \pm 0.043$	$0.001 \pm 0.006$
	Ta <sub>2</sub> O <sub>5</sub> NP	$0.319 \pm 0.045$	$0.001 \pm 0.007$
6MV	XIR	$0.300 \pm 0.021$	N/A
	Ta <sub>2</sub> O <sub>5</sub> NP	$0.335 \pm 0.055$	$0.002 \pm 0.010$
10MV	XIR	$0.187 \pm 0.045$	$0.012 \pm 0.009$
	Ta <sub>2</sub> O <sub>5</sub> NP	$0.381 \pm 0.040$	N/A

#### 4.5.4 Results – Bismuth Oxide (Bi<sub>2</sub>O<sub>3</sub>)

The investigation of using bismuth oxide (Bi<sub>2</sub>O<sub>3</sub>) nanoparticles by the TNT is still preliminary. The investigations of Bi<sub>2</sub>O<sub>3</sub> NPs in the present study only include: the synthesis of the particles, phase and structure characterisation using different techniques (i.e. XRD and TEM), internalisation and testing the cytotoxicity on both cancer cells (9L) and non-malignant cells (MDCK). The cytotoxicity was described before in section 4.3.

##### 4.5.4.1 Phase and structural characterisation of Bi<sub>2</sub>O<sub>3</sub>

The XRD pattern for bismuth oxide nanoparticles synthesised using the precipitate method in argon (530°C) and air (570°C) annealed are shown in Figure 4.29. Data was acquired using an automated GBC®eMMA X-ray Diffractometer. X-ray diffraction peaks were assigned Miller indices in correlation with the ICSD. The Bi<sub>2</sub>O<sub>3</sub> is included here as it is also currently used because its smaller size was observed.

The average crystallite size was calculated to lay in the range 63 – 69 nm and 42 – 55 nm for Bi<sub>2</sub>O<sub>3</sub> NPs synthesised via the precipitation method in argon and citrate gel method, respectively. They are consistent with the crystallite

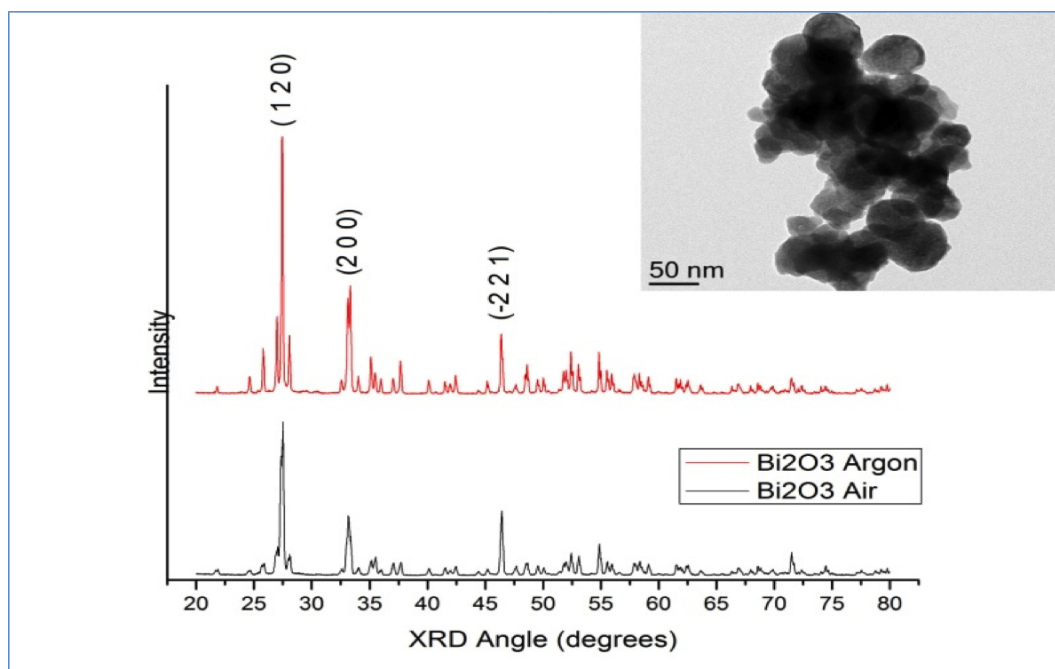


Figure 4.29: XRD spectrum of  $\text{Bi}_2\text{O}_3$  NP via precipitate in argon and air annealed; high resolution TEM (insert). Data was acquired using an automated GBC®eMMA X-ray Diffractometer. X-ray diffraction peaks were assigned Miller indices in correlation with the ICSD [Stewart et al., 2014].

sizes observed in the TEM image Figure 4.30 for both methods, which were flat plates with a micron sized diameter but extremely thin as shown in Figure 4.30.

#### 4.5.4.2 Internalisation of $\text{Bi}_2\text{O}_3$

The internalisation or cellular uptake of the  $\text{Bi}_2\text{O}_3$  NPs were analysed using flow cytometry (Figure 4.31). As for  $\text{Ta}_2\text{O}_5$ , this shows that the  $\text{Bi}_2\text{O}_3$  NPs did not affect cell side scatter, as evidenced by only a slight increase in the mean SSC value (Figure 4.31).



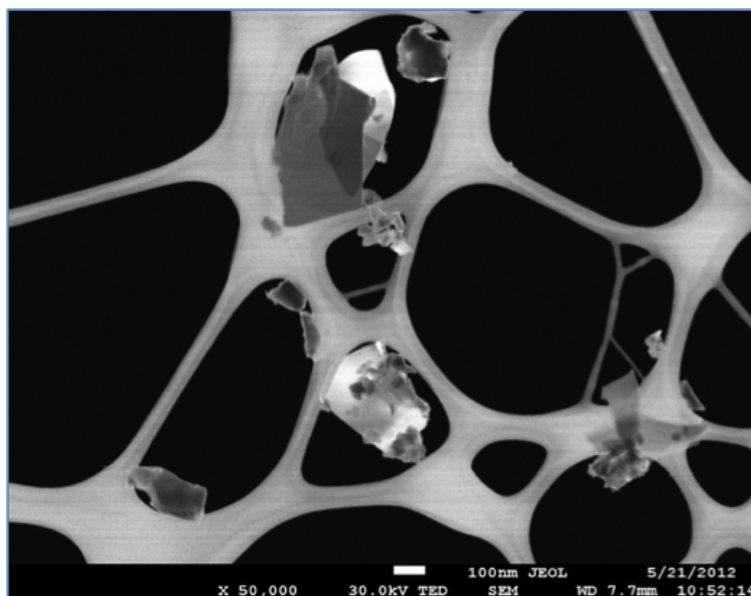


Figure 4.30: TEM image of Bi<sub>2</sub>O<sub>3</sub> [Stewart, 2012].

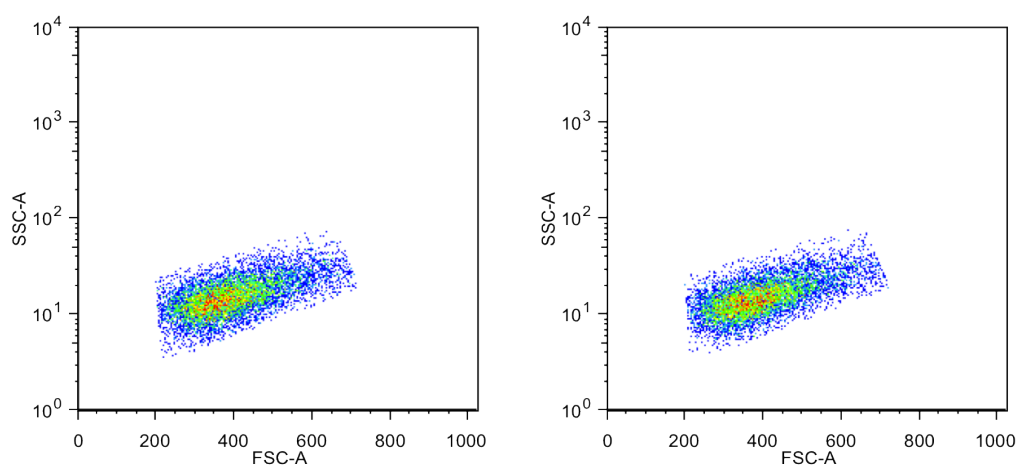


Figure 4.31: Flow cytometric analysis of forward scatter (FSC) and side scatter (SSC) of 9L cells incubated for 24 hours with 50 µg/ml bismuth oxide (Bi<sub>2</sub>O<sub>3</sub>) (right) and its control of untreated cells (left).

### 4.5.5 Discussion

#### 4.5.5.1 Cerium Oxide ( $\text{CeO}_2$ )

Investigations using  $\text{CeO}_2$  NPs explore characteristics such as its biocompatibility or toxicity [Lin et al., 2006; Sager et al., 2007; Buzea et al., 2007], the ability to provide protection against radiation by scavenging free radicals and the selective nature of its protection to normal and cancer cells [Tarnuzzer et al., 2005]. However, to date, the understanding of its effectiveness across a range of beam energies has not been reported in the literature.

Cerium oxide nanoparticles also known as nanoceria are redox-active metal oxide nanoparticles, which are used as protection against radiation-induced damage [Rzigalinski et al., 2003] and in antioxidant therapy [Celardo et al., 2011]. Nanoceria act as antioxidant because the presence of the mixed valence states of  $\text{Ce}^{3+}$  and  $\text{Ce}^{4+}$ , as induced by the oxygen vacancies [Tarnuzzer et al., 2005; Celardo et al., 2011] and provide long term scavenging of reactive oxygen species (ROS) [Rzigalinski et al., 2006].

The application of  $\text{CeO}_2$  NPs to clinical radiation protection has been the subject of numerous studies [Madero-Visbal et al., 2012; Colon et al., 2009; Rzigalinski et al., 2003; Tarnuzzer et al., 2005]. In this study,  $\text{CeO}_2$  NPs were synthesised using a spray pyrolysis techniques for their application in radiation protection. It was proposed that  $\text{CeO}_2$  NPs efficacy to function as a radioprotector is dependent upon the energy of the X-rays used during treatment; we investigated this energy-dependence using 150 kVp X-ray, 6 MV and 10 MV photon beams.

Characterisation of the synthesised sample using XRD revealed important

properties that are essential for our application. Figure 4.17A shows that we have CeO<sub>2</sub> NPs sample with a single cubic phase, existing as CeO<sub>2</sub> upon comparison with the ICSD, with a mean crystallite measured in the range of 6 – 8 nm.

Figure 4.21 and 4.22 clearly indicate that the CeO<sub>2</sub> NPs provide protection against radiation-induced damage to 9L cells when irradiated with 6 and 10 MV photon beams, respectively. This radioprotection is supported by the decrease in  $\alpha$  values following the using of CeO<sub>2</sub> compared to irradiation alone (Table 4.4).

Intriguingly, this study showed that 9L cells have a slight reduction in survival rate when exposed with CeO<sub>2</sub> NPs combined with 150 kVp X-rays in comparison with the exposure to 6 MV and 10 MV combination. A small increase in  $\alpha$  values was observed. This is also reflected in the linearisation of the cell survival curve in figure 4.20, which suggests that CeO<sub>2</sub> NPs enable more direct damage effects to occur at this treatment beam energy. We explained this energy dependent efficacy through a counterbalance between the free radical scavenging ability of CeO<sub>2</sub> and the increased RBE of lower energy radiations, which is in part influenced by the macroscopic dose enhancement from the mass-energy absorption of CeO<sub>2</sub> [McMahon et al., 2008, 2011; Robar et al., 2002].

It is important to consider photoelectric interactions for high-Z compounds [Attix, 2004] such as nanoparticles (e.g. Figure 4.20) and also the drugs used in next sections (i.e. BrUdR). Energies around the K-edge maximise the probability of interaction with X-rays and Ce atoms, which leads to an increased production of Auger electron cascades. These Auger electrons increase the

average LET of the resultant secondary particles, maximising the efficiency of these radiations through denser ionisations. This imparts more direct damage, which in turn reduces the abundance of reactive oxygen species (ROS) responsible for indirect damage [Tubiana et al., 1990].

#### 4.5.5.2 Tantalum pentoxide ( $\text{Ta}_2\text{O}_5$ ) and bismuth oxide ( $\text{Bi}_2\text{O}_3$ )

The use of  $\text{Ta}_2\text{O}_5$  nanoceramics as novel candidates for dose enhancement radiotherapy is one of our pioneering studies.  $\text{Ta}_2\text{O}_5$  acts as biocompatible radiation assistance high-Z agents, this finding lead to the research on  $\text{Bi}_2\text{O}_3$  being used for the same function as  $\text{Ta}_2\text{O}_5$ .

From XRD experiments, the average particle size of our  $\text{Ta}_2\text{O}_5$  NPs was 56 nm. For  $\text{Bi}_2\text{O}_3$ , the average size was in the range of 63 – 69 nm (synthesised via precipitation method) and 42 – 55 nm (synthesised via citrate gel method). Their values are both relatively large compared to the value for  $\text{CeO}_2$  (i.e. 6 – 8 nm). This is also shown in the flow cytometric analysis on 9L cells, where the cellular uptake of  $\text{CeO}_2$  was observed but not  $\text{Ta}_2\text{O}_5$  or  $\text{Bi}_2\text{O}_3$ .

The higher the atomic number ( $Z$ ) the higher the probability that an increased photoelectric absorption would occur due to photoelectric effect is dominant at kilovoltage beam energies. The photoelectric component of the mass energy absorption coefficient is approximately proportional to the  $Z^3$  (Eq. 2.1).

The observed energy dependence of radiosensitisation in  $\text{Ta}_2\text{O}_5$  is contrary to the results observed in  $\text{CeO}_2$ , both above as well as in a later section with BrUdR, the sensitisation enhancement ratio is increase as the energies increase for  $\text{Ta}_2\text{O}_5$  ( $\text{SER}_{10}$  at 150 kVp is lower than  $\text{SER}_{10}$  at 6 and 10 MV energies).

This should not be confused with the  $PER_{10}$  observed in  $CeO_2$ , as the same terminology used represents as no  $SER_{10}$  observed in MV energies. This can be explained by an internalisation mechanism, where smaller particles such as  $CeO_2$  are more likely to be internalised by the cells and therefore can settle closer to the DNA. This closer proximity allows more low energy secondary electrons (low range, high LET) to induce double strand breaks (DSB) due to their close proximity (more details as obvious in the use of BrUdR later in section 4.6 where they incorporated into DNA).

Another possible mechanisms to explain this inverse behaviour involves backscattered electron dose enhancement, which is a well known phenomenon in radiation therapy with MV photon beams (i.e titanium hip prostheses) [Reft et al., 2003]. As with the increasing size and Z number of the NPs aggregates and decreasing electron energy, the backscattering mechanism increases suggests that the dose enhancement tail is produced mostly by lower energy electron, which additionally can be associated with an increase in RBE. At 6 MV, less secondary electrons are produced than at 10 MV, which leads to a lower SER in general.

To our knowledge, there is currently no published research regarding the use of  $Ta_2O_5$  NPs in dose enhancement radiotherapy. Compared to research on gold NPs, which have the greater ability to be internalised due to their much smaller size (1.9 nm) [Butterworth et al., 2010] and concentrated (up to 100  $\mu g/ml$ ) on more relative radiosensitive cell line MDA-MB-231 [Jain et al., 2011], our results with the larger sized  $Ta_2O_5$  NPs on more radioresistant cells, 9L, are extremely interesting.

As in the case of  $Bi_2O_3$ , we expected its function in dose enhancement radio-

therapy should be similar for  $\text{Ta}_2\text{O}_5$ , due to the value of  $Z = 83$  for bismuth and its average large size. In general, our results suggest that the optimum condition for nanoparticles used as a radiosensitiser (i.e.  $\text{Ta}_2\text{O}_5$  and  $\text{Bi}_2\text{O}_3$ ) is that they should be evenly distributed throughout the tumour, and be taken up by tumour cells. Thus, the size of the NPs has the most dominant effect on the distribution and uptake.

#### 4.5.6 Conclusions

In the case of  $\text{CeO}_2$  (a known radioprotector) investigation on 9L cells at concentration of  $50 \mu\text{g}/\text{ml}$  showed significant nanoparticles internalisation. In addition, radioprotection was observed with a protection enhancement ratio (PER) of 1.23 when irradiated in a 10 MV photon field. The high- $Z$  property of the nanoparticle revealed itself under kilovoltage (150 kVp) irradiation fields where the net radioprotection was reduced to zero (i.e.  $\text{PER} = 1.00$ ). It was concluded that there exists a trade off between the radioprotection and radiosensitisation properties of the  $\text{CeO}_2$  nanoparticle. The radiosensitisation was thought to be most prominent at 150 kVp as the nanoparticle is internalised by the 9L cells where low energy secondary electron scattering and auger electron emission from the nanoparticle would be expected to be most effective leading to 9L cell death.

In order to try and isolate the radiosensitising component of nanoparticles, a  $\text{Ta}_2\text{O}_5$  nanoparticle was developed at TNT as a pure radiosensitiser. At an nanoparticle concentration of  $50 \mu\text{g}/\text{ml}$  (so as to directly to compare with the  $\text{CeO}_2$  radioprotector nanoparticle), no internalisation of the nanoparticle was measured by flow cytometry, which was consistent with the nanoparticle size deduced from high resolution TEM. Significant radiosensitisation of the 9L

cells was apparent under irradiation in a 10 MV photon field with an SER of 1.33 measured. This radiosensitisation reduced to zero at 150 kVp (SER =1.07). The less effectiveness of radiosensitisation at 150 kVp is consistent with that expected from the flow cytometry results in combination with the interpretations from the CeO<sub>2</sub> nanoparticle experiments. In the case of the Ta<sub>2</sub>O<sub>5</sub> nanoparticle, it is thought that the sensitisation is most predominant in the 10 MV photon field due to the low energy secondary electron scattering (leading to a very lethal radiation field) combined with the increased secondary electron production (simply due to the presence of the high-Z nanoparticle).

In light of the Ta<sub>2</sub>O<sub>5</sub> excellent result, an ultrahigh-*Z* radiosensitiser was designed and produced in the form of Bi<sub>2</sub>O<sub>3</sub>, (which is still currently under investigation at the time of writing this thesis). Cytotoxicity on the 9L glioma cell line show great potential as a radiosensitiser in radiation therapy. The flow cytometry data indicates that, similar to Ta<sub>2</sub>O<sub>5</sub>, the Bi<sub>2</sub>O<sub>3</sub> will not be significantly internalised in the 9L cells and therefore is expected to be most effective at the higher X-ray energy radiotherapy fields.

Although there are still challenges to be addressed (i.e. further refinement and optimisation of the NPs in terms of particle size, aggregation, and concentration), the ceramic NPs used in this study have shown great promise for the development of effective therapeutic materials such as radioprotectant for CeO<sub>2</sub> and radiosensitiser for successful treatment of the radioresistant cancer cells in the cases of Ta<sub>2</sub>O<sub>5</sub> and Bi<sub>2</sub>O<sub>3</sub>.

## 4.6 Chemo-Auger Approach Part 1: BrUdR, MTX, and X-rays at 125 kVp

This section focuses on the enhancement of the efficacy of kilovoltage X-ray therapy by optimising the combination of chemotherapy drugs (BrUdR and MTX) with external X-rays irradiation (125 kVp radiation field). As mentioned earlier in section 3.1.5.2, it is hypothesised that the optimal energy for this study is 125 kVp. (The effective energy calculation based on the available filter range at the radiation oncology department, Prince of Wales Hospital).

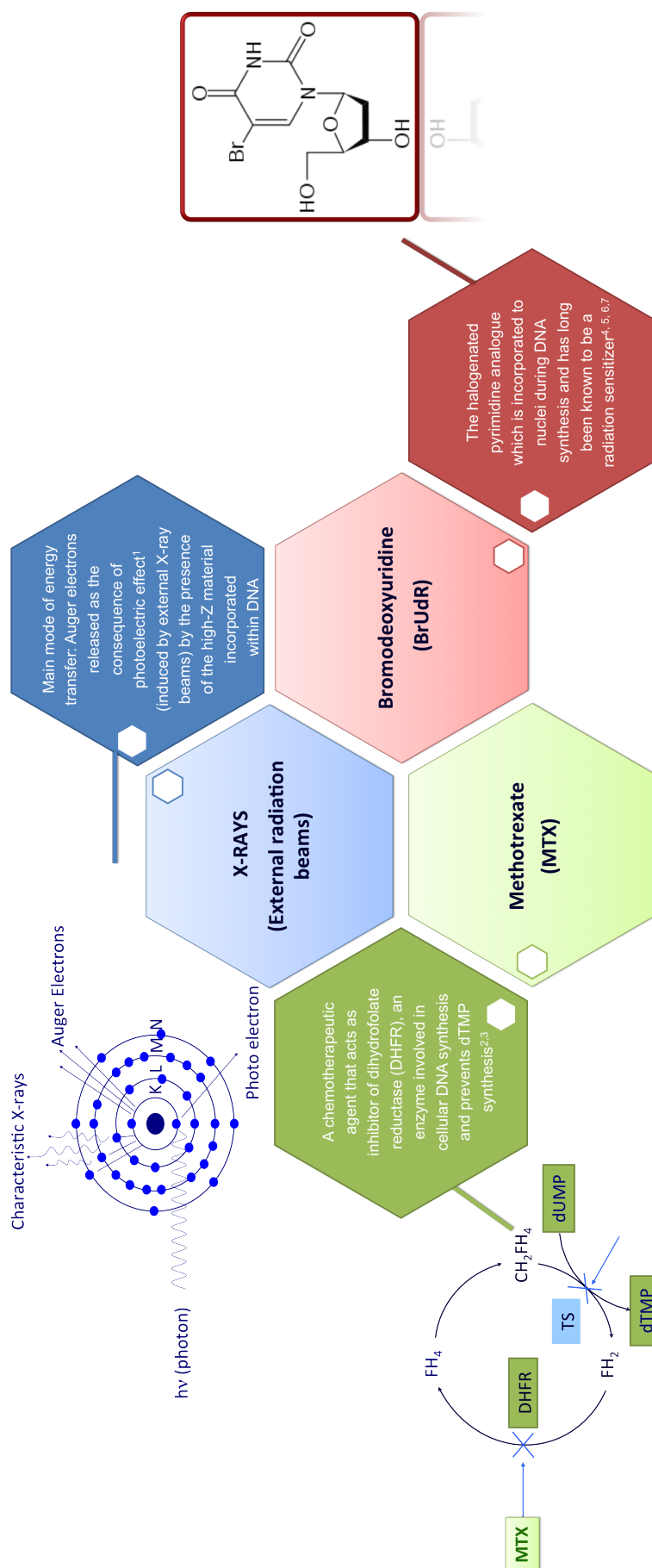
### 4.6.1 Background

#### Need for improved radiotherapy protocols

The treatment of malignant brain tumours remains a major challenge, as the most common brain tumour malignancies tend to recur despite significant advances in surgical techniques including radiation delivery, and chemotherapy. One of the most difficult challenges in the treatment of brain tumours is selectivity, i.e. to develop a treatment that is specific to tumours cells and which therefore maximises the effectiveness of the tumour treatment (better local control) while minimising damage to normal healthy cells as much as possible.

Improvements in radiation dose delivery and more efficient cancer cell killing are needed for targeted cancer treatment. These may provide an improvement in local tumour control and reduce tumour recurrence. For instance, the improvement achieved with photon activation therapy (PAT) which utilises high linear energy transfer (LET) radiations in the form of Auger electron distributions through photoactivation of a high Z-radiosensitiser atoms incorporated into cancer cell DNA as part of a drug.





The main study was designed to investigate a new modality for radioresistant tumour treatments (e.g. high-grade glioma) by using the synergy of pharmacological drugs with radiation. The aim is to allow either for a reduction in the prescribed dose of both radiation and the chemo-drugs, leading to the sparing of critical organs, or to allow one to achieve a higher dose to the target volume by increasing the lethal damage to tumour so as to improve local control.

A method that has been proposed to enhance the effect of ionising radiation is the addition of a high-Z atom loaded compound [Le Sech et al., 2000, 2001; Kobayashi et al., 2002]. The novel approach of this project was to define and optimise the process of increasing the absorbed dose to a target by investigating materials with high atomic number (i.e. bromine), locally in the region of target cancer cells. As described in section 2.4, X-rays can interact with tissues containing such elements via the photoelectric effect, which may induce Auger effects (and Auger electrons), resulting in the enhancement of the dose delivered to the tissue. Chemotherapy drugs are combined with X-ray therapy leading to a novel chemo-Auger methodological route to synergetic treatment.

#### 4.6.2 Brief History of BrUdR Usage

There have been much research carried out in the past into the use of halogenated pyrimidine (e.g. BrUdR and IUdR) as a radiosensitiser drug. The following paragraphs discuss the history of the research on BrUdR combined with radiation as well as with antimetabolites.

In the early 1960s, Djordjevic and Szybalski first reported that the incorporation of BrUdR and IUdR into mammalian cells D98S *in vitro* [Djordjevic

and Szybalski, 1960]. This researchers enhanced the sensitivity to ultraviolet (UV) and X-ray irradiation of the cells then followed by others [Delihas et al., 1962; Kriss and Revesz, 1962; Kaplan et al., 1962; Erikson and Szybalski, 1961; Berry and Andrews, 1962]. In the present study, the enhanced radiosensitivity effects of BrUdR to external X-ray irradiation was confirmed using 9L rat gliosarcoma cells.

BrUdR has been used in the treatment of patients with malignant brain tumours starting with work by by Japanese researchers [Sano et al., 1968; Hoshino and Sano, 1969], who also tried to infuse it with antimetabolites. The rationale of adding the antimetabolite was that the inhibition of thymidine synthesis by the antimetabolite would increase the uptake of the halogenated pyrimidine analogs, BrUdR, into DNA. It was expected to selectively increase the sensitivity of tumour cells to radiation because these analogs were expected to selectively incorporate into the DNA of dividing cells, which are present in higher number in tumour cells than in normal cells [Sano et al., 1965, 1968; Hoshino and Sano, 1969; Bagshaw et al., 1967; Brown et al., 1971]. Theoretically, this halogenated pyrimidine is expected to optimally sensitise rapidly growing tumors that are surrounded by non-proliferative normal tissues such as in the case of brain tumors.

Fairchild et al. [1982] were the first to propose photon activation therapy (PAT) as a technique in which high LET radiation, in the form of Auger electron distributions, are generated through the photoactivation of stable iodine atoms incorporated in DNA via iododeoxyuridine (IUdR). The idea was develop further investigated by Fairchild and Bond [1984], who concluded that a photon energy just above the K-absorption edge of iodine was optimal. In 1993, Laster et al. proposed PAT as a promising form of cancer therapy to improve the

treatment of malignancies, particularly the highly lethal and malignant brain tumour glioblastoma multiform (GBM).

In 2004, Corde et al. proposed this PAT concept in the presence of iodine compounds and irradiate with energy just above the K-absorption edge of iodine (33.2 keV). They succeeded in demonstrating that photons with an energy of 50 keV were the most effective energy. Then in 2009, Laster et al. proposed to improve the treatment of tumour malignancies by using photons from palladium-103 ( $^{103}\text{Pd}$ ) seeds targeted to the L-absorption edge of platinum (Pt) atoms, which bound to the cancer cells DNA [Laster et al., 2009].

As mentioned earlier, the novel idea of our main study is to investigate the enhanced radiosensitising effect of BrUdR. Such enhancement is achieved by the addition of a small amount of antimetabolite (i.e. MTX or 5-FU) that increases the uptake of BrUdR into the cells. The aims of the first part of this study were:

- To establish irradiation conditions for the optimal enhancement of the chemo Auger therapy using conventional kilovoltage X-ray beams from an accessible clinical orthovoltage machine.
- To compare the radiation cell survival curves (with and without drugs) and obtain the sensitisation enhancement ratio at 10% survival fraction ( $\text{SER}_{10}$ ).
- To quantify the level of BrUdR incorporation in the DNA (with and without MTX) and investigate any correlation of this with clonogenic survival.

### 4.6.3 Results

#### 4.6.3.1 Radiosensitisation of BrUdR on 9L cells with X-rays energy of 125 kVp

The survival curves for 9L cells following radiation alone and radiation combined with BrUdR (10  $\mu$ M for 72 hours) are presented in Figure 4.32. The data shows that BrUdR administered concomitantly with 125 kVp X-rays irradiation enhanced the biological effect of the X-ray irradiation by reducing the clonogenic survival of 9L cells (Figure 4.32). This is reflected in the  $\alpha$  value ( $\pm$ SD) for 9L cells irradiated with BrUdR ( $\alpha=0.295\pm0.036$  Gy $^{-1}$ ) being higher than that of irradiated cells without BrUdR (controls) which gave a value of  $\alpha=0.213\pm0.019$  Gy $^{-1}$ .

#### 4.6.3.2 Radiosensitisation of methotrexate on 9L cells with X-rays energy of 125 kVp

The survival curves for 9L cells following radiation alone and radiation combined with MTX (0.01  $\mu$ M for 72 hours) are presented in Figure 4.33. This shows that MTX administered concomitantly with 125 kVp X-rays irradiation led to no enhanced sensitisation effect of the x-ray irradiation on the clonogenic survival of 9L cells (Figure 4.33). This is reflected in the  $\alpha$  value ( $\pm$ SD) for 9L cells irradiated with MTX ( $\alpha=0.191\pm0.013$  Gy $^{-1}$ ), which is not significantly different compared to irradiated cells without exposure to MTX ( $\alpha=0.213\pm0.019$  Gy $^{-1}$ ).

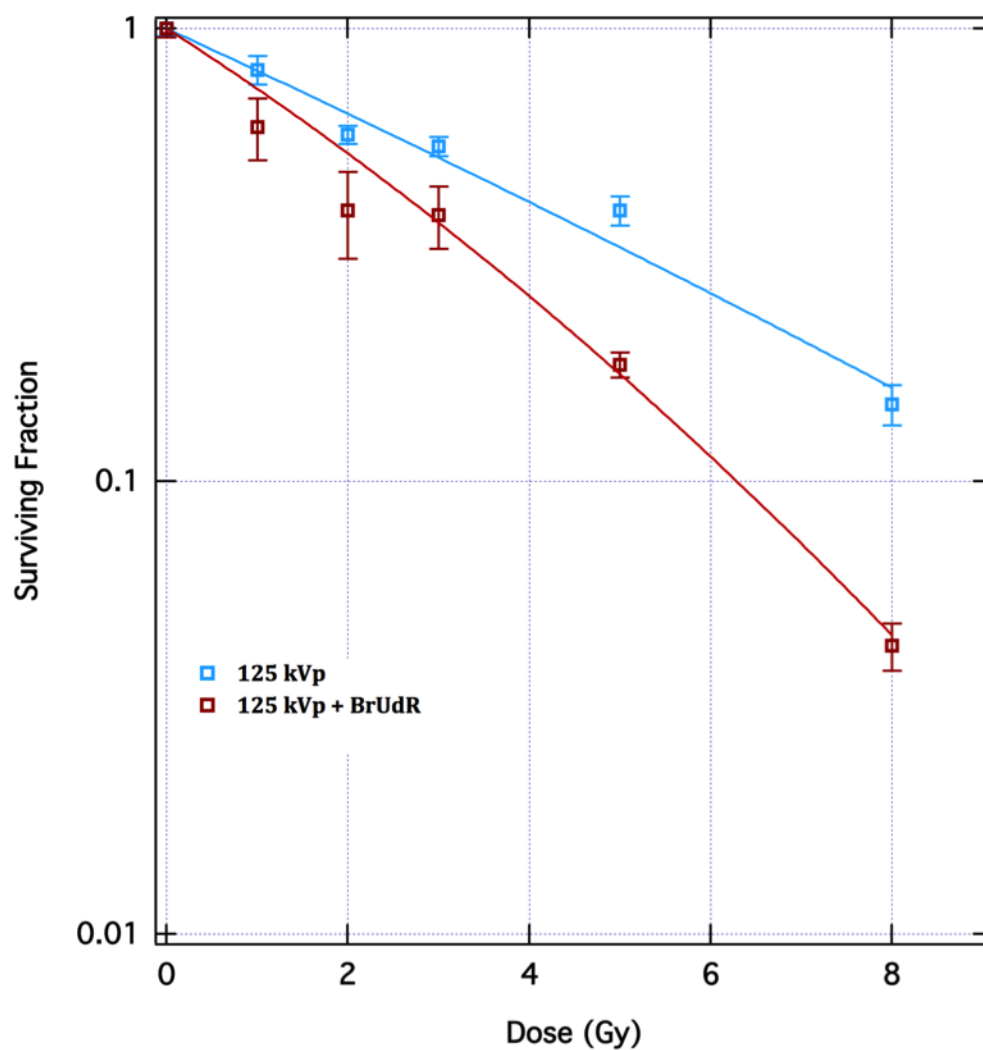


Figure 4.32: Radiation dose-survival curves of confluent cultures of 9L cells after irradiation at energies of 125kVp, with and without exposure to  $10 \mu\text{M}$  BrUdR for 72 hours. Normalised of data for BrUdR-treated cells was done with unirradiated, BrUdR-treated cells sample. Each data point represents the means  $\pm$  standard deviation ( $\pm\text{SD}$ ) of at least three independent experiments.

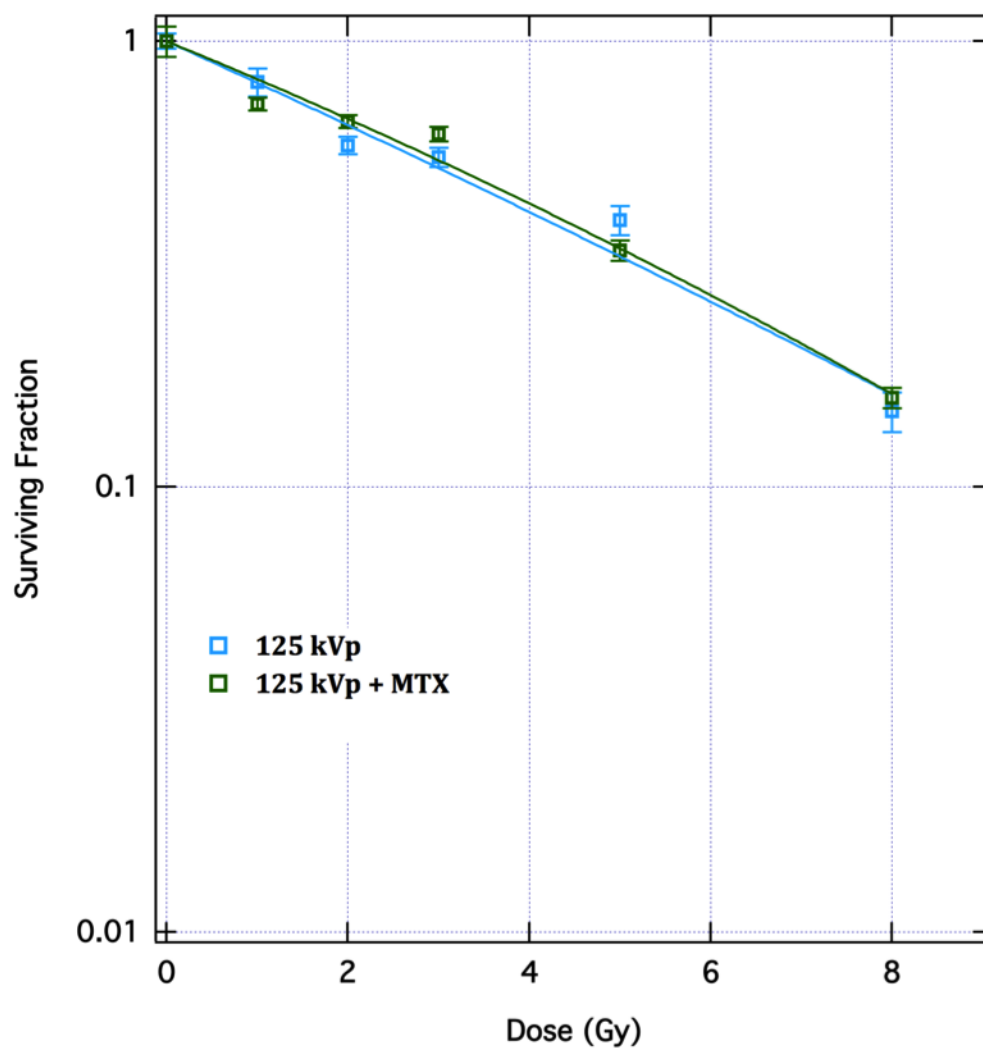


Figure 4.33: Radiation dose-survival curves of confluent cultures of 9L cells after irradiation, at energies of 125 kVp, with or without  $0.01 \mu\text{M}$  MTX treatment for 72 hours. Normalised of data for MTX-treated cells was done with unirradiated, MTX-treated cells sample. Each data point represents the means ( $\pm\text{SD}$ ) of at least three independent experiments.

### 4.6.3.3 Influence of methotrexate on radiosensitising effect of BrUdR

The results for the combined BrUdR (10  $\mu$ M) and MTX (0.01  $\mu$ M) administered concomitantly with 125 kVp X-rays irradiation on 9L cells is shown in Figure 4.34. This shows a cell kill greater than that given by the sum of the results obtained from the individual agents alone, with a significant increase of the  $\alpha$ -value to  $0.486 \pm 0.068 \text{ Gy}^{-1}$ .

To clearly illustrate the synergistic effect of the combination of X-ray treatment with dual drug exposure, Figure 4.35 shows the cell survival curves of the 9L cells after irradiation with 125 kVp x-rays and/or combined with 0.01  $\mu$ M MTX alone, 10  $\mu$ M BrUdR alone, or 0.01  $\mu$ M MTX and 10  $\mu$ M BrUdR.

Table 4.6 summarises the LQ parameters of 9L cells obtained following analyses of the radiation dose-survival curves for irradiation alone and the combined irradiation and drugs at a X-ray photon energy of 125 kVp. These data support the conclusion that radiosensitisation by halogenated pyrimidines (i.e. BrUdR) is mainly due to an increase in the linear parameter  $\alpha$  with the quadratic parameter  $\beta$  unchanged. This is consistent with the work of Franken et al. [2013] who showed that  $\beta$  is not expected to be significantly influenced.

The sensitisation enhancement ratio at 10% surviving fraction ( $\text{SER}_{10}$ ) were also calculated. The SER of irradiated BrUdR plus MTX-treated cells (2.3) was higher than either BrUdR-treated (1.6) or MTX-treated (1) alone. Thus, the effects of combined BrUdR plus MTX appears to be supra additive.



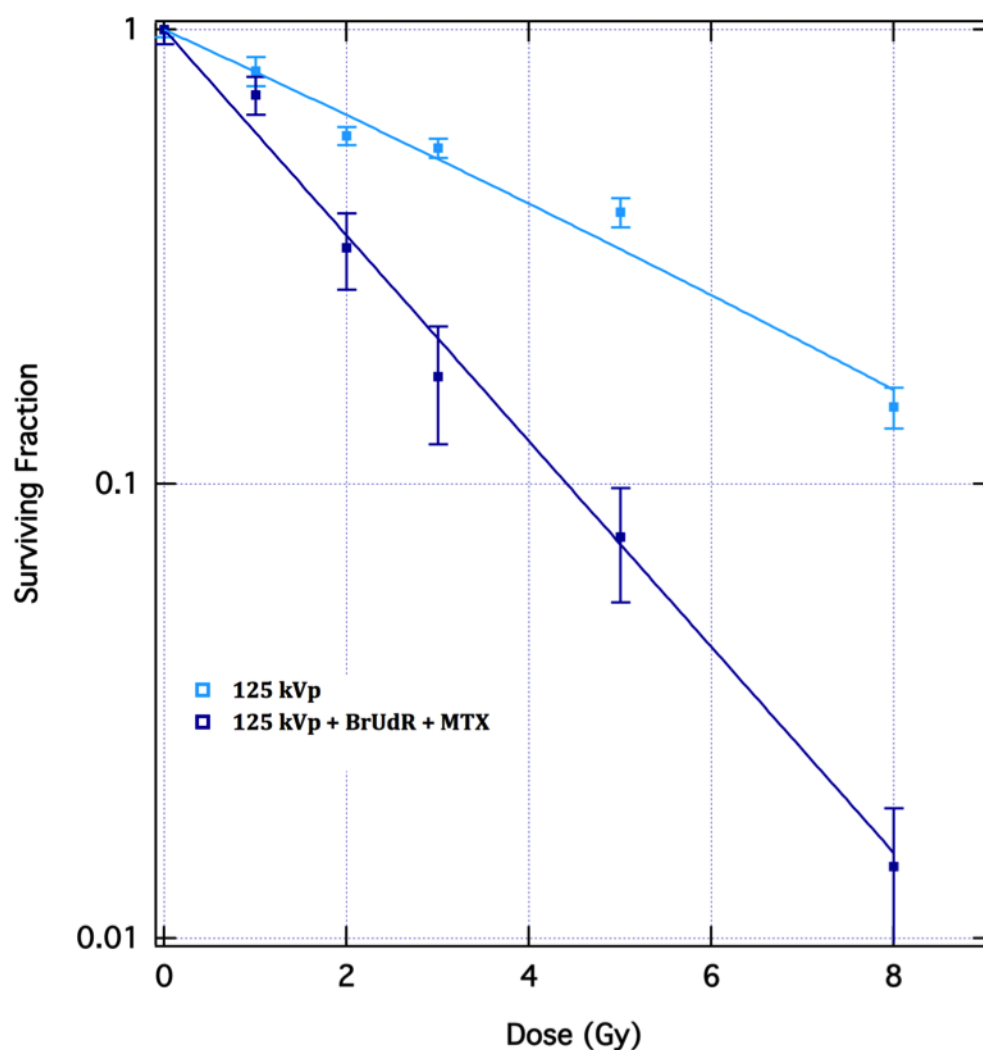


Figure 4.34: Radiation dose-survival curves of confluent cultures of 9L cells after irradiation at energies of 125 kVp, with or without drugs combination ( $0.01 \mu\text{M}$  MTX and  $10 \mu\text{M}$  BrUdR) treatment for 72 hours. Normalised of data for drugs-treated cells was done with unirradiated, drugs-treated cells sample. Each data point represents the means ( $\pm\text{SD}$ ) of at least three independent experiments.

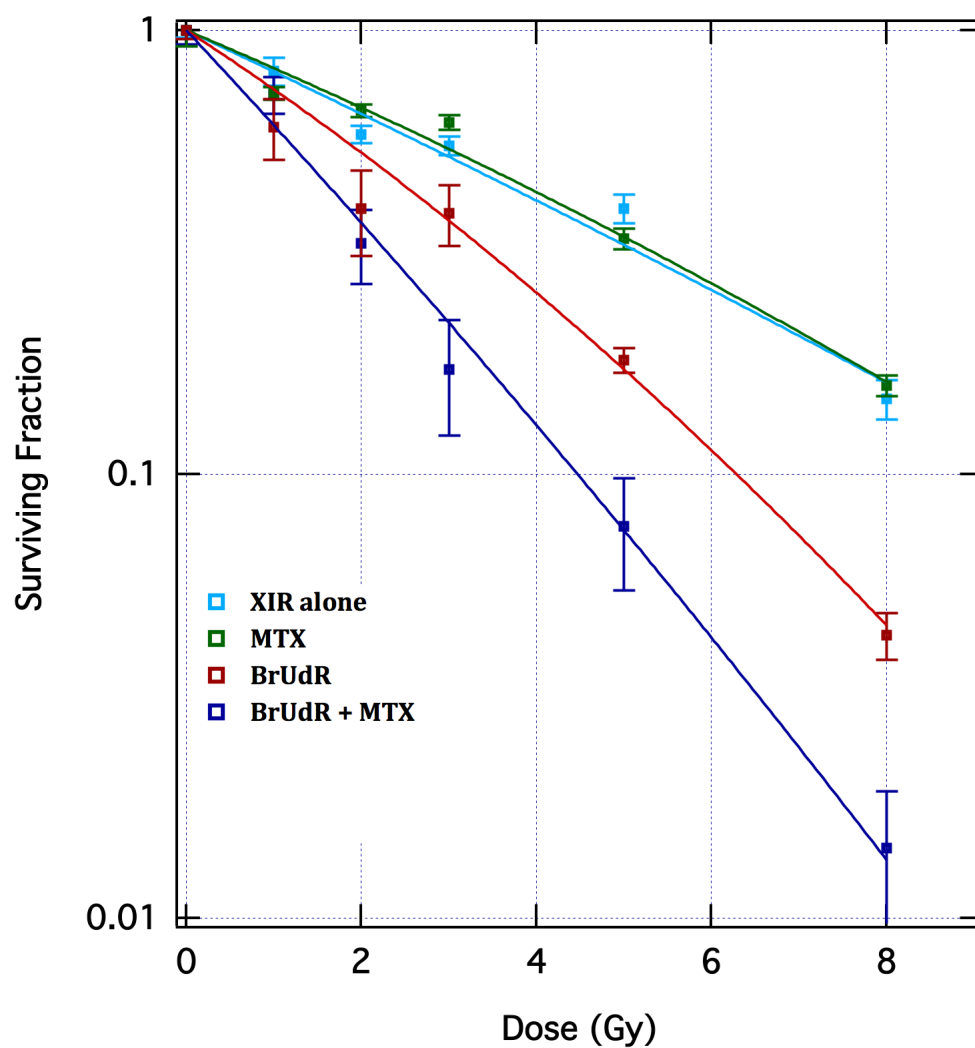


Figure 4.35: Radiation dose-survival curves of confluent cultures of 9L cells after irradiation at energies of 125 kVp, with or without drugs ( $0.01 \mu\text{M}$  MTX and/or  $10 \mu\text{M}$  BrUdR) treatment for 72 hours. Each data point represents the means ( $\pm\text{SD}$ ) of at least three independent experiments.

Table 4.6: Values of the linear-quadratic model parameters  $\alpha$  and  $\beta$ , the  $\alpha/\beta$  ratio, and  $\text{SER}_{10}$  from 9L cells treated with ionising radiation only and MTX/BrUdR-sensitised radiation dose survival curves at energies of 125 kVp. XIR = radiation only; MTX = methotrexate ( $0.01 \mu\text{M}$ ) and BrUdR = bromodeoxyuridine ( $10 \mu\text{M}$ ); N/A = not applicable;  $\text{SER}_{10}$  - sensitisation enhancement ratio at 10% surviving fraction.

Treatment	$\alpha \text{ (Gy}^{-1}\text{)}$	$\beta \text{ (Gy}^{-2}\text{)}$	$\text{SER}_{10}$
XIR alone	$0.213 \pm 0.019$	$0.002 \pm 0.003$	N/A
BrUdR	$0.295 \pm 0.036$	$0.011 \pm 0.006$	1.6
MTX	$0.191 \pm 0.013$	$0.004 \pm 0.002$	1
MTX + BrUdR	$0.486 \pm 0.068$	$0.006 \pm 0.011$	2.3

#### 4.6.3.4 Cell cycle analysis and quantification of BrUdR incorporation into DNA simultaneously

DNA measurements with propidium iodide (PI) were performed to determine whether the drugs and/or radiation combination affected the cell cycle progression and also to calculate the S-phase fraction (SPF) (Eq. 3.6). Bromodeoxyuridine (BrUdR) is a thymidine analog that is taken up by cells in the S-phase of the cell cycle. These cells can be identified by immunohistochemical staining using anti-BrUdR monoclonal antibodies. This technique was developed by Gratzner and Leif [1981] and Gratzner [1982]. Originally it was used to analyse the tumour cell cycle and replaced autoradiograph methods that are applied at intervals after the administration of the tritiated thymidine ( $[^3\text{H}]\text{TdR}$ ). The latter method is time consuming, laborious, and radioactivity dependent. The quick and non-radioactive method of using bivariate flow cytometry analysis, cell cycle distribution and the labeling index (LI) were therefore used in this study. The measurements of LI between the two methods are comparable [Wilson et al., 1985].

Representative DNA histograms of PI stained 9L cells are shown in Figure 4.36. The histogram profile of untreated confluent cells shown in Figure 4.36 exhibited a large peak (first peak on left) representing cells that possess a 2N

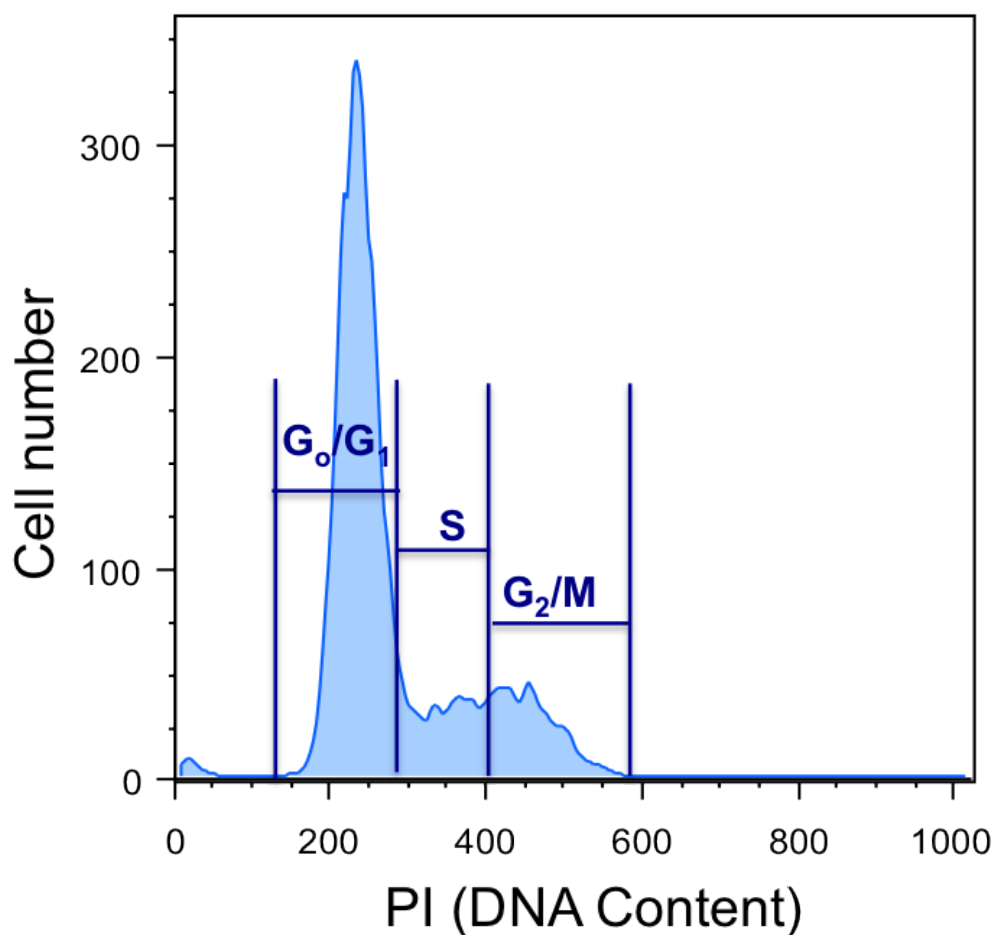


Figure 4.36: Representative of single parametric DNA diagrams of 9L cells stained with PI – gated shown represents each cell phase. DNA histogram were analysed with the FlowJo for Mac software.

(G<sub>0</sub>/G<sub>1</sub> phase) DNA content. The second, smaller, peak on the right represents cells with 4N DNA content, which are the cells are in G<sub>2</sub>/M phase. The interval between the two peaks represents the cells in S-phase.

The SPF is 12.6% under control conditions (untreated) (Figure 4.37a). The result from cell cycle analysis for 9L cells treated with MTX alone (with SPF is 54%) was consistent with S-phase cell cycle arrest as previously reported [Sen et al., 1990; Dabrowska et al., 2007] as MTX treatment caused the accu-

mulation of cells in early S-phase (Figure 4.37b). The results from cell cycle analysis in 9L cells treated with BrUdR alone was consistent with M-phase cell cycle arrest as previously reported [Sen et al., 1990; Dabrowska et al., 2007] (Figure 4.37c).

The accumulation of cells into the S-phase is observed after 72 hour period of MTX and BrUdR incubation, which rapidly elevated the SPF increase to 33% (Figure 4.37d) compare to the control (Figure 4.37a). For the combination of MTX and BrUdR with radiation there was only one obvious apoptotic or pre-apoptotic peak (sub-G<sub>1</sub> peak), the G<sub>2</sub>/M and S phase cells disappeared completely (Figure 4.37e).

Representative bivariate flow cytometry dot plots (i.e DNA/BrUdR distributions) of cells treated with and without BrUdR alone or combined with MTX are shown in Figure 4.38. The average percentage results ( $\pm$  standard deviation) are presented as a percentage of BrUdR-positive cells in relation to the total cell number determined based on the PI staining. LIs of cells treated with BrUdR alone were  $38\% \pm 3.4\%$  whereas combined with MTX the LIs were  $38.4\% \pm 3.1\%$ .

#### 4.6.4 Discussion

The halogenated pyrimidine, BrUdR is an agent that has a similar size and chemical structure with the natural pyrimidines (Figure 2.26). It is hypothesised that during DNA replication these base analogues are mistakenly incorporated into the newly formed DNA chains replacing the natural base thymine [Chadwick and Leenhouts, 1981]. BrUdR is therefore provide high Z-radiosensitiser atoms (i.e bromine) which are incorporated into DNA re-

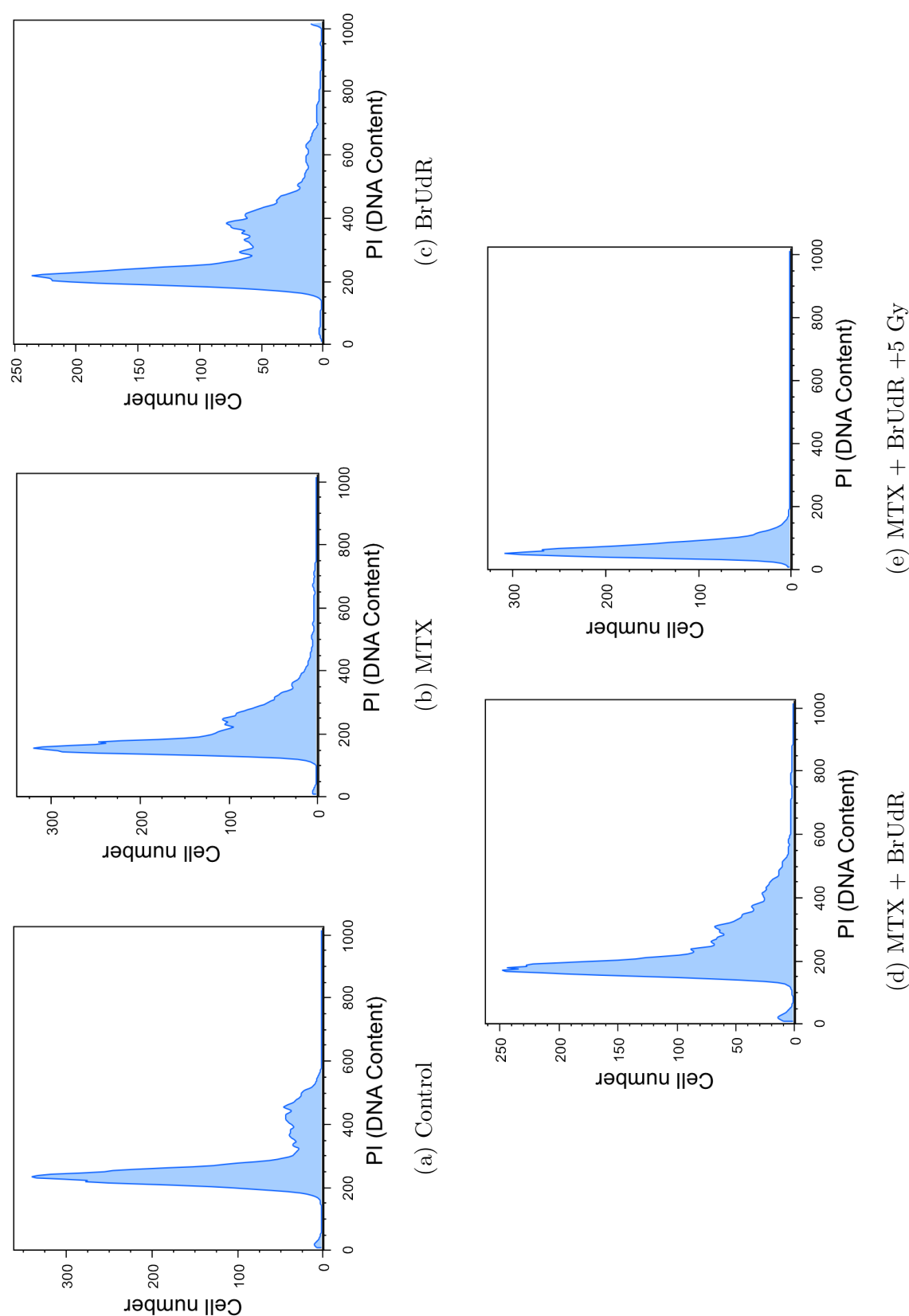


Figure 4.37: Single parametric DNA diagrams of 9L cells stained with PI. Measurements were performed on a FACS LSR II flow cytometer after 72 h without drugs/irradiation (control) (a), 0.01  $\mu$ M MTX (b), 10  $\mu$ M BrUdR (c), 0.01  $\mu$ M MTX + 10  $\mu$ M BrUdR (d), and 0.01  $\mu$ M MTX + 10  $\mu$ M BrUdR combined with 5Gy X-rays radiation of 125 kVp (e). DNA histograms were analysed with the FlowJo for Mac software. The assay was performed at least three times, a representative example is shown.

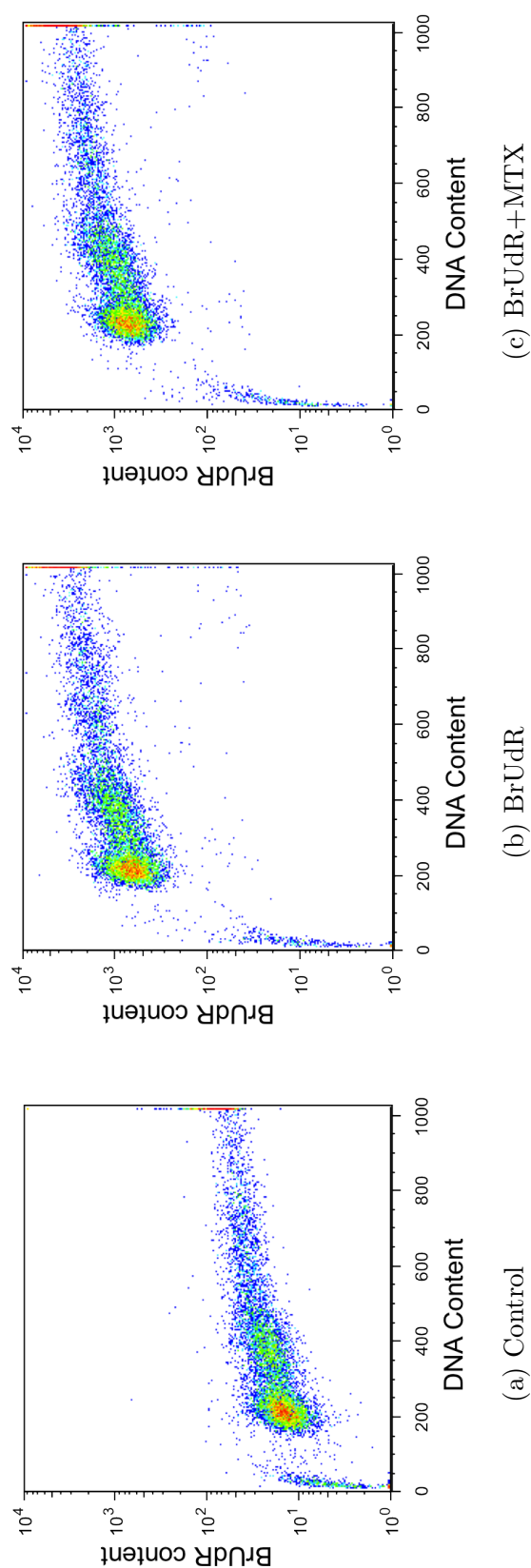


Figure 4.38: Dot plots of bivariate DNA/BrUdR distributions of 9L cells. Measurements were performed on a FACS LSR II flow cytometer after 72 h without drugs/irradiation (control) (a), 10  $\mu$ M BrUdR (b), 0.01  $\mu$ M MTX + 10  $\mu$ M BrUdR (c). Total DNA content (red fluorescence – 575/26-A) versus amount of incorporated BrUdR (green fluorescence – 515/20-A) shown on the x-axis and y-axis, respectively. DNA histograms were analysed with the FlowJo for Mac software. The assay was performed at least three times, a representative example is shown.

sulting in an enhancement of the biological effect of ionising radiation. The rationale to add MTX was that the inhibition of thymidine synthesis by the antimetabolite would increase the uptake of the halogenated pyrimidine analogs, BrUdR, into tumour DNA.

In the present study, the clonogenic survival of 9L cells has also been correlated with FACS results, as it was hypothesised that there might be an association between the decreased clonogenic survival with an increased uptake of the BrUdR by MTX. These comparisons have been motivated by the effort to clarify the radiosensitising effect of BrUdR (with or without the presence of MTX) in biological systems, especially DNA strand breaks and their dependence on the number of BrUdR molecules incorporation into DNA.

As an initial approach the enhanced radiosensitising effect by BrUdR has been studied in clonogenic survival assays of the rat gliosarcoma cell line 9L. As mentioned in earlier section 4.1.1, the 9L cell line was used due to its radioresistant characteristic as compared to other rat brain tumour cell lines. The first part of this investigation was to experimentally investigate the radiosensitising effect by BrUdR (with or without the presence of MTX) on the clonogenic survival of the x-ray irradiated 9L cell line at an energy of 125 kVp, as well as to quantify the predicted increase of  $\alpha$  values.

In the present study, it was demonstrated that the radiosensitisation effect of BrUdR (10  $\mu$ M) on 9L cells with a X-ray energy of 125 kVp resulting in reduced clonogenic cell survival (Figure 4.32). This confirms the hypothesised that BrUdR acts as a radiosensitiser. In turn this supports the studies in drug-radiation interactions, which suggest that the linearisation of a cell survival curve indicate that the agent is additive with itself [Steel and Peckham, 1979].



Unlike the case of BrUdR, no radiosensitisation effect was observed on irradiation concomitantly with MTX alone ( $0.01\ \mu\text{M}$ ) (Figure 4.33). This is inconsistent with the potentiation described by Bagshaw and Doggett [1969], where MTX can cause an increasing cellular damage by x-ray radiation by inhibiting cellular repair. There are two possible explanations for this. Firstly, it could be due to the stationary phase cells at the time of irradiation. This explanation is consistent with studies by Spittle [1978] that indicate MTX act as radiosensitiser of log phase cells and not stationary phase cells. Secondly, it could be due to the dose of MTX used in this study is less than two-hundredth of the  $\text{IC}_{50}$  as anticancer drugs.

The addition of MTX ( $0.01\ \mu\text{M}$ ) did cause an enhancement of the radiosensitising effect of BrUdR ( $10\ \mu\text{M}$ ) (Figure 4.34). These results support the idea that the addition of BrUdR concomitantly with X-ray irradiation increases the spatial distribution of low-energy secondary electrons, resulting in an enhanced biological effect of the radiation. This effect is increased in the presence of MTX (Figure 4.35). These results are also consistent with the hypothesis of the drug-radiation interactions. This showed that the effect of combining the two agents used (i.e. BrUdR and MTX) concomitantly with radiation, lead to the conclusion that they are supra additive (Figure 4.35).

It has been proposed that the loss of the ability of cells to reproduce itself is directly related to the number of radiation-induced DNA-DSB [Chadwick and Leenhouts, 1981]. Thus, our findings suggest that cell death was due to a lethal accumulation of DNA strand breaks. This correlates with the greatly reduced cell survival in the clonogenic assay. This confirms that there is a highly localised energy deposition when the radiosensitiser drug, BrUdR is combined

with MTX ( $0.01 \mu\text{M}$ ) which causes more ionisation clusters in cells. This leads to more DNA strand breaks.

It has been shown that the degree of incorporation of halogenated pyrimidines into DNA depends upon their concentration at the time of exposure [Phillips et al., 1989] and with the time of exposure [Phillips et al., 1995; Lawrence et al., 1990a], which been tested in mammalian cells [Uhl et al., 1992]. Moreover, the amount of chromosomal damage or cell killing increases as the incorporation of the bromodeoxyuridine increases [Kaplan et al., 1962; Erikson and Szybalski, 1963a,b]. This was quantitatively defined by Dewey and Humphrey [1965] and Dewey et al. [1966, 1971] on synchronised Chinese hamster ovary (CHO) cells.

The incorporation of bromodeoxyuridine (BrUdR) during DNA synthesis is frequently used for cell cycle analysis. In this study, cells that have incorporated BrUdR during drug incubation were detected by fluorescently labeled anti-BrUdR antibodies. Dolbeare et al. [1983] developed a procedure to simultaneously measure the amount of BrUdR incorporated into DNA and the total DNA content using flow cytometry. They used an anti-BrUdR monoclonal antibody to analyse BrUdR-treated cells in both in vitro and in vivo of CHO cells. The fluorescence intensity was proportional to the amount of incorporated BrUdR as determined by immunofluorescence [Gratzner and Leif, 1981; Gratzner, 1982; Dolbeare et al., 1983]. Thus, the anti-BrdU mouse monoclonal antibody (Clone MoBU-1) that is highly specific for BrUdR incorporated into DNA was used in this study.

The measured PI fluorescence is directly proportional to the DNA content of cells. The results from cell cycle analysis in 9L cells treated with MTX alone are consistent with S-phase cell cycle arrest as previously reported by others

[Sen et al., 1990; Spittle, 1978; Dabrowska et al., 2007] (Figure 4.37b). An increasing number of 9L cells in the S-phase (i.e SPF), from 12.6% to 33%, was observed when the cells were treated with a combination drugs of 10  $\mu$ M BrUdR and 0.01  $\mu$ M MTX (200-fold below  $IC_{50}$ ) (Figure 4.37d). When the drugs combined with radiation there was only one obvious apoptotic peak (sub- $G_1$  phase) (Figure 4.37e), indicating that most of the cells underwent apoptosis. Some cells are able to repair the damage which is why they still divide, producing the colonies observed in clonogenic assays.

A wide range in the degree of thymidine replacement by BrUdR has been documented in two previous studies. Delihis et al. [1962] reported a 1% replacement of thymidine by BrUdR in HEp cells. Nagashima and Hoshino [1985] found that approximately 49% of thymidine by was replaced BrUdR in 9L cells. Our result, that the LI was  $38.4\% \pm 3.4\%$  (Figure 4.38), is in more in agreement with the results reported by Nagashima and Hoshino [1985]. The figure of  $38.4\% \pm 3.4\%$  is higher than the SPF calculated from the DNA histogram (33%). These results also support the conclusion that the LI obtained from fluorescence analysis is higher than the percentage of S-phase cells obtained from DNA histogram. Dolbeare et al. [1983] concluded that the anti-BrUdR antibodies were very sensitive to identifying the early S-phase cells.

There seems to be a discrepancy between the LI of BrUdR/MTX combination with the cell survival analysed by clonogenic assays. The number of cells that survived decreased significantly but no increase in the BrUdR uptake into DNA by MTX was observed ( $38.4\% \pm 3.1\%$ )(Figure 4.38). This is in agreement with the observations of Aoyama et al. [1964] that there was no change in the radiosensitisation as the percentage of thymidine replaced increased. Hence, the radiosensitising effect does not increased in proportion to the rate of in-

corporation of BrUdR into DNA.

In summary, these results suggest that the increased cell death was due to a lethal accumulation of DNA strand breaks (i.e DNA DSB). The formation of such DNA breaks is probably due to inefficient DNA repair resulting from the inhibition of synthesis of thymidilate and purine nucleotides by MTX. Fornace et al. [1990] and Lawrence et al. [1990b] also suggest that the molecular mechanism of this increase in lethality due to radiosensitisation is most likely related to the hydrolysis of halogenated DNA (i.e. highly reactive uracil free radicals) by ionising radiation. This radiation damages the un-substituted complementary-strand DNA.

#### 4.6.5 Conclusions

These data are in accordance with our theoretical expectations and that radiation and BrUdR interact synergistically. In addition, the combination of BrUdR with low doses of MTX is more cytotoxic than either of these agents alone. Overcoming radio-resistance of 9L cells is an important challenge to improving the outcomes for patients with glioma. Achieving a synergistic interaction by combining BrUdR, MTX, and targeted Auger-electron RT (chemo-Auger therapy) could lead to significantly improved responses, compared with either of these therapies alone.

## 4.7 Chemo-Auger Approach Part 2: BrUdR, MTX, and Influence of Different Energies

As described in section 2.4, a synergistic interaction was achieved by combining BrUdR, MTX, and an external X-ray beam at 125 kVp. In this section, the influence of different physical X-ray energies on the radiosensitisation of BrUdR on 9L cells is explored.

### 4.7.1 Background

The addition of high-Z materials to achieve an enhanced dose has already been proven to be viable experimentally *in vitro* using low energy photons of kVp energies (50 – 250 kVp). As mentioned in section 2.4, within this kilovoltage range dose enhancement is mainly due to photoelectric interactions whose interaction cross sections are highly Z dependant.

In order to determine the photon-energy dependence of the chemo-Auger therapy on cell survival a set of experiments has been carried out to investigate the influence of different X-ray photon energies range, including 50 kVp, 125 kVp, 250 kVp, 6 MVp and 10 MVp, so as to cover a wide range of secondary electron spectra while maintaining the same total energy absorbed per unit mass (the same dose delivered). This investigation was undertaken to verify whether the observed effect in section 2.4 is related to low energy secondary electrons.

Megavoltage (MV) X-rays beam are widely used for anticancer radiotherapy as they have the advantage of greater penetration into tissues, allowing the treatment of deep seated tumours in the body. However, this advantage is

limited by the inverse relationship of absorption to penetration (i.e. inverse square law).

In the higher range of clinical relevant photon energies (6–25 MVp), photon beams mainly interact with matter by Compton scattering and pair production. A recent phantom based study has shown that local dose enhancement of as much as 40% can be achieved by the introduction of high-Z materials (i.e. gold foils) to the region of interest with 18 MV or higher energy photon beams [Alkhatib et al., 2009]. Thus, in this project we also proposed to modify the chemo-Auger approach to a chemo-electron/positron pair creation approach. The aims of part 2 of this study were:

- To establish irradiation conditions for the optimal enhancement of chemo electron/positron pair therapy by conventional megavoltage X-ray beams (i.e. LINAC).
- To compare the radiation cell survival curves and verify the optimal photoactivation source.

## 4.7.2 Results

### 4.7.2.1 Radiosensitisation of BrUdR + MTX on 9L cells with 50 kVp X-rays beam

The results for the combined BrUdR (10  $\mu$ M) and MTX (0.01  $\mu$ M) administered concomitantly with 50 kVp X-rays irradiation on 9L cells is shown in Figure 4.39. This shows a greater cell kill than that expected with irradiation alone with the value of  $\alpha = 0.284 \pm 0.009 \text{ Gy}^{-1}$  being larger than that of the control, with  $\alpha = 0.151 \pm 0.019 \text{ Gy}^{-1}$ .

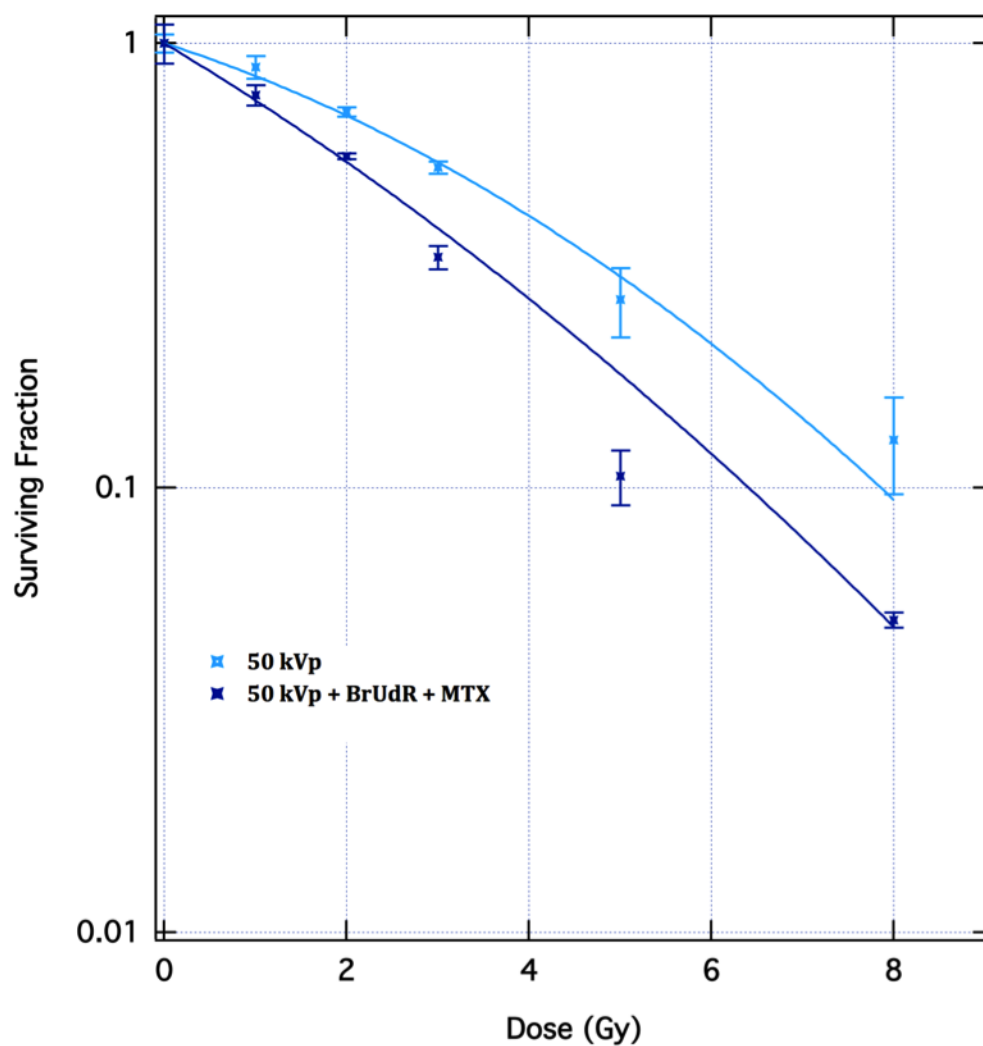


Figure 4.39: Radiation dose-survival curves of confluent cultures of 9L cells after irradiation at energies of 50 kVp, with or without drugs combination ( $0.01 \mu\text{M}$  MTX and  $10 \mu\text{M}$  BrUdR) treatment for 72 hours. Each data point represents the means  $\pm$  standard deviation of at least two independent experiments.

#### **4.7.2.2 Radiosensitisation of BrUdR + MTX on 9L cells with 250 kVp X-rays beam**

The results for the combination of BrUdR (10  $\mu\text{M}$ ) and MTX (0.01  $\mu\text{M}$ ) administered concomitantly with 250 kVp X-rays irradiation on 9L cells is shown in Figure 4.40. This shows a greater cell kill than that expected with irradiation alone with the value of  $\alpha = 0.319 \pm 0.025 \text{ Gy}^{-1}$  being larger than that of the control,  $\alpha = 0.152 \pm 0.019 \text{ Gy}^{-1}$ .

#### **4.7.2.3 Radiosensitisation of BrUdR + MTX on 9L cells with 6 MV X-rays beam**

The results for the combination of BrUdR (10  $\mu\text{M}$ ) and MTX (0.01  $\mu\text{M}$ ) administered concomitantly with 6 MV X-rays irradiation on 9L cells is shown in Figure 4.41. This shows a greater cell kill than that expected with irradiation alone with the value of  $\alpha = 0.335 \pm 0.024 \text{ Gy}^{-1}$  being larger than that of the control, with  $\alpha = 0.294 \pm 0.007 \text{ Gy}^{-1}$ .

#### **4.7.2.4 Radiosensitisation of BrUdR + MTX on 9L cells with 10 MV X-rays beam**

The results for the combination of BrUdR (10  $\mu\text{M}$ ) and MTX (0.01  $\mu\text{M}$ ) administered concomitantly with 10 MV X-rays irradiation on 9L cells is shown in Figure 4.42. This shows a greater cell kill than that expected with irradiation alone with the value of  $\alpha = 0.218 \pm 0.069 \text{ Gy}^{-1}$  being larger than that of the control  $\alpha = 0.200 \pm 0.062 \text{ Gy}^{-1}$ .



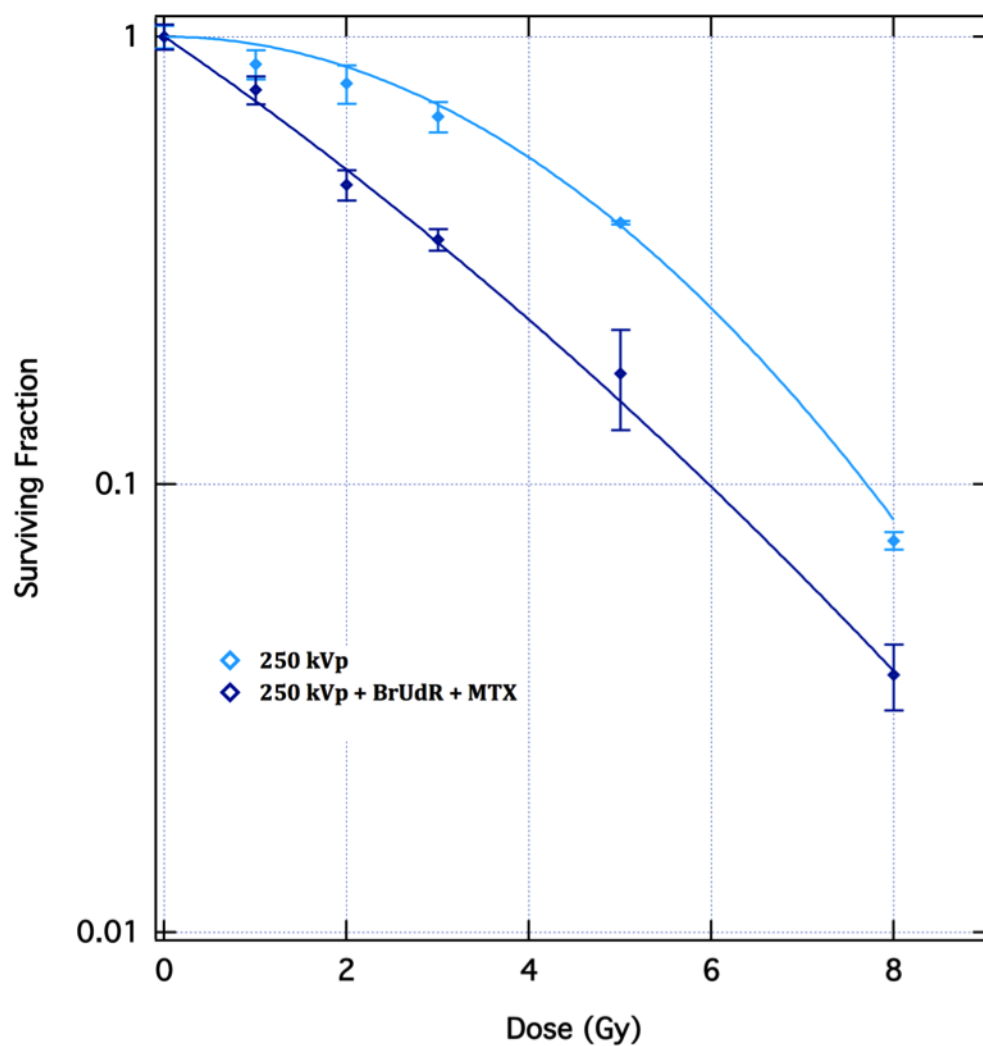


Figure 4.40: Radiation dose-survival curves of confluent cultures of 9L cells after irradiation at energies of 250 kVp, with or without drugs combination ( $0.01 \mu\text{M}$  MTX and  $10 \mu\text{M}$  BrUdR) treatment for 72 hours. Each data point represents the means  $\pm$  standard deviation of at least two independent experiments.

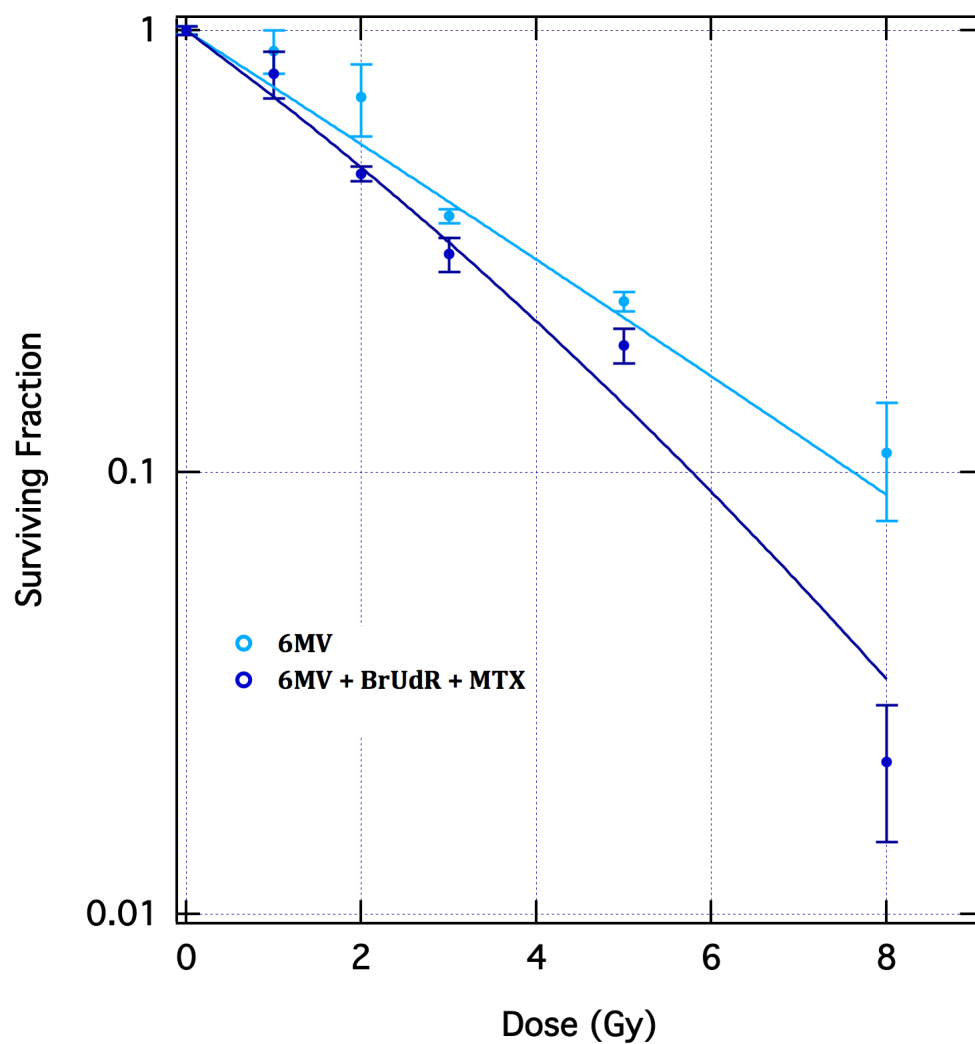


Figure 4.41: Radiation dose-survival curves of confluent cultures of 9L cells after irradiation at energies of 6 MV, with or without drugs combination (0.01  $\mu$ M MTX and 10  $\mu$ M BrUdR) treatment for 72 hours. Each data point represents the means  $\pm$  standard deviation of at least two independent experiments.

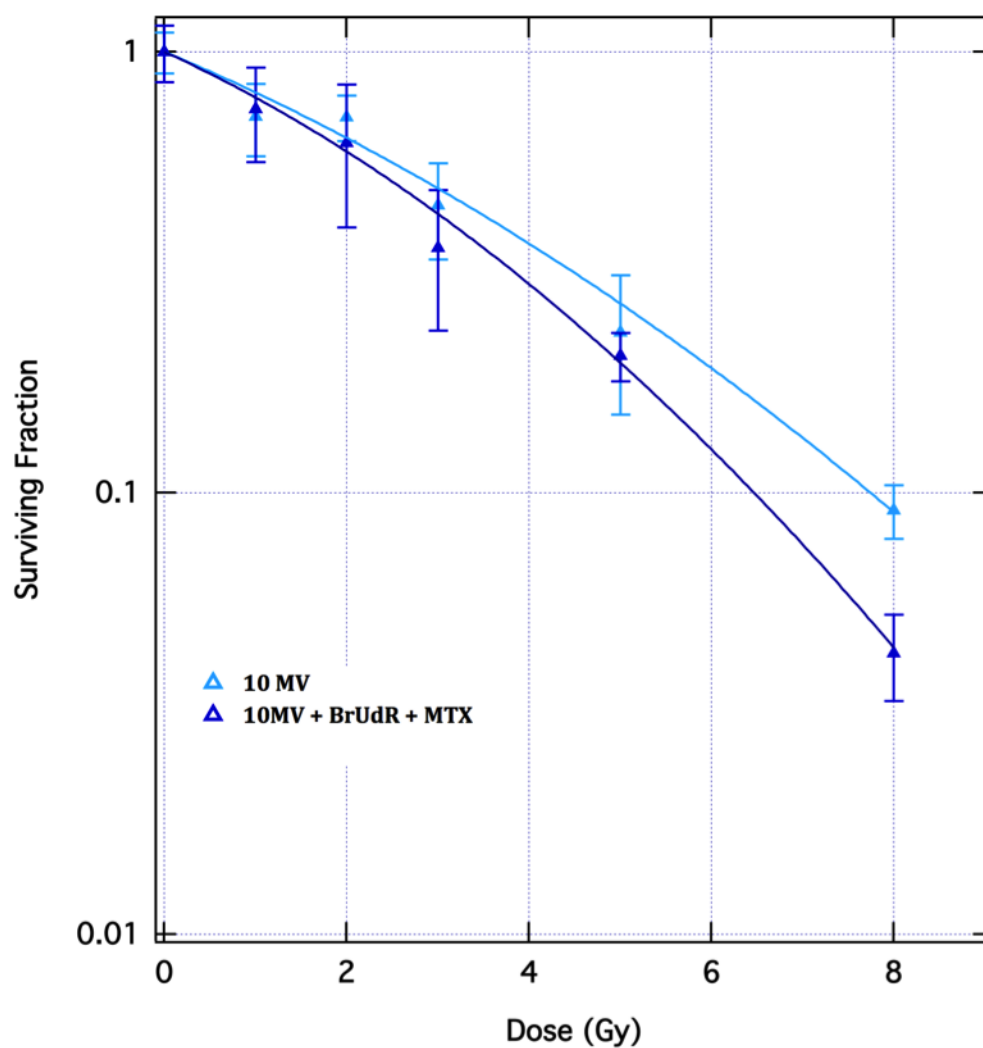


Figure 4.42: Radiation dose-survival curves of confluent cultures of 9L cells after irradiation at energies of 10 MV, with or without drugs combination (0.01  $\mu$ M MTX and 10  $\mu$ M BrUdR) treatment for 72 hours. Each data point represents the means  $\pm$  standard deviation of at least two independent experiments.

#### 4.7.2.5 Correlation between the physical X-rays beam energies and enhancement of radio sensitisation effect of BrUdR combined with MTX

Survival curves following the irradiation of 9L cells containing drugs (BrUdR plus MTX) are plotted in Figure 4.43 with all of the control curves averaged together.

Table 4.7 summarises the LQ parameters for 9L cells obtained from analyses of the radiation dose-survival curves for irradiation alone and following combined irradiation and drugs at all energies.

Table 4.7: Values of the linear-quadratic model parameters  $\alpha$  and  $\beta$ , the  $\alpha/\beta$  ratio, and  $\text{SER}_{10}$  from 9L cells treated with ionising radiation only and MTX/BrUdR-sensitised radiation dose survival curves of different energies. XIR = radiation only; DRUGS = MTX ( $0.01\ \mu\text{M}$ ) and BrUdR ( $10\ \mu\text{M}$ ) combination; N/A = not applicable;  $\text{SER}_{10}$  = sensitisation enhancement ratio at 10% surviving fraction.

Energies	Treatment	$\alpha\ (\text{Gy}^{-1})$	$\beta\ (\text{Gy}^{-2})$	$\text{SER}_{10}$
50 kVp	XIR	$0.151 \pm 0.019$	$0.018 \pm 0.006$	1.2
	DRUGS	$0.284 \pm 0.009$	$0.011 \pm 0.001$	
125 kVp	XIR	$0.213 \pm 0.008$	$0.002 \pm 0.001$	2.3
	DRUGS	$0.521 \pm 0.028$	N/A	
250 kVp	XIR	N/A	$0.038 \pm 0.000$	1.3
	DRUGS	$0.319 \pm 0.025$	$0.011 \pm 0.004$	
6MV	XIR	$0.294 \pm 0.007$	$0.010 \pm 0.002$	1.3
	DRUGS	$0.335 \pm 0.024$	$0.011 \pm 0.005$	
10MV	XIR	$0.200 \pm 0.062$	$0.013 \pm 0.008$	1.2
	DRUGS	$0.218 \pm 0.069$	$0.021 \pm 0.010$	

The most significant increases in the  $\alpha$  value were observed in the irradiation of cells with an energy of 125 kVp, with a  $\text{SER}_{10}$  of 2.3 (Figure 4.44). This radiosensitisation value demonstrates that the damaged DNA was probably due to inefficient DNA repair resulting from the inhibition of synthesis of thymidilate and purine nucleotides by MTX as well as the photoelectrons productions at 125 kVp. This energy is optimal according to the peak of absorption con-

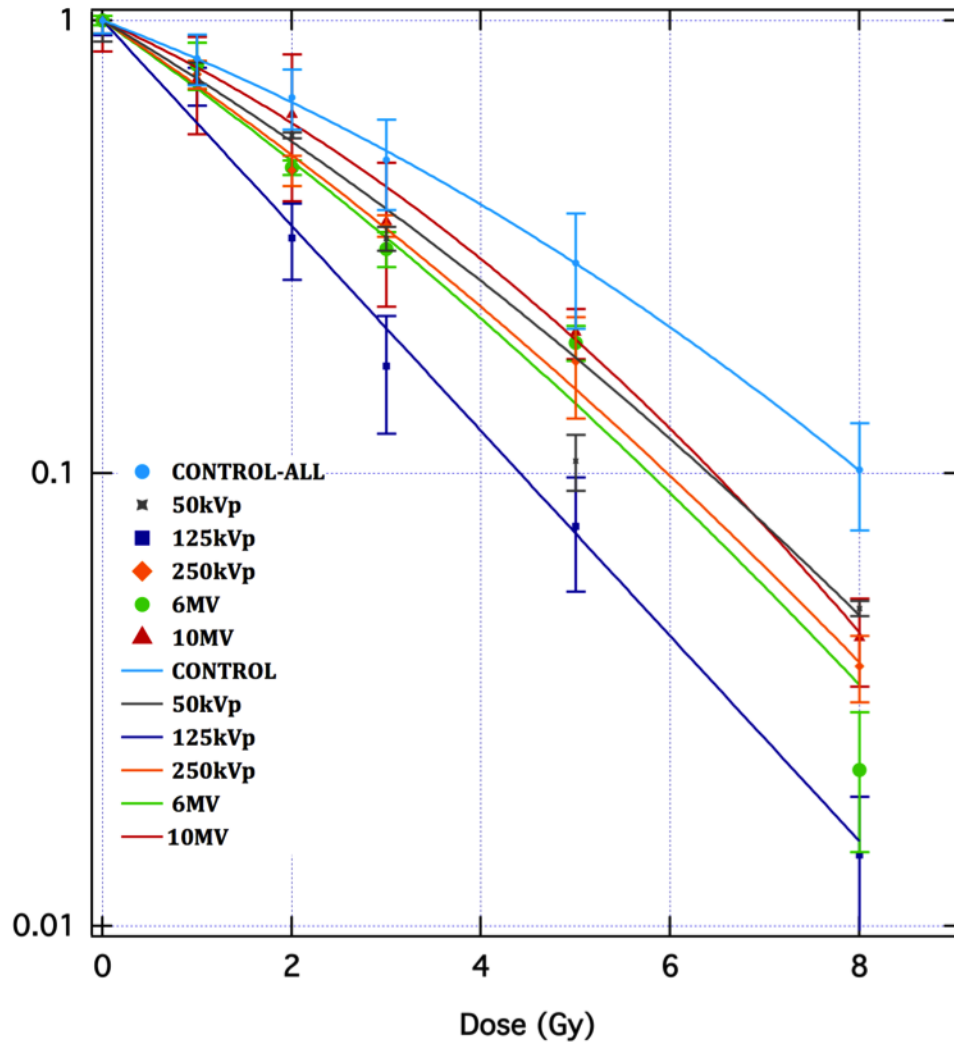


Figure 4.43: The effect of BrUdR plus MTX on 9L cells after irradiation with different energies of radiation analysed with LQ model (Eq.2.6). Each data point represents the means standard deviation of at least two independent experiments are shown. Control represents as the average of the irradiated controls from all different energies without drugs treated.

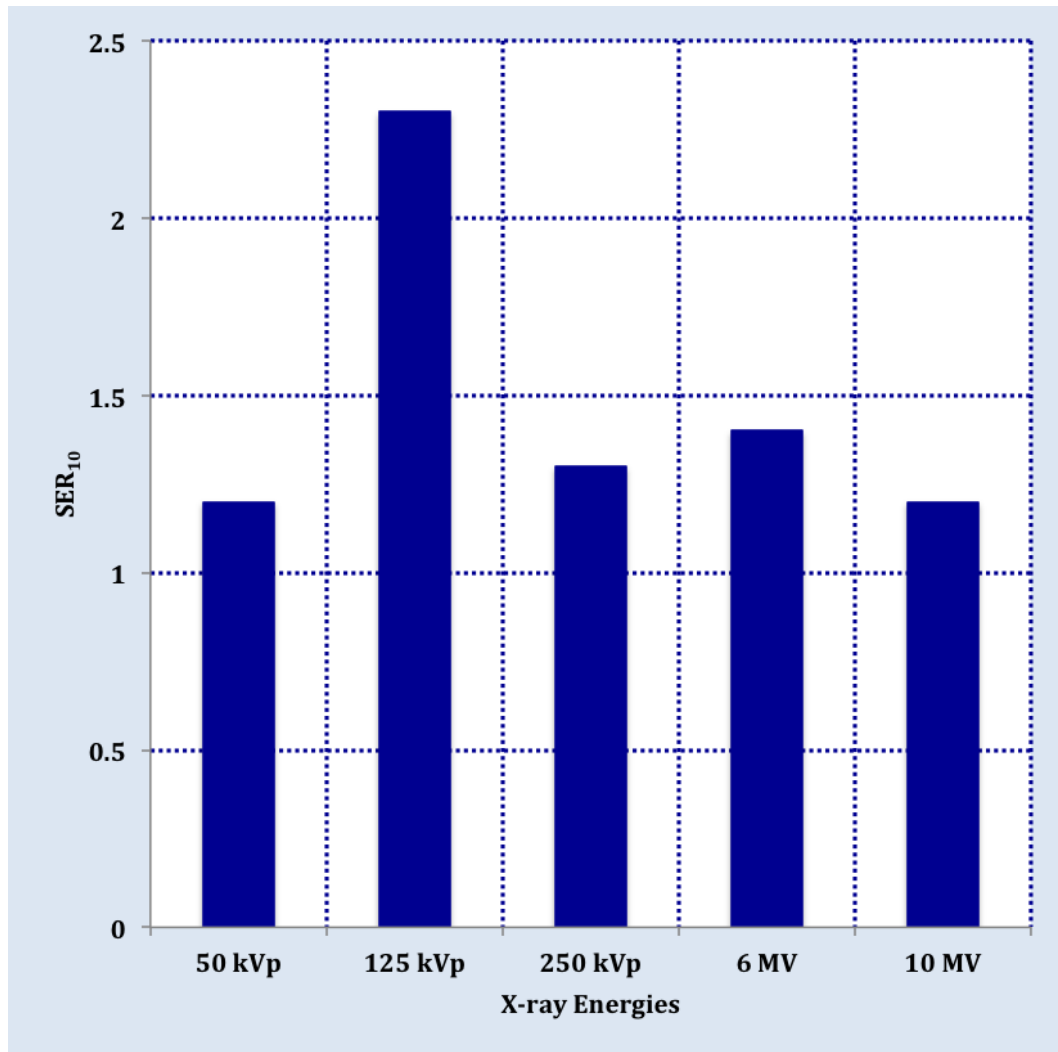


Figure 4.44: Sensitisation enhancement ratio at 10% surviving fraction ( $SER_{10}$ ) in function of radiation energies.

trast of bromine relative to water spectrum which occurs around  $\sim 40$  keV.

Figure 4.45 shows the same trend as demonstrated in section 2.4, i.e. no radiosensitising effect was observed when the cells were irradiated at 5 Gy with MTX alone and an enhanced radiosensitisation was observed with BrUdR plus MTX compared to irradiation alone in all kVp energies. This is illustrated by the reduction in number of clonogenic survival at 5 Gy of irradiated 9L cells concomitantly with drugs (Figure 4.45). It also clearly shows that the optimum energy is 125 kVp where the reduction in number of clonogenic survival

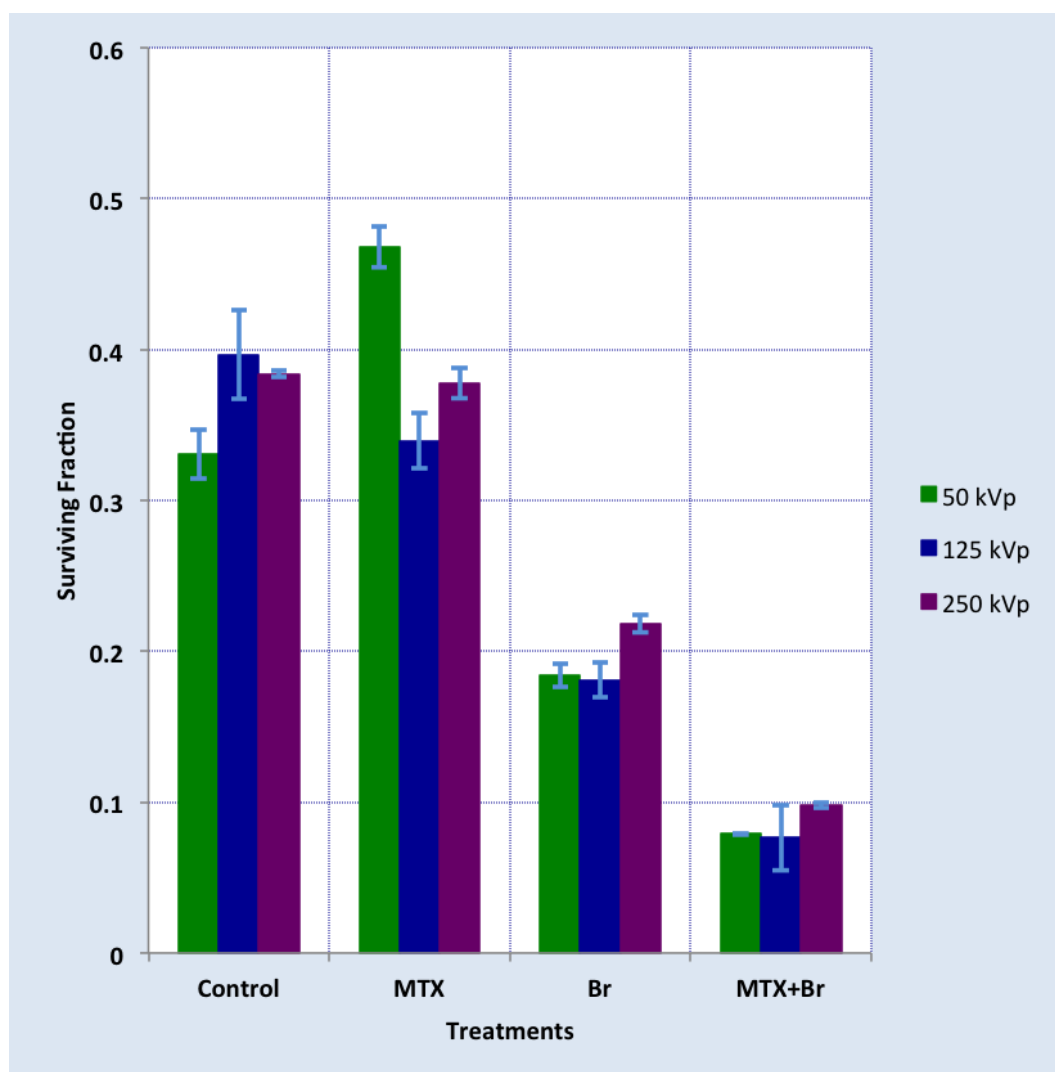


Figure 4.45: The effect of drugs on 9L cells after irradiation with energies of 50, 125, and 250 kVp at dose of 5 Gy. MTX = methotrexate ( $0.01 \mu\text{M}$ ); Br = bromodeoxyuridine ( $10 \mu\text{M}$ ).

is greater compared to the 50 and 250 kVp energies (Figure 4.45).

### 4.7.3 Discussions

For all X-ray energies, the radiation dose-response curves of 9L cells after irradiation concomitantly with  $10 \mu\text{M}$  BrUdR plus  $0.01 \mu\text{M}$  MTX shown an enhanced radiosensitising effect of the irradiation. The data shows the reduction in number of clonogenic survival at 50 kVp (Figure 4.39), 250 kVp (Figure

4.40), the 6 MV (Figure 4.41), and 10 MV (Figure 4.42). These are consistent with the  $\alpha$  values being larger than the corresponding irradiated controls without drugs (i.e. BrUdR plus MTX).

To date there have been no previous reports exploring the correlation between the radiosensitising effect of BrUdR combined with MTX and the external beam radiation energy dependence assessed by comparison of cell survival fraction. From Figure 4.43, it is concluded that the optimum energy for the maximum enhancement of BrUdR (plus MTX) radiosensitisation of 9L cells *in vitro* is obtained with an external X-ray beam irradiation using conventional orthovoltage X-ray machine at an energy of 125 kVp, with highest SER<sub>10</sub> of 2.3 (Figure 4.44). Such enhancement is evidenced by a linearisation of the cell survival curve.

It is well understood from the synchrotron experiments by [Corde et al., 2004] and [Rousseau et al., 2009a], that iodine is most efficiently ionised just above the K-edge (33.2 keV) and the peak of absorption contrast relative to water occurs in the spectrum at 50 keV. The results presented in this study also confirm the theoretical expectation according to the peak of absorption contrast of bromine relative to water in the spectrum occurs around  $\sim 40$  keV (Figure 3.1) and the output spectrum emitted from the orthovoltage X-ray unit used at 125 kVp (Figure 3.3) which defined in section 3.1.5.2. Our results showed that the influence of energy dependence is due to an increased production of photoelectrons. Hence, the photoelectric effect is the most relevant to this study. It is also noteworthy that the spectrum calculation were only for pure bromine atoms, not as a compound in BrUdR.

The SER<sub>10</sub> values were similar for all x-ray energies ( $\sim 1.2 - 1.3$ ) except for



the value at 125 kVp (2.3) (Table 4.7). This is explained by the fact that although, relative to water, bromine absorbs better at all X-ray energies, the ratio of absorption is greatest above the K-edge. Hence, given the simulated X-ray spectrum output of 50 kVp (Figure 3.2) and 250 kVp (Figure 3.5), it falls below the K-edge of bromine. Thus, despite the polychromatic nature of the x-ray tube output these results indicate that orthovoltage x-rays at 125 kVp are the most efficient at photoactivating BrUdR because of optimum peak absorption contrast of bromine relative to water occurs around  $\sim 40$  keV.

Table 4.7 summarises the LQ parameters of 9L cells obtained following analyses of the radiation dose-survival curves for irradiation alone and for combined irradiation and drugs at all energies. These data also support the conclusion that radiosensitisation by halogenated pyrimidines (i.e. BrUdR) is mainly due to an increase in the linear parameter  $\alpha$ , with the quadratic parameter  $\beta$  is rarely influenced [Franken et al., 2013]. The exception to this is energies of 250 kVp, where the  $\beta$  value is dominant as represents the accumulation of damage repair.

The sensitising effects presented in this study are also in agreement with the study by Tym and Todd [1964]. They studied the sensitising effect of another base analog, iododeoxyuridine (IUdR), on cells with different types of radiation. They found a stronger sensitisation for sparsely ionising radiation (i.e X-rays) compared to very heavy densely ionising particles (Carbon-12). In addition, low energy high-LET Auger electrons produced by photoelectric interactions that eject K-shell or other electrons [Karnas et al., 1999; Buchegger et al., 2006] can significantly cause an increase of SSB and DSB [Corde et al., 2003; Le Sech et al., 2001]. This can lead to more effective tumour cell killing *in vitro* [Laster et al., 1993]. *In vivo* studies showed an increased in the sur-

vival of Fisher rats bearing glioma [Biston et al., 2004; Adam et al., 2003] and also tumour growth delay for PAT-treated mice [Laster et al., 2009]. Thus, the overall results in this study are in a good agreement with previous studies that suggest the more effective cell killing by novel radiosensitiser drugs (i.e BrUdR or IUdR) was probably due to an increase in DNA strand breaks.

The change in efficacy of treatments as measured quantitatively by a significant reduction of 20% and 30% in the necessary absorbed radiation dose in order to achieve the same 10% cell surviving fraction was found in 6 and 10 MV irradiation with BrUdR plus MTX (Figure 4.44). Even though this was not as effective as the 125 kVp, it is more feasible to use in clinical practice and much more effective compared to other modalities currently available for the treatment of glioma. These results are also in good agreement with other studies on the use of high-Z elements (i.e platinum) in the form of cisplatin [Rousseau et al., 2010] and carboplatin [Rousseau et al., 2009b; Bobyk et al., 2012]. They both demonstrated an equivalent therapeutic response when the drug is combined with either 6 MV photons or synchrotron x-rays at the K-edge of platinum (at 78.8 keV) [Rousseau et al., 2010; Bobyk et al., 2012].

In order to confirm the effect that the combination of drugs (BrUdR plus MTX) with radiation kills cells greater than either agent alone, we performed a complete set of experiments with MTX-alone and/or BrUdR-alone irradiated concomitantly at a dose of 5 Gy in 50 and 250 kVp x-rays beam. These are shown in Figure 4.45, which shows the same trend as in section 2.4, chemo-Auger approach part 1 that BrUdR acts synergistically with x-rays and is supra additive in the presence of MTX.

The value of  $\alpha$  increases as the  $SER_{10}$  increases whereas the value for  $\beta$  is

nearly constant in both drug and control curves except under exceptional circumstances. The  $\beta$  value for 125kVp and drugs combination was not applicable which represents that there is no accumulation damage repair occurs. However, most importantly, the  $\alpha$  dominance of the irradiated drug-containing survival curves is the main principal thesis of this study. The  $\alpha$  value provide the most information related to sensitisation that in turn leads to the most effective method in killing tumour cells, this can overshadow the  $\beta$ -dependence. Recall the interpretation of the linearisation of the cell survival curve (BrUdR plus MTX at 125 kVp). According to the cell killing mechanism defined in section 2.1.4.4, we can extract some physical meaning of the trend that our mechanism of enhancement mimics the high-LET-like behaviour (i.e. cell survival curves with no shoulder) (Figure 2.10)

In the mid 1960s, BrUdR was given intra-arterially [Hoshino and Sano, 1969; Sano et al., 1965, 1968] and intravenously (i.v) infusion in 1980s [Jackson et al., 1987] in combination with radiotherapy for malignant glioma. The major drawback of this method is that the radiosensitisation of the tumour cells requires them to be continuously exposed to the drugs as the liver can dehalogenate them rapidly [Kriss et al., 1963]. Then, Deutsch et al. [1989] reported for the first time *in vivo* studies of the effects of IUdR administered into cerebrospinal fluid (CSF) and combined with irradiation of the craniospinal axes that can be clinically applicable for glioma treatment. Thus, the optimum mode of BrUdR administration in combination with radiotherapy is another challenging step. Recently, Kassis et al. [2004] have proposed the administration of 125IUdR (radiolabeled IUdR) into CSF for the treatment of advanced neoplastic meningitis. It has been used in the first human treatment of the same disease and proved to be feasible without acute neurological toxicity [Rebischung et al., 2008]. We propose that the mode of IUdR administration into

CSF could also be applied for administering BrUdR as a radiosensitiser simultaneously with MTX in the treatment for glioma.

#### 4.7.4 Conclusions

The hypothesis investigated in the present study was whether a chemo-Auger approach could be successfully applied in the clinical setting by using conventional X-ray machine (e.g. LINAC) that are already widely used in clinical radiotherapy for cancer treatment instead of using monoenergetic synchrotron radiation.

The synergistic effect of enhanced absorption contrast and tumour specificity can still be achieved by using halogenated pyrimidines to provide high-Z elements and irradiated externally by a polychromatic orthovoltage X-rays machine. It has been shown in this study that when combining BrUdR plus MTX with the appropriate energy photon spectrum centralised at the peak of absorption (i.e.  $\sim 40$  keV) the radiosensitisation per unit dose of radiation is optimised.

BrUdR combined with X-rays of energies 125 kVp is more cytotoxic to 9L cells than when combined with other energies (50 kVp, 250 kVp, 6 MV, or 10 MV). Even though the most effective tumour cell killing can be achieved by using orthovoltage X-rays machine, the change in efficacy of treatments as measured quantitatively by a significant reduction of 20% and 30% in the necessary absorbed radiation dose in order to achieve the same 10% cell surviving fraction was found in 6 and 10 MV irradiation with BrUdR combined with small quantities of MTX. This finding can be applied in clinical radiotherapy to increase the therapeutic ratio since the LINAC is a feasible machine for

cancer radiotherapy treatment.

The full efficacy of this combination therapy, i.e. chemo-Auger and chemo-electron/pair production approach, which has been discarded since 1960s (BAR therapy), can now be resumed. Our results suggest that *in vivo* studies and clinical trials of BrUdR photo-activation plus MTX concomitantly with external photon irradiation for treatment of brain tumours merit consideration.

Photoactivation studies of BrUdR combined with other anti-cancer drugs such as 5-FU or its prodrug called Fluorodex also under way in our laboratory.

## 4.8 Groundwork for Confocal Microscopy

This section describes and examines the confocal microscopy work carried out. All experiments were performed in the Illawarra Health and Medical Research Institute (IHMRI) of the University of Wollongong.

### 4.8.1 Reactive Oxygen Species Production in 9L Cells After a 24 Hour Incubation Period with Ta<sub>2</sub>O<sub>5</sub> Nanoparticles

Reactive oxygen species (ROS) are important chemical intermediates in biological studies [Chen et al., 2010]. ROS is used to describe the number of reactive molecules and free radicals (as in section 2.1.4.1). Thus, it is important to be able to quantify their quantity. The most widely used technique to detect ROS was developed more than 40 years ago. This method is based on the oxidation of the non-fluorescent probe 2',7'-Dichlorodihydrofluorescein (DCFH<sub>2</sub>) to produce the highly fluorescent 2',7'-Dichlorofluorescein (DCF) [Chen et al., 2010].

In this study intracellular ROS generated by Ta<sub>2</sub>O<sub>5</sub> nanoparticles in 9L cells were detected using 2',7'-Dichlorofluorescein diacetate (DCF<sub>2</sub>DA) and visualised by the green DCF<sub>2</sub>DA fluorescence shown in Figure 4.46. The DCF<sub>2</sub>DA fluorescence generated by Ta<sub>2</sub>O<sub>5</sub> nanoparticles was predominantly localised in the cytoplasm of 9L cells (Figure 4.46B) compared to control cells (Figure 4.46A). Figure 4.47 shows that 9L cells can uptake the Ta<sub>2</sub>O<sub>5</sub> nanoparticles via normal endocytosis. This suggests that Ta<sub>2</sub>O<sub>5</sub> nanoparticles can act as targeted nanoparticles that can be specifically incorporated into the cell nucleus (Figure 4.47).

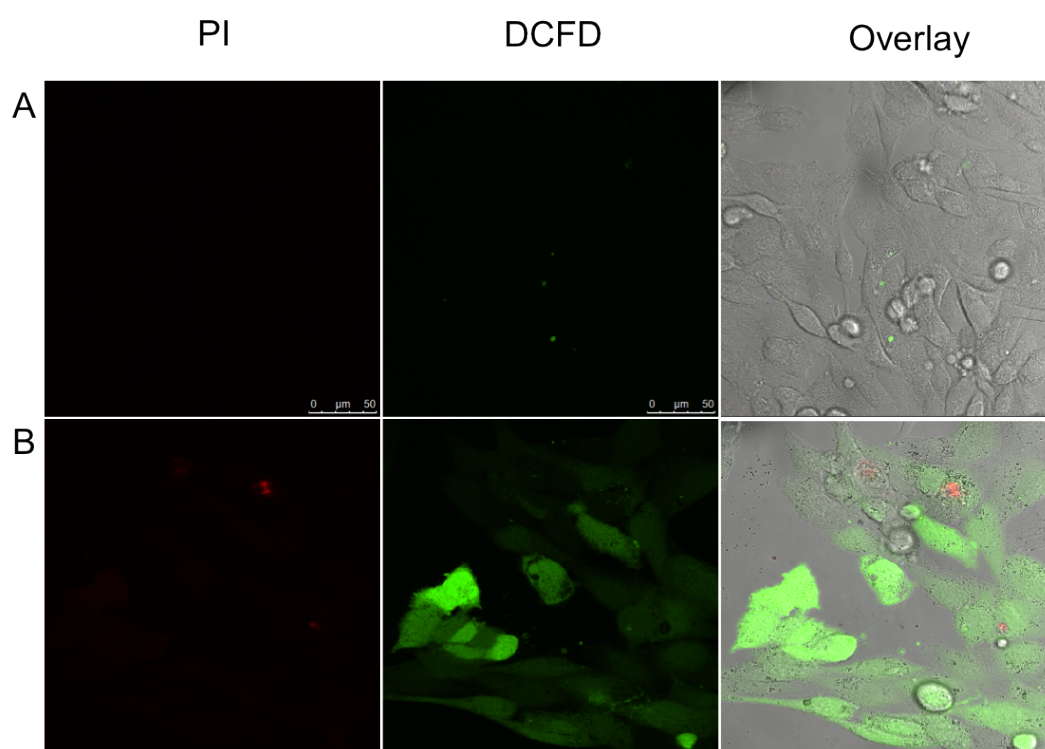


Figure 4.46: Microphotograph of intracellular ROS induced by Ta<sub>2</sub>O<sub>5</sub> nanoparticles in 9L cells detected with DCFD dye and counterstained with PI. (A) Untreated cells (control). (B) Cells were treated with 50 µg/ml of Ta<sub>2</sub>O<sub>5</sub> nanoparticles for 24 hours. All the chamber slides were analysed for fluorescence with a 488 nm excitation laser on a Leica confocal laser scanning microscope and the images were captured using the same parameters to allow comparison. Overlay image corresponding to the fluorescence of intracellular PI and DCFD fluorescence image.

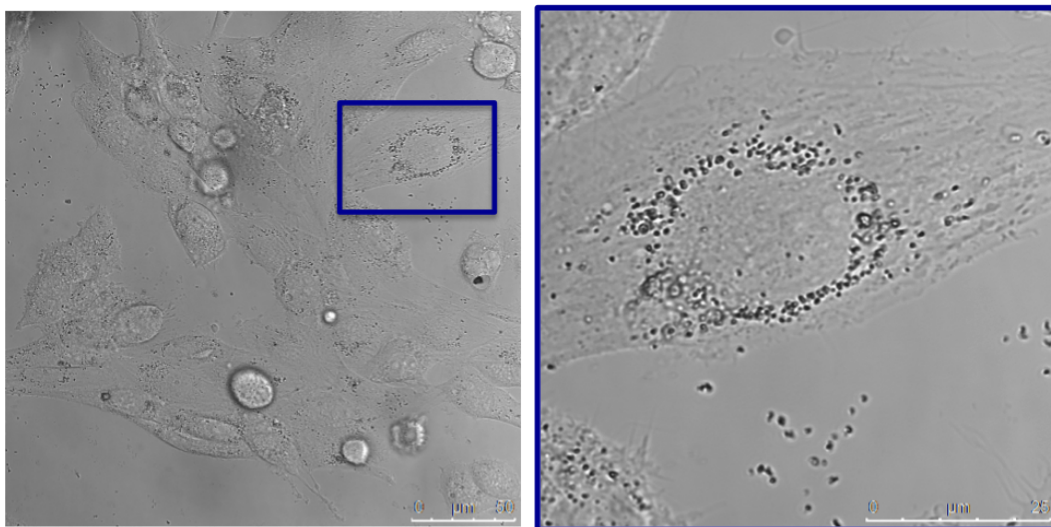


Figure 4.47: Exposure of 9L cells to  $\text{Ta}_2\text{O}_5$  nanoparticles ( $50 \mu\text{g}/\text{ml}$ ) for 24 hours, results in uptake of agglomerates surround the cell nucleus (black dots) (on left) and the magnification (on right). Light microscopy images were obtained using a Leica confocal laser scanning microscope.

#### 4.8.2 BrUdR as a Radiosensitiser Drug that is Specifically Incorporated into DNA in 9L Cells

Cells that had incorporated BrUdR during the drug incubation procedure were detected using fluorescently labelled anti-BrUdR antibodies (MoBU-1) and visualised by the use of a confocal laser scanning microscope. Figure 4.48 supports the hypothesis that BrUdR is incorporated into DNA since the MoBU-1 fluorescent image is predominantly seen only when the cells treated with BrUdR (green signal) (Figure 4.48C) and no green signal is observed in either untreated cells (negative control) (Figure 4.48A) or MTX-treated cells (positive control) (Figure 4.48B).

Due to all the cells have been fixed and permeabilised, all the cells are stained with propidium iodide (PI) and appear red in the fluorescent image. The intensity of the red fluorescence image for BrUdR-treated cells (Figure 4.48C) is stronger than for both controls. A possible explanation is that PI is an intercalate agent that stains DNA, the stronger the fluorescent signal indicates



that there has been a greater cell uptake. Since BrUdR is predominantly in the DNA, we expect that the cells are more vulnerable to permeation.

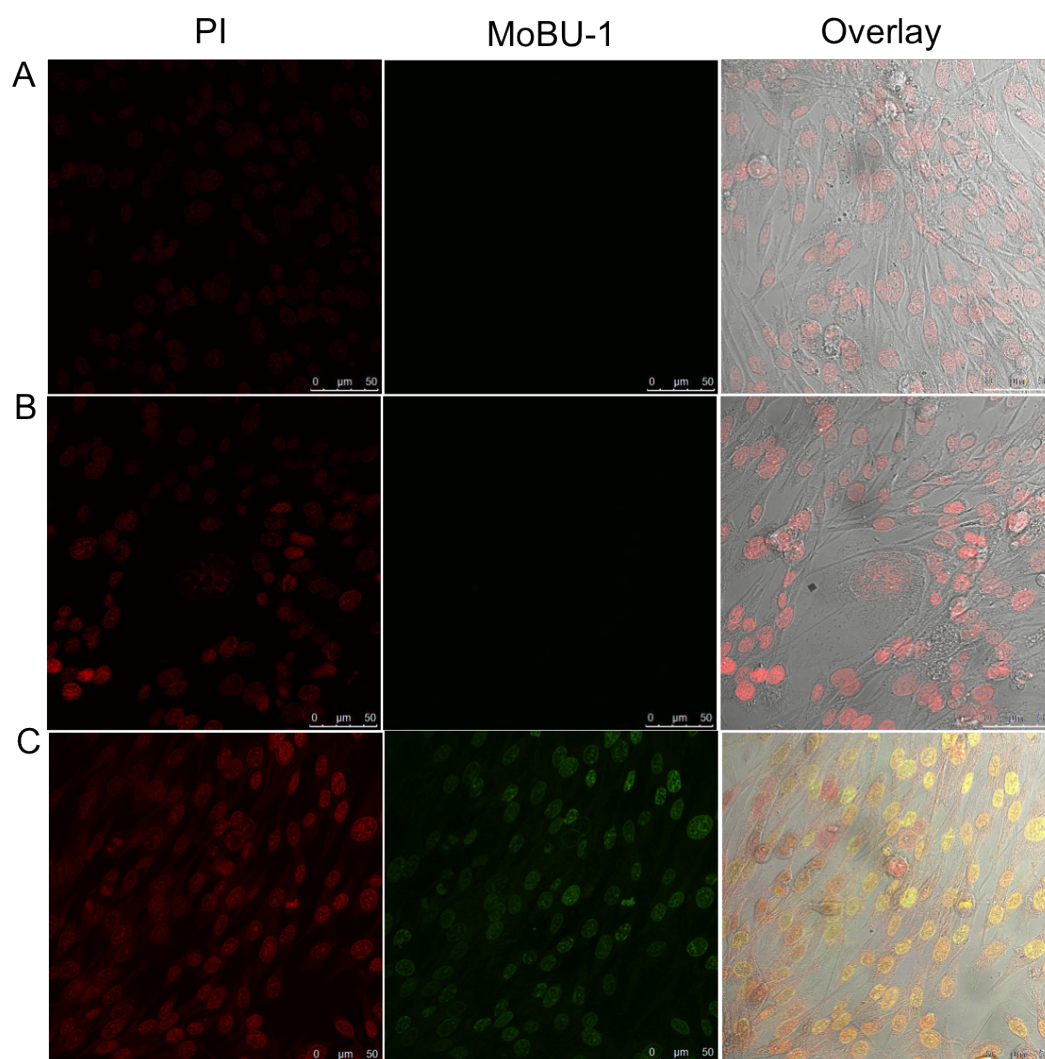


Figure 4.48: Microphotograph of intracellular 5-bromo-2'-deoxyuridine (BrUdR) in 9L cells. (A) Cells with no treatment was used as negative control. (B) Treatment of cells with 0.01 μM of MTX was used as positive control. (C) Cells treated with 10 μM BrUdR. Detection of BrUdR by direct fluorescent microscopy after 30 mins incubation with fluorescently labeled anti-BrUdR antibody (MoBU-1) (green signal) and cell nuclei labeled with PI (red signal). All the chamber slides were analysed for fluorescence with a 488 nm excitation laser on a Leica confocal laser scanning microscope and the images were captured using the same parameters to allow comparison. Overlay image corresponding to the fluorescence of intracellular PI and MoBU-1 fluorescence image.

### 4.8.3 Conclusions

Understanding the cellular uptake mechanism of the nanoparticles may provide important information to assist further development of targeted nanotherapeutic agents in combination with radiation therapy. Further studies that need to be conducted in the future are to continue analysing the nanoparticles treatment in *in vitro* cells using the confocal laser scanning microscope.

In addition to the immunostaining of BrUdR, it is clear that the procedure of fixation and permeabilisation worked successfully. These results also show an excellent correlation to the flow cytometry analysis. The results support that the assumption that BrUdR is incorporated into DNA, as evidenced by the green fluorescence image detected using the monoclonal antibody (clone MoBU-1) that is highly specific for BrUdR.

## Chapter 5

# Conclusions and Future Directions

This study investigated the influence of high-Z materials on the biological effect of X-rays on the cancer cell line 9L which is a rat gliosarcoma. Experiments were designed to quantify the effect of the beam energies upon radiation-induced damage using clonogenic survival analysis.

The halogenated pyrimidine analog 5-bromo-2'-deoxyuridine, also known as bromodeoxyuridine (BrUdR), was used due to its potential as a radiosensitiser drug for clinical radiotherapy. Dose-response curves were obtained using X-ray energies ranging from 50 kVp to 10 MVp at single doses of 1, 2, 3, 5, and 8 Gy. Comparisons were made of the radiation response of 9L cells combined with MTX and BrUdR.

The addition of BrUdR sensitised the 9L cells to 125 kVp X-rays irradiation by a sensitisation enhancement factor ( $SER_{10}$ ) of 1.6 whereas sensitisation following the addition of MTX was either not observed or was insignificant. The combination of MTX and BrUdR together significantly increased the sensi-

sation of the 9L cells ( $SER_{10} = 2.3$ ), though flow cytometry studies showed that it did not increase the degree of replacement of thymidine 5-bromo-2'-deoxyuridine.

The conceptual approach for clinical applications is that the dose of X-ray radiation beams (orthovoltage X-rays or LINAC) absorbed in the tumor region is enhanced by the application of a radiosensitiser drug, BrUdR, combined with an anticancer-drug, MTX. Another suggestion arising from this study is to investigate the general applicability of this concept by testing another combination of potent drugs such as IUdR and 5-FU.

Some cancer cells may have different responses to the increase in DSBs produced by X-ray irradiation in the presence of drugs. This arises because cancer cells are likely to differ in their ability to undergo DNA repair following DNA damage. Thus it is important to predict whether all cancer patients or perhaps only those with particular tumour types or particular genetic lesions, since there is variation in radiosensitivity, will benefit from the combined use of drugs. To determine the general applicability of our chemo-Auger therapy approach additional cell lines must be investigated, including radiosensitive lines such as MCF-7.

Understanding the molecular mechanisms leading to cancer cell death induced by X-ray radiation in the presence of high-Z materials may provide important information to assist in the further development of novel treatment options in radiation therapy. Future studies that need to be conducted are to investigate the effect in other cancer cell lines as well as *in vivo* studies. We have used the 9L rat gliosarcoma cell line, as they will be used in subsequent *in vivo* models of glioma. Thus, to determine whether the observed *in vitro* effects can trans-

late into a useful *in vivo* responses, the next step is to use a rat glioma model (e.g. Fischer 344 gliosarcoma-bearing rat) .

In a second aspect of the project we investigated the effect of radiation in combination with nanoparticles containing a high-Z element: cerium oxide ( $\text{CeO}_2$ ), tantalum pentoxide ( $\text{Ta}_2\text{O}_5$ ), and bismuth oxide ( $\text{Bi}_2\text{O}_3$ ). Although the presence of the nanoparticles enhanced the biological effect of the irradiation in the tumour volume, it is likely that adjacent normal tissue would also be affected. Thus the non-malignant MDCK cell line was chosen for investigation. Only the groundwork, cell growth analysis and toxicity, of the MDCK cell line was carried out in this study. However, it is clear that when lower photon X-rays energies used the high-Z nanoparticles are not as efficiently absorbed into cells as the radiosensitiser material BrUdR.

The main purpose of this thesis was to develop appropriate methods to allow a full investigation as to whether high-Z materials in combination with anti-cancer drugs and EBRT has the potential to provide a valuable cancer therapeutic strategy (i.e chemo-Auger therapy). The application of BrUdR combined with chemotherapeutic drugs and radiation is predicted to bring improvements in the biological effect of a radiation dose delivered to tumour tissue. This is expected to improve local tumour control while reducing the irradiation of healthy tissue. It has been shown that the combination of BrUdR, MTX and radiation significantly increases the biological effect of radiation.

It is concluded that to achieve the best effect from the presence of compounds containing a high-Z element that this compound should not be arbitrarily adsorbed into the cellular environment but must be specifically absorbed into cancer cells. This is evidenced by the uptake of BrUdR into the tumour cell

DNA. Then the most effective cell killing occurs at an optimum radiation energy.

Finally, the sensitisation enhancement ratio (SER) from external radiation beams was found to be the greatest ( $\text{SER} = 2.3$ ) when using both MTX and BrUdR.

# Appendix A

## Cell Line Information

## A.1 9L Cell Line

**Cell line name:** GS-9L

**Description:**

**Species:** Rat

**Organ:** Brain

**Disease:** Glioma

**Depositor:** ECACC (obtained from Westmead Children hospital LOT04/E/015)

**Reference:** Coderre et al. [1990]

**Biosafety level:** 2

**Growth mode:** Adherent

**Morphology:** Fibroblast-like

**Propagation:** Complete DMEM medium: DMEM + 10% FBS + 1% Pen  
Strep (+5,000 Units/mL Pen; +5,000  $\mu\text{g/mL}$  Strep)

**Subculturing:**

**Ratio:** Split 1:2 to 1:4

**Seeding:** at  $2 - 4 \times 10,000$  cells/cm<sup>2</sup>. Remove spent medium, rinse with PBS (w/o Ca and Mg), add fresh 0.05% trypsin/EDTA, incubate at 37°C until the cells detach. Add fresh medium, aspirate, and transfer into new flask. Incubate in incubator at 37°C (and 5% (v/v)CO<sub>2</sub>).

**Preservation:** Culture medium 90%; DMSO 10% (v/v)

**Passage number:** 46

**Sterility:** Mycoplasma negative



## A.2 MCF-7 Cell Line

**Cell line name:** MCF-7

**Description:**

**Species:** Human

**Organ:** Breast

**Disease:** Adenocarcinoma

**Depositor:** ATCC (kindly provided by A/Prof. M. Ranson at IHMRI)

**Reference:** CM McGrath

**Biosafety level:** 2

**Growth mode:** Adherent

**Morphology:** Epithelial

**Propagation:** Complete DMEM medium: DMEM + 10% FBS + 1% Pen Strep (+5,000 Units/mL Pen; +5,000  $\mu\text{g/mL}$  Strep)

**Subculturing:**

**Ratio:** Split 1:3 to 1:6

**Seeding:** at  $2 - 4 \times 10,000 \text{ cells/cm}^2$ . Remove spent medium, rinse with PBS (w/o  $\text{Ca}^{2+}$ ,  $\text{Mg}^{2+}$ ), add fresh 0.05% trypsin/EDTA, incubate at  $37^\circ\text{C}$  until the cells detach. Add fresh medium, aspirate, and transfer into new flask. Incubate in incubator at  $37^\circ\text{C}$  (and 5% (v/v) $\text{CO}_2$ ).

**Preservation:** Complete culture medium 95%; DMSO 5% (v/v)

**Passage number:** 11

**Sterility:** Mycoplasma negative

## A.3 U-87 MG Cell Line

**Cell line name:** U-87 MG

**Description:**

**Species:** Human

**Organ:** Brain

**Disease:** Glioblastoma; astrocytoma

**Depositor:** ECACC (obtained from Sigma-Aldrich Cat. No. 89081402)

**Reference:** Pontén and Macintyre [1968]

**Biosafety level:** 2

**Growth mode:** Adherent

**Morphology:** Epithelial-like

**Propagation:** Complete DMEM medium: DMEM with sodium pyruvate + 10% FBS + 1% Pen Strep (+5,000 Units/mL Pen; +5,000  $\mu\text{g/mL}$  Strep)

**Subculturing:**

**Ratio:** Split 1:3 to 1:6

**Seeding:** at  $2 - 4 \times 10,000 \text{ cells/cm}^2$ . Remove spent medium, rinse with PBS (w/o  $\text{Ca}^{2+}$ ,  $\text{Mg}^{2+}$ ), add fresh 0.05% trypsin/EDTA, incubate at  $37^\circ\text{C}$  until the cells detach. Add fresh medium, aspirate, and transfer into new flask. Incubate in incubator at  $37^\circ\text{C}$  (and 5% (v/v) $\text{CO}_2$ ).

**Preservation:** Culture medium 95%; DMSO 5% (v/v)

**Passage number:** 12

**Sterility:** Mycoplasma negative

## A.4 MDCK Cell Line

**Cell line name:** MDCK (Madin Darby Canine Kidney)

**Description:**

**Species:** Dog

**Organ:** Kidney

**Disease:** –

**Depositor:** ECACC (obtained from Sigma LOT05/L/009)

**Reference:** Madin and Darby [1958]; Gaush et al. [1966]

**Biosafety level:** 2

**Growth mode:** Adherent

**Morphology:** Epithelial

**Propagation:** Complete DMEM medium: DMEM + 10% FBS + 1% Pen  
Strep (+5,000 Units/mL Pen; +5,000  $\mu\text{g/mL}$  Strep)

**Subculturing:**

**Ratio:** Split 1:3 to 1:10

**Seeding:** at  $1 - 3 \times 10,000 \text{ cells/cm}^2$  Remove spent medium, rinse with PBS (w/o  $\text{Ca}^{2+}$ ,  $\text{Mg}^{2+}$ ), add fresh 0.05% trypsin/EDTA, incubate at  $37^\circ\text{C}$  until the cells detach. Add fresh medium, aspirate, and transfer into new flask. Incubate in incubator at  $37^\circ\text{C}$  (and 5% (v/v)  $\text{CO}_2$ ). Cells attach firmly and require at least  $2 \times$  PBS washes prior to addition of Trypsin/EDTA.

**Preservation:** Complete culture medium 90%; DMSO 10% (v/v)

**Passage number:** 61

**Sterility:** Mycoplasma negative

## Appendix B

### Subculture Adherent Cells – Protocol

## B.1 Subculture Adherent Cells – Protocol

### Materials

#### Sterile materials

- Healthy, 80-90% confluent cell culture in T75cm<sup>2</sup> flask
- c-DMEM medium (complete DMEM supplemented with 10% FBS and 1% PenStrep)
- PBS (without Ca<sup>2+</sup> and Mg<sup>2+</sup>)
- Trypsin-EDTA
- 1, 5, 10 and 25 mL pipettes
- T75 cm<sup>2</sup> flasks

#### Other materials

- Pippetor, Eppendorf tubes, tube racks, hemocytometer, vortex, hand-counter, microscope, calculator, gloves, ethanol, wipes, etc. Access to water bath set at 37°C and incubator at 37°C (and 5% (v/v) CO<sub>2</sub>).

### Procedure

1. Warm up an aliquot of the medium, PBS, and trypsin-EDTA in water bath at 37°C
2. Check the confluence of the cells under microscope
3. Using aseptic technique, in BSC: Open and handle the lid of the flask of the cells (dont put it on the bench)
4. Remove the spent medium

5. Wash with PBS (e.g 10 ml)\*; shake several times; discard the PBS
6. Add 2 ml of trypsin; shake it several times\*
7. Placed in incubator at 37°C for 5 minutes
8. Gently tapped the edge of flask; check under microscope (the cells should be detach/floating now)
9. Re-suspend with fresh medium\*; gently pipette it up and down to re-suspend it well; and aliquot small sample to perform cell count (see next protocol)
10. Transfer the required number of cells into new-labeled flask (labeled with initial, date, cell type, passage number, etc.).
11. Incubate in the incubator at 37°C (and 5% (v/v) CO<sub>2</sub>).

\* Put the pipette tip on the top of the neck of flask (and shake it while adding); cover it all of the surface; shake it several times

## Appendix C

### Cells Counting – Protocol



## C.1 Cells Counting – Protocol

### Materials

- Tube containing a cell line
- Hemocytometer
- Trypan blue
- Pipette and tips
- Vortex mixer

### Procedure

1. Before sampling, vortex the tube containing a cell to resuspend the cells.
2. Take a 10  $\mu\text{l}$  sample and add to 10  $\mu\text{l}$  of Trypan blue solution (1:2 dilution); mix thoroughly (pipette up and down).
3. Remove 10  $\mu\text{l}$  of cell suspension/Trypan blue sample with a pipette and place tips to the edge of a coverslip on the haemocytometer. Gently dispense the suspension into the space between coverslip and the haemocytometer (the counting chamber) until the counting chamber is filled, shown in Figure C.1.
4. Allow the cells to settle. Place on the microscope stage and using low power focus on the ruled area, looking at the four corner grids where each square millimetre is divide into 16 squares (A-D) and the middle one (E) which divide into 25 square, as shown in Figure C.2.
5. Count the cells in each 5 grids (A-E; figure 2). Average the 5 counts to the number of cells per grid. This value represents the number of cells in 0.1  $\mu\text{l}$  of suspension applied to the haemocytometer. Thus, to calculate

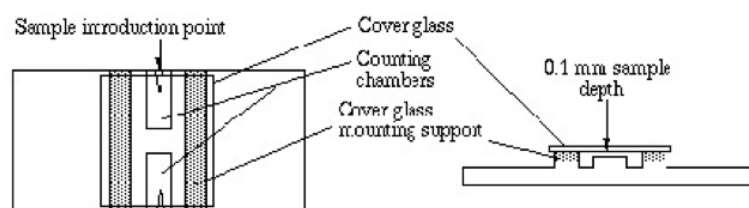


Figure C.1: A typical hemocytometer

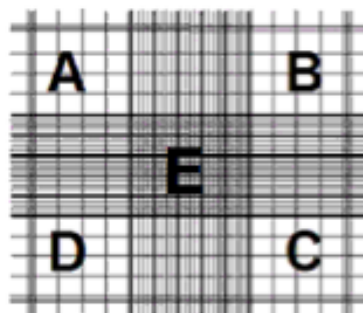


Figure C.2: Counting chamber of a hemocytometer

the concentration of cells in the original suspension: (Average number of cells per grid)  $\times$  (dilution factor)  $\times$  (10,000)

## Appendix D

### Cryopreservation – Protocol

## D.1 Freezing Protocol

### Materials

#### Sterile materials

- Healthy, 80-90% confluent cell culture in T75cm<sup>2</sup> flask (need at least 4 flasks)
- c-DMEM medium (complete DMEM supplemented with 10% FBS and 1% PenStrep)
- Cell culture freezing medium (mix well and store at 2° to 8°C / in ice bucket until use)
- PBS (without Ca<sup>2+</sup> and Mg<sup>2+</sup>)
- Trypsin-EDTA
- 1, 5, 10 and 25 mL pipettes
- Centrifuge tubes
- 2mL Cryogenic vials (labelled before)

#### Other materials

- Pippetor, Eppendorf tubes, tube racks, hemocytometer, vortex, hand-counter, microscope, calculator, gloves, ethanol, wipes, etc. Access to bench centrifuge, water bath set at 37°C and incubator at 37°C (and 5% (v/v) CO<sub>2</sub>).

### Procedure

1. The culture medium should be replaced 24h prior to freezing

2. Gently detach the cells: Discard all the old media; wash the cell monolayer with 10 ml of PBS (twice) and discard; treated with 2 mL of the trypsin-EDTA; put in incubator at 37°C for 2–5 mins; check under microscope (cells should be detach now)
3. Resuspend with fresh c-DMEM medium (pre-warmed) and pipette it up and down. Transferred into the centrifuged tubes and placed on ice. Take a small aliquot of cells to an Eppendorf tube, vortex and count the viability cells (with the Trypan blue) using hemocytometer
4. Obtain cell pellet: centrifuge at 1500 rpm for 7mins
5. Discard the supernatant from the centrifuged cells and resuspend the cell pellet in the appropriate freezing medium to give final cell concentration  $2\text{--}4 \times 10^6$  cells/mL; pipette 1 mL into each Cryogenic vials
6. Place the Cryogenic vials in Mr. Frosty container (containing 250 mL isopropanol and should be cooled prior to use); place in  $-80^\circ\text{C}$  freezer (at least 4 hour)
7. After 24h, transfer all the Cryogenic vials to a gas phase liquid nitrogen permanent storage vessel.

A schematic diagram of creating batch of master and working stocks of cells is shown in figure D.1.

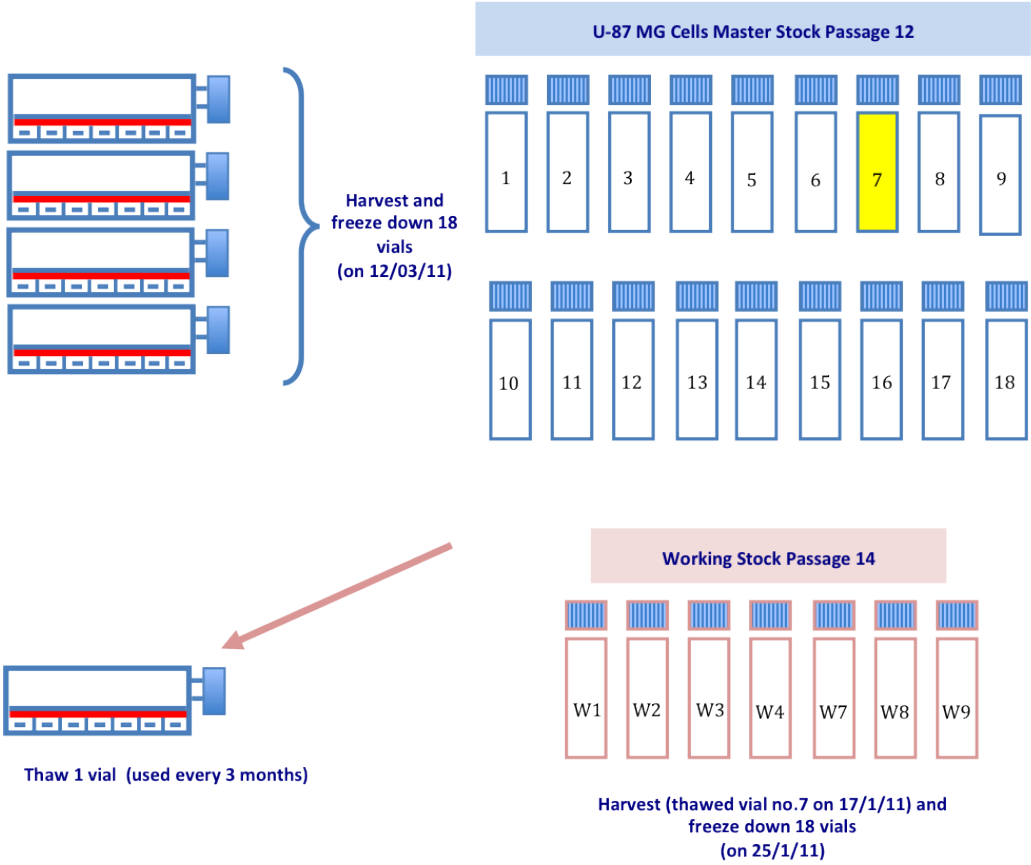


Figure D.1: Schematic diagram of master and working stocks of cells (e.g. U-87 MG cells)

## D.2 Thawing Protocol

### Materials

#### Sterile materials

- c-DMEM medium (complete DMEM supplemented with 10% FBS and 1% PenStrep)
- T75cm<sup>2</sup> or T25cm<sup>2</sup> flasks
- 50 mL Falcon<sup>TM</sup> tubes

#### Other materials

- Pippetor, Eppendorf tubes, tube racks, hemocytometer, vortex, hand-counter, microscope, calculator, gloves, ethanol, wipes, etc. Access to bench centrifuge, water bath set at 37°C and incubator at 37°C (and 5% (v/v) CO<sub>2</sub>).

### Procedure

1. Warm up an aliquot of media (e.g. cDMEM) at 37°C water bath
2. Get 1 cryovial of frozen cells
3. Using antiseptic technique, in BSC class 2, hold a tissue soaked in 70% ethanol around the cap of the frozen sample and turn the cap a quarter turn. Re-tighten the cap.
4. Quickly and gently warm the frozen sample (Put the vial in the tube with pre-warmed ethanol) in 37°C water bath until just thawed (1–2 min).
5. Using antiseptic technique, in BSC class 2, transfer the thawed cells into:

New sterile flask\* and add warm media to the cells drop wise while gently swirling the flask in a circular motion to slowly equilibrate the cells to the medium first few mLs very slow (e.g. 1 drop per second then speed up)

Or

New conical tube with 5ml pre-warmed media and may centrifuge on low spin.

6. Lay the flask down and check the cells condition under the microscope. If highly clumped, gently pipette the cells up and down a bit to disperse them
7. Take a small aliquot of cells and count the viability cells
8. Incubate cells in incubator at 37°C (and 5% (v/v) CO<sub>2</sub>) and leave for couple hours or until attached (or leave overnight)
9. Once the cells have attached and had a chance to expel the DMSO, remove the media and add fresh media
10. Maintain the cells and subculture as necessary

\* Flask size depends on cell number T25cm<sup>2</sup> for low cell number or cells requiring close contact or T75cm<sup>2</sup> for higher cell number or extremely fast growing cells. For T25cm<sup>2</sup> flask, use 5-8 mls total volume of media. For T75cm<sup>2</sup> flask, use 10-20 mls total volume of media.



## Appendix E

### Cells Growth Assay – Protocol

## E.1 9L Cell Line

### Materials

#### Sterile materials

- Healthy, 80-90% confluent cell culture in T75cm<sup>2</sup> flask (need at least 4 flasks)
- c-DMEM medium (complete DMEM supplemented with 10% FBS and 1% PenStrep)
- PBS (without Ca<sup>2+</sup> and Mg<sup>2+</sup>)
- Trypsin-EDTA
- 1, 5, 10 and 25 mL pipettes
- Centrifuge tubes
- BD Falcon<sup>TM</sup> Primaria petri dishes 60 × 15 mm (growth area = 21.3 cm<sup>2</sup>; vol. = 6 –7 mL)

#### Other materials

- Pippetor, Eppendorf tubes, tube racks, hemocytometer, vortex, hand-counter, microscope, calculator, gloves, ethanol, wipes, etc. Access to bench centrifuge, water bath set at 37°C and incubator at 37°C (and 5% (v/v) CO<sub>2</sub>).

### Procedure

1. Gently detach the cells: Discard all the old media; wash the cell monolayer with 10 ml of PBS and discard; treated with 2 mL of the trypsin-EDTA; put in incubator at 37°C for 2 mins; check under microscope.

2. Resuspend with 10 ml of fresh c-DMEM medium (pre-warmed) and pipette it up and down. Take a small aliquot of cells to an Eppendorf tube, vortex and count the cells using haemocytometer.
3. Adjust the final cell concentration of  $5 \times 10^4$  cells/petri dish (to be optimum, it should be  $5 \times 10^5$  cells/petri dish based on  $2 - 4 \times 10^4$  cells/cm<sup>2</sup>).
4. Take 5 mL into each petri dish (triplicate for each day data points for 14 days (make up total of 42 petri dishes).
5. Place all 42 petri dishes in incubator at 37°C (and 5% (v/v) CO<sub>2</sub>).
6. Counts the cells from triplicate petri dishes daily for 14 days (repeat the first two procedure above, but with only 5 ml PBS, 1 ml Trypsin-EDTA, and 5 ml c-DMEM).
7. The cells counted will be averaged for each time interval and the doubling time of cell will the calculated from the linear phase of the growth curve.

## E.2 MCF-7 Cell Line

### Materials

#### Sterile materials

- Healthy, 80-90% confluent cell culture in T75cm<sup>2</sup> flask (need at least 4 flasks)
- c-DMEM medium (complete DMEM supplemented with 10% FBS and 1% PenStrep)\*
- PBS (without Ca<sup>2+</sup> and Mg<sup>2+</sup>)
- Trypsin-EDTA
- 1, 5, 10 and 25 mL pipettes
- Centrifuge tubes
- BD Falcon<sup>TM</sup> Primaria petri dishes 100 × 15 mm (growth area = 58.95 cm<sup>2</sup>; vol. = 16 –17.5 mL)

#### Other materials

- Pippetor, Eppendorf tubes, tube racks, hemocytometer, vortex, hand-counter, microscope, calculator, gloves, ethanol, wipes, etc. Access to bench centrifuge, water bath set at 37°C and incubator at 37°C (and 5% (v/v) CO<sub>2</sub>).

### Procedure

1. Gently detach the cells: Discard all the old media; wash the cell monolayer with 10 ml of PBS and discard; treated with 2 mL of the trypsin-EDTA; put in incubator at 37°C for 2 mins; check under microscope.

2. Resuspend with 10 ml of fresh c-DMEM medium (pre-warmed) and pipette it up and down. Take a small aliquot of cells to an Eppendorf tube, vortex and count the cells using haemocytometer.
3. Adjust the final cell concentration of  $2 \times 10^5$  cells/petri dish (to be optimum, it should be  $5 \times 10^5$  cells/petri dish based on  $2 - 4 \times 10^4$  cells/cm<sup>2</sup>).
4. Take 10 mL into each petri dish (triplicate for each day data points for 10 days (make up total of 30 petri dishes).
5. Place all 30 petri dishes in incubator at 37°C (and 5% (v/v) CO<sub>2</sub>).
6. Counts the cells from triplicate petri dishes daily for 10 days (repeat the first two procedure above, but with only 5 ml PBS, 2 ml Trypsin-EDTA, and 5 ml c-DMEM).
7. The cells counted will be averaged for each time interval and the doubling time of cell will be calculated from the linear phase of the growth curve.

\* Or complete RPMI-1640 supplemented with 5% FBS and 1% PenStrep.

## E.3 U-87 MG Cell Line

### Materials

#### Sterile materials

- Healthy, 80-90% confluent cell culture in T75cm<sup>2</sup> flask (need at least 4 flasks)
- c-DMEM medium (complete DMEM with sodium pyruvate – supplemented with 10% FBS and 1% PenStrep)
- PBS (without Ca<sup>2+</sup> and Mg<sup>2+</sup>)
- Trypsin-EDTA
- 1, 5, 10 and 25 mL pipettes
- Centrifuge tubes
- BD Falcon™ Primaria petri dishes 60 × 15 mm (growth area = 21.3 cm<sup>2</sup>; vol. = 6 – 7 mL)

### Procedure

1. Gently detach the cells: Discard all the old media; wash the cell monolayer with 10 ml of PBS and discard; treated with 2 mL of the trypsin-EDTA; put in incubator at 37°C for 2 mins; check under microscope.
2. Resuspend with 10 ml of fresh c-DMEM medium (pre-warmed) and pipette it up and down. Take a small aliquot of cells to an Eppendorf tube, vortex and count the cells using haemocytometer.
3. Adjust the final cell concentration of  $5 \times 10^4$  cells/petri dish (to be optimum, it should be  $5 \times 10^5$  cells/petri dish based on  $2 - 4 \times 10^4$  cells/cm<sup>2</sup>).
4. Take 5 mL into each petri dish (triplicate for each day data points for 14 days (make up total of 42 petri dishes)).

5. Place all 42 petri dishes in incubator at 37°C (and 5% (v/v) CO<sub>2</sub>).
6. Counts the cells from triplicate petri dishes daily for 14 days (repeat the first two procedure above, but with only 5 ml PBS, 1 ml Trypsin-EDTA, and 5 ml c-DMEM).
7. The cells counted will be averaged for each time interval and the doubling time of cell will the calculated from the linear phase of the growth curve.

## E.4 MDCK Cell Line

### Materials

#### Sterile materials

- Healthy, 80-90% confluent cell culture in T75cm<sup>2</sup> flask (need at least 4 flasks)
- c-DMEM medium (complete DMEM supplemented with 10% FBS and 1% PenStrep)\*
- PBS (without Ca<sup>2+</sup> and Mg<sup>2+</sup>)
- Trypsin-EDTA
- 1, 5, 10 and 25 mL pipettes
- Centrifuge tubes
- BD Falcon™ Primaria petri dishes 100 × 15 mm (growth area = 58.95 cm<sup>2</sup>; vol. = 16 –17.5 mL)
- T75cm<sup>2</sup> and T175cm<sup>2</sup> flasks

#### Other materials

- Pippetor, Eppendorf tubes, tube racks, hemocytometer, vortex, hand-counter, microscope, calculator, gloves, ethanol, wipes, etc. Access to bench centrifuge, water bath set at 37°C and incubator at 37°C (and 5% (v/v) CO<sub>2</sub>).

### Procedure

1. Gently detach the cells: Discard all the old media; wash the cell monolayer with 10 ml of PBS and discard; treated with 5 – 10 mL of the



trypsin-EDTA; put in incubator at 37°C for 5 – 10 mins; check under microscope.

2. Resuspend with 10 ml of fresh c-DMEM medium (pre-warmed) and pipette it up and down (at least 10 times). Take a small aliquot of cells to an Eppendorf tube, vortex and count the cells using haemocytometer.
3. Adjust the final cell concentration of  $2 \times 10^5$  cells/petri dish (to be optimum, it should be  $5 \times 10^4$  cells/petri dish based on  $2 - 4 \times 10^4$  cells/cm<sup>2</sup>).
4. Take 10 mL into each petri dish (triplicate for each day data points for 10 days (make up total of 30 petri dishes).
5. Place all 30 petri dishes in incubator at 37°C (and 5% (v/v) CO<sub>2</sub>).
6. Counts the cells from triplicate petri dishes daily for 10 days (repeat the first two procedure above, but with only 5 ml PBS, 2 ml Trypsin-EDTA, and 5 ml c-DMEM).
7. The cells counted will be averaged for each time interval and the doubling time of cell will be calculated from the linear phase of the growth curve.

## Appendix F

### Drugs Treatment and Cytotoxicity – Protocol

## F.1 Drugs Treatment and Cytotoxicity – Protocol

This appendix provide an example of the complete procedure start from preparation of the cells (Day 0) until the last day of experiment (Day 28) on 9L cells.

### Cell Culture Preparation (24/03/11)

#### Sterile Materials

- Cell culture (9L cells) in T75 cm<sup>2</sup> flasks (Passage 55)
- Complete DMEM medium (DMEM contain L-glutamine supplemented with
- FBS + 1% PenStrep)
- PBS (without Ca<sup>2+</sup> and Mg<sup>2+</sup>)
- 0.05% Trypsin-EDTA
- 2, 5, and 10 mL pipettes
- T12.5 cm<sup>2</sup> flasks (with vented cap)

#### Other materials

- Pippetor, Eppendorf tubes, tube racks, hemocytometer, vortex, hand-counter, microscope, calculator, gloves, ethanol, wipes, etc. Access to bench centrifuge, water bath set at 37°C and incubator at 37°C (and 5% (v/v) CO<sub>2</sub>).

#### Procedure

1. Pre-warmed the DMEM, PBS, and Trypsin-EDTA at 37°C water bath.

2. Remove the spent medium from the flask; wash the cell monolayer with 10 ml of PBS and discard; treated with 2 ml of trypsin-EDTA; put in incubator at 37°C for 5mins; check under microscope (cells should be detach now).
3. Resuspend with 10 ml of DMEM pipetting the cells up and down; take a small aliquot in Eppendorf tube; count with hemocytometer; Adjust the number of cells required (i.e 100,000 cells/flask).
4. Pipette the amount of volume of cells required (e.g.  $\sim 100\mu\text{l}$ ) into each new T12.5 cm<sup>2</sup> flask labeled .
5. Add 5 ml of fresh DMEM into each flask; wiped with ethanol; place in cell culture incubator at 37C (with 5% (v/v) CO<sub>2</sub>).
6. After 5 days of culture (at  $\sim 60\%$  confluence), the drugs (5-FU,MTX, and BrUdR) will be added to each flask (according to the dose as shown in F.1).

Table F.1: summarised of drugs concentration for cytotoxicity test on 9L cells

Flask	Drugs ( $\mu\text{M}$ )		
	5-FU	MTX	BrUdR
Control-1			
Control-2			
3	0.01		
4	0.1		
5		0.01	
6		0.1	
7			1
8			10
9	0.01		1
10	0.1		1
11	0.01		10
12	0.1		10
13		0.01	1
14		0.1	1
15		0.01	10
16		0.1	10

**Cell Culture – Drugs incubation (29/03/11)**Sterile Materials

- 16 flasks of the 9L cells seeded on 24/3/11
- P20-P1000 pipette tips
- Drugs dilution (5-FU,MTX, and BrUdR)

Other Materials

- Pippetor, Eppendorf tubes, tube racks, hemocytometer, vortex, hand-counter, microscope, calculator, gloves, ethanol, wipes, etc. Access to bench centrifuge, water bath set at 37°C and incubator at 37°C (and 5% (v/v) CO<sub>2</sub>).

Procedure

1. Add the required volume of drugs (5-FU,MTX, and BrUdR) according to the dose into each appropriate flask (Table F.1); wipe the flask with

EtOH; place in cell culture incubator at 37°C (with 5% (v/v) CO<sub>2</sub>) for 3 days.

### **Cytotoxicity Test and Clonogenic Assays (01/04/11)**

After 3 days incubated with drugs, the toxicity of the drugs will be assessed and the clonogenic survival assays will be performed.

#### Sterile Materials

- 16 flasks of the 9L cells
- c-DMEM medium (complete DMEM supplemented with 10% FBS + 1% PenStrep)
- PBS (without Ca<sup>2+</sup> and Mg<sup>2+</sup>)
- 0.05% Trypsin-EDTA
- 2, 5, and 10 mL pipettes
- P20-P1000 pippete tips
- 50 ml Falcon<sup>TM</sup> tubes
- BD Falcon<sup>TM</sup> Primaria petri dishes 100 × 15 mm (growth area = 58.95 cm<sup>2</sup>; vol. = 16 –17.5 mL) (total needed = 14 flasks × 3 densities × 3plicates = 126 + 6 controls = 132 plates) (Table F.2)

#### Other Materials

- Pippetor, Eppendorf tubes, tube racks, hemocytometer, vortex, hand-counter, microscope, calculator, gloves, ethanol, wipes, etc. Access to bench centrifuge, water bath set at 37°C and incubator at 37°C (and 5% (v/v) CO<sub>2</sub>).

### Procedure

1. Pre-warmed the DMEM, PBS, and Trypsin-EDTA at 37°C water bath (while waiting labeled each 132 petri dish).
2. Remove the spent medium from the flask; wash the cell monolayer with 5ml of PBS and discard; treated with 1ml of trypsin-EDTA; put in incubator at 37°C for 5mins; check under microscope (cells should be detach now).
3. Resuspend with 1ml of DMEM pipetting the cells up and down; transfer 100  $\mu$ l of cells into 2 ml of DMEM (or HBSS buffer) for dilution in 50 ml FALCONtubes; count with haemocytometer (dispense the cells inside the BSC).
4. Adjust the number of cells required for seeding based on the percentage toxicity rate (r%) of each treated cells condition compared to the untreated cells (control cells as reference) as followed:

$$N = \left(1 + \frac{r}{100}\right) \times 1500 \text{ cells,}$$

where N is the number of cells and r is the toxicity death rate of the treated cells. We will make a set of three different densities for each flask (of treated cells only) in order to get a good range number of cells plating for the next experiment. See the template for more details (Table F.2),

5. Fill all the 132 plates with 10ml of fresh complete DMEM.
6. Vortex the cells before pipetting the into each petri dish.
7. Pipette the amount of volume required according to the number of cells/petri dish (Table F.2) into each appropriate petri dish labeled (For each cell sample density in triplicates).

8. When finished (e.g. 6 petri dishes plated), shake the petri dish clockwise, anti-clockwise, up-down and right-left directions; wiped with ethanol; place in cell culture incubator at 37°C (with 5% (v/v) CO<sub>2</sub>); start again for plating the next one.
9. After 21 days of culture, the cell colonies will fix and stain with crystal violet.



**Fix and Staining – 22/04/11**

After 21 days, the cells will fix and stain with mixture solution of 25% crystal violet + 75% of EtOH (v/v).

Materials

- All plates of the 9L cells seeded on 01/04/11
- Dulbeccos PBS (with  $\text{Ca}^{2+}$  and  $\text{Mg}^{2+}$ )
- Crystal violet
- 70% ethanol
- 2 ml pipettes
- waste jerry can or container
- Pipettor, gloves, ethanol, wipes, access to tap water

Procedure

1. Remove the spent medium from each plate; wash the cell monolayer with approximate 5 ml of DPBS and discard; add approximate 2ml of mixture solution of 25% crystal violet and 75% ethanol and leave for about 5 minutes.
2. Rinse with tap water into waste container; invert the plates and allow them to dry (on a carton cover with wipes paper).

Then, only the number of colonies containing more than 50 cells will counted and check by microscope.

Table F.2: Template for the cytotoxicity test of drugs and clonogenic assays on 01/04/11

<b>Cytotoxicity test of drugs and clonogenic assays on 01/04/11</b>							
Flask no.	5-FU ( $\mu$ M)	MTX ( $\mu$ M)	BrUdR ( $\mu$ M)	Plate no.	cells ( $\mu$ L)	cells/plate	$\mu$ L
1-control	–	–	–	1–3		1500	
2-control	–	–	–	4–6		1500	
3	0.01			7–9 10–12 13–15		N= 3N= 9N=	
4	0.1			16–18 19–21 22–24		N= 3N= 9N=	
5		0.01		25–27 28–30 31–33		N= 3N= 9N=	
6		0.1		34–36 37–39 40–42		N= 3N= 9N=	
7			1	43–45 46–48 49–51		N= 3N= 9N=	
8			10	52–54 55–57 58–60		N= 3N= 9N=	
9	0.01		1	61–63 64–66 67–69		N= 3N= 9N=	
10	0.1		1	70–72 73–75 76–78		N= 3N= 9N=	
11	0.01		10	79–81 82–84 85–87		N= 3N= 9N=	
12	0.1		10	88–90 91–93 94–96		N= 3N= 9N=	
13		0.01	1	97–99 100–102 103–105		N= 3N= 9N=	
14		0.1	1	106–108 109–111 112–114		N= 3N= 9N=	
15		0.01	10	115–117 118–120 121–123		N= 3N= 9N=	
16		0.1	10	124–126 127–129 130–131		N= 3N= 9N=	

## Appendix G

### Nanoparticles Treatment and Cytotoxicity – Protocol

## G.1 Nanoparticles Treatment and Cytotoxicity – Protocol

### Cell Culture Preparation

#### Sterile Materials

- Healthy, ~80-90% confluent cell culture in T75cm<sup>2</sup> flask
- c-DMEM medium (complete DMEM supplemented with 10%(v/v) FBS and 1%(v/v) PenStrep)
- DPBS (without Ca<sup>2+</sup> and Mg<sup>2+</sup>)
- 0.05% Trypsin-EDTA
- 2, 5, 10, and 25 mL pipettes
- BD Falcon™ Primaria Petri dish 60 × 15 mm (growth area = 21.3 cm<sup>2</sup>; vol. = 6 – 7 ml)
- BD T12.5cm<sup>2</sup> flasks (with vented cap)
- P20-P1000 pipette tips

#### Other Materials

- Pippetor, Eppendorf tubes, tube racks, hemocytometer, vortex, hand-counter, microscope, calculator, gloves, ethanol, wipes, etc. Access to bench centrifuge, water bath set at 37°C and incubator at 37°C (and 5% (v/v) CO<sub>2</sub>).

#### Procedure

1. Pre-warmed c-DMEM, DPBS, and Trypsin in water bath at 37°C

2. Gently detach the cells: Discard the old media; wash the monolayer cells with 10 mL of DPBS and discard; treated with 2mL Trypsin-EDTA; placed in incubator at 37°C for 2-3mins
3. Re-suspend with 10mL of fresh DMEM; pipette it gently up and down. Take a small aliquot of cells to an Eppendorf tube, vortex and count the cells using haemocytometer
4. Adjust the final cell concentration of  $\sim 4 \times 10^5$  cells/flask (total make up to 2 flasks 1 flask of treated cells and 1 flasks of control) and place in incubator at 37°C (and 5% (v/v) CO<sub>2</sub>) for 2 days (cell should be reach  $\sim 70\%$  confluence)
5. After 2 days, add the sterile NP prepared (refer to NP preparation step below) into 1 flasks (labeled +NP).
6. After 1day incubation time, counts the cells as followed:
  - Gently detach the cells: Discard the old media; wash the monolayer cells with 5mL of DPBS and discard; treated with 1mL Trypsin-EDTA; placed in incubator at 37C for 2-3mins.
  - Re-suspend with 2mL of fresh DMEM; pipette it gently up and down. Take a small aliquot of cells to an Eppendorf tube, vortex and count the cells using hemocytometer.
  - Adjust the number of cells required for seeding based on the percentage toxicity rate ( $r\%$ ) of each treated cells condition compared to the untreated cells (control cells as reference) as followed:

$$N = \left(1 + \frac{r}{100}\right) \times 1500 \text{ cells,}$$

where N is the number of cells and r is the toxicity death rate of the treated cells. We will make a set of three different densities for each

flask (of treated cells only) in order to get a good range number of cells plating for the next experiment. See the template for more details (Table G.1).

Table G.1: An example of template for the cytotoxicity test and clonogenic assay of nanoparticles on 9L cells

<b>Cytotoxicity and clonogenic test of Bi<sub>2</sub>O<sub>3</sub> on 9L cells (22–24 Nov 2011)</b>					
Flask no.	Bi <sub>2</sub> O <sub>3</sub> ( $\mu\text{g}/\text{ml}$ )	Plate no.	cells/ $\mu\text{L}$	cells/plate	$\mu\text{L}$
1-control	–	1–3		1500	
DAY1	50	4–6		N=	
	50	7–9		2N=	
	50	10–12		4N=	
2-control	–	13–15		1500	
DAY2	50	16–18		N=	
	50	19–21		2N=	
	50	22–24		4N=	

## Nanoparticle (NP) Samples Preparation

### Drying the NP samples

- Crush the NP into powder and place on foil. Place in 70°C oven (including the glass vials) for no less than 2 hours, and then transfer the NP into the glass vial.

### Sterilising the NP samples

- Placed the glass vial containing the NP, into a small beaker cover with foil and autoclave at 121°C.
- Upon completion, if doing the experiments on the same day, start immediately step 3. Otherwise, placed the glass vial into a drying oven (70°C) for couple hours (to avoid condensation) then it can be stored

at room temperature (placing the vial inside a tube containing silica to avoid moisture re-absorption).

#### Suspend the NP samples in PBS

- Inside the BSC, transferred the sterile NP (e.g. 5 mg) into 50 mL Falcon<sup>TM</sup> tube and add 10 mL of sterile PBS (make up concentration of 500  $\mu\text{g/mL}$ ). To have the required concentration of 50  $\mu\text{g/mL}$  of the NP, the volume of 1ml will need to be added into each flask.

#### Sonicate the NP samples

- Wipe the fine tip probe of the sonifier with 70% ethanol.
- Place the Falcon<sup>TM</sup> tube (containing the NP) into a beaker filled with water (make sure about 2 – 3 cm of the fine tip probe is immersed in the water without touching the side or the bottom of the beaker). Then, place the beaker into another bigger beaker or container surrounding with ice (to avoid the probe overheating the solution).
- Set-up the sonifier (depend on what sonifier to be used high or ultra-high): strength at level 7 (no higher than 7!); duty cycle control at constant; and timer for 5 minutes (repeat 6 times to give total duration of 30 mins).

#### Add the NP samples into cells

- Immediately after the sanitation finish, inside the BSC, adds the volume of NP required (e.g. 1 ml) into flask prepared before (containing  $\sim 1 \times 10^6$  cells).

## Appendix H

### Complete Procedure of X-rays Irradiation Experiments



## H.1 Experimental dose rate on LINAC

### Cell Culture Preparation

1. Healthy,  $\sim 90\%$  confluent cell culture in T12.5cm<sup>2</sup> flasks with vented cap  
– seeding at  $1 \times 10^5$  cells/flask 3 days before X-ray irradiation.
2. After 3 days incubation, just prior the irradiation, fill the flask of cells with approximately 30ml of pre-warm HBSS buffer (w/Phenol); sealed the lid with parafilm (not to cover the filter on top).
3. Placed vertically all the flasks in the container surround by silica gel; then in a carry bag.
4. Transport to POWH.

### Cells Irradiations

Irradiate the cells in flask vertically at room temperature randomly (as showed previously in methods section). After irradiation of all cell samples completed, bring all the cell samples back to IHMRI lab and plate immediately.

### Clonogenic Assays Plating

#### **Materials**

#### Sterile materials

- Cell culture in T12.5cm<sup>2</sup> flasks
- c-DMEM medium (complete DMEM supplemented with 10% FBS and 1% PenStrep)
- PBS (without Ca<sup>2+</sup> and Mg<sup>2+</sup>)
- Trypsin-EDTA

- 1, 5, 10 and 25 mL pipettes
- BD Falcon™ Primaria petri dishes 100 × 15 mm (growth area = 58.95 cm<sup>2</sup>; vol. = 16 –17.5 mL)
- 50mL Falcon™ tubes
- P20-P1000 pipette tips

#### Other materials

- Pippetor, Eppendorf tubes, tube racks, hemocytometer, vortex, hand-counter, microscope, calculator, gloves, ethanol, wipes, etc. Access to bench centrifuge, water bath set at 37°C and incubator at 37°C (and 5% (v/v) CO<sub>2</sub>).

### **Procedure**

1. Pre-warmed the c-DMEM, PBS, and Trypsin-EDTA 37°C water bath (while waiting – labeled each petri dish).
2. Prepare for assay: Transfer 10ml of DMEM into each petri dish.
3. Remove the spent medium from the flask; wash the cell monolayer with 5 ml of PBS and discard; treated with 1ml of trypsin-EDTA; put in incubator at 37°C for 2 mins; check under microscope (cells should be detach now).
4. Resuspend with 1 ml of DMEM pipetting the cells up and down; transfer either 300 or 500  $\mu$ l of cells into 5 ml of DMEM for dilution in 50ml Falcon™ tubes; count with hemocytometer; Adjust the number of cells required (Table H.1)
5. Vortex the cells before pipetting the into petri dish.

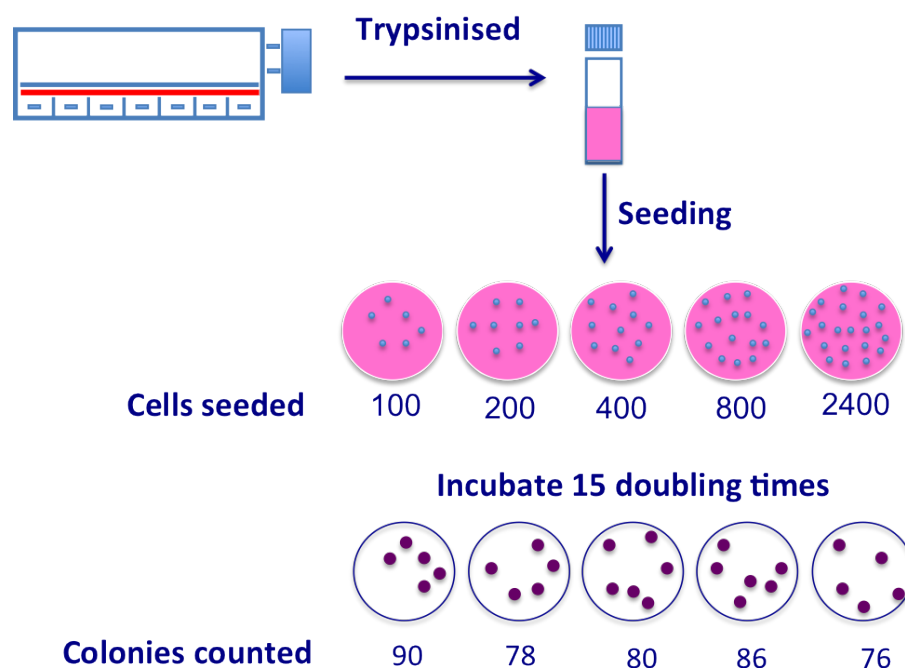


Figure H.1: Schematic diagram of cell culture technique (i.e clonogenic assay).

6. Pipette the amount of volume required according to the number of cells/petri dish (Table H.1) into each appropriate petri dish labeled (for each cell sample density in triplicates).
7. When finished (e.g. 6 petri dishes plated), shake the petri dish clockwise, anti-clockwise, up-down and right-left directions; wiped with ethanol; place in cell culture incubator at  $37^{\circ}\text{C}$  (with 5% (v/v)  $\text{CO}_2$ ); start again for plating the next flask.
8. After 15 doubling time (e.g 21 days for 9L) of culture, the cell colonies was fix and stain with mixture solution of 25% crystal violet (v/v) and 75% (v/v) ethanol.

A schematic diagram of the clonogenic assay procedure is illustrated in figure H.1.

Table H.1: A representative of summarised of X-rays irradiation of 9L cells for clonogenic assay. The number of cell densities used are different depend on the energy of X-rays and the cell line

<b>Irradiation of 9L cells with 10 MV X-rays (HDR and LDR)</b>						
Flask no.	Dose (Gy)	Dose rate	Petri dish no.	cells/petri dish	Cells/ $\mu$ L	$\mu$ L
1	Control 1-0	—	1–3	1500		
2	Control 2-0	—	4–6	1500		
3	1	HDR	7–9	2100		
4	2	HDR	10–12	2300		
5	3	HDR	13–15 16–18 19–21	2300 3400 4200		
6	5	HDR	22–24 25–27	4000 6000		
7	8	HDR	28–30 31–33 34–36	8000 12000 16000		
8	1	LDR	37–39	1500		
9	2	LDR	40–42 43–45	1500 2300		
10	3	LDR	46–48 49–51	2300 3400		
11	5	LDR	52–54 55–57	4500 6000		
12	8	LDR	58–60 61–63 64–66	12000 14000 16000		

HDR: High-Dose Rate (5 Gy/min); LDR: Low-Dose Rate (0.5 Gy/min).

## H.2 Chemotherapy Drugs Combination

### Cell Culture Preparation

1. Healthy, ~90% confluent cell culture in T12.5cm<sup>2</sup> flasks with vented cap  
– seeding at  $1 \times 10^5$  cells/flask, incubate for 2 days before adding the drugs.
2. After 3 days incubation with drugs, just prior the irradiation, fill the flask of cells with approximately 30ml of pre-warm HBSS buffer (w/Phenol) for the controls (no drugs). For the drugs-treated cells, the concentration being adjusted; sealed the lid with parafilm (not to cover the filter on top).
3. Placed vertically all the flasks in the container surround by silica gel; then in a carry bag.
4. Transport to POWH.

### Cells Irradiations

refer to previous section in Appendix F1 cells irradiations.

### Clonogenic Assays Plating

refer to previous section in Appendix F1 clonogenic assays plating.

Only the tables are different. A representative tables are shown below (Table H.2 and Table H.3).

Table H.2: A representative of summarised of kVp X-rays irradiation of 9L cells for clonogenic assay. The number of cell densities used are different depend on the energy of X-rays used

<b>Irradiation of 9L cells with 125 kVp X-rays (NO DRUGS)</b>						
Flask no.	Dose (Gy)	Dose rate	Petri dish no.	cells/petri dish	Cells/ $\mu$ L	$\mu$ L
1	Control 1-0	—	1–3	1500		
2	Control 2-0	—	4–6	1500		
3	1	—	7–9	2000		
4	2	—	10–12	2300		
5	3	—	13–15	2500		
			16–18	3400		
6	5	—	19–21	4000		
			22–24	6000		
7	8	—	25–27	8000		
			28–30	10000		
			31–33	12000		

Table H.3: A representative of summarised of kVp X-rays irradiation of 9L cells for clonogenic assay. The number of cell densities used are different depend on the energy of X-rays and single/combination of drugs used

<b>Irradiation of 9L cells with 125 kVp X-rays (0.01 <math>\mu</math>M MTX)</b>						
Flask no.	Dose (Gy)	Dose rate	Petri dish no.	cells/petri dish	Cells/ $\mu$ L	$\mu$ L
1	Control 1-0	—	1–3	4000		
2	Control 2-0	—	4–6	4000		
3	1	—	7–9	4000		
		—	10–12	8000		
		—	13–15	16000		
4	2	—	16–18	5000		
		—	19–21	10000		
		—	22–24	20000		
5	3	—	25–27	8000		
		—	28–30	16000		
		—	31–33	32000		
6	5	—	34–36	16000		
		—	37–39	32000		
		—	40–42	64000		
7	8	—	43–45	50000		
			46–48	100000		
			49–51	200000		

## H.3 Nanoparticles Combination

### Nanoparticle (NP) Samples Preparation

#### **Drying the NP samples**

- Crush the NP into powder and place on foil. Place in 70°C oven (including the glass vials) for no less than 2 hours, and then transfer the NP into the glass vial.

#### **Sterilising the NP samples**

- Placed the glass vial containing the NP, into a small beaker cover with foil and autoclave at 121°C.
- Upon completion, if doing the experiments on the same day, start immediately step 3. Otherwise, placed the glass vial into a drying oven (70°C) for couple hours (to avoid condensation) then it can be stored at room temperature (placing the vial inside a tube containing silica to avoid moisture re-absorption).

#### **Suspend the NP samples in PBS**

- Inside the BSC, transferred the sterile NP (e.g. 5 mg) into 50 mL Falcon<sup>TM</sup> tube and add 10 mL of sterile PBS (make up concentration of 500 µg/mL). To have the required concentration of 50 µg/mL of the NP, the volume of 1ml will need to be added into each flask.

#### **Sonicate the NP samples**

- Wipe the fine tip probe of the sonifier with 70% ethanol.
- Place the Falcon™ tube (containing the NP) into a beaker filled with water (make sure about 2 – 3 cm of the fine tip probe is immersed in the water without touching the side or the bottom of the beaker). Then, place the beaker into another bigger beaker or container surrounding with ice (to avoid the probe overheating the solution).
- Set-up the sonifier (depend on what sonifier to be used high or ultra-high): strength at level 7 (no higher than 7!); duty cycle control at constant; and timer for 5 minutes (repeat 6 times to give total duration of 30 mins).

### **Add the NP samples into cells**

- Immediately after the sanitation finish, inside the BSC, adds the volume of NP required (e.g. 1 ml) into flask prepared before (containing  $\sim 1 \times 10^6$  cells).

### **Cells Irradiations**

1. Healthy,  $\sim 90\%$  confluent cell culture in T12.5cm<sup>2</sup> flasks with no vented cap (with or without nanoparticles).
2. After 1 days incubation with nanoparticles, just prior the irradiation, fill the flask of cells with approximately 30 ml of pre-warm HBSS buffer (w/Phenol) for MV irradiations only (6 ml in total volume for kV irradiation; sealed the lid with parafilm).
3. Placed horizontally all the flasks in the container surround by silica gel; then in a carry bag.
4. Transport to POWH.



5. Irradiate the cells in flask horizontally at room temperature randomly (as showed previously in methods section). After irradiation of all cell samples completed, bring all the cell samples back to IHMRI lab and plate immediately.

Next procedure of clonogenic assay plating are exactly the same like in previous section in Appendix F1. Only the numbers of cells being plated are adjusted.

# Appendix I

## Flow Cytometric Detection

## I.1 Cell Cycle Analysis

### Materials

- Healthy, ~100% confluent cell culture in T12.5cm<sup>2</sup> flask
- c-DMEM medium (complete DMEM supplemented with 10% FBS and 1% PenStrep)
- PBS (without Ca<sup>2+</sup> and Mg<sup>2+</sup>)
- 0.05% trypsin-EDTA
- 50 mL Falcon™ tube

### Reagents and other Materials

- Ice-cold 70% Ethanol and PBS
- PI master mix (100 µg/mL RNase A, 40µg/mL PI, and PBS pH 7.4)
- Fluorescence-activated cell sorting (FACS) machine, FACS tube, pipetor, pippets and tips, Eppendorf tubes, tube racks, hemocytometer, vortex, hand-counter, microscope, calculator, gloves, ethanol, wipes, etc. Access to bench centrifuge, water bath set at 37°C and incubator at 37°C (and 5% (v/v) CO<sub>2</sub>).

### Procedure

1. Pre-warmed the DMEM, PBS and trypsin-EDTA at 37°C water bath.
2. Harvest the cells in the appropriate manner (refer to Appendix B of cell culture protocol).

3. Take a small aliquot of cells in Eppendorf tube; count with haemocytometer.
4. Transfer the amount of cells required ( $2 \times 10^4 - 1 \times 10^6$  cells/200  $\mu$ L) into 50 ml tubes.
5. Wash: Top up with cold PBS and centrifuge (4°C) at 1500rpm for 5mins. This step removes the serum.
6. Fixation: Aspirate the supernatant. Gently resuspend the cells pellet with 1 mL cold 70% Ethanol by adding drop-wise with a Pasteur pipette while vortexing (note: this is to prevent clustering of cells during the fixation). Leave the cells for at least 60 mins up to a week at  $-20^{\circ}\text{C}$ .
7. Remove ethanol by centrifuge (4°C) at 1500rpm for 5mins and wash twice with PBS (as in step 5). This step removes the fixative. Aspirate the supernatant.
8. Stain: Add 200  $\mu$ L PI master mix and incubate for 60 mins at  $37^{\circ}\text{C}$  protected from light (cover w/foil).
9. Put sample on ice. Run sample on FACS machine.
10. Analyse by flow cytometry: using BD LSR II FACSort flow cytometry collecting 10,000 events per sample. DNA content was then measured and the proportion of cells in  $G_0/G_1$ , S and  $G_2/M$  phases of cell cycle were calculated on the basis of histograms using FlowJo software.

Notes:

- Master stock for both PI and RNase is made of 1mg/ml. Aliquot can be stored for up to 2 months at  $4^{\circ}\text{C}$  or 2 years at  $-20^{\circ}\text{C}$  for PI (protected from light) and RNase for up to 6 months at  $4^{\circ}\text{C}$  or frozen at  $-20^{\circ}\text{C}$ .

- PI is very light sensitive. Do not keep it long at RT. Discard if it turns to dark red colour. It is also suspected as carcinogen. Take appropriate safety precautions when working with this dye.

## I.2 Immunocytochemical Protocol

### *Analysis of DNA content and BrUdR incorporation simultaneously*

#### Materials

- Cells culture in appropriate medium.
- FACS tube (or round bottom polystyrene tubes/centrifuge tube)
- 50 mL Falcon™ tubes
- Pipette tips and pipettes
- Centrifuge, vortex, Ice bucket, timer
- Fluorescence-activated cell sorting (FACS) machine

#### Reagents

- Phosphate Buffered Saline (PBS)
- 0.05% Trypsin-EDTA
- Cells and culture media (fresh complete DMEM)
- Ice-cold 70% Ethanol
- 4N Hydrochloric acid (HCl)
- Phosphate/citric acid buffer, pH 7.4
  - Mix 182 ml of 0.2 M  $\text{Na}_2\text{HPO}_4$  with 18 ml of 0.1 M citric acid. Check the pH, which should be 7.4. if not, adjust with 1 M HCl or 1 M NaOH. Store up to 2 months at 2°C to 6°C.
- Antibody diluting buffer (prepare fresh). PBS containing:

- 0.1% (v/v) Triton X-100
- 1% (w/v) bovine serum albumin (BSA)
- Propidium Iodide staining solution (protect from light)
  - 100  $\mu$ g PI
  - 1 mg RNase A
  - 10 mL PBS
- BrdU-Mouse monoclonal antibodies-clone MoBU-1 Alexa Fluor 488 conjugate (Invitrogen-B35139)

## **Procedure**

### ***Incorporate BrUdR***

1. Add BrUdR to the cell culture medium to obtain a final concentration of 10  $\mu$ M. Incubate for 3 days at 37°C.

### ***Harvest and fix the cells***

2. Harvest cells by Trypsin-EDTA. Transfer into centrifuge tubes.
3. Centrifuge the tube at 1500 rpm for 5mins at room temperature. Discard the supernatant.
4. Wash: Top up the cells with 10 mL PBS and mix well. Centrifuge at 1500 rpm for 5mins at room temperature. Discard the supernatant. This step removes the serum.
5. Dislodge the cells by shaking.

6. Fixation: Add 10 mL ice-cold 70% ethanol by adding drop-wise to the cell pellet while vortexing.
7. Store for a minimum of 4 hour (and for as long as several months) at  $-20^{\circ}\text{C}$ .

***Prepare the cells for labelling***

8. Remove the cell suspension from the freezer and centrifuge at 1500 rpm for 5mins at room temperature. Discard the supernatant.
9. Dislodge the cells by shaking.
10. Wash: Top up the cells with 10 mL PBS and mix well. Centrifuge at 1500 rpm for 5 mins at room temperature. Discard the supernatant. This step removes the fixative.
11. Dislodge the cells by shaking.
12. Denaturation: Add 2 mL of 4 M HCl to the cell pellet and mix well. Incubate for 20 minutes at room temperature.
13. Add 10 mL phosphate/citric acid buffer, mix well, and centrifuge at 1500 rpm for 5mins at room temperature. Discard the supernatant.
14. Dislodge the cells by shaking.
15. Add 10 mL antibody diluting buffer to the cell pellet, mix well, and centrifuge at 1500 rpm for 5mins at room temperature. Discard the supernatant.
16. Repeat the wash as described in step 13.
17. Dislodge the cells by shaking.



18. Resuspend the cells at a concentration of  $1 \times 10^7$  cells/mL in antibody diluting buffer.
19. Add 100  $\mu$ L of cells suspension to FACStube.

***Label the cells with antibody to detect BrUdR***

20. Stain: Add 5  $\mu$ L of BrdU-Mouse monoclonal antibodies-clone MoBU-1 Alexa Fluor 488 conjugate (Invitrogen-B35139) and incubate for 30 minutes, protected from light.
21. Wash: add 3 mL antibody diluting buffer into each tube, mix well, and centrifuge at 1500 rpm for 5 mins at room temperature. Discard the supernatant.

***Label with DNA staining dye***

22. Counter-stain: Add 0.5 ml of PI solution.
23. Incubate for 30 minutes at room temperature, protected from light.

***Set up flow cytometric data collection***

24. Acquire events on flow cytometer, collecting at 10,000 events. Collect fluorescence as follows:
  - Collect green fluorescence using 488-nm excitation for detection of Alexa Fluor 488 anti-BrUdR
  - Collect far red fluorescence using 488-nm excitation for PI detection

# Appendix J

## List of Abbreviations

Abbreviation	Meaning
$\alpha$	alpha
$\beta$	beta
3D-CRT	three-dimensional conformal external radiotherapy
9L	mouse gliosarcoma cell line
5-FU	5-fluorouracil
A	adenine
ATCC	American type culture collection
ATM	ataxia telangiectasia mutated
BBB	blood-brain barrier
BIM	biologically important molecule
Bi	bismuth
$\text{Bi}(\text{NO}_3)_3$	bismuth (III) nitrate penthydrate
$\text{Bi}_2\text{O}_3$	bismuth oxide
BrUdR	5-bromo-2'-deoxyuridine
BSA	bovine serum albumin
BT	brachytherapy
C	cytosine

---

Ca	calcium
Ce	cerium
CeO <sub>2</sub>	cerium oxide
CH <sub>2</sub> FH <sub>4</sub>	5,10-methylene tetrahydrofolate
CO <sub>2</sub>	carbondioxide
CMMB	Centre for Medical and Molecular Bioscience
CMRP	Centre for Medical Radiation Physics
CNS	central nervous system
D	dose
DHFR	dihydrofolate reductase
DCFH <sub>2</sub>	2',7'-Dichlorodihydrofluorescein
DCF	2',7'-Dichlorofluorescein
DCFD	2',7'-Dichlorofluorescein diacetate
DNA	deoxyribonucleic acid
DMEM	Dulbecco's modified eagles medium
DMSO	Dimethylsulfoxide
DSB	double-strand break
dTMP	deoxythymidine monophosphate
dUMP	deoxyuridine monophosphate
EBRT	external beam radiation therapies
EC	electron capture
ECACC	european collection of cell cultures
E <sub>q</sub>	equation
F	fluorine
FFF	flattening filter free
FH <sub>2</sub>	dihydrofolate
FH <sub>4</sub>	tetrahydrofolate
FACS	fluorescence-activated cell sorting

---

FCS	flow cytometer standard
FdUMP	2'-deoxyuridylic acid monophosphate
FSC	forward scatter
G <sub>0</sub>	phase where cells are quiescent
G <sub>1</sub>	gap 1; phase where cells are preparing for DNA synthesis
G <sub>2</sub>	gap 2; phase where cells are preparing for mitosis
G	guanine
H	hydrogen atom
H <sub>2</sub> O <sup>+</sup>	water ion
HBSS	Hanks' balanced salt solution
HCl	Hydrochloric acid
HDR	high-dose rate
HVL	half-value layer
HR	homologous recombination
I	iodine
ICRU	International Commission on Radiation Units and Measurements
ICSD	Inorganic Crystal Structure Database
IHMRI	Illawarra Health and Medical Research Institute
IMAT	intensity modulated arc therapy
IMRT	intensity modulation radiation therapy
IC	internal conversion
IR	ionising radiation
Ir	iridium
IRT	indirect radiation therapy
ISEM	Institute for Superconducting and Electronic Materials
IUdR	iododeoxyuridine
i.v	intravenously
kV	kilovolt

---

kVp	kilovolt peak
LAS AF	Leica application suite advanced fluorescence
LDR	low-dose rate
LET	linear energy transfer
LINAC	linear accelerator
LMDS	local multiply damaged sites
LQ	linear-quadratic
M-phase	mitosis, phase where cells divide into two daughter cells
MCF-7	human breast carcinoma
MDA-MB-231	human breast carcinoma
MDCK	madin darby canine kidney cell line
Mg	magnesium
MoBU-1	anti-BrUdR antibodies
MTX	methotrexate
MU	monitor unit
MV	megavoltage
NIGMS	National Institute of General Medical Science
NIST	National Institute of Standards and Technology
NHEJ	non-homologous end joining
NP	nanoparticle
NSP	nanosstructure particle
NADP <sup>+</sup>	nicotinamide adenine dinucleotide phosphate
NADPH	reduced form of NADP <sup>+</sup>
OH <sup>•</sup>	hydroxyl radical
P	phosphorus
PAT	photon activation therapy
PBS	phosphate buffer solution
PE	plating efficiency

---

PenStrep	penicillin/streptomycin
PER	protection enhancement ratio
PI	propidium iodide
PMT	photomultiplier tube
POWH	Prince of Wales hospital
RBE	relative biological effectiveness
RNA	ribose nucleic acid
ROS	reactive oxygen species
RT	radiation therapy
S-phase	phase where DNA synthesis occurs
SD	standard deviation
SER	sensitisation enhancement ratio
SF	surviving fraction
SSA	single-strand annealing
SSB	single-strand break
SSC	side scatter
SPF	S-phase fraction
SRT	stereotactic radiotherapy
T	thymine
Ta	tantalum
Ta <sub>2</sub> O <sub>5</sub>	tantalum pentoxide
TEM	transmission electron microscopy
TNT	targeted nano-therapies team
Trypin-EDTA	trypsin-ethylenediaminetetraacetic acid
TS	thymidilate synthetase
U-87MG	human glioblastoma cell line
UOW	University of Wollongong
VMAT	volumetric-modulated arc therapy

XRD	X-ray diffraction
Yt	yttrium
Z	atomic number

**Units used**

°C	degrees Celcius
g	gram
mg	milligram
cGy	centi Gray
Gy	Gray
keV	kilo-electron volt
cm	centimeter
nm	nanometer
J	Joule
kg	kilogram
M	Molar (concentration mole/L)
$\mu$	micro
min	minute
h	hour
l	litre
ml	millilitre
rpm	revolution per minute
v/v	concentration expressed as volume/volume ratio
w/v	concentration expressed as weight/volume ratio

# Appendix K

## List of Publications and Conference Abstracts

The following publications are associated with the work contained in this thesis.

1. A. Briggs, S. Corde, S. Oktaria, R. Brown, A. Rosenfeld, M. Lerch, K. Konstantinov, M. Tehei, Cerium oxide nanoparticles: influence of the high-Z component revealed on radioresistant 9L cell survival under X-ray irradiation. *Nanomedicine: Nanotechnology, Biology, and Medicine* (2013); 9:1098-1105.
2. R. Brown, M. Tehei, S. Oktaria, A. Briggs, C. Stewart, K. Konstantinov, A. Rosenfeld, S. Corde, M. Lerch, High-Z nanostructured ceramics in radiotherapy: first evidence of Ta<sub>2</sub>O<sub>5</sub>-induced dose enhancement on radioresistant cancer cells in an MV photon field. *Particle and Particle Systems Characterisation* (2013) (Accepted for publication).
3. C. Stewart, K. Konstantinov, M. McDonald, D. Cardillo, K. Bogusz, S. Oktaria, D. Shi, M. Lerch, T. Devers, S. Corde, A. Rosenfeld, M. Tehei. Engineering of bismuth oxide nanoparticles to induce differential biochemical activity in malignant and non-malignant cells. *Particle and*



Particle Systems Characterisation (2014) (Accepted for publication).

4. S. Oktaria, S. Corde, M. Lerch, A. Rosenfeld, M. Tehei. *In vitro* investigation of the dose-rate effect on the biological effectiveness of megavoltage X-ray radiation doses (2014) (submitted).
5. S. Oktaria, S. Corde, M. Lerch, A. Rosenfeld, M. Tehei, Radiation induced chemo-beta therapy I: *in vitro* demonstration of the radiosensitisation enhancement on a rat gliosarcoma cell line (2014) (submitted).
6. S. Oktaria, S. Corde, M. Lerch, A. Rosenfeld, M. Tehei, Radiation induced chemo-beta therapy II: *in vitro* demonstration of the radiosensitisation enhancement on a rat gliosarcoma cell line and influence of different X-ray energies (2014) (manuscript in preparation).

The following poster and oral presentations have been made at conferences connected with the work in this thesis.

1. The 14th International Congress of Radiation Research, Warsaw, Poland, 28th August – 1st September 2011, *In vitro* investigation of the dose-rate effect on the biological effectiveness of megavoltage X-ray radiation doses. (Poster)
2. The 25th Annual Chemistry & IPRI Conference, Fitzroy Falls Conference Centre, NSW, Australia 31st – 2nd November 2011, *In vitro* investigation of the dose-rate effect on the biological effectiveness of megavoltage X-ray radiation doses. (Oral)
3. Australian Institute of Physics (AIP) and Royal Australian Chemical Institute (RACI), Sydney, Australia, 10th November 2011, *In vitro* investigation of the dose-rate effect on the biological effectiveness of megavoltage X-ray radiation doses. (Poster)

- 
4. Prince of Wales Hospital Radiation Oncology Meeting, Randwick, NSW, Australia, 29th November 2011, *In vitro* investigation of the dose-rate effect on the biological effectiveness of megavoltage X-ray radiation doses. (Oral)
  5. The 6th Student Research Symposium of the ACT/NSW Branch of the Australian College of Physical Scientists and Engineering in Medicine (ACPSEM), University of Sydney, Australia, 1st December 2011, Investigation of the dose-rate effect on the biological effectiveness of 10 MV X-ray in cancer cell lines assessed by clonogenic assay. (Oral)
  6. Radiation 2012 Conference, AINSE, Lucas Heights, NSW, Australia, 15-17th February 2012, Investigation of the dose-rate effect on the biological effectiveness of 10 MV X-ray in cancer cell lines assessed by clonogenic assay. (Oral)
  7. Radiation 2012 Conference, AINSE, Lucas Heights, NSW, Australia, 15-17th February 2012, Enhanced radiosensitisation of resistant tumour cells to radiotherapy: a novel approach on biomodulation in DNA by chemotherapy drug. (Poster)
  8. 2012 Engineering and Physical Sciences in Medicine (EPSM) Conference, Gold Coast, QLD, Australia, 2-6th December 2012, Enhanced radiosensitisation of resistant tumour cells to radiotherapy: a novel approach on biomodulation in DNA by chemotherapy drug. (Poster)
  9. Mini- Micro- Nano- Dosimetry (MMND 2012) and International Prostate Cancer Treatment (IPCT 2012) International Workshop, The University of Wollongong, 6-9th December 2012, Enhanced radiosensitisation of resistant tumour cells to radiotherapy: a novel approach on biomodulation in DNA by chemotherapy drug. (Oral)

10. The 20th Australian Institute of Physics Congress and 37th Australian Conference on Optical Fibre Technology (ACOFT), The University of New South Wales, 9-13th December 2012, Enhanced radiosensitisation of resistant tumour cells to radiotherapy: a novel approach on biomodulation in DNA by chemotherapy drug. (Poster)

# References

- Adam, J., Elleaume, H., Joubert, A., Biston, M., Charvet, A., Balosso, J., Le Bas, J., Estève, F., 2003. Synchrotron radiation therapy of malignant brain glioma loaded with an iodinated contrast agent: first trial on rats bearing f98 gliomas. *International Journal of Radiation Oncology, Biology, Physics* 57 (5), 1413–1426.
- Adams, G. E., 1989. Temporal stages of radiation action: free radical processes. In: Steel, G. G., Adams, G. E., Horwich, A. (Eds.), *The Biological Basis of Radiotherapy*. Lippincott Williams & Wilkins, Philadelphia.
- Alkhatib, A., Watanabe, Y., Broadhurst, J., 2009. The local enhancement of radiation dose from photons of mev energies obtained by introducing materials of high atomic number into the treatment region. *Med Phys* 36, 3543–3548.
- Allard, E., Jarnet, D., Vessieres, A., Vinchon-Petit, S., Jaouen, G., Benoit, J. e. a., 2010. Local delivery of ferrociphenol lipid nanocapsules followed by external radiotherapy as a synergistic treatment against intracranial 9l glioma xenograft. *Pharm Res* 27, 5664.
- Anilkumar, M., Pasricha, R., Ravi, V., 2005. Synthesis of bismuth oxide nanoparticles by citrate gel method. *Ceramics International* 31 (6), 889–891.

- Aoyama, T., Kondo, T., Horikawa, M., Sugahara, T., 1964. Effect of halogenated pyrimidines on radiosensitivity of mouse strain 1 cells and their radioresistant variant. *J Radiat Res (Tokyo)* 29, 39–48.
- Attix, F. H., 2004. Introduction to radiological physics and radiation dosimetry. Wiley–VCH Verlag GmbH & Co. KGaA.
- Avendaño, C., Menéndez, J., 2008. Medicinal chemistry of anticancer drugs. Elsevier B.V, Oxford, UK.
- Bagshaw, M., Doggett, R., 1969. A clinical study of chemical radiosensitization. *Front. Radiation Ther. Onc.* 4, 164–173.
- Bagshaw, M., Doggett, R., Smith, K., Kaplan, H., Nelsen, T., 1967. Intra-arterial 5-bromodeoxyuridine and x-ray therapy. *Am J Roentgenol Radium Ther Nucl Med* 99, 886–894.
- Barendsen, G. W., 1991. Interpretation of the let dependence of radiation induced lethal and sublethal lesions in mammalian cells. In: K. H. Chadwick, G. M., Varma, M. N. (Eds.), *Biophysical modelling of radiation effects*. Adam Hilger, Bristol, United Kingdom.
- Barendsen, G. W., 1994. RBE-LET relationships for different types of lethal radiation damage in mammalian cells: comparison with dna dsb and an interpretation of differences in radiosensitivity. *International Journal of Radiation Biology* 66 (5), 433–436.
- Barth, R., 1998. Rat brain tumor models in experimental neuro-oncology: the 9L, c6, t9, f98, RG2 (D74), RT-2 and CNS-1 gliomas. *Journal of neuro-oncology* 36 (1), 91–9102.
- BD, B., 2000. Introduction to flow cytometry: a learning guide. Becton, Dickinson and Company, San Jose, CA.

- BD, B., 2007. BD LSR II user's guide. Becton, Dickinson and Company, San Jose, CA.
- Bencokova, Z., Pauron, L., Devic, C., Joubert, A., Gastaldo, J., Massart, C., Balosso, J., Foray, N., 2008. Molecular and cellular response of the most extensively used rodent glioma models to radiation and/or cisplatin. *Journal of Neuro-oncology* 86 (1), 13–21.
- Benedict, S., Cardinale, R., Wu, Q., Zwicker, R., Broaddus, W., Mohan, R., 2001. Intensity-modulated stereotactic radiosurgery using dynamic micro-multileaf collimation. *International Journal of Radiation Oncology, Biology, Physics* 50 (3), 751–758.
- Bernier, J., Hall, E., Giaccia, A., 2004. Radiation oncology: a century of achievements. *Nature Reviews. Cancer* 4 (9), 737–747.
- Berry, R., Andrews, J., 1962. Modification of the radiation effect on the reproductive capacity of tumor cells in vivo with pharmacological agents. *Radiation Research* 16, 82–88.
- Biade, S., Stobbe, C. C., Chapman, J. D., 1997. The intrinsic radiosensitivity of some human tumor cells throughout their cell cycles. *Radiation Research* 147, 416–421.
- Bischoff, P., Altmeyer, A., Dumont, F., 2009. Radiosensitising agents for the radiotherapy of cancer: advances in traditional and hypoxia targeted radiosensitisers. *Expert opinion on therapeutic patents* 19 (5), 643–662.
- Biston, M., Joubert, A., Adam, J., Elleaume, H., Bohic, S., Charvet, A., Estève, F., Foray, N., Balosso, J., 2004. Cure of fisher rats bearing radioreistant f98 glioma treated with cis-platinum and irradiated with monochromatic synchrotron x-rays. *Cancer Research* 64 (7), 2317–2323.

- Bobyk, L., Edouard, M., Deman, P., Rousseau, J., Adam, J., Ravanat, J., Estève, F., Balosso, J., Barth, R., Elleaume, H., 2012. Intracerebral delivery of carboplatin in combination with either 6 MV photons or monoenergetic synchrotron x-rays are equally efficacious for treatment of the f98 rat glioma. *Journal of Experimental & Clinical Cancer Research* 31 (78).
- Borek, C., Hall, E., 1973. Transformation of mammalian cells in vitro by low doses of x-rays. *Nature* 243, 450–453.
- Briggs, A., 2011. The implementation of cerium oxide nanoparticles for radiation protection using cancerous brain cells. Master's thesis, School of Engineering Physics.
- Briggs, A., Corde, S., Oktaria, S., Brown, R., Rosenfeld, A., Lerch, M., Konstantinov, K., Tehei, M., 2013. Cerium oxide nanoparticles: influence of the high-Z component revealed on radioresistant 9L cell survival under x-ray irradiation. *Nanomedicine: Nanotechnology, Biology, and Medicine* 9, 1098–1105.
- Brown, J., Goffinet, D., Cleaver, J., Kallman, R., 1971. Preferential radiosensitization of mouse sarcoma relative to normal skin by chronic intra-arterial infusion of halogenated pyrimidine analogs. *Journal of the National Cancer Institute* 47, 75–89.
- Brown, R., 2011. Investigation into the dose enhancing effects of tantalum pentoxide nanoparticles on cancerous brain cells under irradiation. Master's thesis, School of Engineering Physics.
- Brown, R., Tehei, M., Oktaria, S., Briggs, A., Stewart, C., Konstantinov, K., Rosenfeld, A., Corde, S., Lerch, M., 2013. High-z nanostructured ceramics in radiotherapy: first evidence of Ta<sub>2</sub>O<sub>5</sub> induced dose enhancement on radio

- resistant cancer cells in an X-ray photon field. Accepted for publication in *Particle and Particle Systems Characterisation*.
- Bryant, P. E., 1989. Mechanisms of repair of dna damage induced by ionising radiation. In: Steel, G., Adams, G., Horwich, A. (Eds.), *The Biological Basis of Radiotherapy*. Elsevier Science, Amsterdam, Netherlands.
- Buchegger, F., Florence, P., Dupertuis, Y., Delaloye, A., 2006. Auger radiation targeted into DNA: a therapy perspective. *European Journal of Nuclear Medicine and Molecular Imaging* 33 (11), 1352–1363.
- Butterworth, K., Coulter, J., Jain, S., Forker, J., McMahon, S., Schettino, G., Prise, K. M., Currell, F. J., Hirst, D., 2010. Evaluation of cytotoxicity and radiation enhancement using 1.9nm gold particles: Potential application for cancer therapy. *Nanotechnology* 21 (29), 295101–295709.
- Buzea, C., Pacheco, I., Robbie, K., 2007. Nanomaterials and nanoparticles: sources and toxicity. *BioInterphases* 2, 1771.
- Casarett, A., 1968. *Radiation Biology*. Englewood Cliffs, USA.
- Celardo, I., De Nicola, M., Mandoli, C., Pedersen, J., Traversa, E., Ghibelli, L., 2011.  $\text{Ce}^{3+}$  ions determine redox-dependent anti-apoptotic effect of cerium oxide nanoparticles. *ACS Nano* 5 (6), 4537–4549.
- Chadwick, K., Leenhouts, H., 1973. A molecular theory of cell survival. *Physics in medicine and biology* 18 (1), 78–87.
- Chadwick, K., Leenhouts, H., 1981. *The molecular theory of radiation biology*. Springer-Verlag, Berlin.Heidelberg.
- Charlton, D., Pomplun, E., J., B., 1987. Some consequences of the Auger effect: Fluorescence yield, charge potential, and energy imparted. *Radiation Research* 111, 553–564.



- Chen, X., Zhong, Z., Xu, Z., Chen, L., Wang, Y., 2010. 2',7'-dichlorofluorescein as fluorescent probe for reactive oxygen species measurement: forty years of application and controversy. *Free Radic Res* 44 (6), 587–604.
- Cheung, K., 2006. Intensity modulated radiotherapy: advantages, limitations and future developments. *Biomedical Imaging and Intervention Journal* 2 (1).
- Coderre, J., Glass, J., Fairchild, R., Micca, P., Fand, I., Joel, D., 1990. Selective delivery of boron by the melanin precursor analogue p-boronophenylalanine to tumors other than melanoma. *Cancer Research* 50, 138–141.
- Collis, S., Sangar, V., Tighe, A., Roberts, S., Clarke, N., Hendry, J., Margison, G., 2002. Development of a novel rapid assay to assess the fidelity of dna double-strand-break repair in human tumour cells. *Nucleic Acids Research* 30 (2), e1–e6.
- Collis, S., Schwaninger, J., Ntambi, A., Keller, T., Nelson, W., Dillehay, L., Deweese, T., 2004. Evasion of early cellular response mechanisms following low level radiation-induced DNA damage. *The Journal of Biological Chemistry* 279 (48), 49624–49632.
- Colon, J., Herrera, L., Smith, J., Patil, S., Komanski, C., Kupelian, P., et al, 2009. Protection from radiation-induced pneumonitis using cerium oxide nanoparticles. *Nanomedicine* 5, 225231.
- Corde, S., Balosso, J., Elleaume, H., Renier, M., Joubert, A., Biston, M., Adam, J., Charvet, A., Brochard, T., Le Bas, J., Estève, F., Foray, N., 2003. Synchrotron photoactivation of cisplatin elicits an extra number of DNA breaks that stimulate RAD51-mediated repair pathways. *Cancer Research* 63 (12), 3221–3227.

- Corde, S., Joubert, A., Adam, J., Charvet, A., Le Bas, J., Estève, F., El-leaume, H., Balosso, J., 2004. Synchrotron radiation-based experimental determination of the optimal energy for cell radiotoxicity enhancement following photoelectric effect on stable iodinated compounds. *British journal of cancer* 91 (3), 544–551.
- Curtis, S., 1986. Lethal and potentially lethal lesions induced by radiation—a unified repair model. *Radiation Research* 106 (2), 252–270.
- Dabrowska, M., Hendrikx, P., Skierski, J., Malinowska, M., Bertino, J., Rode, W., 2007. EGFP fluorescence as an indicator of cancer cells response to methotrexate. *European Journal of Pharmacology* 555 (2-3), 93–99.
- Deacon, J., Peckham, M. J., Steel, G. G., 1984. The radioresponsiveness of human tumours and the initial slope of the cell survival curve. *Radiotherapy and Oncology: Journal of the European Society for Therapeutic Radiology and Oncology* 2, 317–323.
- Dean, P., Hoffman, R., 2007. Overview of flow cytometry instrumentation. *Current protocols in cytometry / editorial board, J. Paul Robinson Chapter 1:1.1.1-1.1.8.*
- Delaney, G., Jacob, S., Featherstone, C., Barton, M., 2005. The role of radiotherapy in cancer treatment: estimating optimal utilization from a review of evidence-based clinical guidelines. *Cancer* 104, 1129–1137.
- Delilhas, N., Rich, M., Eidinoff, M., 1962. Radiosensitization of a mammalian cell line with 5-bromodeoxyuridine. *Radiation Research* 17, 479–491.
- DeNardo, S., Denardo, G., 2006. Targeted radionuclide therapy for solid tumors: an overview. *International Journal of Radiation Oncology, Biology, Physics* 66 (2 Suppl), S89–S95.

- Denekamp, J., 1986. Cell kinetics and radiation biology. *International Journal of Radiation Biology* 49, 357–380.
- Deschavanne, P. J., Fertil, B., et al., 1990. The relationship between radiosensitivity and repair of potentially lethal damage in human tumor cell lines with implications for radioresponsiveness. *Radiation Research* 122, 29–37.
- Deutsch, M., Rewers, A., Redgate, E., Fisher, E., Boggs, S., 1989. 5-iodo-2-deoxyuridine administered into the lateral cerebral ventricle as a radiosensitizer in the treatment of disseminated glioma. *J Natl Cancer Inst* 81, 1322–1325.
- Dewey, W., Humphrey, R., 1965. Increase in radiosensitivity to ionizing radiation related to replacement of thymidine in mammalian cells with 5-bromodeoxyuridine. *Radiation Research* 26, 538–553.
- Dewey, W., Sedita, B., Humphrey, R., 1966. Radiosensitization of x-chromosome of chinese hamster cells related to incorporation of 5-bromodeoxyuridine. *Science* 152, 519–521.
- Dewey, W., Stone, L., Miller, H., Gibrak, R., 1971. Radiosensitization with 5-bromodeoxyuridine of chinese hamster cells x-irradiated during different phases of the cell cycle. *Radiation Research* 47, 672–688.
- Djordjevic, B., Szybalski, W., 1960. Genetics of human cell lines. III. Incorporation of 5-bromo- and 5-iododeoxyuridine into the deoxyribonucleic acid of human cells and its effect on radiation sensitivity. *The Journal of Experimental Medicine* 112, 509–531.
- Dolbeare, F., Gratzner, H., Pallavicini, M., Gray, J., 1983. Flow cytometric measurement of total dna content and incorporated bromodeoxyuridine. *Proceedings of the National Academy of Sciences of the United States of America* 80, 5573–5577.

- Durand, R. E., Sutherland, R., 1973. Growth and radiation survival characteristics of v79-171b chinese hamster cells: a possible influence of intercellular contact. *Radiation Research* 56, 513–527.
- Erikson, R., Szybalski, W., 1961. Molecular radiobiology of human cell lines. i. comparative sensitivity to x-rays and ultraviolet light of cells containing halogen-substituted dna. *Biochem Biophys Res Commun* 4, 258–261.
- Erikson, R., Szybalski, W., 1963a. Molecular radiobiology of human cell lines. iii. radiation-sensitizing properties of 5-iododeoxyuridine. *Radiation Research* 20, 252–262.
- Erikson, R., Szybalski, W., 1963b. Molecular radiobiology of human cell lines. v. comparative radiosensitizing properties of 5-halodeoxycytidines and 5-halodeoxyuridines. *Radiation Research* 20, 252–262.
- Fairchild, R., Bond, V., 1984. Photon activation therapy. *Strahlentherapie* 160, 758–763.
- Fairchild, R., Brill, A., Ettinger, K., 1982. Radiation enhancement with iodinated deoxyuridine. *Invest Radiol* 17, 407–416.
- Feinendegen, L., 1990. 1989 douglas lea memorial lecture. the cell dose concept: potential application in radiation protection. *Physics in Medicine and Biology* 35 (5), 597–612.
- Felsenfeld, G., Groudine, M., 2003. Controlling the double helix. *Nature* 421 (6921), 448–453.
- Ferreira, B., Mavroidis, P., Adamus-Gorka, M., Svensson, R., Lind, B., 2008. The impact of different doseresponse parameters on biologically optimized IMRT in breast cancer. *Physics in Medicine and Biology* 53, 2733–2752.

- Fertil, B., Malaise, E., 1981. Inherent cellular radiosensitivity as a basic concept for human tumor radiotherapy. *Int J Radiat Oncol Biol Phys* 7 (5), 621–629.
- Fertil, B., Malaise, E., 1985. Intrinsic radiosensitivity of human cell lines is correlated with radioresponsiveness of human tumors: analysis of 101 published survival curves. *Int J Radiat Oncol Biol Phys* 11, 1699–1707.
- Fornace, A., Dobson, J. P., Kinsella, T., 1990. Enhancement of radiation damage in cellular DNA following unifilar substitution with iododeoxyuridine. *Int J Radiat Oncol Biol Phys* 18, 873–878.
- Fowler, J., Welsh, J., Howard, S., 2004. Loss of biological effect in prolonged fraction delivery. *Int J Radiat Oncol Biol Phys* 59 (1), 242–249.
- Franken, N., Rodermond, H., Stap, J., Haveman, J., van Bree, C., 2006. Clonogenic assay of cells *in vitro*. *Nature Protocols* 1 (5), 2315–2319.
- Franken, N. A., Oei, A., Kok, H., Rodermond, H., Sminia, P., Crezee, J., Stalpers, L., Barendsen, G., 2013. Cell survival and radiosensitisation: Modulation of the linear and quadratic parameters of the LQ model (review). *International Journal of Oncology* 42, 1501–1515.
- Friedberg, E. C., 2003. DNA damage and repair. *Nature* 421, 436–440.
- Fu, W., Dai, J., Hu, Y., Han, D., Song, Y., 2004. Delivery time comparison for intensity-modulated radiation therapy with/without flattening filter: a planning study. *Phys Med Biol* 49, 1535–1547.
- Fugiwara, Y., Mitani, M., Yasuike, S., Kurita, J., Kaji, T., 2005. An organobismuth compound that exhibits selective cytotoxicity to vascular endothelial cells *in vitro*. *Journal of Health Science* 51 (3), 333–340.

- Furre, T., Koritzinsky, M., Olsen, D. R., Pettersen, E., 1999. Inverse dose-rate effect due to pre-mitotic accumulation during continuous low dose-rate irradiation of cervix carcinoma cells. *Int J Radiat Biol* 75, 699–707.
- Furusawa, Y., H., Maezawa, H., Suzuki, K., 1991. Enhanced killing effect on 5-bromodeoxyuridine labelled bacteriophage t1 by monoenergetic synchrotron x-ray at the energy of bromine k-shell absorption edge. *Journal of Radiation Research* 32 (1), 1–12.
- Garberg, P., Ball, M., Borg, N., Cecchelli, R., Fenart, L., Hurst, R., Lindmark, T., Mabondzo, A., Nilsson, J. E., Raub, T., Stanimirovic, D., Terasaki, T., Oberg, J., Osterberg, T., 2005. *In vitro* models for the blood-brain barrier. *Toxicology In Vitro* 19, 299–334.
- Gaush, C., Hard, W., Smith, T., 1966. Characterization of an established line of canine kidney cells. *Proceedings of the Society for Experimental Biology and Medicine* 122, 931–935.
- Georgakilas, A. G., 2008. Processing of DNA damage clusters in human cells: current status of knowledge. *Molecular Biosystems* 4, 30–35.
- Ghulam Muhammad, A., Candolfi, M., King, G., Yagiz, K., Foulad, D., Mineharu, Y., Kroeger, K., Treuer, K., Nichols, W., Sanderson, N., Yang, J., Khayznikov, M., Van Rooijen, N., Lowenstein, P., Castro, M., 2009. Antiglioma immunological memory in response to conditional cytotoxic/immune-stimulatory gene therapy: humoral and cellular immunity lead to tumor regression. *Clinical cancer research : an official journal of the American Association for Cancer Research* 15 (19), 6113–6127.
- Gofman, J., 1990. The special interaction of ionizing radiation with living tissue. In: O'Connor, E. (Ed.), *Radiation-Induced Cancer from Low-Dose*

- Exposure: An Independent Analysis. Committee for Nuclear Responsibility, San Fransisco, California.
- Goodhead, D., 1994. Initial events in the cellular effects of ionizing radiations: clustered damage in DNA. *International Journal of Radiation Biology* 65 (1), 7–17.
- Goodhead, D., 1999. Mechanisms for the biological effectiveness of high-LET radiations. *Journal of Radiation Research* 40 Suppl, 1–13.
- Goodhead, D., 2006. Energy deposition stochastics and track structure: what about the target? *Radiation Protection Dosimetry* 122 (1-4), 3–15.
- Goodhead, D., Munson, R., Thacker, J., Cox, R., 1980. Mutation and inactivation of cultured mammalian cells exposed to beams of accelerated heavy ions. IV. biophysical interpretation. *International Journal of Radiation Biology and Related Studies in Physics, Chemistry, and Medicine* 37 (2), 135–167.
- Gratzner, H., 1982. Monoclonal antibody to 5-bromo- and 5-iododeoxyuridine: A new reagent for detection of dna replication. *Science* 218, 474–475.
- Gratzner, H., Leif, R., 1981. An immunofluorescence method for monitoring DNA synthesis by flow cytometry. *Cytometry* 1 (6), 385–393.
- Griffiths, T. D., Tolmach, L. J., 1975. Age-dependence of the X-ray-induced deficiency in DNA synthesis in HeLa S3 cells during generation 1. *Radiation Research* 63, 501–520.
- Group, I. M. R. T. C. W., 2001. Intensity-modulated radiotherapy: current status and issues of interest. *Int J Radiat Oncol Biol Phys* 51 (4), 880–914.
- Hahn, S., Maity, A., 2009. General principles of radiation and chemoradiation. *Retina (Philadelphia, Pa.)* 29 (6 Suppl), S30–S31.

- Hall, E., Giaccia, A., 2012. Radiobiology for the Radiologist. Lippincott Williams & Wilkins, Philadelphia.
- Hall, E. J., 1972. Radiation dose-rate: a factor of importance in radiobiology and radiotherapy. *Br J Radiol* 45, 81–97.
- Hatse, S., De Clercq, E., Balzarini, J., 1999. Role of antimetabolites of purine and pyrimidine nucleotide metabolism in tumor cell differentiation. *Biochemical Pharmacology* 58 (4), 539–555.
- Helleday, T., Lo, J., van Gent, D., Engelward, B., 2007. DNA double-strand break repair: from mechanistic understanding to cancer treatment. *DNA repair* 6 (7), 923–935.
- Henderson, S., Kimler, B., Morantz, R., 1981. Radiation therapy of 9L rat brain tumors. *Int J Radiat Oncol Biol Phys* 7 (4), 497–502.
- Hill, M., Stevens, D., Marsden, S., Allot, R., Turcu, I., Goodhead, D., 2002. Is the increased relative biological effectiveness of high LET particles due to spatial or temporal effects? characterization and OER in V79-4 cells. *Physics in Medicine and Biology* 47 (19), 3543–3555.
- Hirst, D., 2007. The importance of radiobiology to cancer therapy: current practice and future perspectives. *Clinical Oncology (Royal College of Radiologists (Great Britain))* 19 (6), 367–369.
- Hofer, K., 2000. Biophysical Aspects of Auger Processes. *Acta Oncologica* 39 (6), 651–657.
- Hombach, J., Bernkop-Schnurch, A., 2009. Chitosan solutions and particles: evaluation of their permeation enhancing potential on mdck cells used as blood brain barrier model. *International Journal of Pharmaceutics* 376, 104–109.



- Hoshino, T., Sano, K., 1969. Radiosensitization of malignant brain tumours with bromouridine (thymidine analogue). *Acta Radiol Ther Phys Biol* 8, 15–26.
- Howell, R., 2008. Auger processes in the 21st century. *International Journal of Radiation Biology* 84 (12), 959–975.
- Hueneekens, F. M., 1994. The methotrexate story: a paradigm for development of cancer chemotherapeutic agents. *Adv Enzyme Regul.* 34, 397–419.
- Iliakis, G., Kurtzman, S., 1989. Application of non-hypoxic cell sensitizers in radiobiology and radiotherapy: rationale and future prospects. *Int J Radiat Oncol Biol Phys* 16 (5), 1235–1241.
- Iwadata, Y., Fujimoto, S., 1997. Prediction of drug cytotoxicity in 9l rat brain tumor by using flow cytometry with a deoxyribonucle acid-binding dye. *Neurosurgery* 40 (4), 782–788.
- Jackson, D., Kinsella, T., Rowland, J., Wright, D., Katz, D., Main, D., Collins, J., Kornblith, P., Glatstein, E., 1987. Halogenated pyrimidines as radiosensitizers in the treatment of glioblastoma multiforme. *Am J Clin Oncol* 10, 437–443.
- Jain, S., Coulter, J., Hounsell, A., Butterworth, K., McMahon, S., Hyland, W., Muir, M., Dickson, G., Prise, K., Currell, F., O’Sullivan, J., Hirst, D., 2011. Cell-specific radiosensitization by gold nanoparticles at megavoltage radiation energies. *Int J Radiat Oncol Biol Phys* 79 (2), 531–539.
- Jensen, R., 1998. Growth factor-mediated angiogenesis in the malignant progression of glial tumors: a review. *Surgical Neurology* 49 (2), 189–95; discussion 196.

- John, H., Cunningham, J., 1983. The physics of radiology, 4th edition. Charles C Thomas, Springfield IL.
- Kamen, B., Drachtman, R., 2000. The use of methotrexate in the treatment of childhood malignancies. In: Cronstein, B., Bertino, J. (Eds.), *Methotrexate. Milestones in Drug Therapy*. Birkhuser Basel, pp. 49–63.
- Kao, J., Rosenstein, B., Peters, S., Milano, M., Kron, S. J., 2005. Cellular response to DNA damage. *Ann N Y Acad Sci* 1066, 243–258.
- Kaplan, H., Smith, K., Tomlin, P., 1962. Effect of halogenated pyrimidines on radiosensitivity of *E. coli*. *Radiation Research* 16, 98–113.
- Karnas, S., Yu, E., R, M., Battista, J., 1999. Optimal photon energies for IUdR K-edge radiosensitization with filtered x-ray and radioisotope sources. *Physics in Medicine and Biology* 44 (10), 2537–2549.
- Karp, G., 2005. *Cell and molecular biology: concepts and experiments*, 4th Edition. John Wiley & Sons, Hoboken, NJ, United States of America.
- Kassis, A., 2003. Cancer therapy with auger electrons: are we almost there? *Journal of Nuclear Medicine: Official Publication, Society of Nuclear Medicine* 44 (9), 1479–1481.
- Kassis, A., Kirichian, A., Wang, K., Semnani, E., Adelstein, S., 2004. Therapeutic potential of 5-[125I]iodo-2'-deoxyuridine and methotrexate in the treatment of advanced neoplastic meningitis. *International Journal of Radiation Biology* 80 (11-12), 941–946.
- Khan, F. M., 2010. *The physics of radiation therapy* 4th ed. Lippincott Williams & Wilkins.
- Khanna, K., Jackson, S., 2001. DNA double-strand breaks: signaling, repair and the cancer connection. *Nature Genetics* 27 (3), 247–254.

- Kiefer, J., 1990. Biological radiation effects. Springer-Verlag, Berlin, Heidelberg.
- Kimler, B., 1994. The 9L rat brain tumor model for pre-clinical investigation of radiation-chemotherapy interactions. *Journal of Neuro-oncology* 20 (2), 103–109.
- Kimler, B. F., Henderson, S. D., 1982. Cyclic responses of cultured 9l cells to radiation. *Radiation Research* 91, 155–168.
- Knox, S. J., Sutherland, W., Goris, M. L., 1993. Correlation of tumor sensitivity to low-dose-rate irradiation with G2/M-phase block and other radiobiological parameters. *Radiation Research* 135, 24–31.
- Kobayashi, K., Frohlich, H., Usami, N., Takakura, K., Le Sech, C., 2002. Enhancement of x-ray-induced breaks in DNA bound to molecules containing platinum: a possible application to hadrontherapy. *Radiation Research* 157, 32–37.
- Kobayashi, K., Usami, N., Porcel, E., Lacombe, S., Le Sech, C., 2010. Enhancement of radiation effect by heavy elements. *Mutation Research* 704 (1-3), 123–131.
- Kominami, H., Miyakawa, M., ya Murakami, S., Yasuda, T., Kohno, M., ichi Onoue, S., Kera, Y., Ohtani, B., 2001. Solvothermal synthesis of tantalum(V) oxide nanoparticles and their photocatalytic activities in aqueous suspension systems. *Physical Chemistry Chemical Physics* 3, 2697–2703.
- Kragl, G., af Wetterstedt, S., Knäusl, B., Lind, M., McCavana, P., Knöös, T., McClean, B., Georg, D., 2009. Dosimetric characteristics of 6 and 10MV unflattened photon beams. *Radiotherapy and Oncology : Journal of the European Society for Therapeutic Radiology and Oncology* 93 (1), 141–146.

- Krex, D., Klink, B., Hartmann, C., von, A., Pietsch, T., 2007. Long-term survival with glioblastoma multiforme. *Brain: A Journal of Neurology* 130 (Pt10), 2596–2606.
- Kriss, J., Maruyama, Y., Tung, L., Bond, S., Révész, L., 1963. The fate of 5-bromodeoxyuridine, 5-bromodeoxycytidine, and 5-iododeoxycytidine in man. *Cancer Research* 23, 260–268.
- Kriss, J., Revesz, L., 1962. The distribution and fate of bromodeoxyuridine and bromodeoxycytidine in the mouse and rat. *Cancer Research* 22, 254–265.
- Lajtha, L., Oliver, R., 1961. Some radiobiological considerations in radiotherapy. *Br J Radiol* 34, 252–257.
- Lambert, J., Midolo, P., 1997. The action of bismuth in the treatment of *Helicobacter pylori* infection. *Aliment Pharmacol Ther* 11 (suppl.1), 27–33.
- Larson, D., Bodell, W., et al, 1989. Auger electron contribution to bromodeoxyuridine cellular radiosensitization. *Int J Radiat Oncol Biol Phys* 16 (1), 171–176.
- Laster, B., Dixon, D., Novick, S., Feldman, J., Seror, V., Goldbart, Z., Kalef-Ezra, J., 2009. Photon activation therapy and brachytherapy. *Brachytherapy* 8, 324–330.
- Laster, B., Popenoe, E., Wielopolski, L., Commerford, S., Gahbauer, R., Goodman, J., Meek, A., Fairchild, R., 1990. Analysis of 5-iodo-2'-deoxyuridine incorporation in murine melanoma for photon activation therapy. *Radiotherapy and Oncology : Journal of the European Society for Therapeutic Radiology and Oncology* 19 (2), 169–178.
- Laster, B. H., Thomlinson, W., et al, 1993. Photon activation of iododeoxyuri-

- dine: biological efficacy of auger electrons. *Radiation Research* 133 (2), 219–224.
- Lawrence, C. W., 1971. *Cellular Radiobiology*. Edward Arnold Limited, London.
- Lawrence, T., Davis, M., Maybaum, J., Stetson, P., Ensminger, W., 1990a. The dependence of halogenated pyrimidine incorporation and radiosensitization on the duration of drug exposure. *Int J Radiat Oncol Biol Phys* 18, 1393–1398.
- Lawrence, T., Davis, M., Maybaum, J., Stetson, P., Ensminger, W., 1990b. The effect of single versus double-strand substitution on halogenated pyrimidine-induced radiosensitization and DNA strand breakage in human tumor cells. *Radiation Research* 123, 192–198.
- Le Sech, C., Takakura, K., C, S., Frohlich, H., Charlier, M., Usami, N., Kobayashi, K., 2000. Strand break induction by photoabsorption in DNA-bound molecules. *Radiation Research* 153 (4), 454–458.
- Le Sech, C., Takakura, K., C, S., Frohlich, H., Charlier, M., Usami, N., Kobayashi, K., 2001. Enhanced strand break induction of DNA by resonant metal-innershell photoabsorption. *Canadian Journal of Physiology and Pharmacology* 79 (2), 196–200.
- Leith, J., Cook, S., Chougule, P., Calabresi, P., Wahlberg, L., Lindquist, C., Epstein, M., 1994. Intrinsic and extrinsic characteristics of human tumors relevant to radiosurgery: comparative cellular radiosensitivity and hypoxic percentages. *Acta Neurochirurgica. Supplement* 62, 18–27.
- Lin, W., Huang, Y., Zhou, X., Ma, Y., 2006. Toxicity of cerium oxide nanoparticles in human lung cancer cells. *Int J Toxicol* 25, 451–456.

- Ling, C. C., Guo, M., Chen, C. H., Deloherey, T., 1995. Radiation-induced apoptosis: effects of cell age and dose fractionation. *Cancer Research* 55, 5207–5212.
- Locke, J., Stutchbury, T., Vine, K., Gamble, A., Clingan, P., Bremmer, J., Ranson, M., 2009. Development and assessment of novel all-in-one parenteral formulations with integrated anticoagulant properties for the concomitant delivery of 5-fluorouracil and calcium folinate. *Anti-Cancer Drugs* 20, 822–831.
- Lodge, M., Madelon, P., Stirk, L., Munro, A., De Ruyscher, D., Jefferson, T., 2007. A systematic literature review of the clinical and cost-effectiveness of hadron therapy in cancer. *Radiotherapy and Oncology : Journal of the European Society for Therapeutic Radiology and Oncology* 83 (2), 110–122.
- Lohse, I., Lang, S., Hrbacek, J., Scheidegger, S., Bodis, S., Macedo, N., Feng, J., Lütolf, U., Zaugg, K., 2011. Effect of high dose per pulse flattening filter-free beams on cancer cell survival. *Radiotherapy and Oncology : journal of the European Society for Therapeutic Radiology and Oncology* 101 (1), 226–232.
- Macleod, K. G., Langdon, S., 2004. Essential techniques of cancer cell culture. In: Langdon, S. P. (Ed.), *Cancer Cell Culture*. Vol. 88 of *Methods in Molecular Medicine*. Humana Press, pp. 17–29.
- Madero-Visbal, R., Alvarado, B., Colon, J., Baker, C., Wason, M., Das, S., et al, 2012. Harnessing nanoparticles to improve toxicity after head and neck radiation. *Nanomedicine* 8 (7), 1223–1231.
- Madin, S., Darby, J. N., 1958. Established kidney cell lines of normal adult bovine and ovine origin. *Proceedings of the Society for Experimental Biology and Medicine* 98 (3), 574–576.

- Malaise, E., Fertil, B., Deschavanne, P., Chavaudra, N., Brock, W., 1987. Initial slope of radiation survival curves is characteristic of the origin of primary and established cultures of human tumor cells and fibroblasts. *Radiation Research* 111 (2), 319–333.
- Marples, B., 2004. Is low-dose hyper-radiosensitivity a measure of G2-phase cell radiosensitivity? *Cancer Metastasis Rev* 23, 197–207.
- Matthews, J., Meeker, B., Chapman, J., 1989. Response of human tumor cell lines *in vitro* to fractionated irradiation. *Int J Radiat Oncol Biol Phys* 16 (1), 133–138.
- McGinn, C., Kinsella, T., 1993. The clinical rationale for S-phase radiosensitization in human tumors. *Current Problems in Cancer* 17 (5), 273–321.
- McMahon, S., Hyland, W., Muir, M., Coulter, J., Jain, S., Butterworth, K., et al, 2011. Biological consequences of nanoscale energy deposition near irradiated heavy atom nanoparticles. *Sci Rep* 1, 1–9.
- McMahon, S., Mendenhall, M., Jain, S., Currell, F., 2008. Radiotherapy in the presence of contrast agents: a general figure of merit and its application to gold nanoparticles. *Phys Med Bio* 53, 5635–5651.
- Mendonca, M. S., Rodriguez, A., Alpen, E., 1989. Quiescence in 9L cells and correlation with radiosensitivity and PLD repair. *Radiation Research* 117, 433–447.
- Metcalf, P., Kron, T., Hoban, P., 2007. The physics of radiotherapy x-rays and electrons. Medical Physics Publishing, Madison, Wisconsin.
- Michalik, V., 1992. Model of DNA damage induced by radiations of various qualities. *International Journal of Radiation Biology* 62 (1), 9–20.

- Mitchell, J. B., Bedford, J. S., 1977. Dose-rate effects in synchronous mammalian cells in culture. ii. a comparison of the life cycle of HeLa cells during continuous irradiation or multiple-dose fractionation. *Radiation Research* 71, 547–560.
- Mitchell, J. B., Bedford, J. S., Bailey, S. M., 1979. Dose-rate effects in plateau-phase cultures of s3 Hela and V79 cells. *Radiation Research* 79, 552–567.
- Mitchell, J. B., Russo, A., Kuppusami, P., Krishna, M. C., 2000. Radiation, radicals, and images. *Ann N Y Acad Sci* 899 (1), 28–43.
- Moiseenko, V., Duzenli, C., Durand, R., 2007. *In vitro* study of cell survival following dynamic MLC intensity-modulated radiation therapy dose delivery. *Medical Physics* 34 (4), 1514–1520.
- Moreno-Vega, A., Gómez-Quintero, T., Nuñez-Anita, R., Acosta-Torres, L., no, V. C., 2012. Polymeric and ceramic nanoparticles in biomedical applications. *Journal of Nanotechnology* 2012.
- Mu, X., Lofroth, P., Karlsson, M., Zackrisson, B., 2003. The effect of fraction time in intensity modulated radiotherapy: theoretical and experimental evaluation of an optimisation problem. *Radiother Oncol* 68, 181–187.
- Mundt, A., Roeske, J., Weichselbaum, R., 2000. Physical and biologic basis of radiation oncology. In: Bast, R. J., Kufe, D., Pollock, R. (Eds.), *Holland-Frei Cancer Medicine*. 5th edition. BC Decker, Hamilton.
- Munshi, A., Hobbs, M., Meyn, R., 2005. Clonogenic cell survival assay. *Methods in Molecular Medicine* 110, 21–28.
- Nagashima, T., Hoshino, T., 1985. Rapid detection of S-phase cells by anti-bromodeoxyuridine monoclonal antibody in 9L brain tumor cells *in vitro* and *in situ*. *Acta Neuropathol* 66, 12–17.



- Nawroth, T., Glube, N., Peters, T., Buch, P., Buch, K., Langguth, P., Pairet, B., Decker, H., Bickes-Kelleher, D., Vaupel, P., Konerding, M., Schmidberger, H., Alexiou, C., Gähler, R., Lauss, B., Jentschel, M., May, R., Corde, S., Boesecke, P., Bravin, A., LeDuc, G., 2008. Nano-IRT: indirect radiation therapy development with target nanoparticles. <http://www.mpsd.de/irt/IRT.html>.
- Nelson, D. L., Cox, M., 2005. *Lehninger principles of biochemistry*. W.H. Freeman and Company, New York.
- Nias, A., 1990. *An introduction to radiobiology*. John Wiley & Sons, England.
- Nikjoo, H., Uehara, S., Wilson, W., Hoshi, M., Goodhead, D., 1998. Track structure in radiation biology: theory and applications. *International Journal of Radiation Biology* 73 (4), 355–364.
- Njeh, C., Saunders, M., Langton, C., 2012. Accelerated partial breast irradiation using external beam conformal radiation therapy: a review. *Critical Reviews in Oncology/Hematology* 81 (1), 1–20.
- Norbury, C. J., Hicson, I., 2001. Cellular responses to DNA damage. *Annu. Rev. Pharmacol. Toxicol* 41, 367–401.
- of General Medical Science, N.-N. I., 2006. *The new genetics*. U.S: National Institute of General Medical Science.
- Olive, P., 1998. The role of DNA single- and double-strand breaks in cell killing by ionizing radiation. *Radiation Research* 150, S42–S51.
- on Radiation Units, I. C., Measurements, I., 1979. *Quantitative concepts and dosimetry in radiobiology*. International Commission on Radiation Units and Measurements, Washington.

- Ormerod, M., 1999. Flow cytometry: Second Edition. Springer-Verlag, New York.
- Patil, M., Deshpande, V. V., Dhage, S., Ravi, V., 2005. Synthesis of bismuth oxide nanoparticles at 100°C. *Materials Letters* 59, 2523–2525.
- Patrick, G. L., 2005. An introduction to medicinal chemistry, third edition. Oxford University Press Inc., New York.
- Patterson, A., 1939. The scherrer formula for x-ray particle size determination. *Phys. Rev.* 56 (10), 978–982.
- Petti, P., Lennox, A., 1994. Hadronic radiotherapy. *Annu. Rev. Nucl. Part. Sci* 44, 155–197.
- Phillips, T., Bodell, W., Uhl, V., Ross, G., Rasmussen, J., Mitchell, J., 1989. Correlation of exposure time, concentration and incorporation of IdUrd in V-79 cells with radiation response. *Int J Radiat Oncol Biol Phys* 16, 1251–1255.
- Phillips, T., Scott, C., Leibel, S., Rotman, M., Weigensberg, I., 1995. Results of a randomized comparison of radiotherapy and bromodeoxyuridine with radiotherapy alone for brain metastases: report of RTOG trial 89-05. *Int J Radiat Oncol Biol Phys* 33, 339–348.
- Pinedo, H., Peters, G., 1988. Fluorouracil: biochemistry and pharmacology. *J Clin Oncol* 6 (10), 1653–1664.
- Plumb, J., 2004. Cell sensitivity assays: clonogenic assay. *Methods in Molecular Medicine* 88, 159–164.
- Poludniowski, G., Landry, G., F, D., Evans, P., Verhaegen, F., 2009. SpekCalc: a program to calculate photon spectra from tungsten anode x-ray tubes. *Physics in Medicine and Biology* 54 (19), N433–N438.

- Pontén, J., Macintyre, E., 1968. Long term culture of normal and neoplastic human glia. *Acta Pathol Microbiol Scand* 74 (4), 465–486.
- Powsner, R. A., Powsner, E. R., 2006. Chapter 11: Radiation biology. In: Powsner, R. A., Powsner, E. R. (Eds.), *Essential Nuclear Medicine Physics*.
- Prasad, K. N., 1995. *Handbook of radiobiology* second edition. CRC Press, Boca Raton, Florida.
- Puck, T., Marcus, P., 1956. Action of x-rays on mammalian cells. *The Journal of Experimental Medicine* 103 (5), 653–666.
- Radbruch, A., 1992. Immunofluorescence: Basic consideration. In: Radbruch, A. (Ed.), *Flow cytometry and cell sorting*. Springer Laboratory, Berlin Heidelberg.
- Radcliff, G., Jaroszeski, M. J., 1997. Basics of flow cytometry. In: Jaroszeski, M. J., Heller, R. (Eds.), *Methods in Molecular Biology*. Humana Press Inc, Totowa, NJ.
- Radford, I. R., 1986. Evidence for a general relationship between the induced level of dna double-strand breakage and cell killing after x-irradiation of mammalian cells. *International Journal of Radiation Biology* 49 (4), 611–620.
- Rafehi, H., Orlowski, C., Georgiadis, G., Ververis, K., Assam, E., Karagiannis, T., 2011. Clonogenic assay: adherent cells. *Journal of Visualized Experiments : JoVE* 49.
- Ramsay, J., Ward, R., Bleehen, N. M., 1992. Radiosensitivity testing of human malignant gliomas. *Int J Radiat Oncol Biol Phys* 24, 675–680.
- Rebischung, C., Hoffmann, D., Stefani, L., Desruet, M., Wang, K., Adelstein, S., Artignan, X., Vincent, F., Gauchez, A., Zhang, H., Fagret, D., Vuillez,

- J., Kassis, A., Balosso, J., 2008. First human treatment of resistant neoplastic meningitis by intrathecal administration of MTX plus (125)IUdR. *International Journal of Radiation Biology* 84 (12), 1123–1129.
- Reft, C., Alecu, R., Dad, I., Gerbi, B., Keall, P., Lief, E., Mijnheer, B., Papanikolaou, N., Sibata, C., Dyk, J., 2003. Dosimetric consideration for patients with HIP prostheses undergoing pelvic irradiation. report of the AAPM radiation therapy committee task group 63. *Am. Assoc. Phys. Med.* 30 (6), 1162–1182.
- Robar, J., Riccio, S., Martin, M., 2002. Tumour dose enhancement using modified megavoltage photon beams and contrast media. *Phys Med Bio* 47, 24332449.
- Rothkamm, K., Kruger, I., Thompson, L., Lobrich, M., 2003. Pathways of dna double-strand break repair during the mammalian cell cycle. *Molecular and Cellular Biology* 23 (16), 5706–5715.
- Rousseau, J., Adam, J., Deman, P., Wu, T., Jean, G., Gouget, B., Barth, R., Estève, F., Elleaume, H., 2009a. Intracerebral delivery of 5-iodo-2'-deoxyuridine in combination with synchrotron stereotactic radiation for the therapy of the f98 glioma. *Journal of synchrotron radiation* 16 (Pt 4), 573–581.
- Rousseau, J., Barth, R., Fernandez, M., Adam, J., Balosso, J., Estève, F., Elleaume, H., 2010. Efficacy of intracerebral delivery of cisplatin in combination with photon irradiation for treatment of brain tumors. *Journal of Neuro-oncology* 98 (3), 287–295.
- Rousseau, J., Barth, R., Moeschberger, M., Elleaume, H., 2009b. Efficacy of intracerebral delivery of carboplatin in combination with photon irradiation

- for treatment of f98 glioma-bearing rats. *Int J Radiat Oncol Biol Phys* 73 (2), 530–536.
- Rowley, R., Leeper, D. B., 1985. Cell cycle age dependence for radiation-induced G2 arrest: evidence for time-dependent repair. *Radiation Research* 103, 326–336.
- Russell, P. J., 2006. *iGenetics: a molecular approach*. Pearson Benjamin Cummings, San Fransisco, United States of America.
- Rzagalinski, B., Meehan, K., Davis, R., Xu, Y., Miles, W., Cohen, C., 2006. Radical nanomedicine. *Nanomedicine* 1, 399412.
- Rzagalinski, B.A.and Bailey, D., Chow, W., Kuiry, S., Patil, S., Merchant, S., 2003. Cerium oxide nanoparticles increase the lifespan of cultured brain cells and protect against free radical and mechanical trauma. *FASEB J* 17, A606.
- Sager, T., Porter, D., Robinson, V., Lindsley, W., Schwegler-Berry, D., Castanova, V., 2007. Improved method to disperse nanoparticles for *in vitro* and *in vivo* investigation of toxicity. *Nanotoxicology* 1, 118129.
- Sancar, A., Laura, L., Keziban, U., Linn, S., 2004. Molecular mechanisms of mammalian DNA repair and the DNA damage checkpoints. *Annual review of biochemistry* 73, 39–85.
- Sano, K., Hoshino, T., Nagai, M., 1968. Radiosensitization of brain tumor cells with a thymidine analogue (bromouridine). *J Neurosurg* 28, 530–538.
- Sano, K., Sato, F., Hoshino, T., Nagai, M., 1965. Experimental and clinical studies of radiosensitizers in brain tumors, with special reference to budr-antimetabolite continuous regional infusion-radiation therapy (BAR therapy). *Neurol Med Chir (Tokyo)* 7, 51–72.
- Saphiro, H. M., 1988. *Practical flow cytometry*. Alan R. Liss, Inc., New York.

- Sastry, K. S. R., 1992. Biological effects of the auger emitter iodine-125: a review. report no 1 of aapm nuclear medicine task group no.6a. *Med. Phys.* 19 (6), 1361–1370.
- Seiwert, T., Salama, J., Vokes, E., 2007. The concurrent chemoradiation paradigm—general principles. *Nature clinical practice. Oncology* 4 (2), 86–8100.
- Sen, S., Erba, E., D’Incalci, M., 1990. Synchronisation of cancer cell lines of human origin using methotrexate. *Cytometry* 11, 595–602.
- Shewach, D., Lawrence, T., 2007. Antimetabolite radiosensitizers. *J Clin Oncol* 25 (26), 4043–4050.
- Shinohara, K., Ohara, H., et al, 1985. Enhanced killing of HeLa cells pre-labeled with 5-bromodeoxyuridine by monochromatic synchrotron radiation at 0.9 a: an evidence for Auger enhancement in mammalian cells. *Journal of Radiation Research (Tokyo)* 26 (3), 334–338.
- Simons, K., Virta, H., 2006. Chapter 15 growing madin-darby canine kidney cells for studying epithelial cell biology. In: Celis, J. (Ed.), *Cell Biology (Third Edition)*. Elsevier Inc., pp. 127–131.
- Siochi, R., 1999. Minimizing static intensity modulation delivery time using an intensity solid paradigm. *Int J Radiat Oncol Biol Phys* 43 (3), 671–680.
- Siu, L., Moore, M., 2005. Pharmacology of anticancer drugs. In: Tannock, I., Hill, R., Bristow, R., Harrington, L. (Eds.), *The Basic Science of Oncology*. 4th ed. McGraw-Hill, New York, NY, pp. 322–348.
- Sohn, T., Yeo, C., Cameron, J., Koniaris, L., 2000. Resected adenocarcinoma of the pancreas616 patients: results, outcomes, and prognostic indicators. *Journal of Gastrointestinal Surgery* 4 (6), 567–1579.

- Spittle, M., 1978. Methotrexate and radiation. *Int J Radiation Oncology Biol Phys* 4, 103–107.
- Stathakis, S., Esquivel, C., Gutierrez, A., Buckey, C., Papanikolaou, N., 2009. Treatment planning and delivery of IMRT using 6 and 18MV photon beams without flattening filter. *Applied Radiation and Isotopes : Including Data, Instrumentation and Methods for Use in Agriculture, Industry and Medicine* 67 (9), 1629–1637.
- Steel, G., Peckham, M., 1979. Exploitable mechanisms in combined radiotherapy-chemotherapy: the concept of additivity. *Int J Radiation Oncology Biol Phys* 5, 85–91.
- Steel, G. G., 1989. Survival of clonogenic cells: cell-survival curves. In: Steel, G., Adams, G., Horwich, A. (Eds.), *The Biological Basis of Radiotherapy*. Elsevier Science, Amsterdam, Netherlands.
- Stewart, C., 2012. Application of advanced high-z nanoceramics for radiation assisted cancer therapy. NANO301 Final report.
- Stewart, C., Konstantinov, K., McDonald, M., Cardillo, D., Bogusz, K., Oktaria, S., Shi, D., Lerch, M., Devers, T., Corde, S., Rosenfeld, A., Tehei, M., 2014. Engineering of bismuth oxide nanoparticles to induce differential biochemical activity in malignant and non-malignant cells. Accepted for publication in *Particle and Particle Systems Characterisation*.
- Stutchbury, T., Vine, K., Locke, J., Chrisp, J., 2010. Preclinical evaluation of novel all-in-one formulations of 5-Fluorouracil and folinic acid with reduced toxicity Profiles-Supplementary data. In Press.
- Suntharalingam, N., Podgorsak, E. B., Hendry, J. H., 2005. Basic radiobiology. *Radiation Oncology Physics: A Handbook for Teachers and Students*, 485–504.

- Sutherland, B., Bennett, P., Sidorkina, O., Laval, J., 2000. Clustered DNA damages induced in isolated DNA and in human cells by low doses of ionizing radiation. *Proceedings of the National Academy of Sciences of the United States of America* 97 (1), 103–108.
- Srensen, B., Vestergaard, A., Overgaard, J., Præstegaard, L., 2011. Dependence of cell survival on instantaneous dose rate of a linear accelerator. *Radiotherapy and oncology : journal of the European Society for Therapeutic Radiology and Oncology* 101 (1), 223–225.
- Tarnuzzer, R., Colon, J., Patil, S., Seal, S., 2005. Vacancy engineered ceria nanostructures for protection from radiation induced cellular damage. *Nano Letter* 5, 2573–2577.
- Tehei, M., Smith, J., Monk, C., Ollivier, J., Oetl, M., Kurkal, V., Finney, J., Daniel, R., 2006. Dynamics of immobilized and native escherichia coli dihydrofolate reductase by quasielastic neutron scattering. *Biophysical Journal* 90 (3), 1090–1097.
- Tripathi, D., Amresh, G., Tripathi, D., Kant, R., 2011. Antimicrobial and antitumor studies of some organic derivatives of bismuth. *Journal of Medicinal Chemistry Letters* 1 (1), 1–6.
- Tubiana, M., Dutreix, J., Wambersie, A., 1990. *Introduction to radiobiology*. Taylor & Francis, London.
- Tubiana, M., Eschwege, F., 2000. Conformal radiotherapy and intensity-modulated radiotherapy—clinical data. *Acta Oncol* 39 (5), 555–567.
- Tutt, A., Yarnold, J., 2006. Radiobiology of breast cancer. *Clinical oncology (Royal College of Radiologists (Great Britain))* 18 (3), 166–178.



- Tym, R., Todd, P., 1964. The sensitization by iododeoxyuridine of cultured human cells to the lethal effect of x-rays and heavy ions. *Int J Radiat Biol Relat Stud Phys Chem Med* 8, 589–603.
- Uhl, V., Phillips, T., Ross, G., Bodell, W., Rasmussen, J., 1992. Iododeoxyuridine incorporation and radiosensitization in three human tumor cell lines. *Int J Radiat Oncol Biol Phys* 22, 489–494.
- Veronesi, B., 1996. Characterization of the mdck cell line for screening of neurotoxicants. *Neurotoxicology* 17, 433–443.
- Vinchon-Petit, S., Jarnet, D., Jadaud, E., Feuvret, L., Garcion, E., Menei, P., 2010. External irradiation models for intracranial 9L glioma studies. *Journal of Experimental & Clinical Cancer Research* 29 (142).
- Vine, K., Locke, J., Ranson, M., Pyne, S., Bremner, J., 2007. An investigation into the cytotoxicity and mode of action of some novel n-alkyl-substituted isatins. *Journal of medicinal chemistry* 50 (21), 5109–5117.
- Von Recklinghausen, U., Hartmann, L., Rabieh, S., Hippler, J., Hirner, A. V., Rettenmeier, A. W., Dopp, E., 2008. Methylated bismuth, but not bismuth citrate or bismuth glutathione, induces cyto- and genotoxic effects in human cells in vitro. *Chem Res Toxicol* 21 (6), 1219–1228.
- Wagner, D., Christiansen, H., Wolff, H., Vorwerk, H., 2009. Radiotherapy of malignant gliomas: comparison of volumetric single arc technique (RapidArc), dynamic intensity-modulated technique and 3D conformal technique. *Radiotherapy and Oncology : Journal of the European Society for Therapeutic Radiology and Oncology* 93 (3), 593–596.
- Wakisaka, S., 1979. In vitro correlation of drug concentrations and radiosensitization in combination therapy with 5-bromo-2'-deoxyuridine, methotrexate, and radiation. *Cancer Research* 39 (1), 244–249.

- Wang, J. Z., Li, X., D'Souza, W. D., Stewart, R. D., 2003. Impact of prolonged fraction delivery times on tumor control: A note of caution for intensity-modulated radiation therapy (IMRT). *Int J Radiat Oncol Biol Phys* 57 (2), 543–552.
- Ward, J. F., 1981. Some biochemical consequences of the spatial distribution of ionizing radiation produced free radicals. *Radiation Research* 86, 185–195.
- Ward, J. F., 1994. The complexity of DNA damage - relevance to biological consequences. *International Journal of Radiation Biology* 66, 427–432.
- Willers, H., Dahm-Daphi, J., Powell, S., 2004. Repair of radiation damage to dna. *British Journal of Cancer* 90, 1297–1301.
- Williams, J., Zhang, Y., Zhou, H., Gridley, D., Koch, C., Russell, J., Slater, J., Little, J., 2008. A quantitative overview of radiosensitivity of human tumor cells across histological type and TP53 status. *International Journal of Radiation Biology* 84 (4), 253–264.
- Wilson, G., 2004. Radiation and the cell cycle, revisited. *Cancer metastasis reviews* 23 (3-4), 209–225.
- Wilson, G., Marples, B., 2007. Flow cytometry in radiation research: past, present and future. *Radiation research* 168 (4), 391–403.
- Wilson, G., McNally, N., Dunphy, E., Kärcher, H., Pfragner, R., 1985. The labelling index of human and mouse tumours assessed by bromodeoxyuridine staining *in vitro* and *in vivo* and flow cytometry. *Cytometry* 6 (6), 641–647.
- Wong, J., 2006. Systemic targeted radionuclide therapy: potential new areas. *Int J Radiat Oncol Biol Phys* 66 (2 Suppl), S74–S82.
- Wouters, B., Begg, A., 2009. Chapter 2. the dna damage response. In: Joiner,

- M., Kogel, A. V. D. (Eds.), Basic Clinical Radiobiology Fourth Edition. A Hodder Arnold Publication, Great Britain.
- Xia, T., Kovoichich, M., Liong, M., Madler, L., Gilbert, B., Shi, H., et al, 2008. Comparison of the mechanism of toxicity of zinc oxide and cerium oxide nanoparticles based on dissolution and oxidative stress properties. ACS Nano 2, 2121–2134.
- Zardiackas, L., Parsell, D., Dillon, L., Mitchell, D., Nunnery, L., Poggie, R., 2001. Structure, metallurgy, and mechanical properties of a porous tantalum foam. J Biomed Mater Res 58 (2), 180–187.